



HAL
open science

On the stochastic response of rotor-blade models with Floquet modal theory: applications to time-dependent reliability of tidal turbine blades

Oscar Sánchez Jiménez

► **To cite this version:**

Oscar Sánchez Jiménez. On the stochastic response of rotor-blade models with Floquet modal theory: applications to time-dependent reliability of tidal turbine blades. Mechanical engineering [physics.class-ph]. Normandie Université, 2023. English. NNT : 2023NORMIR39 . tel-04544344

HAL Id: tel-04544344

<https://theses.hal.science/tel-04544344>

Submitted on 12 Apr 2024

HAL is a multi-disciplinary open access archive for the deposit and dissemination of scientific research documents, whether they are published or not. The documents may come from teaching and research institutions in France or abroad, or from public or private research centers.

L'archive ouverte pluridisciplinaire **HAL**, est destinée au dépôt et à la diffusion de documents scientifiques de niveau recherche, publiés ou non, émanant des établissements d'enseignement et de recherche français ou étrangers, des laboratoires publics ou privés.



Normandie Université

THÈSE

Pour obtenir le diplôme de doctorat

Spécialité **MECANIQUE DES SOLIDES, GENIE MECANIQUE, PRODUCTIQUE, TRANSPORT
ET GENIE CIVIL**

Préparée au sein de l'**INSA Rouen Normandie**

On the stochastic response of rotor-blade models with Floquet modal theory: applications to time-dependent reliability of tidal turbine blades

Présentée et soutenue par
OSCAR SANCHEZ JIMENEZ

Thèse soutenue le 21/12/2023
devant le jury composé de :

M. EMMANUEL PAGNACCO	MAITRE DE CONFERENCES DES UNIVERSITES HDR - INSA de Rouen Normandie	Directeur de thèse
M. ERIC JACQUELIN	PROFESSEUR DES UNIVERSITÉS - Université Claude Bernard Lyon 1	Président du jury
MME ROBERTA DE QUEIROZ LIMA	ASSISTANT PROFESSOR - Pontifícia Universidade Católica do Rio de Janeiro	Membre
M. GREGORY GERMAIN	CHERCHEUR - Institut français de recherche pour l'exploitation de la mer	Membre
M. DANIEL JEAN RIXEN	PROFESSEUR - Technische Universität München, Germany	Membre
M. CLAUDE BLANZE	PROFESSEUR DES UNIVERSITÉS - Conservatoire National des Arts et Métiers, Paris	Rapporteur

Thèse dirigée par **EMMANUEL PAGNACCO** (LABORATOIRE DE MECANIQUE DE NORMANDIE)



Acknowledgments

Following the tradition of Laplacian causal determinism, one is compelled to acknowledge the antecedents that made this thesis possible and contributed to the transformation experienced by the one presenting it. This work would not have been possible without the influence of these individuals and institutions, to which I owe a great deal.

I acknowledge the opportunity created by the government of my home country, the Dominican Republic, and that of the country that has received me, the Republic of France. The Caliope program, which I have participated in, emerged as a manifestation of this collaboration between France and the Dominican Republic. I also acknowledge the financial support of the Ministry of Higher Education, Science and Technology of the Dominican Republic (MESCYT).

My director, Prof. Emmanuel Pagnacco, played a foundational role in the making of this thesis. His patience, creativity, and intellectual rigor have been instrumental in developing this work. It has been a privilege to be able to work alongside him for the past five years.

I express my most profound appreciation to the jury members, especially for accepting such a task late in the calendar year. I thank the commentary and recommendations of the reviewers, Prof. Éric Jacquelin and Prof. Claude Blanzé; their remarks contributed to a more robust and complete work. Thanks to Dr. Gregory Germain, his observations were of great value given his expertise in the application domain and will undoubtedly shape future research efforts. Thanks to Prof. Daniel J. Rixen for his insightful commentary and questions, but also for the general influence of his work. Special acknowledgment and appreciation to Prof. Roberta De Queiroz Lima for her valuable observations and recommendations on the general thesis, but also for her detailed and insightful commentary on a very early version of what eventually became a large part of chapters 3 and 5 of this thesis: that collaboration resulted in a more concise and clear exposition, and ultimately, in a deeper understanding of the problem and the results obtained.

I would like to thank the members of my Comité de suivi individuel, Prof. Fabrice Barbe and Prof. Eduardo Souza. Prof. Fabrice Barbe provided insightful remarks and productive criticism. His suggestions were valuable.

Prof. Eduardo Souza has my thanks in many of his multiple roles. As a member of my CSI, for his thoughtful observations. As the representative of INSA de Rouen Normandie in the context of the Caliope program, I am grateful for allowing me to embark on this project. Perhaps most of all, as a professor in many courses, but particularly in a field that is very dear to my heart: the fascinating, profound, and elegant theory of Analytical Mechanics.

I thank Prof. Rubens Sampaio for his interest in my work and for his thoughtful, profound observations during the various collaborations we have worked together on.

Although my interest in scientific inquiry has been with me as early as I have memories (presumably thanks to my father), my interactions with three individuals transformed this interest into something more concrete. Thanks to Prof. Inna F. Samson, who allowed me to work on my first research project, and to Prof. Felix Emilio Lara, for his encouragement and massive contribution to improving my mathematical literacy. Thanks to Prof. Maria Penkova Vassileva for her encouragement and teaching in mechanics, mathematics, and scientific research in general; my interactions with her were transformative in profound ways, and it is a privilege to consider myself one of her students.

Mots clés : Systeme pale-rotor, Theorie de Floquet, Systeme lineaire periodique, Processus stochastique, Champs aleatoires spatio-temporels, Hydrolienne, Fiabilité.

Keywords: Rotor-blade system, Floquet theory, Linear Time-periodic Systems, Stochastic processes, Spatio-temporal random fields, Tidal turbines, Reliability.

This thesis has been prepared at the Laboratoire de mécanique de Normandie (LMN), UR3828, in the Institut National des Sciences Appliquées (INSA) de Rouen, Avenue de l'université, BP 8, 76801 Saint-Etienne du Rouvray, cedex, France.

Nomenclature

Throughout this text, bold symbols denote vector and matrix quantities. Calligraphic typesetting is reserved for stochastic fields, except for the Lagrangian.

Latin symbols

A	Area of cross-section of the blade
$\mathbf{A}(t)$	State matrix of time-periodic system
$\mathbf{B}(t)$	State load matrix of time-periodic system
\mathbf{B}_b	Matrix of Fourier coefficients of state load matrix for $b - th$ harmonic
C_m, C_d	Morison's inertia and drag coefficients
C_j^\bullet	Rayleigh-Ritz modal coefficients
D_{pile}	Diameter of pile
\mathbf{D}	Damping component of velocity coefficient matrix
$E[\bullet]$	Mathematical expectation
f_p	Frequency of the system, pumping frequency
$\bar{\mathbf{f}}$	Modally adapted excitation or force
$\mathbf{F}(t)$	Load vector, excitation vector
F_H	Hydrodynamic force
$\text{FT}[\bullet]$	Fourier Transform
f^*	Frequency variable
G	Limit state function of reliability problem; objective function of optimization problem
$\tilde{\mathbf{G}}$	Coordinate of the center of mass of rotor component, or disc
G_x, G_y, G_z	Components of \mathbf{G}
$\mathbf{G}(t)$	Gyroscopic matrix, velocity coefficient matrix;
\mathbf{G}_G	Gyroscopic component of velocity coefficient matrix
H_{sea}	Sea depth

H_{pile}	Pile height
$\mathbf{h}(t)$	First order impulse response function
$\mathbf{h}_2(t_1, t_2)$	Second order impulse response function
i_b, j_m	Indexes of blade and modal discretization, respectively
I_d, J_d	Diametral moment of inertia of the disc
I_p, J_p	Polar moment of inertia of the disc
$\mathbf{K}(t)$	Stiffness matrix, displacement coefficient matrix
KE, PE	Kinetic and potential energy
KED, PED	Kinetic and potential energy of disc/hub/rotor
KEB_{i_b}, PEB_{i_b}	Kinetic and potential energy of blade i_b
L_b	Length of blade
L_ρ	Correlation length
$\mathbf{L}(t)$	Matrix of left periodic modes
\mathbf{L}_l	Matrix of Fourier coefficients of left periodic modes for $l - th$ harmonic
\mathcal{L}	Lagrangian
M_r	Mass of rotor component
$\mathbf{M}(t)$	Mass matrix, inertia matrix
n_H	Higher integer multiple in Fourier series expansion
n_j	Total number of terms in Fourier series expansion
$\mathcal{N}(a, b)$	Normal, or Gaussian distribution of mean a and variance or covariance or PSD b
$N(u, a, b)$	Number of crossings over level u , interval (a, b)
O_{xyz}	Origin of inertial reference frame, inertial reference frame
$\mathbf{p}(t)$	Modally adapted excitation or force
$\mathbb{P}[\star]$	Probability operator
$\mathbf{P}_1, \mathbf{P}_2$	Coordinate vector of supports of rotor-shaft assembly
P_X, p_X	Cumulative Distribution function (CDF), Probability Density Function (PDF) of X
P_{X_M}	Extreme value distribution (EVD) of X , CDF of X_M
$\mathbf{q}, \dot{\mathbf{q}}$	Vector of modal generalized coordinates and velocities
R	Available resistance
R_r	Radius of disc or rotor
R_{FF}	Correlation function of F
$\mathbf{R}(t)$	Matrix of right periodic modes

\mathbf{R}_q	Matrix of Fourier coefficients of right periodic modes for $q - th$ harmonic
$\tilde{\mathbf{R}}(t)$	Rotation matrix
s	Pole of characteristic equation, eigenvalue problem
S	Response in reliability problem
S_{XX}	Power Spectral Density (PSD) of X
T_p	Period of the system, pumping period
TI	Turbulence Intensity Index
u	Crossing level, threshold
V	Flow velocity
$\mathbf{W}_i; W_i^s, W_i^f$	Beam or blade displacement field of blade i ; spanwise component; flapwise component
\mathbf{W}	Block diagonal Hill matrix
$\mathbf{x}, \dot{\mathbf{x}}, \ddot{\mathbf{x}}$	Position, velocity, acceleration vector of physical coordinates
\mathbf{x}_h	Coordinate vector of the center of mass of the hub or disc
X_M	Extreme value of process X
\mathcal{X}	Spatio-temporal stochastic field
$\mathbf{y}, \dot{\mathbf{y}}$	State vectors
\mathbf{Y}	Fundamental solution matrix
$Z(t)$	Stochastic process, output of an integral transformation

Greek symbols

α	Steepness coefficient
β	Directional/angular variable in stochastic sea simulation
λ	Eigenvalue, Lagrange multiplier, Lamé coefficient
$\lambda_X^+(u)$	Mean number of upcrossings by process X over threshold u
$\mathbf{\Lambda}(f)$	Modal Frequency response matrix
$\mathbf{\Lambda}_0, \mathbf{\Lambda}_m$	Group or set of characteristic exponents
ξ	Spatial dummy variable
ξ_i	Damping ration
ρ	Blade density
ρ_f	Fluid density
$\boldsymbol{\rho}$	Matrix of characteristic multipliers
θ_1, θ_2	Tilt angles, Euler angles, Generalized angular coordinates

τ	Time shift, time delay, time difference
κ_0	Initial configuration of rigid body
$\Theta(m)$	Function of passage of characteristic exponents and periodic modes from group zero
$\Phi(t, t_0)$	State transition matrix, Floquet transition matrix
$\phi_j^*(X_b,)$	Modal shape form, blade mode shape
ϕ	Eigenvector
ϕ_i^*	Rayleigh-Ritz modal basis
$\phi_{(i,j),k}$	First influence factor
$\Psi_{j,k}(t)$	Wavelet function of scale j and translation k
$\Psi_{i,j}$	Second influence factor
Ψ^R, Ψ_i^L	Right and left eigenvector, LTI system
μ_F	Mean of F
μ_i	i – th Floquet multiplier
σ_{FF}	Variance of F
σ_x	Normal stress on x direction
Σ_{FF}	Covariance function of F
η	Surface elevation
γ	Spatial frequencies on stochastic simulation of sea state
ρ_i	i – th Lyapunov characteristic exponent
v_u^+	Crossing intensity or rate of upcrossing over threshold u
$v(f)$	Frequency shift function
ω	Natural frequency, circular natural frequency
$\bar{\omega}$	Subset of probability space Ω , probabilistic event
Ω	Angular velocity, parametric term in periodic component
Ω	Probability space
Ω_G	Angular velocity vector

Abbreviations

BEM	Blade Element Momentum
BVP	Boundary Value Problem
CDF	Cumulative Distribution Function
DOF	Degree of Freedom
EPSD	Evolutionary Power Spectral Density
EOM	Equation of Motion
EVD	Extreme Value Distribution
FT	Fourier Transform
IVP	Initial Value Problem
IFT	Inverse Fourier Transform
LTI	Linear time-invariant
LTP	Linear time-periodic
MCS,MCM	Monte-Carlo simulation, Monte-Carlo method
ODE	Ordinary Differential Equation
PDF	Probability Density Function
PGHW	Periodic Generalized Harmonic Wavelet
RBM	Root Bending Moment
STFT	Short Time Fourier Transform

Contents

Acknowledgments	1
Nomenclature	5
Contents	11
Introduction	14
Chapter 1 : Previous works	23
1 Rotor-blade model	24
2 Linear time-periodic systems	24
2.1 The Floquet-Lyapunov-Hill approach	24
2.2 Alternative approaches	27
3 Stochastic modeling, simulation, and extreme value theory	28
3.1 Stochastic force models and simulation	29
3.2 Extreme value distribution	32
Chapter 2 : Dynamics of rotating mechanical systems: The rotor-blade model	37
1 Architecture of rotor-blade systems	38
2 Kinematic description	40
3 Equation of motion: Energy and Lagrangian	43
3.1 Kinetic energy	43
3.2 Potential energy	44
3.3 Energy of blades	46
3.4 Lagrangian and equation of motion	51
4 Blade modeling and modal discretization	55
4.1 Modal determination by kinematic methods	55
4.2 Load determination in modal basis	59
4.3 Stress determination from modal variables	59
4.4 Numerical implementation: example and comparisons	61
5 Numerical example of the dynamical model	61
Chapter 3 : Theory of ordinary differential equations with periodic coefficients with applications to deterministic mechanical systems with stochastic input	69
1 Results for LTI systems	70

2	Free Response of LTP systems and Floquet modal analysis	71
2.1	Free response and modal analysis: Elements of Floquet theory	72
2.2	Hill's method for modal analysis of LTP systems	75
2.3	PGHW representation of Floquet modes: change of basis approach	78
2.4	Selected examples	82
3	Forced response of LTP systems	91
3.1	Time-domain resolution in modal variable	91
3.2	Spectral approach	92
Chapter 4 : Load description and moment propagation with PDF estimation		97
1	Notation	98
1.1	Generalities	98
1.2	Extension to vector processes	103
1.3	Extension to fields	105
2	Morison force in offshore engineering	105
2.1	General results	106
2.2	Covariance result for a stationary Gaussian process input	106
2.3	Comparison with two existing results in the literature	107
3	Morison load with stochastic field input and PDF reconstruction	109
3.1	System description and input field	109
3.2	PDF reconstruction from moments	111
3.3	Results	112
Chapter 5 : Moment propagation in LTP systems with periodic modal representation		117
1	Moment transformation of nonstationary processes	117
1.1	Cyclic Gaussian scalar process	117
1.2	On Withers' theorem and Gaussian moments	120
2	Extreme value distribution of periodic zero-mean nonstationary processes	125
2.1	Moment propagation of derivative process	126
3	Analyzing upcrossings of Gaussian periodically modulated processes	127
3.1	Preliminaries	127
3.2	Method of interval approximation	128
4	Floquet moment transformation	129
4.1	Convolution relationships	131
4.2	Transformations of the adapted excitation	136
5	Illustrative example	139
5.1	Load description	139
5.2	Response and analysis	141
Chapter 6 : Application: reliability of a tidal turbine model		151
1	Background	151
1.1	Tidal stream turbines	151
1.2	Time-dependent reliability	153

2	System description	155
2.1	Dynamical model	155
2.2	Modal analysis	157
3	Load modeling and simulation	160
3.1	Preliminaries	160
3.2	modeling the velocity field	163
4	Methodology	165
4.1	MCS-ODE method	167
4.2	Modal spectral MCS method	168
4.3	Floquet modal convolution	168
5	Results	170
5.1	Transient to steady transition	170
5.2	Floquet modal convolution: early transient regime	175
5.3	Steady-state	180
5.4	Synthesis of extreme values and reliability indicators	182
	Conclusion and future work	185
	Bibliography	191
	Appendix A : Matrix specification of various dynamical systems developed	201
1	The 2 DOF mass-blade	202
2	The 21 DOF model	204
	Appendix B : Description of the stochastic load	210
1	Description of the stochastic load	211
	Appendix C : Energy expression of beam from continuum mechanics and material constitutive laws	215
	Appendix D : Generation of stochastic processes	219
1	Preliminaries	220
1.1	Karhunen-Loève representation	221
2	Simulation of Gaussian processes	221
2.1	Multivariate case	223
3	Simulation of non-Gaussian processes	225
	Résumé	227
	Abstract	229

Introduction

“It is possible I already had some presentiment of my future.”

Gene Wolfe, *The Book of the New Sun*

General motivation

Technological innovation relies on the robustness of the body of knowledge that allows implementation and execution to be carried out effectively. This manifests in the design and analysis tools that intervene in the implementation process, impacting the performance, reliability, and cost-efficiency of systems, machines, and structures. The field of mechanics serves as a foundational discipline in a large proportion of technologies in various domains. This has resulted in an ever-increasing degree of complexity and sophistication in studying mechanical systems. This degree of complexity is evidenced in two conceptual axes:

- System complexity: modeling the mechanical behavior that arises from the interaction between multiple components, the variability or uncertainty of system properties, and such behaviors as nonlinearity, parametric effects, and time-varying properties;
- Excitation complexity: modeling the environmental interactions in more general forms, such as stochastic descriptions of forces;

this increase in complexity requires the extension of existing analytical tools to these new considerations and the development of new techniques to accommodate these constraints.

In a similar vein, the approaches to address the challenges mentioned above can be placed on a gradient: from simplified models that permit the application of analytical tools and result in profound insights into the behavior of the system under study to very detailed models that require efficient and procedural computation yielding realistic results. In the case of stochastic mechanics, the broad class of Monte-Carlo methodologies plays a key role, given the generality of its underlying principle. Nonetheless, the drawback of this approach is the steep, often prohibitive computation time entailed in the simulation and analysis of large and realistic systems. Additionally, analysis under this approach is limited with respect to the other side of the spectrum. Conversely, analytical methods are limited to simplified models, and the degree of simplification could lead to a loss of fidelity with respect to the desired application.

This thesis focuses on studying the vibrational motion of deterministic mechanical systems undergoing large rotations and under stochastic loads within the previously established framework. A central model in this category is the rotor-blade system, composed of a rigid, often discrete, component that can be described in terms of the theory of rotordynamics; in addition, continuum elements are attached to this component, and these can be modeled in terms of standard vibrating beam theory, with the particularity that the rotational effect results in a significant behavior change. This model category describes various technologies: wind and tidal turbines, helicopter propulsion, steam and gas turbines, compressors, and mechatronics or robotic devices.

In terms of loading, the environmental interactions over a structure or machine can feature a high degree of variability or complexity, making them suitable candidates for a stochastic description instead of a fully deterministic one. Oceanic environments are a primary example of high variability, featuring the effects of waves, tides, swell, turbulence, and wind effects over the state of the waters. This variability manifests itself through two key design considerations: the advent of extreme events and random fatigue damage.

The methodological approach is semi-analytical: the aim is to develop simplified models that are sufficiently accurate to apply and develop methods that give some insight into the behavior of the system as opposed to merely a solution. This inherently multi-disciplinary task involves applied mechanics and rotordynamics, probability and stochastic processes, extreme value theory, theory of ordinary differential equations and dynamical systems, numerical analysis, signal processing, and scientific computing. We now introduce a conceptual framework to consider the type of problems inherent to the engineering practice. This will permit a more precise discussion of this work's objectives and further developments.

Conceptual framework

From a broader perspective, the goals of this study are primarily concerned with analyzing systems, although considerable attention is paid to enabling the applicability to design problems. It is of practical and conceptual use to formally distinguish between different classes of problems in the engineering and design practice, some of which are perhaps shared with other disciplines. We take an abstract approach to construct this distinction, dwelling on the particulars as the need arises. . Let S stand for a system in the broadest sense possible, its behavior described by some mathematical structure: from systems of equations to systems of partial differential equations.

- • Type A: some perturbation, say F , acts on S , producing a response q . The objective is: given F and with known S , determine q , the response: $F, S \rightarrow q$. We call this type of problem an analysis problem. In the practice of mechanics, the most fundamental response is expressed in terms of motion: movement, displacement, velocity, and momentum (quantity of motion, quantity of angular motion). From this fundamental response, one may apply certain behavior laws or some additional transformation to obtain kinetic quantities: reaction force, stress, mechanical moment, or torque. Applying more intricate relationships and obtaining complex responses as complex as fatigue is also possible. The importance of these second or third-order quantities of the response is related to the assessment of the performance of S . The obtention of these second or third-order quantities of the response from the fundamental response we will call post-processing. Of course, the fact that motion is the most fundamental form of obtaining the response does not preclude the existence of methods of analysis formulated in such a way that the fundamental response is some other quantity: in this sense, we will call the raw output of a method the fundamental response quantity. Second and third-order responses are established in terms of the intervention or not of intermediate quantities for the calculation.
- • Type B: Some perturbation F is known, and restrictions ψ_q on the admissible q are established. The objective is to select the appropriate system S such that, given F , the response q conforms to the restrictions $\psi_q : \{F, \psi_q\} \rightarrow \{S, q \in \psi_q\}$. We call this type of problem a design or synthesis problem. In practice, the general architecture of S is known in this type of problem, and what needs to be selected is some set of specific parameters to fully define it. One may think of a spring-mass-damper system $S \rightarrow M, C, K$ where the behavior is well known, but one may need to select the appropriate value of C to ensure a prescribed dynamical behavior. This type of problem forces one to confront an issue in terminology. Rather than considering one particular system, considering them broad families of possible systems is often useful. Not a system but a manifold of them. An $S \rightarrow M, C, K$ system is characterized by its behavior, but the particular details will depend on the specific values of each parameter. Once the values of M, C, K are specified, we say we have an instance of system S . In this light, Type B problems become a search for the appropriate instance of S .

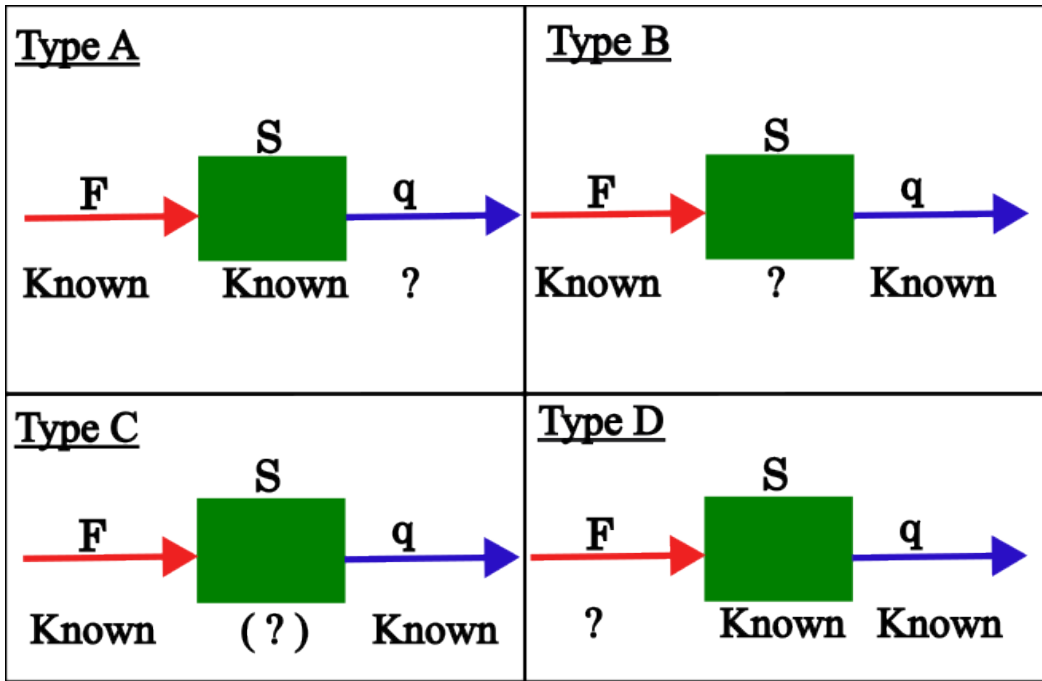


Figure 1: Representation of problem-type framework

- Type C: The response q is known along with F . The objective is to determine the unspecified quantity $s \subset S$, the system. The determination of s is not the same as the one previously discussed in type B: here, we seek to determine a subset of S that produces q given F . In practice, this type of problem arises when the particular characteristics of an already existing instance need to be found. We call this type of problem a system characterization problem. We may write $\{q, F\} \rightarrow S(s)$.
- Type D: The response q is known along with S . The objective is to determine the unspecified quantity F , the excitation. In practice, this problem arises when the instance of S is known, and q is available from some measurement, so one seeks to characterize F for external purposes. We call this type of problem a load characterization problem. We may write $\{q, S\} \rightarrow F$.

The value of this conceptual framework is twofold: First, a method to address one type of problem might be modified to tackle another type of problem. This modification can result in important variations in the advantages and disadvantages, so it is important to have a conceptual tool to distinguish each instance; second, it helps disentangle the different but related notions of a system S , which can be a broad category of instances that share a similar behavior but which have particular characteristics.

Determinism, randomness, and stochasticity

We call deterministic any quantity fully specified within an established numerical error threshold from the information available. On the other hand, random is a quantity that can not be fully specified in the same way since its behavior will incur an unpredictable evolution. While random quantities can not be fully determined, these can usually still be characterized or described in some way: if the quantity can be "sampled" (measured, evaluated, repeated), then it is often possible to describe general trends that hold if the number of samples is sufficiently descriptive. This description of general trends relies heavily on an interconnection between probability theory and statistical tools. Finally, we call stochastic a quantity that displays some measure of randomness but is subject to stringent deterministic relationships.

Conceptually, one may think of the stochastic category as containing a gradient going from deterministic to random: to see this, we can imagine a simple variable specified by its mean and variance. The mean and variance are deterministic quantities, so we conceptualize the behavior of this variable for different variances while the mean remains fixed: when the variance is infinite, the determination of general trends previously discussed becomes less meaningful in characterizing the variable; when the variance degenerates to zero, there is no randomness in the variable, and we recover a deterministic variable identical to the mean.

We call a system causal when its past fully determines its present. In contrast, when a system's present is not fully determined by its past, the system is said to be acausal. This terminology results in the emergence of two obvious and distinct types of acausal systems: 1) systems that are deterministic but whose present is caused not only by the past but also by its future (this implies the propagation of information backward in time); 2) systems that are not fully determined by the past because there is an element of randomness intrinsic to them. This further leads to the notions of deterministic acausality and random acausality.

One final observation concerns the notion of randomness. There are physical phenomena that happen to be intrinsically random; this is known from direct observation. On the other hand, some phenomena emerge from some complex interactions but are still deterministic in principle. While deterministic, characterizing these complex phenomena is either impractical or impossible. It is sometimes useful to model these deterministic complex phenomena using the same or similar mathematical theory to describe random ones. When this modeling is performed, one may refer to the modeling quantities as random in the mathematical sense, but the underlying phenomena modeled by these are not truly random. This suggests the classification of pseudo-random, or perhaps even epistemically random or random in the epistemic sense: it is practically impossible to obtain (or process) the necessary information to determine the phenomenon, so it is random not from some intrinsic physical trait, but from our limited knowledge of the relevant information associated with it.

Approaches to Type A problems in mechanics

- Analytical: integration of Equations of Motion.
- Numerical: time-domain integration.
- Numerical: frequency domain resolution.
- Numerical: Monte-Carlo successive numerical resolution with statistical post-processing.

Criteria of interest in Type B problems in mechanics

- Maximum stress and strain.
- Vibration amplitude.
- Other extreme events.
- Reliability.
- Fatigue and long-term events.

Taxonomy of mechanical systems

- Based on the system: deterministic or uncertain.
- Based on rotation: natural (no rotational motion along a principal axis), rotodynamical (rotational motion along a principal axis).
- Based on motion: static, dynamic.

- Based on behavior: linear, nonlinear.
- Based on temporal characteristics: time-invariant, periodically time-variant, quasi-periodically-time-variant, generally time-variant.
- Based on dimensionality: discrete, continuous, mixed or complex.
- Based on number of subsystem: single-body, multi-body.

Objectives

The first part of this work aims to develop and describe the deterministic mechanical system under study. To this end, the approach selected is that of analytical mechanics in the vein of the following texts: [96], [6], [43]. The Lagrangian formalism is utilized, and results from rotordynamics, as covered in [42] and [39], inform the modeling choices. The flexible elements are described from the general Continuum mechanics theory, and kinematic discretization methods are imposed on the continuum, as well as the relevant beam theory hypotheses and material behavior. The aim is to arrive at a concrete model while laying the theoretical foundation to adjust for different cases of interest. The description of the dynamical system is then analyzed using the theory of ordinary differential equations with periodic coefficients. The Floquet- Lyapunov and Hill methods are examined and applied. Besides the comprehensive review of these methods, pertinent extensions are proposed: time-frequency and modal tools are implemented to describe the response.

As shown in the next chapter, the model developed can be seen as a generalization of the rotating blade problem. The study of this type of system is not new, being the intense object of research during the last century in aerospace disciplines. Similarly, studying LTP systems and ODE with periodic coefficients is a robust, established area that intersects many domains. This manuscript's goal remains to review and synthesize the existing body of knowledge in both areas and adapt it for the study at hand. This need arises from considering stochastic inputs into this type of system, especially when these inputs are considered with some degree of complexity.

The second part focuses on the stochastic aspects of the excitation and response. We follow the developments introduced by [134] to describe stochastic processes and fields. Simulation aspects and propagation techniques are discussed and presented; an emphasis is placed on the moment propagation of nonstationary processes. This type of transformation plays a key role given the following facts: first, nonstationarity arises when force models are applied to rotating systems as a result of the relative motion between solid and medium; second, the response of LTP systems will be shown to be generally nonstationary even to a stationary input, this fact can be readily noticed from the study of Floquet's theorem, as the Floquet periodic modes act as periodic modulation of the response; finally, nonstationarity expresses environmental states of interest in many applications, such as tidal turbines.

Probabilistic moments provide useful information about the stochastic response, and they are prioritized because their obtention has practical advantages. However, they only provide a full description in specific cases, such as Gaussian processes. Thus, the advantages and limitations of this approach are discussed and exemplified, particularly in the approximation of the distribution of extremes of the response. The Monte-Carlo approach is taken to contrast these findings as the generality of the method serves as a baseline comparison. At the same time, the steep computational requirements to reach a valid result from MCS constitute a major motivation for the semi-analytical approach taken in this work.

Finally, the third part consists of concrete applications of the established results. The main application pertains to tidal turbines, their analysis, and potential design schemes. The bibliography of the field is reviewed, and based on current trends and research needs, the techniques developed are used. Several contributions are proposed: the dynamical model and Floquet analysis applied to this type of machine, the detailed stochastic model to represent and simulate the current-tide-turbulence medium, and applications of reliability criteria under these circumstances. Throughout the thesis, the interplay between theoretical and computational aspects is analyzed. While the central problem is of type A, insights into problems of type B are considered.

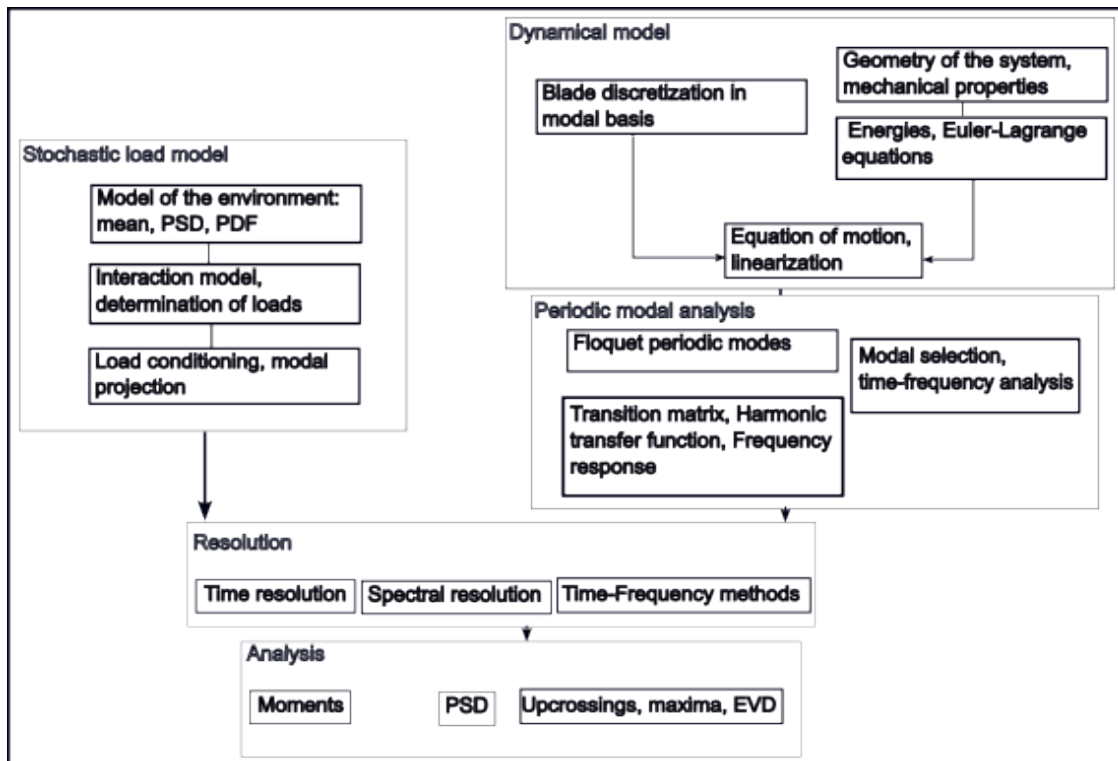


Figure 2: Conceptual flow of the thesis

Contributions

The main contributions of the thesis are summarized here, providing a concise description and the innovative elements.

- In chapter 2:
 - a. A new reduced-order rotor-blade theoretical model is proposed, valid for constant intrinsic spin or rotational velocity. The model is based on a 5 DOFs rigid rotor and Euler-Bernoulli beam theory with modal representation describing the blades. The innovative aspects include 1) the use of a relatively general rotor in a reduced-order model; 2) the inclusion of spanwise-flapwise motion on the blades, including possible coupling arising from blade section asymmetry; 3) theoretical developments allowing the description of blades with different material behavior.
 - b. A fast Rayleigh-Ritz algorithm is proposed, providing a polynomial approximation of the modal parameters of the rotating beam problem in spanwise and flapwise directions. The algorithm is flexible regarding the range of angular velocities that can be considered and the number of modes and degree of desired polynomial approximation.
- In chapter 3:
 - a. A synthesis of Floquet modal analysis is proposed. It combines results from different fields of application, such as ODE theory, Aerospace/helicopter analysis, and control theory. The synthesis aims to recover key results established in the literature and make them accessible from a unified framework.

- b. A detailed study of Floquet Periodic Modes is presented. The existing methods for calculating the Floquet Periodic Modes are discussed and contrasted. The indeterminacy of the characteristic exponents is reinterpreted, using the results from Peters et al., and extended to a simple rule allowing the determination of the periodic mode corresponding to a shifted characteristic exponent.
- c. A change of basis theorem on Hilbert spaces is applied to analyzing periodic modes, focusing on the Fourier-PGHW bases. The result facilitates time-frequency analysis of the periodic modes using Wavelet theory.
- d. The Campbell-Lyapunov diagram is proposed: it is a parametric diagram showing the evolution of the Lyapunov characteristic exponents of the Floquet system with varying rotational velocity or pump frequency.
- e. A new development of LTP systems' existing spectral response formula is presented. The development, based on the combination of the Fourier series representation of Floquet Periodic Modes and the Fourier transform of the input, aims to provide clarity in the use and interpretation of the formula.
- In chapter 4:
 - a. An Extreme value distribution approximation method is proposed: it consists of analytical moment propagation from loads to response, followed by PDF reconstruction using the principle of maximum entropy relying on optimization techniques. The method is applied to the rigid submerged pile under the action of a Morison load, with Gaussian input velocity field and acceleration.
- In chapter 5:
 - a. Analytical expressions for moment propagation of periodic stochastic processes and their derivative are presented.
 - b. The Wither conjecture is presented and tested: application of Wither theorem to Gaussian stochastic processes for moment propagation, allowing the determination of moments of polynomial transformations of Gaussian processes.
 - c. An Interval approximation method to estimate the Extreme value distribution of periodic stochastic processes is proposed and tested. The method circumvents a limitation in the corresponding literature, particularly for processes with moments that cross zero, resulting in the indeterminacy of the quantities involved.
 - d. Analytical expressions for moment propagation in Floquet modal variables are proposed. These expressions are more detailed than those found in the literature and include high-order moments, a result not identified in the literature.
- In chapter 6:
 - a. Synthesis showing the connection between: the time-dependent reliability problem and extreme value theory, particularly for a limit-state of constant available resistance and nonstationary response. The result aims to bridge the gap between the results in both domains and to facilitate the application of results to the study of tidal turbine blades.
 - b. A Monte-Carlo method based on Floquet modal theory (spectral formula) is proposed, providing the steady-state response of LTP systems subjected to nonstationary non-gaussian loads.
 - c. A Convolution semi-analytical method based on Floquet modal theory is proposed, providing the transient response of LTP systems subjected to nonstationary non-gaussian loads. The practical limitations of this approach are explored and described.
 - d. The concept of moment modal decomposition is presented and tested: it contributes to each periodic mode to the moments of the response.
 - e. A reliability analysis of a simplified tidal turbine model in three loading regimes is presented. The failure mode under analysis is formulated in terms of the normal stress associated with the root bending moment from the combined spanwise-flapwise vibration of the blade.

Structure of the thesis

The structure of this thesis is as follows:

1. The first chapter presents an overview of previous relevant results: Floquet ODE theory, the evolution of the physical problem in the literature, developments in different disciplines, stochastic models, and extreme value and reliability results.
2. The second chapter develops the dynamical model to be studied: kinematics and geometry, the Euler-Lagrange formalism, and the kinematic modal discretization of the blade elements are treated.
3. Chapter 3 presents the results of the modal analysis of the system from the Floquet, Hill, and an innovative approach adopted for the analysis of the Floquet periodic modes based on Wavelet analysis. An example of the modal solution of a simplified Floquet system describing a rotor-blade system is presented.
4. In Chapter 4, some notational and technical developments for moment propagation are presented, with examples including Morison's model in memoryless integral transformation. The problem of moments for this type of transformation is addressed and formulated in terms of the maximum entropy distribution as an optimization problem.
5. Chapter 5 combines the results from chapters 3 and 4 to study the stochastic response of time-periodic systems through moment propagation. A first example is proposed considering the time-modulation of a stationary point process, followed by a study of the upcrossing and maxima estimation of the Gaussian case. Moment transformations are established regarding Floquet modal theory for the steady-state response of Floquet systems.
6. Chapter 6 presents an application of the developed results to a tidal turbine model. Reliability criteria are applied to analyze the blades.

Chapter 1

Previous works

“The miracle of hindsight is how it transforms great military geniuses of the past into incompetent idiots, and incompetent idiots of the present into great military geniuses.”

Steven Erikson, Toll the Hounds

This chapter presents the most relevant antecedents of the research problem and surveys some alternative approaches that have been explored. The different aspects of the problem are covered. First, a review of the evolution of the dynamical problem is presented, starting from the rotating beam problem in the early 20th century. Then, the results of LTP theory are addressed, covering various fields that have contributed to the current state of knowledge. Finally, the advancements in stochastic analysis and extreme value distribution are discussed.

The general equation of the system under consideration takes the following form:

$$\mathbf{M}(t, \Omega) \ddot{\mathbf{x}} + \mathbf{G}(t, \Omega) \dot{\mathbf{x}} + \mathbf{K}(t, \Omega) \mathbf{x} = \mathbf{f}(t) \quad (1.1)$$

where \mathbf{x} is a vector of generalized displacements, the usual over dot notation is adopted for differentiation with respect to time, the matrices involved are such that, for instance, $\mathbf{M}(t + nT_p) = \mathbf{M}(t)$ of any $n \in \mathbb{Z}$; the vector $\mathbf{f}(t)$ here consists of a stochastic vector process which is not necessarily Gaussian and generally nonstationary. This system can be cast into first order or state form:

$$\dot{\mathbf{y}} = \mathbf{A}(t, \Omega) \mathbf{y} + \mathbf{B}(t, \Omega) \mathbf{f}(t), \quad (1.2)$$

with the substitution $\mathbf{y} = [\mathbf{x}, \dot{\mathbf{x}}]^T$.

System Eq. 1.2 is known as a Floquet system of period T_p . This type of equation of motion emerges when modeling a broad class of mechanical systems we refer to as rotor-blade models. They consist of a rotor component, which undergoes large continuous rotation around a main axis, and additional elements radially attached undergoing deformation. The periodicity of the system is associated with the rotational velocity of the rotor $\Omega = 2\pi f_p$, $T_p = \frac{1}{f_p}$, respectively the angular velocity, rotating frequency, and period. In the sequel, the explicit functional dependence on Ω of the matrices in Eq. 1.1 and Eq. 1.2 is omitted to facilitate readability. Given the periodic parameters, the dynamical behavior of this type of system is qualitatively more complex than that of natural systems. We begin our review with the emergence of an associated problem whose generalization leads to this: the rotating blade problem.

1 Rotor-blade model

Considering a system like Eq. 1.1 with the simplifying assumption that the rotor element is fixed in translation, we arrive at a system of the form:

$$\mathbf{M}\ddot{\mathbf{x}} + \mathbf{G}(\Omega)\dot{\mathbf{x}} + \mathbf{K}\mathbf{x} = \mathbf{f}(t), \quad (1.3)$$

this system, while not LTP, is dependent on the parameter Ω . It has been used to study the vibration of a blade in turbo-machinery since the early 20th century. The model is that of a disc with radially attached blades; a description of the transverse vibration of the blades is the subject. The terminology spanwise and flapwise refer to the direction of the deformation: in-plane or out-of-plane, respectively, referencing the plane of rotation. The distinguishing features of this class of system are the stress stiffening and spin softening effects on the dynamics of the blade and from the associated eigenvalue problem [44]:

$$(s^2\mathbf{M} + s\mathbf{G}(\Omega) + \mathbf{K})\Psi = \mathbf{0} \quad (1.4)$$

the next important feature can be observed: the vibration frequency of the system will depend on the parameter Ω . This type of system can display parametric resonance, which results in peak amplitudes for critical angular velocity values.

Early techniques to analyze this type of system rely on the Southwell method which relies on the approximation of small Ω , and more accurate techniques started emerging in the mid-20th century. The paper by [17] provides a formal deduction of the equation of motion of such a system. It utilizes energetic analytical techniques to study the frequency of the system with respect to the parametric term. Similarly, [149] studies the modal behavior of the problem with an added tip mass, accentuating the centrifugal stiffness effect. In the reference [108], the finite element method is used to calculate the system frequency and normal modes for a range of angular velocities. Further, it shows the effects on different beam models. In [70], an adapted finite element method is used to study the frequencies of the system with an added tip mass. From our perspective, the main limitations of these results lie in two factors: first, the rotor was considered fixed, thus the study of the blade led to the study of a rotating beam or plate; second, analysis was confined to the modal and frequency behavior, and the type of excitation considered, if any, were relatively simple and usually deterministic functions. This, however, helps to illustrate the types of effects that result from parametric behavior.

The problem described by Eq. 1.4 is characteristic of rotor systems, as exposed in texts such as [42] and [39]. Following [42], a rotor is understood as a system component undergoing rotation with significant angular momentum. When the motion of the rotor (other than its angular velocity) is included in the description, the interplay between the different reference frames results in periodicity in the parameters. From a physical perspective, this effect includes the gyroscopic term seen in Eq. 1.4 and a time-dependent change in the system's inertial \mathbf{M} and stiffness \mathbf{K} parameters.

2 Linear time-periodic systems

2.1 The Floquet-Lyapunov-Hill approach

The mathematical theory of differential equations with periodic coefficients began to emerge with the works of Mathieu ([86]), who found the namesake equation when studying the vibration of elliptical membranes; Hill ([54]) who arrived at his equation and method in his study of Lunar motion; more formally with the work of Floquet in his treaty on the subject[35]. The main result from this period is a series of theorems and methods by Floquet, Lyapunov, and Hill. Floquet's theorem provides the form of the fundamental solution of this type of system. Lyapunov reducibility theorem demonstrates the existence of a change of variable that renders the associated homogeneous equation to Eq. 1.2 into a time-independent form. Consider the homogeneous associate of Eq. 1.2:

Stability of Solution	Condition
Stability of trivial solution	$\text{Re}(\rho_k) \leq 0, \forall k$
Asymptotic stability	$\text{Re}(\rho_k) < 0, \forall k$
Instability of trivial solution	$\text{Re}(\rho_k) > 0, \exists k$
Existence of T_p -periodic solution	$\rho_k T_p = 2\pi ni, \exists k, n \in \mathbb{Z}$
Existence of T_p -anti-periodic solution	$\rho_k T_p = 2\pi(n+1)i, \exists k, n \in \mathbb{Z}$

Table 1.1: Stability criteria of solutions of Floquet system from characteristic exponents

$$\dot{\mathbf{y}} = \mathbf{A}(t)\mathbf{y}, \quad (1.5)$$

a fundamental solution of Eq. 1.5, \mathbf{Y} , is a linearly independent set of solutions. Floquet's theorem states [119]:

Theorem 1. Floquet's theorem: *Let $\mathbf{Y}(t)$ be a fundamental solution matrix of the Floquet system Eq. 1.5 with period T_p , that is, a matrix whose columns are solutions to the system. Then the matrix $\mathbf{Z}(t) = \mathbf{Y}(t+T_p)$ is also a fundamental solution matrix of the Floquet system. There is a function $\mathbf{R}(t)$ of period T_p and a constant matrix $\boldsymbol{\rho}$ such that: $\mathbf{Y}(t) = \mathbf{R}(t) \exp[\boldsymbol{\rho}t]$,*

where $\exp[\boldsymbol{\rho}t]$ is understood as the matrix exponential of $\boldsymbol{\rho}$. The matrix function $\mathbf{R}(t)$ is what we interpret as the Floquet modal matrix, each column being a Floquet periodic mode. This theorem guarantees the existence of $\mathbf{R}(t)$, while Hill's method provides a concrete procedure to compute it. The matrix $\boldsymbol{\rho}$ contains the so-called characteristic exponents of the Floquet system. The stability of the solutions of Eq. 1.5 can be established from the analysis of the characteristic exponents, as synthesized in [119], see Tab. 1.1.

Hill's method consists of the Fourier series expansion of the periodic terms, and the solution reduces to finding the unknown Fourier coefficients of the solution. Modern texts on the subject of ODE, such as [119], [20] and [69], provide a comprehensive treatment of the subject from a mathematical perspective.

These works focus predominantly on results for the homogeneous equation. The application of these mathematical tools to engineering problems can be found in earlier works on helicopter dynamics and design. In the text [66] (initial version is from 1980), Hill's method is applied to the modal analysis of an LTP system modeling the helicopter rotor-blade system. In the work [25], Hill's method is used to study the stability of the aeroelastic response of helicopters in forward fly. In contrast, in works such as [99] during the 1970s, Peters expands the application of Floquet theory to this domain. Notably, Peters introduces the formula:

$$\mathbf{R}(t) = \Phi(t, 0) \mathbf{R}(0) \boldsymbol{\rho}(t) \quad (1.6)$$

which allows the determination of the Floquet modal matrix from the transition matrix of the system. In the following years, numerical approaches to Floquet analysis of this type of system greatly develop. Friedmann and Hammond, in [37] and [38] discuss the numerical aspects of computing the transition matrix of LTP systems while proposing efficient methods for its determination. The state transition matrix $\Phi(t, 0)$ permits the representation of the homogeneous solution given initial conditions. The methods developed by Friedmann and Hammond are relatively general, making their application to any other LTP system other than helicopter rotor blades straightforward. In the same vein, [124] later presents sophisticated numerical schemes that use orthogonal polynomial integration to study stability from the state transition matrix.

Xu and Gasch, in [151], present the development of Floquet Modal analysis of an arbitrary LTP system. Parallels with the modal analysis of LTI systems are emphasized. The connection between Floquet-Lyapunov and Hill's method is exploited. The non-homogeneous (forced) response of the Floquet system is obtained using the modal basis, convolution integral, and Fourier transform. Their development leads to an LTP equivalent of the mechanical compliance matrix used in LTI mechanical systems. Finally, an application is provided in the form of a wind turbine subjected to an arbitrary wind excitation. Building on their work, [22] applies the same modal approach to design active control strategies.

In his thesis [144], Wereley studies general LTP systems with applications in control theory. The thesis provides a detailed exposition of both Floquet's and Hill's methods, introducing useful theoretical manipulations that are absent in the literature up to that point. The Harmonic Transfer Function (HTF) is introduced here as an LTP equivalent to the LTI transfer function. As with the work of Xu and Gasch, this development facilitates studying the forced response of LTP systems.

Although most of the research thus far presented focuses on stability analysis or deterministic response, some exceptions are worth highlighting for completeness. These exceptions will help frame the innovative elements of the present work. In note [103], the problem of helicopter flapping with random inputs is considered. An LTP system as Eq. 1.2 is studied with a stochastic force that is weakly periodic nonstationary:

$$\begin{aligned}\mu_f(t) &= \mu_f(t + T_p) \\ R_{ff}(t_1, t_2) &= R_{ff}(t_1 + T_p, t_2 + T_p),\end{aligned}\tag{1.7}$$

where $\mu_f(t)$ is the mean function of the process $f(t)$ and $R_{ff}(t_1, t_2)$ is its correlation function, periodic on T_p . The transition matrix and convolution integral are used to establish some of the probabilistic moments of the response. Expressions for the mean function, correlation function, and a version of an evolutive Power Spectral Density (EPSD) are established.

In the reference [141], the flapping motion with a rigid rotor is considered under random forces. No mention is made of results from Floquet theory. Still, it can be seen by comparison that the impulse response function utilized here is equivalent to the state transition matrix of the system, which is obtained by direct successive integration. Different stochastic models are used for the forces, including white and correlated noise. In addition to moments, the response is characterized by upcrossing intensity.

Reference [131] proposes a numerical method using Chebyshev polynomials to estimate the state transition matrix and then compares two methods to obtain the response. Deterministic and random inputs are considered. Two types of processes are considered: a modulated white noise and a process with an exponential correlation function.

These early solutions to the stochastic response of LTP systems have certain limitations that we aim to address in this thesis. While results from Floquet theory are capitalized on, little attention is paid to the behavior and characteristics of the Floquet periodic vectors, which offer valuable information about the behavior of the total solution. These works also demonstrate the fact that the LTP forced response to a stochastic input is, in general, a nonstationary stochastic process, but the rich theory of this class of process is not involved in the analysis. For instance, different proposals to generalize the PSD in nonstationary cases have been proposed, and time-frequency distributions can be utilized to study the time evolution of the spectrum: Harmonic Wavelets, Short-time Fourier Transform, and the Wigner-Ville distribution, among others. The stochastic excitations selected in these publications are relatively simple, but a more detailed description of the force processes is possible, which leads to a more realistic application of the results obtained. These points are addressed in our work, and the connection between the stochastic description of the response and design criteria is made, particularly with reliability criteria.

Having covered the classic results from the literature, we now turn to more recent developments. In his thesis, [22] applies an approach similar to that of [151] to the modal analysis of an LTP system. The goal of this work is active control strategies for LTP systems. An important difference with respect to other efforts is that the blades in his proposed model are deformable bodies, and the interaction between blade modes and rotor modes is presented in the Floquet modes obtained. A fully spectral method is proposed in the reference [3], the frequency response of the LTP system is determined iteratively, and the stability of the response is also analyzed. Comparisons are made to a Monte-Carlo resolution scheme.

In the reference [9], an LTP system describing a wind turbine is considered, and a coordinate transformation is proposed for this type of system. The Multi-blade coordinate transformation is used to express the response in the fixed reference frame. The relevant part of the analysis is related to the evolution of the modal frequencies; this is done numerically using specialized analysis software. Floquet analysis is integrated into the modal analysis after the coordinate transformation.

Hansen [51] focuses on the modal analysis of a wind turbine using Hill's method. A rotor-blade model describes two types of turbines: two-bladed and three-bladed. The periodic modes are contrasted for each case, and the particularities of Hill's method are discussed. The redundancy of modes inherent to Hill's method is solved by applying filtering criteria to the obtained candidate eigenvalues. Additionally, the paper provides a synthetic review of the emergence of Floquet and Hill techniques in wind turbine technologies from the late 2000s to mid-2010s, in publications by himself (Hansen) and Skjoldan [125], Bottasso and Cacciola [14], among others.

To conclude the wind energy review, in [118], the forced response is studied using modal techniques from the results found in the preceding publications. A reduced-order model is selected to describe the key aspects of floating wind turbine motion. The Colemann transformation and Floquet analysis are applied. Special attention is paid to the effect of system anisotropy on the stability of the solution. Different wind velocities are also considered, and the loads are calculated using Blade Element Momentum Theory (BEMT). No stochastic description of loads is presented.

In recent years, other domains have integrated Floquet analysis and proposed adapted stability and response analysis methods. For instance, in reference [49] Floquet analysis is applied to studying periodic flexible multi-body systems. A numerical technique is proposed for the determination of the stability and the simulation of such systems. The Galerkin method is the basis of the numerical method, which aims to find the system's periodic solutions.

2.2 Alternative approaches

We now briefly summarize some alternative approaches that have been explored for the resolution of the problem in this thesis; as detailed in [50], three trends can be identified:

- Artificial intelligence tools: [4] proposes an emulator to study the response as a function of uncertain mistuning; [19] utilizes different machine learning methodologies to study uncertainties inherent to the manufacture of rotor blades in helicopters.
- Experimental techniques have been implemented to characterize in-service systems: [143] proposes a novel experimental technique based on optical fiber to measure the response of a helicopter rotor blade system; [101] utilizes a hybrid method involving digital image correlation to characterize the properties (particularly the sectional stiffness) of a helicopter rotor blade.
- Computational and analytical developments have been applied to the study of stochastic LTP systems: [76] combines a reduced-order model with an arbitrary polynomial chaos (aPC) basis with random spatial heterogeneities; [81] takes an analytical and experimental approach to study multi-source nonlinearities in rotor-blade systems; [36] proposes a method based in chaos exponentials (related to polynomial chaos method) to project the Blade Element Momentum equations that describe the loading on a wind turbine to obtain estimations of the unsteady long-term load; [16] takes an analytical approach based in stochastic calculus to address error and noise in the inputs of wind turbines with a particular emphasis on the flutter-type dynamical instability; [156] focuses on the dynamic reliability of a compressor rotor system with stochastic stresses and strengths. In reference [31], the approach to determining the forced response of time-varying systems is developed using a Wavelet representation to extend the concept of transmissibility in LTI systems to the case of time-varying ones.

Some of the ideas in these alternative approaches might prove useful to our purposes. Yet, many are aimed at fundamentally different tasks: some are focused on addressing nonlinear systems, others are formulated for type C or type D problems, and others consider uncertainties in the system rather than the excitation. This summary, however, offers a modern perspective on the state of the field. This concludes the review of the system side of the problem. The following section addresses developments in stochastic load modeling and other relevant aspects of the stochastic component of our work.

3 Stochastic modeling, simulation, and extreme value theory

This section recovers some existing results useful to our treatment of stochastic quantities. We follow many of the ideas and methods introduced in his thesis [134] by Suptille, adapting them to our application. Other key references covering fundamental topics are the monographs by Papoulis [98] for probability theory, Preumont [104] and Lutes and Sarkani [85] for the application of random processes to mechanical vibrations, and Christakos [21] for the treatment of spatio-temporal stochastic fields. We first present some definitions and notational aspects that will be used throughout this work.

A scalar stochastic process $X(t)$ in the probability space $\{\Omega, \mathcal{F}, \mathbb{P}\}$, where Ω is a sample space, \mathcal{F} is a sigma-algebra over Ω , and \mathbb{P} is a probability measure, continuous t , is an infinite set of random variables indexed by time, each random variable is characterized by its Cumulative Distribution Function (CDF):

$$P_X(x, t) = \mathbb{P}[X(t) \leq x], \quad (1.8)$$

for a fixed t ; this is also referred to as the marginal CDF of process $X(t)$ at the indicated time and also the first-order distribution of the process. A more thorough description of the process requires the finite-dimensional distributions (FDDs) of the process, which are the joint CDFs of a finite number of the constituent random variables, for instance, the second-order distributions read:

$$P_{XX}(x_1, x_2, t_1, t_2) = \mathbb{P}[X(t_1) \leq x_1, X(t_2) \leq x_2], \quad (1.9)$$

and similarly, the n -th order distributions read:

$$P_{X\dots X}(x_1, \dots, x_n, t_1, \dots, t_n) = \mathbb{P}[X(t_1) \leq x_1, \dots, X(t_n) \leq x_n]. \quad (1.10)$$

The instantaneous n -th probabilistic moment with respect to the origin, also called ordinary moment, of process $X(t)$, is defined as:

$$\mu_{X^n}(t) = \mathbb{E}[X^n(t)] = \int_{\mathbb{R}} x^n p_X(x, t) dx, \quad (1.11)$$

where $\mathbb{E}[\bullet]$ denotes the expectation operator, x covers the range of the possible values of the process, and $p_x(x, t)$ is its marginal Probability Density Function (PDF): $p_x(x, t) = \frac{\partial P_X(x, t)}{\partial x}$ if the derivative exists. For the ordinary moments, we may also expand the subscript and write $\mu_{X^n} = \mu_{X \times X \dots \times X}$ (n times); for instance the following equivalences are often practical: $\mu_{X^2}(t) = \mu_{XX}(t)$, $\mu_{X^3}(t) = \mu_{XXX}(t)$ and $\mu_{X^4}(t) = \mu_{XXXX}(t)$, but after the fourth moment the subscript expansion becomes cumbersome so the original form is given preference in our developments when $n > 4$. We refer to the first ordinary moment as the mean of process $X(t)$. Similarly, the instantaneous n -th probabilistic moment with respect to the mean, so-called central moment, is defined as:

$$\sigma_{X^n}(t) = \mathbb{E}[(X(t) - \mathbb{E}[X(t)])^n], \quad (1.12)$$

we observe that with this indicial notation: ordinary moments are invariant under index permutation, while central moments are not. We refer to the second central moment as the variance of process $X(t)$.

The instantaneous moments can be generalized to the inter-instant moments:

$$\begin{aligned} R_{XX}(t_1, t_2) &= \mathbb{E}[X(t_1)X(t_2)] \\ \Sigma_{XX}(t_1, t_2) &= \mathbb{E}[(X(t_1) - \mathbb{E}[X(t_1)])(X(t_2) - \mathbb{E}[X(t_2)])] \end{aligned} \quad (1.13)$$

the correlation function and covariance function of process $X(t)$, respectively; more generally:

$$\begin{aligned}
R_{X^n}(t_1, t_2, \dots, t_n) &= \mathbb{E} \left[\prod_{i=1}^n X(t_i) \right] \\
\Sigma_{X^n}(t_1, t_2, \dots, t_n) &= \mathbb{E} \left[\prod_{i=1}^n (X(t_i) - \mathbb{E}[X(t_i)]) \right], \tag{1.14}
\end{aligned}$$

for $n = 3$ we have the bi-correlation and bi-covariance, for $n = 4$ the tri-correlation and tri-covariance, and so on.

A process is strongly stationary if its marginal distributions are invariant to time. A weakly stationary process up to the second order is one such that:

$$\begin{aligned}
\mu_X(t) &= \mu_X \\
\Sigma_{XX}(t_1, t_2) &= \Sigma_{XX}(t_2 - t_1), \tag{1.15}
\end{aligned}$$

the mean is constant and the covariance function depends on the time difference $\tau = t_2 - t_1$ rather than the time instants. The Wiener-Khinchin theorem provides the following result:

$$S_{XX}(f) = \text{FT}[\Sigma_{XX}(\tau)], \tag{1.16}$$

where $\text{FT}[\bullet]$ is the Fourier transform, and $S_{XX}(f)$ is the Power Spectral Density (PSD) of process $X(t)$.

A stochastic process can be interpreted as a sequence of random variables indexed by a time variable. In many domains, a sequence of random variables is called a stochastic field. The term spatio-temporal stochastic field (see [21]) denotes a sequence of random variables indexed by time and space variables. Throughout this work, the term stochastic field refers to spatio-temporal fields. We thus note a stochastic field by $\mathcal{X}(\mathbf{x}, t)$, which depends on the 3D space coordinate \mathbf{x} and time t . The moments of field $\mathcal{X}(\mathbf{x}, t)$ are expressed as:

$$\begin{aligned}
\mu_{\mathcal{X}(\mathbf{x}_1) \dots \mathcal{X}(\mathbf{x}_n)}(t) &= \mathbb{E}[\mathcal{X}(\mathbf{x}_1, t) \dots \mathcal{X}(\mathbf{x}_n, t)] \\
\sigma_{\mathcal{X}(\mathbf{x}_1) \dots \mathcal{X}(\mathbf{x}_n)}(t) &= \mathbb{E}[(\mathcal{X}(\mathbf{x}_1, t) - \mathbb{E}[\mathcal{X}(\mathbf{x}_1, t)]) \dots (\mathcal{X}(\mathbf{x}_n, t) - \mathbb{E}[\mathcal{X}(\mathbf{x}_n, t)])] \\
R_{\mathcal{X}(\mathbf{x}_1) \dots \mathcal{X}(\mathbf{x}_n)}(t_1, \dots, t_n) &= \mathbb{E}[\mathcal{X}(\mathbf{x}_1, t_1) \dots \mathcal{X}(\mathbf{x}_n, t_n)] \\
\Sigma_{\mathcal{X}(\mathbf{x}_1) \dots \mathcal{X}(\mathbf{x}_n)}(t_1, \dots, t_n) &= \mathbb{E}[(\mathcal{X}(\mathbf{x}_1, t_1) - \mathbb{E}[\mathcal{X}(\mathbf{x}_1, t_1)]) \dots (\mathcal{X}(\mathbf{x}_n, t_n) - \mathbb{E}[\mathcal{X}(\mathbf{x}_n, t_n)])], \tag{1.17}
\end{aligned}$$

where the index quantities are to be interpreted as varying on the \mathbf{x} space. For instance, the instantaneous second ordinary moment of field $\mathcal{X}(\mathbf{x}, t)$ is $\mu_{\mathcal{X}(\mathbf{x}_1)\mathcal{X}(\mathbf{x}_2)}(t)$, a function of a time variable and two space variables.

3.1 Stochastic force models and simulation

Stochastic modeling is a powerful tool that allows us to take into account the high variability in structural properties and physical phenomena. This approach results in mechano-probabilistic models with an intrinsic, probabilistic notion of risk/safety, from which emerges the study of system reliability in probabilistic mechanics. Already in the 1990s, as can be noted in reference [127], probabilistic approaches had been gaining traction to the point of being integrated into international guidelines and reports in the context of structural design (for instance, the JCSS's *General Principles on Reliability for Structural Design*, used by ISO in the revision of ISO 2394, as well as in the ISO in the revision of ISO 2394; the Commission of the European Communities followed these guidelines in a first draft of the Eurocode n° 1 (EUR 8847, 1984), and subsequently in the drafting of Eurocodes 2 to 8). Schuller [121] offers an insightful perspective of the field in the mid-2000s, highlighting the fact that offshore applications have led the way in stochastic methods and reliability applications.

Given the complexity of the physical phenomena involved in their dynamics, marine and oceanic mediums are strong candidates for stochastic modeling. An offshore or submerged structure or machine is potentially subject to wind, waves, tides, currents, and additional turbulent effects that characterize the background sea environment. The question of how to characterize these effects and determine the behavior or response of structures and machines subject to them has been a subject of research for a long time.

In the classic work of Morison [90], the namesake and popular semi-empirical formula is proposed with the objective of calculating the forces produced by waves on slender offshore structures:

$$F_H = \rho_f C_m \frac{\pi}{4} D_{\text{pile}}^2 \dot{V} + \frac{1}{2} \rho_f C_d D_{\text{pile}} V |V|, \quad (1.18)$$

where ρ_f is the density of the water, D_{pile} is the effective diameter of the slender element, C_m and C_d are empirical constants describing inertial and drag effects, V and \dot{V} are the particle velocity and acceleration of the fluid respectively, and F_H is the hydrodynamic force per unit of area. While the original result was proposed in a deterministic context, it was soon extended to the stochastic domain. Borgmann pioneered the early efforts in this front in reference [12], where he considered the particle velocity and acceleration as centered Gaussian stochastic processes and obtained expressions for the PDF and moments of the response.

The investigation of the stochastic version of Eq. 1.18 eventually led to the question of determining the extremes of such forces and the consideration of deformable elements and their dynamic response. In the paper [47], Grigoriu studies the extremes of Morison force when the particle velocity is Gaussian. He utilizes the upcrossing rate of the force and the theory of Translated Gaussian Processes to compute the crossing intensity. The paper identifies an important issue: statistical linearization yields a Gaussian response and does not provide a good approximation except for inertially dominated regimes. The nonlinearity of the Morison model breaks Gaussianity and leads to underestimation of mean and variance, so the maxima are poorly approximated. We remark that given a stochastic process $X(t)$ under consideration in the interval $[0, T]$, we call the extreme value distribution (EVD) the CDF of the quantity:

$$X_M = \max_{[0, T]} [X(t)] \quad (1.19)$$

that is, for a process $X(t)$, the largest value in $[0, T]$ is described as the random variable X_M , its CDF $P_{X_M}(x_M) = \mathbb{P}[X_M \leq x_M]$ expressing the probability that the largest value attained by the process in the interval is at most x_M .

The extremes and statistics of Morison-type loading have been extensively researched with different types of methods being proposed: Moe [89] utilizes probabilistic and spectral methods and discusses the distinction between short-term and long-term statistics; Baar [2] studies the extremes of Morison forces using approximations and compares the different regimes, the qualitative difference of the distribution when one term is dominant over the other; Lindgren [82] studies the extremes using probabilistic methods and applies Rice formula, which will be discussed in more detail in the next subsection; Naess [91] uses analytical methods to describe extreme value statistics. We stress the fact that these results are about the Morison force itself, not the response of a given structure or machine to it.

Apart from the previous developments, the study of the response to Morison-type loads has also been studied in depth. Koliopoulos [71] studied the case of a single-degree-of-freedom linear system, described the response in terms of moments, deduced PDF estimations, and used Rice's formula to determine the upcrossing of the response process. More recent works include Zheng and Liaw's [158] study of a linear oscillator subject to a Morison-type force, proposing a method based on Cumulants, and spectral analysis is used to obtain the response; Najafian [94] proposed probabilistic models for the response validated by simulation; Naess et al. [92] propose a Monte-Carlo approach to obtain the extremes of the drag-dominated response to a Morison load. Winterstein [145] considers nonlinear oscillators and describes the response through its moments, introducing probabilistic models compatible with the analytically obtained moments. The model proposed is compared to Charlier and Edgeworth series representation of the response PDF based on moments; the results include extremes and fatigue descriptors. This approach has been further explored by Winterstein and collaborators and intersects with wind energy applications: [146] and [147].

Algorithm 1.1 Moment propagation conceptual flow

1. Describe the stochastic input and system.
 2. Propagate moments from input to output.
 3. Use the output or response moments to “reconstruct” the PDF of the response.
-

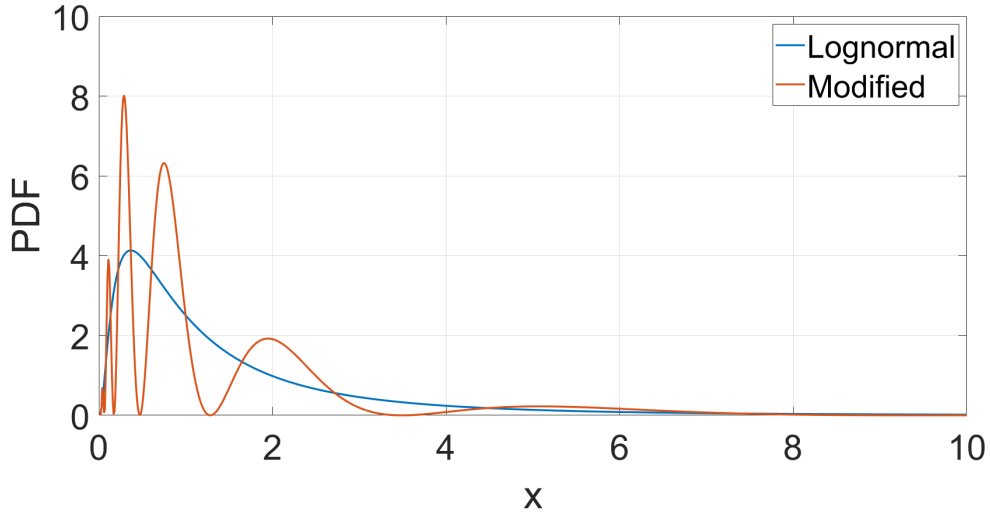


Figure 1.1: Example of Lognormal and modified Lognormal distributions

Analytical results for complex systems and general excitation, like nongaussian and nonstationary input processes, are limited. The strategy exemplified by Winterstein and others (see Alg. 1.1) is based on the fact that moment propagation is often convenient for these complex cases, yet different approaches are possible to this reconstruction of the response PDF, and much of the previously cited research focuses on the practicality and accuracy of these different approaches: from Maximum entropy to Charlier or Edgeworth series. An additional theoretical limitation must be considered in this approach: finite moments do not fully determine the PDF of a general process, as put by Diaconis in [28]: “Natural examples show that distributions can match in many moments and still not be equal”. As an example, consider the following two distributions characterized by the following PDF:

$$\begin{aligned}
 p(x) &= \frac{1}{\sqrt{2\pi}} \left(\frac{1}{x}\right) \exp\left[-\frac{(\log[x])^2}{2}\right] \\
 p_a(x) &= p(x) (1 + a \sin[2\pi \log[x]])
 \end{aligned}
 \tag{1.20}$$

with $x \geq 0$ and $-1 < a < 1$, these PDF can be visualized in Fig. 1.1, the non-central moments up to 4 for $a = -1$ are: $\mu_f = 10.359$, $\mu_{ff} = 46.427$, $\mu_{fff} = 565.57$, $\mu_{ffff} = 18730$; it can be shown (see: [30]) that these two different distributions have equal moments.

Another approach available to determine the response in complex situations is what we will call Monte-Carlo methods or Monte-Carlo simulations (MCM or MCS) throughout this work, as shown in Alg. 1.2. If sufficient realizations have been simulated, then the statistical descriptors should approach the probabilistic quantities of the response process. This approach is taken in the previously referenced work by Naess. The advantages of the MCM approach are its generality and conceptual simplicity and its compatibility with computational

Algorithm 1.2 MCM conceptual flow

1. Describe the stochastic input and system.
 2. Simulate the stochastic input for a sufficiently large number of independent realizations.
 3. Solve the dynamic equation subject to each input realization in a deterministic fashion.
 4. Perform statistical analysis on the solutions.
-

parallelization owing to the independence between realizations. Among the disadvantages we note scaling constraints, as convergence in the statistical sense may require a very large number of realizations, and for large systems the resolution time can be substantial or even prohibitive in the computational time sense; the implementation requires efficient methods to simulate the stochastic input, which is available for Gaussian and stationary processes, but are much more limited for more general processes. The scaling problem is particularly pronounced when the quantity under estimation is related to the extremes of the response: by definition, these are rare events and an accurate description requires either a very large number of realizations or the implementation of some modification of the standard MCM, such as biased sampling. For the simulation of Gaussian stationary processes, a widely popular method was proposed in reference [123], and many alternatives and versions have been developed over the years, for instance, [135] based on the inverse Fourier Transform. Alternatives to the nongaussian and nonstationary cases include: Gaussian Translation ([122]) and Karhunen–Loève–based approaches ([102]).

Using the problem category presented in the introduction, further remarks are made with respect to the MCS approach to response characterization with stochastic inputs. MCS is usually well adapted to type A or analysis problem since a single execution of the sequence Alg. 1.2 is required. The previously discussed scaling problems can be addressed with parallelization and code optimization (vectorization, selection of an efficient solver). In the case of type B problems, the MCS approach becomes impractical: since this type of problem can be framed as a search of parameters in a design space, a generally large number of executions of Alg. 1.2 would be required. On the other hand, design specifications can be expressed in terms of constraints to be met by moments in Alg. 1.1, which would then allow a much more effective implementation of a solution.

3.2 Extreme value distribution

The study of the largest value attained by a process on an interval $[0, T]$ plays a central role in the analysis of applied stochastic phenomena. From an engineering perspective, the motivation is straightforward: extreme response is one of the main design considerations of systems. The connection between the descriptive concept of EVD and design concept of probability of failure P_f can be evidenced by considering a sufficiently high failure level u_f and considering the CDF of Eq. 1.19:

$$P_f = 1 - P_{X_M}(u_f), \quad (1.21)$$

the probability of failure P_f in the observation time $[0, T]$ is the probability of the random variable X_M attaining or surpassing the level u_f . The complement of P_f in the probabilistic sense is the probability of no failure (safety), or reliability: $P_R = 1 - P_f = P_{X_M}(u_f)$.

A pivotal result in the study of extremes of stochastic processes was made by Rice in references [112] and [113], where the namesake formula is proposed for the zero crossings of a differentiable stochastic process, yielding the crossing intensity of rate of upcrossing $v_X(t)$:

$$v_X(t) dt = dt \int_{-\infty}^{\infty} |y| p_{X\dot{X}}(0, y, t) dy \quad (1.22)$$

where $p_{X\dot{X}}$ is the joint PDF of the stochastic process $X(t)$ and its derivative $\dot{X}(t)$. When applied to a stationary Gaussian process, this yields:

$$v_X^+(t) = \exp\left[-\frac{u^2}{2\Sigma_{XX}(0)}\right] \left(\frac{1}{2\pi}\right) \left(\frac{\ddot{\Sigma}_{XX}(0)}{\Sigma_{XX}(0)}\right)^{\frac{1}{2}}, \quad (1.23)$$

where Σ_{XX} is the covariance function of the process, $\ddot{\Sigma}_{XX} = \frac{\partial^2 \Sigma_{XX}}{\partial t^2}$.

More broadly, and considering the number of crossings over the level u on $[0, T]$ as $N(u, 0, T)$ one has:

$$\begin{aligned} \lambda_X^+(u) &= \mathbb{E}[N(u, 0, T)] \\ \mathbb{E}[N(u, 0, T)] &= \int_0^T v_X^+(u, t) dt, \end{aligned} \quad (1.24)$$

where $\lambda_X^+(u)$ is the mean number of upcrossings of X over u in $[0, T]$. To obtain $\lambda_X^+(u)$ here, Eq. 1.22 can be applied, although the main difficulty consists in the accurate determination of the joint PDF of the processes involved, particularly in this case of time-varying processes. With λ_X^+ known, the Poisson hypothesis can be used to seek an EVD of the form:

$$P_{X_M}(u) = P_X(u, t=0) \times \exp[-\lambda_X^+(u)], \quad (1.25)$$

where $P_X(u, t=0)$ is the probability of the process $X(t)$ remaining below the threshold u at the initial time of observation $t=0$.

In the subsequent decades, these two formulas saw application in many fields, from ocean engineering ([132]) to vibration theory ([24]). Theoretical and practical developments were published in the same period: Leadbetter [78] and Yang [152] worked to ameliorate the understanding of nonstationary and nongaussian cases. A historical and technical perspective on the influence of Rice's formula is given in the reference [83].

We now turn to two results of interest in the literature on nonstationary Gaussian processes related to their EVD and first-passage time. A more formal approach is taken in [74].

Hasofer and Petocz [52] This result is enunciated in terms of the following quantities:

$$\begin{aligned} \sigma_{YY}(t) &= \mathbb{E}[Y^2(t)] = R_{YY}(t_1, t_1); \\ \sigma_{Y\dot{Y}}(t) &= \mathbb{E}[Y(t)\dot{Y}(t)] = \dot{R}_{YY}(t_1, t_1); \\ \sigma_{\dot{Y}\dot{Y}}(t) &= \mathbb{E}[\dot{Y}(t)\dot{Y}(t)] = \ddot{R}_{YY}(t_1, t_1); \end{aligned} \quad (1.26)$$

where $\dot{Y}(t) = \frac{d}{dt}[Y(t)]$, and $\dot{R}_{YY} = \frac{\partial}{\partial t}[R_{YY}]$. The following time-dependent functions are introduced:

$$\begin{aligned} \gamma(t) &= \left[1 - \frac{\sigma_{Y\dot{Y}}^2(t)}{\sigma_{YY}(t)\sigma_{\dot{Y}\dot{Y}}(t)}\right]^{\frac{1}{2}} \\ \eta(t) &= \frac{u\sigma_{Y\dot{Y}}(t)}{\gamma(t)\sigma_{YY}(t)\sqrt{\sigma_{\dot{Y}\dot{Y}}(t)}} \end{aligned} \quad (1.27)$$

then the rate of upcrossings over a level u are expressed as :

$$v_Y^+(u;t) = \frac{\gamma(t)}{\sqrt{2\pi}} \sqrt{\frac{\sigma_{\dot{Y}\dot{Y}}(t)}{\sigma_{YY}(t)}} \exp\left[-\frac{u^2}{2\sigma_{YY}(t)}\right] \left[\frac{\phi(\eta(t))}{\eta(t)\Phi(\eta(t))} \right] \quad (1.28)$$

where ϕ is the standard normal PDF and Φ the standard normal CDF. Asymptotically, $u \rightarrow \infty$:

$$v_Y^+(u;t) \approx \frac{1}{\sqrt{2\pi}} \left[\frac{\gamma(t)}{\sigma_{YY}(t)} \right] \left[\frac{u}{\sqrt{\sigma_{YY}(t)}} \right] \exp\left[-\frac{u^2}{2\sigma_{YY}(t)}\right]. \quad (1.29)$$

Knowing that the rate of upcrossings over a sufficiently high level u allows for the computation of the first passage :

$$L_Y(u;t) = \Pr[T_Y(u) > t] = \exp\left[-\int_0^t v_Y^+(u;\tau) d\tau\right] \quad (1.30)$$

with $T_Y(u)$ is the first time at which Y surpasses the level u in the interval under study. This last formula relies on the assumption that the random variable counting the exceedances has a Poisson distribution. The Poisson hypothesis (particularly with respect to the independence of peaks) tends to break down with narrow-band processes because of the clumping of extremes. Under such situations, the envelope of the process can be studied in the same manner as here.

Ambetkar, Kuppa and Gupta [1] Considering a random vector of components $Y_i(t)$, the number of crossings of level u_i on the $[0, T]$ interval is introduced as $N_i(u_i, 0, T)$, with $Y_{m_i} = \max_{[0, T]} Y_i(t)$. The joint EVD is written as:

$$P_{Y_m}(u_1, \dots, u_i) = \exp\left[-\sum_{j=1}^{\frac{(u+1)u}{2}} \lambda_j\right], \quad (1.31)$$

which means the problem is reduced to finding or estimating the Poisson parameters λ_j .

Limitations The results on both of these references seem to have a similar limitation: the modulating function is of a very specific type composed of decaying exponentials. Our interest is in periodic or quasi-periodic modulations. The consequence of this disparity is that, in the postulated modulation we explore, of type $a(t) = \sum_i a_i(t, \omega)$, the introduced functions such as $\eta(t)$ in [52] and [1] are arbitrarily large due to the variance in the denominator approaching zero, resulting in issues evaluating: Eq. 1.28.

An important limitation in the applicability of equation Eq. 1.22 is the fact that realistic loading processes are often nongaussian and, as we shall see in detail in Chapter 3, lead to nonstationary response processes when applied to LTP systems; these two facts lead to serious challenges in the determination of the joint PDF of the response process and its derivative in analytical terms. As illustrated in Fig. 1.1, moment propagation is a powerful tool but moments might not be sufficient to reproduce the required PDF accurately, a problem compounded by the fact that usually, limited moments are available for the response. In practice, usually, the first 4 moments are considered in much of the literature. The few examples where this limit is crossed are from very specific types of prescribed distributions and not in applied fields of study. Additionally, in the case of stochastic processes, the instantaneous moments may not be a good descriptor, so higher-order covariances might need be computed. Higher order covariances increase their dimension with order, and the scaling from a computational perspective is cumbersome. We proceed by example:

1. A load process in a type of LTP system, the rotor-blade system, emerges from a governing law such as Morison's Eq. 1.18, but from a physical perspective, even if the velocity field is assumed stationary, it is the relative velocity that is required in the cited equation. Because of this, the Morison force perceived by the system is nonstationary.

2. The breaking in Gaussianity comes from nonlinearities in the interaction laws. Assume a stationary Gaussian velocity point process $X(t) \sim N(\mu_X, \Sigma_{XX}(\tau))$. Gaussianity implies that the moments must follow the following relationship:

$$\mu_{XXX} = \mu_X^3 + 3\mu_X \sigma_{XX}, \quad (1.32)$$

now considering the drag term of Eq. 1.18: $F = aX^2$, we have:

$$\begin{aligned} \mu_F &= a\mu_{XX} \\ \sigma_{FF} &= a^2\sigma_{XX} \end{aligned} \quad (1.33)$$

and since $\mu_{FFF} = a^3\mu_{X^6}$, $\mu_{X^6} = \mu_X^6 + 15\mu_X^4\sigma_{XX} + 45\mu_X^2\sigma_{XX}^2 + 15\sigma_{XX}^3$:

$$a^3 \left(\mu_X^6 + 15\mu_X^4\sigma_{XX} + 45\mu_X^2\sigma_{XX}^2 + 15\sigma_{XX}^3 \right) \neq a^3 \left(\mu_{XX}^3 + 3\mu_{XX}\sigma_{XX} \right) \quad (1.34)$$

we conclude that F can not be Gaussian.

3. The Floquet modal transformation of Eq. 1.1 with $\mathbf{x}(t) = \mathbf{R}(t)\mathbf{q}(t)$ leads to the modal (LTI) form of the problem: $\dot{\mathbf{q}}(t) - \boldsymbol{\rho}\mathbf{q}(t) = \bar{\mathbf{f}}(t)$, whose forced response is ([151]):

$$\mathbf{q}(t) = - \int_0^{+\infty} [\exp[\boldsymbol{\rho}(t-\tau)]] \bar{\mathbf{f}}(\tau) d\tau \quad (1.35)$$

taking the expectation:

$$\boldsymbol{\mu}_q(t) = - \int_0^{+\infty} [\exp[\boldsymbol{\rho}(t-\tau)]] \boldsymbol{\mu}_F(\tau) d\tau \quad (1.36)$$

as discussed in the previous point, $\boldsymbol{\mu}_F(t)$ is not constant since \mathbf{f} is not stationary in general, but further, even if $\boldsymbol{\mu}_F(t) = \boldsymbol{\mu}_F$ is assumed constant and $\boldsymbol{\mu}_q$ is too, the physical response is: $\boldsymbol{\mu}_X = \mathbf{R}(t)\boldsymbol{\mu}_q$, with $\mathbf{R}(t)$ the Floquet modal matrix of period T_p , the mean response, in this case, is nonstationary due to the periodic modulation of the periodic eigenvectors. In any case, the response is not stationary.

Nevertheless, different strategies have been developed to address these limitations:

- Moment propagation and probabilistic models based on the available moments have proved effective in specific domains: [146],[147].
- The theory of Gaussian Translation introduced by Grigoriu [46] has been expanded to some effect into the nonstationary domain [34], [157].
- Approximate formulas [84] have been developed for the nonstationary nongaussian case.
- Efficient MCS-based approaches to the study of extremes have been proposed [63], in some cases using reliability methods and numerical tools [62].
- The case of multivariate extremes has been explored to some extent [48].

The determination of the EVD of nongaussian nonstationary processes remains a challenge.

Chapter 2

Dynamics of rotating mechanical systems: The rotor-blade model

“As stated, every constraint that is not holonomic is nonholonomic. One will readily understand that it is not possible to give a general discussion of nonholonomic constraints such as can be done for holonomic ones because the latter is a narrowly circumscribed class while the former is not. (Thus, bananas are readily discussed, while nonbananas are not.) Nevertheless, some classification of frequently encountered nonholonomic constraints is possible.”

Reinhardt M. Rosenberg, *Analytical Dynamics of Discrete Systems*

In this chapter, the dynamical model of a rotor-blade system is constructed. The kinematic description of the system is established, informed by a priori knowledge of rotordynamics and relevant applications. The energetic expressions are deduced for general cases and then adapted to our case of interest. The Euler-Lagrange formulation of classical mechanics is chosen to establish a general equation of motion for a family of mechanical systems. The parameters of this family of systems consist of the constituents' geometric, physical, and mechanical properties, as well as the selected architecture of the structure under analysis.

A key aspect is the description of blade elements. A section is devoted to the modeling of blades taking a similar approach to that of the general system case: geometry of motion, energetic expressions derived from a continuum onto which we impose classical beam hypotheses and material behavior laws, and derivation of the equations of motion. Modal kinematic discretization is then applied to the equations of motion to obtain a discrete modal representation of blade vibration of arbitrary order. A balance between generality and practicality is sought.

Several innovative aspects of our development will be highlighted during the chapter. First, the application of a rich body of results in analytical mechanics of rigid bodies, as presented in [96], to this type of model, to our knowledge not present in the corresponding literature; second, we relax some restrictions usually found in the available literature concerning the description of the "hub/disc" or rotor component, leading to coupling terms that affect the modal and vibration behavior of the system; third, many approaches found in the pertinent literature either consider a rigid body, or discretize the entire system in terms of Finite Elements (FE), in contrast our model considers a multi-body system in which only the rotor element is rigid while mounted on elastic supports, and the blades are deformable. These modeling choices permit us to study the vibration behavior of

blades, considering the inherent coupling of this type of system. The fact that kinematic discretization methods are used instead of Finite Element techniques implies that the interpretation and analysis are more intuitive and manageable, particularly when the stochastic aspects come into play.

1 Architecture of rotor-blade systems

The rotor-blade model comprises two main types of constituents: a rotor subsystem, also called a hub out of practicality, and the blade elements. Depending on the application, additional elements, such as blade tip masses, vibration control, or suppression devices, can be integrated into the model. Additionally, the rotor-blade system can be integrated into a support structure: in tidal energy applications, the supports can be towers fixed to the sea floor or suspended floating platforms; in wind energy, various types of tower structures are utilized, and in offshore cases, floating and fixed supports exist. Two and three blades are the most common configurations for horizontal tidal turbines.

The rotor subsystem consists of an axisymmetric shaft with a mounted disc. The system has a spin or angular velocity parallel to the axis of symmetry of the disc. A diversity of models have been proposed concerning the characteristics of the shaft and kinematic hypotheses of motion([42],[39]):

1. Concerning the shaft and supports of the shaft, the following models have been proposed: rigid shaft on flexible supports, flexible shaft on rigid supports, and flexible shaft and supports.
2. Concerning kinematic considerations: the Jeffcott rotor in which motion is confined to the rotational plane (2 DOFs); different 4 DOFs models with different configurations, the degrees of freedom being two translations of the center of mass of the disc, and two angles describing the orientation of the disc. The spin is usually a prescribed quantity and, thus, is not a motion parameter. Translation in the direction of spin is usually neglected. The Stodola-Green rotor is characterized by the cantilever support conditions of the shaft.

Qualitatively, 2-DOF models such as the Jeffcott rotor do not display gyroscopic effects, a key feature of 4-DOF rotors. The gyroscopic term, which appears as a consequence of the conservation of angular momentum in the system, is the source of parametric vibrations in this type of model. To see this, consider the general equation:

$$\mathbf{M}\ddot{\mathbf{x}} + \mathbf{G}(\Omega)\dot{\mathbf{x}} + \mathbf{K}\mathbf{x} = \mathbf{0} \quad (2.1)$$

where the matrix $\mathbf{G}(\Omega)$ has the form:

$$\mathbf{G}(\Omega) = \begin{pmatrix} 0 & 0 & 0 & 0 \\ 0 & 0 & 0 & 0 \\ 0 & 0 & 0 & -I_p\Omega \\ 0 & 0 & I_p\Omega & 0 \end{pmatrix} \quad (2.2)$$

with I_p the polar moment of inertia of the disc and Ω the angular speed. This system can be cast into modal form seeking a solution of the form:

$$\mathbf{x} = \alpha\boldsymbol{\Psi}\exp(st); \quad \alpha, s \in \mathbb{C} \quad (2.3)$$

which results in the following eigenvalue problem:

$$(s^2\mathbf{M} + s\mathbf{G}(\Omega) + \mathbf{K})\boldsymbol{\Psi} = \mathbf{0} \quad (2.4)$$

making it evident that the resonant frequencies associated with this problem's eigenvalues will depend on the angular speed Ω . The Campbell diagram is a parametric plot that displays the values of the frequencies of the system for a selected range of Ω . A schematic representation of this type of system is shown in Fig. 2.1. An example of a Campbell diagram is shown in Fig. 2.2.

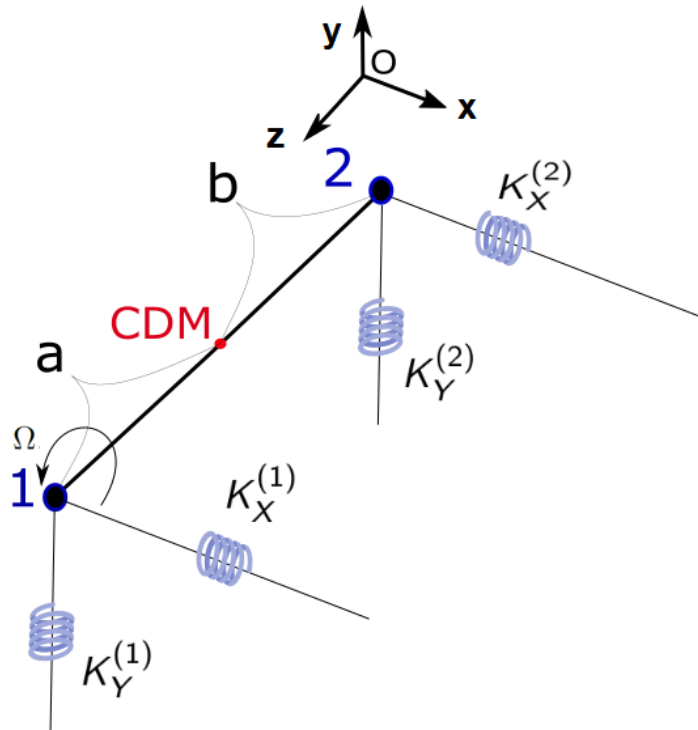


Figure 2.1: Schematic representation of 4 DOFs rotor system with rigid shaft and flexible supports

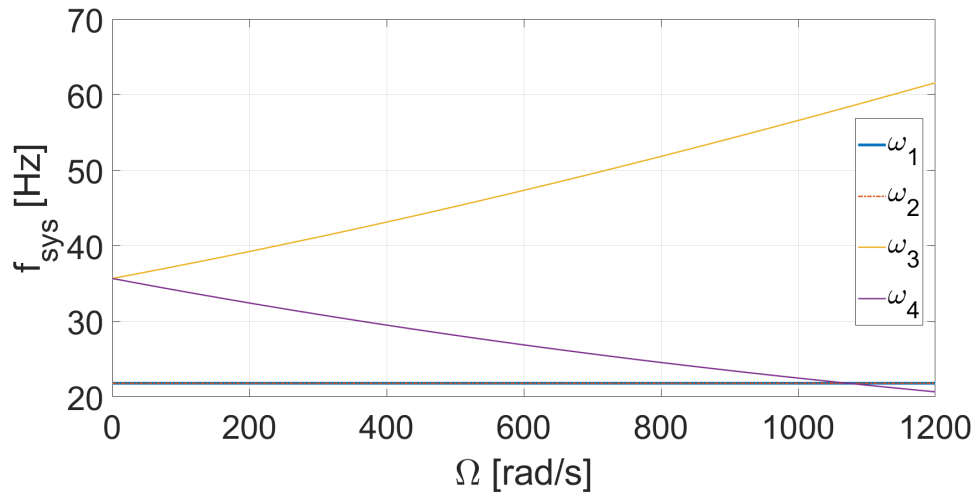


Figure 2.2: Example of Campbell diagram for 4 DOF rotor model

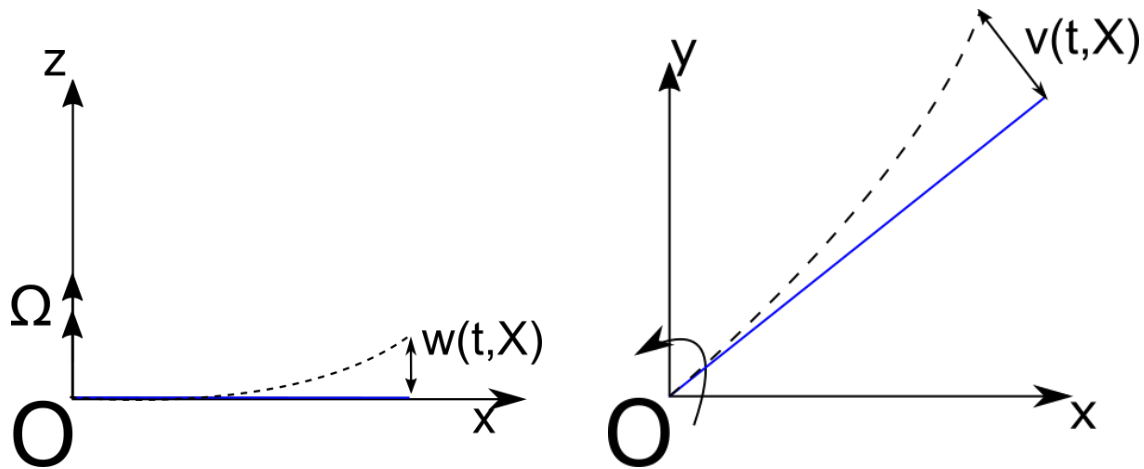


Figure 2.3: Transverse vibration of blade: a) flapwise; b) spanwise

The modeling of the blades, as described in the next chapter, is closely associated with the problem of the rotating beam. The blades are radially attached to the disc and undergo transverse vibration. Depending on the application, different directions are prioritized in the blade description. A variety of terms have been coined to refer to these ([108],[40],[75]): the transverse vibration inside the plane of rotation is called spanwise, lead-lag or in-plane, the transverse vibration is called flapwise or out-of-plane. The Euler-Bernoulli and Timoshenko beam models are often employed ([40],[108],[68]). Two boundary conditions are predominant based on application: cantilever, often selected in wind and tidal applications, and pinned, more often found in helicopter ones.

Centrifugal stiffening (also called geometric stiffening) and spin softening are the main effects that make the rotating beam problem qualitatively different from the non-rotating one. These effects manifest in the stiffness property of the system, as the centrifugal force acts similarly to the pre-stress effect in beams ([43]).

2 Kinematic description

Based on the previous section, we make the following modeling choices to start the kinematic description of the system:

- The rotor model selected has 5 DOFs: three translations of the center of mass of the disc, two rotations describing its orientation, and the spin is prescribed and considered constant.
- A rigid shaft on flexible supports is assumed.
- As the focus is the vibration of the rotor-blade assembly, the modeling of support is ignored, although its integration process is outlined.
- The blade is described as an Euler-Bernoulli (slender) beam undergoing bending-bending deformation in both flapwise and spanwise directions.

While we adopt these hypotheses for the following development, some of the analysis will go into relaxing them if necessary and the type of change these would entail.

We describe the initial, undeformed configuration κ_0 with respect to an inertial reference frame O_{xyz} that remains fixed, that remains fixed; its origin coincides with the center of mass of the disc in this configuration $\tilde{\mathbf{G}} =$

$[G_x, G_y, G_z]^T$, the disc is contained in the $x - y$ plane, while z coincides with the axis of symmetry of the disc-shaft assembly. The disc is characterized by its mass M_r , radius R_r , and, given its axial symmetry, by the following moments of inertia [60]:

$$\begin{aligned} J_p = I_Z &= \int_A (Y^2 + X^2) dm \\ I_X = I_Y &= \int_A (X^2 + Z^2) dm \\ J_d = I_X = I_Y \end{aligned} \quad (2.5)$$

where we have adopted the rotor-dynamics convention: J_p is called the polar moment of inertia of the disc, and J_d is the diametral moment of inertia of the disc. Additionally, the shaft's mass and inertia are considered negligible with respect to the disc. The position of the supports of the shaft with respect to the referential in this configuration can be done using the following vectors: $\mathbf{P}_1 = [0, 0, L_1]$ and $\mathbf{P}_2 = [0, 0, L_2]$. Notice that if both L_1 and L_2 are negative, the model resembles the Stodola-Green cantilever rotor; if they have different signs, we have a model that resembles the standard 4-DOF rotor (that is, pinned-pinned boundary condition). In any event, the characteristics of the support can always be reduced to equivalent terms; the difference between these choices is the relationships among the corresponding stiffness and damping coefficients. Given this fact, we ignore any particular sign on L as the particular case can be applied once the model has been established.

The final aspect in the description of the system in configuration κ_0 concerns the description of the blades. We will assume the existence of the vector functions $\mathbf{W}_{i_b}(\xi, t) = [\xi, W_{i_b}^s(\xi, t), W_{i_b}^f(\xi, t)]^T$, that describe the position of an arbitrary point over the $i_b - th$ blade with respect to its axis, here ξ is dummy variable specifying the coordinate along the length of the beam, the superscript distinguished the spanwise and flapping component of the deflection of the beam. It is the case that $0 \leq \xi \leq L_b$, where L_b is the length of the blade. We assume all blades are identical, so $L_{b_i} = L_b$ for all i . We will show the existence of such functions and their construction in section 4. With this, the position of an arbitrary point over the $i_b - th$ blade with respect to O_{xyz} is $\mathbf{P}_{i_b}(\xi, t) = \mathbf{W}_{i_b}(\xi, t) + [R_r, 0, 0]^T$. In configuration κ_0 , $\mathbf{P}_{i_b}(\xi, 0) = [R_r + \xi, 0, 0]^T$. The other blades can be specified by their angle with respect to the first one, and for convenience, we will write α_i , where $\alpha_1 = 0$. For the two-blade case $\alpha_2 = \pi$ is the most useful case as it describes a symmetric configuration. A visual representation of this configuration is presented in Fig. 2.4.

We now introduce an arbitrary perturbed configuration κ . The kinematic description of the system requires the passage $\kappa_0 \rightarrow \kappa$; to this end, a series of intermediate reference systems will be defined. First, a non-inertial reference frame G_{xyz} follows the center of mass and keeps the same orientation as O_{xyz} , the passage between the two is a translation that coincides with the displacement of the point \mathbf{G} . Second, three rotations are required to pass from the referential G_{XYZ} which preserves the orientation of the disc, and G_{xyz} . These rotations are describes using a 3 – 2 – 1 sequence of Euler angles ([96],[42]):

$$\begin{aligned} \mathbf{R}_1 &= \begin{pmatrix} 1 & 0 & 0 \\ 0 & \cos(\theta_1) & \sin(\theta_1) \\ 0 & -\sin(\theta_1) & \cos(\theta_1) \end{pmatrix} \\ \mathbf{R}_2 &= \begin{pmatrix} \cos(\theta_2) & 0 & -\sin(\theta_2) \\ 0 & 1 & 0 \\ \sin(\theta_2) & 0 & \cos(\theta_2) \end{pmatrix} \\ \mathbf{R}_3 &= \begin{pmatrix} \cos(\theta_3) & \sin(\theta_3) & 0 \\ -\sin(\theta_3) & \cos(\theta_3) & 0 \\ 0 & 0 & 1 \end{pmatrix} \end{aligned} \quad (2.6)$$

where θ_1 , θ_2 and θ_3 are the respective Euler angles: θ_1 corresponds to a rotation around the instantaneous x axis, θ_2 a rotation around the instantaneous y axis (clearly not the same axis as y in the κ_0 configuration since

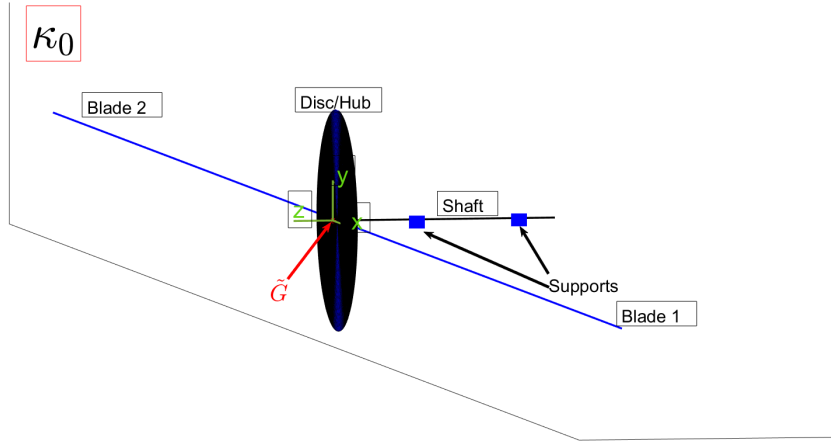


Figure 2.4: Diagram of the rotor-blade model with two blades

the first rotation has been applied) and θ_3 is a large rotation called the spin or intrinsic rotation of the rotor, in this application $\theta_3 = \Omega t$; $\dot{\theta}_3 = \Omega = \text{constant}$. Thus, the passage from an arbitrary vector \mathbf{r}_G in the referential G_{XYZ} to the inertial referential O_{xyz} is:

$$\begin{aligned} \mathbf{r}_O &= \tilde{\mathbf{G}} + \tilde{\mathbf{R}}(t) \mathbf{r}_G \\ &= \tilde{\mathbf{G}} + (\mathbf{R}_1^T \mathbf{R}_2^T \mathbf{R}_3^T) \mathbf{r}_G \end{aligned} \quad (2.7)$$

where $\tilde{\mathbf{R}}(t) = \mathbf{R}_1^T \mathbf{R}_2^T \mathbf{R}_3^T$ is:

$$\tilde{\mathbf{R}}(t) = \begin{pmatrix} \cos(\theta_2) \cos(\theta_3) & -\cos(\theta_2) \sin(\theta_3) & \sin(\theta_2) \\ \sin(\theta_1) \sin(\theta_2) \cos(\theta_3) + \cos(\theta_1) \sin(\theta_3) & \cos(\theta_3) \cos(\theta_1) - \sin(\theta_1) \sin(\theta_2) \sin(\theta_3) & -\sin(\theta_1) \cos(\theta_2) \\ -\cos(\theta_1) \sin(\theta_2) \cos(\theta_3) + \sin(\theta_1) \sin(\theta_3) & \cos(\theta_1) \sin(\theta_2) \sin(\theta_3) + \sin(\theta_1) \cos(\theta_3) & \cos(\theta_1) \cos(\theta_2) \end{pmatrix}. \quad (2.8)$$

The energies can be obtained from this kinematic description, as will be shown in the next section. An interesting result can be established at this point. Each one of the matrices in Eq. 2.6 is a proper orthogonal matrix: $\mathbf{R}_i^T \mathbf{R}_i = \mathbf{I}$, $\det(\mathbf{R}_i) = 1$. It follows that $\tilde{\mathbf{R}}(t)$ is a proper orthogonal matrix. This implies that the following eigenvalue problem is guaranteed to have one solution such that $\Lambda = 1$:

$$\tilde{\mathbf{R}} \mathbf{r} = \Lambda \mathbf{r} \quad (2.9)$$

or: $\tilde{\mathbf{R}} \mathbf{r} = \mathbf{r}$. The corresponding eigenvector \mathbf{r} is the instantaneous axis of rotation. An analytic expression for \mathbf{r} is ([96]):

$$\begin{pmatrix} r_1 \\ r_2 \\ r_3 \end{pmatrix} = -\frac{1}{2 \sin[\Psi]} \begin{pmatrix} -\cos(\theta_1) \sin(\theta_1) - \cos(\theta_3) \sin(\theta_1) + \cos(\theta_1) \sin(\theta_2) \sin(\theta_3) \\ \sin(\theta_1) \sin(\theta_3) - \cos(\theta_1) \cos(\theta_3) \sin(\theta_2) - \sin(\theta_2) \\ -\cos(\theta_2) \sin(\theta_3) - \cos(\theta_3) \sin(\theta_1) \sin(\theta_2) - \cos(\theta_1) \sin(\theta_3) \end{pmatrix} \quad (2.10)$$

where $\cos[\Psi] = \frac{1}{2} (\cos(\theta_2) \cos(\theta_3) + \cos(\theta_1) \cos(\theta_3) - \sin(\theta_1) \sin(\theta_2) \sin(\theta_3) + \cos(\theta_1) \cos(\theta_2) - 1)$.

3 Equation of motion: Energy and Lagrangian

In this section, we build on the parametrization of motion to obtain the energies of the system. With the energies available, the Lagrangian of the system is obtained, and thus, the equations of motion.. With the energies available, the Lagrangian of the system is obtained and thus the equations of motion. The generalized coordinates of the system are: $\mathbf{x} = [G_x, G_y, G_z, \theta_1, \theta_2, q_{i_b, j_m}^*]^T$, where the first five variables correspond to the position and orientation of the disc, and the variables q_{i_b, j_m}^* are generalized modal variables resulting from the discretization of the blades, subindex j_m denotes the corresponding mode, i_b denotes the corresponding blade and the overdot is a placeholder for s referencing spanwise motion or f referencing flapping motion.

At this stage, it is also important to discuss the nonlinear nature of the general rotation expressed by $\tilde{\mathbf{R}}(t)$. The presence of nonlinear terms, combined with the quadratic form of the energetic expressions applicable to this type of system, leads to strong nonlinearities in the equations of motion. If the standard small angle assumptions are made on the angles other than the spin: $\cos(\theta_i) \approx 1, \sin(\theta_i) \approx \theta_i; i \in [1, 2]$ we arrive at what we will call reduced rotation matrix:

$$\mathbf{R}_{\text{red}} = \begin{pmatrix} \cos(\theta_3) & -\sin(\theta_3) & \theta_2 \\ \theta_1 \theta_2 \cos(\theta_3) + \sin(\theta_3) \cos(\theta_3) - \theta_1 \theta_2 \sin(\theta_3) & \cos(\theta_3) - \theta_1 \theta_2 \sin(\theta_3) & -\theta_1 \\ \theta_1 \sin(\theta_3) - \theta_2 \cos(\theta_3) & \theta_1 \cos(\theta_3) + \theta_2 \sin(\theta_3) & 1 \end{pmatrix} \quad (2.11)$$

which still will produce nonlinearities. A stronger hypothesis must be made to fully linearize the result: $\theta_1 \theta_2 \approx 0$:

$$\mathbf{R}_{\text{lin}} = \begin{pmatrix} \cos(\theta_3) & -\sin(\theta_3) & \theta_2 \\ \sin(\theta_3) & \cos(\theta_3) & -\theta_1 \\ \theta_1 \sin(\theta_3) - \theta_2 \cos(\theta_3) & \theta_1 \cos(\theta_3) + \theta_2 \sin(\theta_3) & 1 \end{pmatrix} \quad (2.12)$$

the latter we call linearized rotation matrix. In practice, this hypothesis seems justified given the structural characteristics of the type of system we seek to model: operating conditions of tidal turbines and wind turbines demand a high degree of alignment, which is often enforced by control mechanisms. Nevertheless, exploring the nonlinear problem in this context seems like a promising research problem. The justification for this interest comes mainly from the opportunities in type B problems (design) and from the exploration of nonlinear time-periodic phenomena.

The linearized version will be used in the sequel unless otherwise specified. Using the complete matrix and the linearization of the energetic terms that result from it will help illustrate the challenge involved in the nonlinear case.

3.1 Kinetic energy

The energies of the system consist of the following contributions: kinetic energies $KE = KED + \sum_{i_b} KEB_{i_b}$ of disc and i_b blades; potential energies: $PE = PED + \sum_{i_b} PEB_{i_b}$ of the elastic supports of the disc and i_b blades; the kinetic energies will consist of a translation term and a rotation term. The rotational kinetic energy requires the angular velocity expressed in the referential G_{XYZ} . We introduce the following:

$$\tilde{\mathbf{G}} = \begin{pmatrix} G_x \\ G_y \\ G_z \end{pmatrix}; \dot{\tilde{\mathbf{G}}} = \begin{pmatrix} \dot{G}_x \\ \dot{G}_y \\ \dot{G}_z \end{pmatrix}, \quad (2.13)$$

now the angular velocity vector takes the following representation ([42]):

$$\begin{aligned}
\boldsymbol{\Omega}_G &= \mathbf{R}_3 \left(\mathbf{R}_2 \begin{pmatrix} \dot{\theta}_1 \\ 0 \\ 0 \end{pmatrix} + \begin{pmatrix} 0 \\ \dot{\theta}_2 \\ 0 \end{pmatrix} \right) + \begin{pmatrix} 0 \\ 0 \\ \dot{\theta}_3 \end{pmatrix} \\
&= \begin{pmatrix} \dot{\theta}_1 \cos(\theta_2) \cos(\theta_3) + \dot{\theta}_2 \sin(\theta_3) \\ -\dot{\theta}_1 \cos(\theta_2) \sin(\theta_3) + \dot{\theta}_2 \cos(\theta_3) \\ \dot{\theta}_1 \sin(\theta_2) + \dot{\theta}_3 \end{pmatrix}, \tag{2.14}
\end{aligned}$$

the interpretation of this representation is the following: in the passage from G_{xyz} to G_{XYZ} after the first rotation we transform the angular velocity vector around the local axis by \mathbf{R}_2 and add it to the angular velocity vector around the local axis in this second referential; the sum of the two are then transformed by \mathbf{R}_3 into the referential G_{XYZ} , where it is added to the spin. The kinetic energy of the disc is then:

$$KED = \frac{1}{2} \dot{\mathbf{G}}^T \begin{pmatrix} M & 0 & 0 \\ 0 & M & 0 \\ 0 & 0 & M \end{pmatrix} \dot{\mathbf{G}} + \frac{1}{2} \boldsymbol{\Omega}_G^T \begin{pmatrix} J_d & 0 & 0 \\ 0 & J_d & 0 \\ 0 & 0 & J_p \end{pmatrix} \boldsymbol{\Omega}_G \tag{2.15}$$

where the first term is the translation energy and the second term is the energy of the angular motion. This results in the following:

$$KED = \frac{J_p \dot{\theta}_3^2}{2} + \frac{1}{2} M \dot{G}_x^2 + \frac{1}{2} M \dot{G}_y^2 + \frac{1}{2} M \dot{G}_z^2 + \frac{1}{2} J_d (\dot{\theta}_1^2 + \dot{\theta}_2^2) + J_p \dot{\theta}_1 \dot{\theta}_2 \dot{\theta}_3 \tag{2.16}$$

we recognize in this expression the source of the characteristic gyroscopic term $\dot{\theta}_1 \dot{\theta}_2 \dot{\theta}_3$, and since $\dot{\theta}_3$ is constant, we also note that the term $\frac{J_p \dot{\theta}_3^2}{2}$ is a constant and so it entails no variation of energy.

3.2 Potential energy

First, we compute the elastic energy in the flexible supports of the shaft. We assume springs at points $\mathbf{P}_1 = [0, 0, -L_1]$ and $\mathbf{P}_2 = [0, 0, -L_2]$ in κ_0^1 , we also write the following elastic matrices for each support, which assumes linear elastic behavior of the springs:

$$\begin{aligned}
\mathbf{K}_1 &= \begin{pmatrix} K_{X_1} & 0 & 0 \\ 0 & K_{Y_1} & 0 \\ 0 & 0 & K_{Z_1} \end{pmatrix} \\
\mathbf{K}_2 &= \begin{pmatrix} K_{X_2} & 0 & 0 \\ 0 & K_{Y_2} & 0 \\ 0 & 0 & K_{Z_2} \end{pmatrix}. \tag{2.17}
\end{aligned}$$

In the configuration κ the coordinates of these points in the inertial referential are:

¹As mentioned earlier, the signs are related to the support condition of the rotor. They can be taken into account at the stage in which the equivalent elastic matrix is constructed.

$$\begin{aligned}
(\mathbf{P}_1)_{\kappa_0} &= \tilde{\mathbf{G}} + \mathbf{R}_{\text{in}}(\mathbf{P}_1)_{\kappa} \\
&= \tilde{\mathbf{G}} + \begin{pmatrix} \cos(\theta_3) & -\sin(\theta_3) & \theta_2 \\ \sin(\theta_3) & \cos(\theta_3) & -\theta_1 \\ \theta_1 \sin(\theta_3) - \theta_2 \cos(\theta_3) & \theta_1 \cos(\theta_3) + \theta_2 \sin(\theta_3) & 1 \end{pmatrix} \begin{pmatrix} 0 \\ 0 \\ -L_1 \end{pmatrix} \\
&= \tilde{\mathbf{G}} + \begin{pmatrix} -L_1 \theta_2 \\ L_1 \theta_1 \\ L_1 \end{pmatrix} \\
&= \begin{pmatrix} G_x - L_1 \theta_2 \\ G_y + L_1 \theta_1 \\ G_z - L_1 \end{pmatrix} \tag{2.18}
\end{aligned}$$

and after a similar development for the second support the corresponding expression is obtained:

$$\mathbf{P}_2 = \begin{pmatrix} G_x - L_2 \theta_2 \\ G_y + L_2 \theta_1 \\ G_z - L_2 \end{pmatrix}, \tag{2.19}$$

then the displacement on each support at an arbitrary configuration of motion can be expressed in terms of the parameters of motion and the constants characterizing the architecture of the system:

$$\begin{aligned}
\delta \mathbf{P}_1 &= \begin{pmatrix} G_x - L_1 \theta_2 \\ G_y + L_1 \theta_1 \\ G_z - L_1 \end{pmatrix} - \begin{pmatrix} 0 \\ 0 \\ -L_1 \end{pmatrix} = \begin{pmatrix} G_x - L_1 \theta_2 \\ G_y + L_1 \theta_1 \\ G_z \end{pmatrix} \\
\delta \mathbf{P}_2 &= \begin{pmatrix} G_x - L_2 \theta_2 \\ G_y + L_2 \theta_1 \\ G_z - L_2 \end{pmatrix} - \begin{pmatrix} 0 \\ 0 \\ -L_2 \end{pmatrix} = \begin{pmatrix} G_x - L_2 \theta_2 \\ G_y + L_2 \theta_1 \\ G_z \end{pmatrix}. \tag{2.20}
\end{aligned}$$

The potential energy can then be written as follows:

$$PED = \frac{1}{2} \delta \mathbf{P}_1^T \begin{pmatrix} K_{X_1} & 0 & 0 \\ 0 & K_{Y_1} & 0 \\ 0 & 0 & K_{Z_1} \end{pmatrix} \delta \mathbf{P}_1 + \frac{1}{2} \delta \mathbf{P}_2^T \begin{pmatrix} K_{X_2} & 0 & 0 \\ 0 & K_{Y_2} & 0 \\ 0 & 0 & K_{Z_2} \end{pmatrix} \delta \mathbf{P}_2, \tag{2.21}$$

which, upon expansion results in:

$$\begin{aligned}
PED &= \frac{1}{2} \left(K_{X_1} (G_x - L_1 \theta_2)^2 + K_{Y_1} (G_y + L_1 \theta_1)^2 + K_{Z_1} G_z^2 \right) \\
&\quad + \frac{1}{2} \left(K_{X_2} (G_x - L_2 \theta_2)^2 + K_{Y_2} (G_y + L_2 \theta_1)^2 + K_{Z_2} G_z^2 \right). \tag{2.22}
\end{aligned}$$

It can be seen from equation Eq. 2.22 that this potential will lead to elastic coefficients on these 5 degrees of freedom, some of which will be a combination of the spring constant at each support and the relationship between the positions of each support. Consequently, the support condition of the shaft results in particular relationships among these coefficients and the equivalent elastic matrix. This type of analysis is well-known in the field of rotordynamics ([39],[42],[60]), and we will apply to the equations of motion in the upcoming section.

3.3 Energy of blades

It is convenient to introduce the first aspects of the modal discretization scheme that will be completed in section 4 to the calculation of the energy. As previously introduced, we will assume the existence of such functions that, in G_{XYZ} an arbitrary point over the blade can be described by the function $\mathbf{P}_{i_b}(X_b, t) = W_{i_b}^\bullet(X_b, t) + [R_r, 0, 0]^T$, $R_r < X_b < R_r + L_b$, these functions have the form $W_{i_b}^\bullet(X_b, t) = \sum_{j_m} \varphi_{j_b}^\bullet(X_b) q_{i_b, j_m}^\bullet$ where $\varphi_{j_m}^\bullet$ is a mode shape function dependent on X_b ; q_{i_b, j_m}^\bullet is a generalized modal coordinate. Since a beam is a continuum and thus has infinite degrees of freedom and modes, in principle, the previous expression is an approximation in the sense that modal truncation has been applied ([43],[111]):

$$\begin{aligned} W_{i_b}^\bullet(X_b, t) &= \sum_{j_m=1}^{\infty} \varphi_{j_m}^\bullet(X_b) q_{i_b, j_m}^\bullet \\ \sum_{j_m=1}^{\infty} \varphi_{j_m}^\bullet(X_b) q_{i_b, j_m}^\bullet &\approx \sum_{j_m=1}^{N_{modes}} \varphi_{j_m}^\bullet(X_b) q_{i_b, j_m}^\bullet, N \rightarrow \infty \end{aligned} \quad (2.23)$$

in practice, the higher order terms tend to decay quickly. A few modes give an accurate description of the vibration of the system. We relegate the rest of the arguments justifying this choice to the section concerning the computation of the mode shapes.

The velocity field of the blade from the inertial reference frame is:

$$\begin{aligned} (\mathbf{P}_i)_{\kappa_0} &= \tilde{\mathbf{G}} + \tilde{\mathbf{R}}(t) (\mathbf{P}_i)_{\kappa} \\ (\mathbf{V}_i^2)_{\kappa_0} &= (\dot{\mathbf{P}}_i)_{\kappa_0} \cdot (\dot{\mathbf{P}}_i)_{\kappa_0} \end{aligned} \quad (2.24)$$

and considering a blade modeled as an Euler-Bernoulli (or slender) beam, with cross-section area $A(X_b) = A$, Young's modulus $E(X_b) = E$, moment of inertia $I(X_b) = I$, density $\rho(X_b) = \rho$, we can write the kinetic energy density of the $i_b - th$ blade as:

$$KEB_{i_b} = \frac{1}{2} \rho A \int_0^{L_b} \dot{\mathbf{P}}_{i_b, O} \cdot \dot{\mathbf{P}}_{i_b, O} dx, \quad (2.25)$$

it turns out that this kinetic energy density contains a large number of nonlinear terms. The symbolic computation of this expression has been carried out using Wolfram Mathematica 12.1, and 6,271 terms result from the corresponding inner product. The reduced version of $\tilde{\mathbf{R}}(t)$ has been used to overcome the difficulties imposed by the nonlinearities, and the resulting expression has been linearized by hand. By way of verification, the result has been compared to the one obtained using the linearized version of $\tilde{\mathbf{R}}(t)$, and the results coincide. After linearization, the kinetic energy densities of the $i_b - th$ blade take the form:

$$KEB_{i_b} = KEBF_{i_b} + KEBS_{i_b} + KEBC_{i_b} \quad (2.26)$$

with the following expressions for each term:

$$\begin{aligned}
KEBF_{ib} = & \frac{1}{2} \int_0^{L_b} \rho A \left(\dot{W}_{ib}^f \right)^2 dx - \Omega \rho A R_r \cos(t\Omega) \dot{\theta}_1 \int_0^{L_b} \left(W_{ib}^f \right) dx \\
& - \Omega \rho A R_r \sin(t\Omega) \dot{\theta}_2 \int_0^{L_b} \left(W_{ib}^f \right) dx + \rho A R_r \sin(t\Omega) \dot{\theta}_1 \int_0^{L_b} \left(\dot{W}_{ib}^f \right) dx \\
& + \rho A \dot{G}_z \int_0^{L_b} \left(\dot{W}_{ib}^f \right) dx - \rho A \cos(t\Omega) \dot{\theta}_2 \int_0^{L_b} x \left(\dot{W}_{ib}^f \right) dx \\
& + \rho A \sin(t\Omega) \dot{\theta}_1 \int_0^{L_b} x \dot{W}_{ib}^f dx - \Omega \rho A \cos(t\Omega) \dot{\theta}_1 \int_0^{L_b} x W_{ib}^f dx \\
& - \rho A R_r \cos(t\Omega) \dot{\theta}_2 \int_0^{L_b} \dot{W}_{ib}^f dx \\
& - \rho A \Omega \sin(t\Omega) \dot{\theta}_2 \int_0^{L_b} x W_{ib}^f dx
\end{aligned} \tag{2.27}$$

$$\begin{aligned}
KEBS_{ib} = & \frac{1}{2} \rho A \int_0^{L_b} \left(\dot{W}_{ib}^s \right)^2 dx + \frac{1}{2} \Omega^2 \rho A \int_0^{L_b} \left(W_{ib}^s \right)^2 dx \\
& - \rho A \sin(t\Omega) \dot{G}_x \int_0^{L_b} \left(\dot{W}_{ib}^s \right) dx + \rho A \cos(t\Omega) \dot{G}_y \int_0^{L_b} \left(\dot{W}_{ib}^s \right) dx \\
& - \rho A \Omega \cos(t\Omega) \dot{G}_x \int_0^{L_b} \left(W_{ib}^s \right) dx - \rho A \Omega \sin(t\Omega) \dot{G}_y \int_0^{L_b} \left(W_{ib}^s \right) dx
\end{aligned} \tag{2.28}$$

$$\begin{aligned}
KEBC_{ib} = & \frac{1}{12} A \rho L_b \left(2\Omega^2 \theta_2^2 \left(3R_r L_b + L_b^2 + 3R_r^2 \right) \sin^2(t\Omega) + 2\Omega^2 \dot{\theta}_1^2 \left(3R_r L_b + L_b^2 + 3R_r r^2 \right) \cos^2(t\Omega) + 6\dot{G}_x^2 + 6\dot{G}_y^2 + 6\dot{G}_z^2 \right) \\
& + \frac{1}{12} A \rho L_b \left(-3R_r L_b \dot{\theta}_1^2 \cos(2t\Omega) + 3R_r L_b \dot{\theta}_1^2 + 12L_b \dot{\theta}_1 \sin(t\Omega) \dot{G}_z - 3R_r^2 \dot{\theta}_1^2 \cos(2t\Omega) + 3R_r^2 \dot{\theta}_1^2 + 12R_r \dot{\theta}_1 \sin(t\Omega) \dot{G}_z \right) \\
& + \frac{1}{12} A \rho L_b \left(-L_b^2 \dot{\theta}_1^2 \cos(2t\Omega) + L_b^2 \dot{\theta}_1^2 - 12L_b \dot{\theta}_2 \cos(t\Omega) \dot{G}_z - 6r^2 \dot{\theta}_1 \dot{\theta}_2 \sin(2t\Omega) - 12r \dot{\theta}_2 \cos(t\Omega) \dot{G}_z \right) \\
& + \frac{1}{12} A \rho L_b \left(-12R_r L_b \dot{\theta}_1 \dot{\theta}_2 \sin(2t\Omega) + 3R_r L_b \dot{\theta}_2^2 \cos(2t\Omega) + 3R_r L_b \dot{\theta}_2^2 - 4L_b^2 \dot{\theta}_1 \dot{\theta}_2 \sin(2t\Omega) + 3R_r^2 \dot{\theta}_2^2 \cos(2t\Omega) + 3R_r^2 \dot{\theta}_2^2 \right) \\
& + \frac{1}{12} A \rho L_b \left(2\Omega \theta_2 \sin(t\Omega) \left(2 \left(3R_r L_b + L_b^2 + 3R_r^2 \right) \left(\dot{\theta}_1 \sin(t\Omega) - \dot{\theta}_2 \cos(t\Omega) \right) + 3 \left(L_b + 2R_r \right) \dot{G}_z \right) \right. \\
& \left. + L_b^2 \dot{\theta}_2^2 \cos(2t\Omega) + L_b^2 \dot{\theta}_2^2 \right) \\
& + \frac{1}{12} A \rho L_b 2\Omega \theta_1 \cos(t\Omega) \left(2 \left(3R_r L_b + L_b^2 + 3R_r^2 \right) \left(\dot{\theta}_1 \sin(t\Omega) - \dot{\theta}_2 \cos(t\Omega) \right) \right. \\
& \left. + 2\Omega \theta_2 \left(\left(3R_r + 1 \right) L_b + 3R_r^2 \right) \sin(t\Omega) + 3 \left(L_b + 2R_r \right) \dot{G}_z \right)
\end{aligned} \tag{2.29}$$

where the explicit dependence of $W_{i_b}^*(X_b, t)$ has been dropped for convenience and given that clarity is ensured. Here we note:

- The terms $KEBF_{i_b}$ describe kinetic energy associated with the vibration in the flapwise sense.
- The terms $KEBS_{i_b}$ describe kinetic energy associated with the vibration in the spanwise sense.
- The term $KEBC_{i_b}$ contains coupling terms between the degrees of freedom of the disc and those of the blade.

The first term in $KEBF_{i_b}$ and $KEBS_{i_b}$ remain identical to those of planar rotation (as presented in [22] or [17]); however, coupling terms manifest in both the spanwise and flapwise sense, the drastic change in the flapwise case is remarkable since many references consulted neglect the rotor translation in the z direction, so the effect recovered in this development can not be obtained with such hypothesis.

The elastic deformation potential can be deduced by considering a traditional continuum, applying the corresponding kinematic hypotheses, introducing a selected constitutive material law, and finally, including the inertial centrifugal effect. The general displacement for a continuum is:

$$\begin{aligned} U_x &= U_x(X, Y, Z, t) \\ U_y &= U_y(X, Y, Z, t) \\ U_z &= U_z(X, Y, Z, t) \end{aligned} \quad (2.30)$$

the Green strain tensor:

$$\mathbf{E} = \begin{pmatrix} E_{xx} & E_{xy} & E_{yz} \\ E_{xy} & E_{yy} & E_{zy} \\ E_{yz} & E_{zy} & E_{zz} \end{pmatrix} \quad (2.31)$$

with the following components:

$$\begin{aligned} E_{xx} &= \frac{\partial U_x}{\partial X} + \frac{1}{2} \left(\left(\frac{\partial U_x}{\partial X} \right)^2 + \left(\frac{\partial U_y}{\partial X} \right)^2 + \left(\frac{\partial U_z}{\partial X} \right)^2 \right) \\ E_{yy} &= \frac{\partial U_y}{\partial Y} + \frac{1}{2} \left(\left(\frac{\partial U_x}{\partial Y} \right)^2 + \left(\frac{\partial U_y}{\partial Y} \right)^2 + \left(\frac{\partial U_z}{\partial Y} \right)^2 \right) \\ E_{zz} &= \frac{\partial U_z}{\partial Z} + \frac{1}{2} \left(\left(\frac{\partial U_x}{\partial Z} \right)^2 + \left(\frac{\partial U_y}{\partial Z} \right)^2 + \left(\frac{\partial U_z}{\partial Z} \right)^2 \right) \\ E_{xy} &= \frac{1}{2} \left(\frac{\partial U_x}{\partial Y} + \frac{\partial U_y}{\partial X} \right) + \frac{1}{2} \left(\frac{\partial U_x}{\partial X} \frac{\partial U_x}{\partial Y} + \frac{\partial U_y}{\partial X} \frac{\partial U_y}{\partial Y} + \frac{\partial U_z}{\partial X} \frac{\partial U_z}{\partial Y} \right) \\ E_{xz} &= \frac{1}{2} \left(\frac{\partial U_x}{\partial Z} + \frac{\partial U_z}{\partial X} \right) + \frac{1}{2} \left(\frac{\partial U_x}{\partial X} \frac{\partial U_x}{\partial Z} + \frac{\partial U_y}{\partial X} \frac{\partial U_y}{\partial Z} + \frac{\partial U_z}{\partial X} \frac{\partial U_z}{\partial Z} \right) \\ E_{yz} &= \frac{1}{2} \left(\frac{\partial U_y}{\partial Z} + \frac{\partial U_z}{\partial Y} \right) + \frac{1}{2} \left(\frac{\partial U_x}{\partial Y} \frac{\partial U_x}{\partial Z} + \frac{\partial U_y}{\partial Y} \frac{\partial U_y}{\partial Z} + \frac{\partial U_z}{\partial Y} \frac{\partial U_z}{\partial Z} \right). \end{aligned} \quad (2.32)$$

From these expressions and with a constitutive law, the stresses are obtained as $\sigma_{ij} = C_{ijkl} \epsilon_{kl}$, where C_{ijkl} is a tensor describing the material behavior. The stress allows for the definition of strain energy densities:

$$W(\epsilon_{ij}) = \int_0^{\epsilon_{ij}} \sigma_{ij} d\epsilon_{ij}. \quad (2.33)$$

The Euler-Bernoulli beam is a uni-dimensional model, which can be expressed as:

$$\begin{aligned} U_x &= U_x(X, Y, Z, t) \\ U_y &= U_y(X, t) \\ U_z &= U_z(X, t), \end{aligned} \quad (2.34)$$

furthermore, it entails the following relationship:

$$U_x(X, Y, Z) = -Y \frac{\partial U_y}{\partial X} - Z \frac{\partial U_z}{\partial X}. \quad (2.35)$$

From these assumptions we can simplify the displacement field:

$$\begin{aligned} \frac{\partial U_x}{\partial X} &= -Y \frac{\partial^2 U_y}{\partial X^2} - Z \frac{\partial^2 U_z}{\partial X^2} \\ \frac{\partial U_x}{\partial Y} &= -\frac{\partial U_y}{\partial X} \\ \frac{\partial U_x}{\partial Z} &= -\frac{\partial U_z}{\partial X}, \end{aligned} \quad (2.36)$$

and the non-vanishing strain terms are :

$$\begin{aligned} E_{xx} &= \left(-Y \frac{\partial^2 U_y}{\partial X^2} - Z \frac{\partial^2 U_z}{\partial X^2} \right) + \frac{1}{2} \left(\left(Y \frac{\partial^2 U_y}{\partial X^2} \right)^2 + \left(Z \frac{\partial^2 U_z}{\partial X^2} \right)^2 + 2YZ \frac{\partial^2 U_y}{\partial X^2} \frac{\partial^2 U_z}{\partial X^2} + \left(\frac{\partial U_y}{\partial X} \right)^2 + \left(\frac{\partial U_z}{\partial X} \right)^2 \right) \\ E_{yy} &= \frac{1}{2} \left(\frac{\partial U_y}{\partial X} \right)^2 \\ E_{zz} &= \frac{1}{2} \left(\frac{\partial U_z}{\partial X} \right)^2 \\ E_{xy} &= \frac{1}{2} \left(Y \frac{\partial^2 U_y}{\partial X^2} \frac{\partial U_y}{\partial X} + Z \frac{\partial^2 U_z}{\partial X^2} \frac{\partial U_y}{\partial X} \right) \\ E_{xz} &= \frac{1}{2} \left(Y \frac{\partial^2 U_y}{\partial X^2} \frac{\partial U_z}{\partial X} + Z \frac{\partial^2 U_z}{\partial X^2} \frac{\partial U_z}{\partial X} \right) \\ E_{yz} &= \frac{1}{2} \left(-\frac{\partial U_y}{\partial X} \frac{\partial U_x}{\partial Z} \right). \end{aligned} \quad (2.37)$$

At this point, the choice of the constitutive law is required. For the sake of simplicity, an isotropic material will be assumed in what follows. However, the same procedure presented here can be carried out with an alternative constitutive law. The importance of this is the fact that in many fields of interest to our investigation, composite blades with particular material behavior have gained popularity. The constitutive law for an isotropic material is expressed in terms of the so-called Lamé parameters as follows:

$$\begin{bmatrix} \sigma_{xx} \\ \sigma_{yy} \\ \sigma_{zz} \\ \sigma_{yz} \\ \sigma_{xz} \\ \sigma_{xy} \end{bmatrix} = \begin{bmatrix} \lambda + 2\mu & \lambda & \lambda & 0 & 0 & 0 \\ \lambda & \lambda + 2\mu & \lambda & 0 & 0 & 0 \\ \lambda & \lambda & \lambda + 2\mu & 0 & 0 & 0 \\ 0 & 0 & 0 & \mu & 0 & 0 \\ 0 & 0 & 0 & 0 & \mu & 0 \\ 0 & 0 & 0 & 0 & 0 & \mu \end{bmatrix} \begin{bmatrix} E_{xx} \\ E_{yy} \\ E_{zz} \\ 2E_{yz} \\ 2E_{xz} \\ 2E_{xy} \end{bmatrix}, \quad (2.38)$$

the linear part of strain energy V can be obtained considering the linear terms: $E_{xx} = -Y \frac{\partial^2 U_y}{\partial X^2} - Z \frac{\partial^2 U_z}{\partial X^2}$; $E_{yy} = 0$; $E_{zz} = 0$; $E_{xy} = 0$; $E_{xz} = 0$; $E_{yz} = 0$:

$$\begin{aligned} E_{xx}^2 &= \left(-Y \frac{\partial^2 U_y}{\partial X^2} - Z \frac{\partial^2 U_z}{\partial X^2} \right)^2 \\ &= Y^2 \left(\frac{\partial^2 U_y}{\partial X^2} \right)^2 + Z^2 \left(\frac{\partial^2 U_z}{\partial X^2} \right)^2 + 2YZ \frac{\partial^2 U_y}{\partial X^2} \frac{\partial^2 U_z}{\partial X^2} \end{aligned} \quad (2.39)$$

$$\begin{aligned} EP &= \left(\frac{1}{2} \right) (\lambda + 2\mu) \int_A \int_{L_b} Y^2 \left(\frac{\partial^2 U_y}{\partial X^2} \right)^2 + Z^2 \left(\frac{\partial^2 U_z}{\partial X^2} \right)^2 + 2YZ \frac{\partial^2 U_y}{\partial X^2} \frac{\partial^2 U_z}{\partial X^2} dx dA \\ &= \left(\frac{1}{2} \right) (\lambda + 2\mu) I_{ZZ} \int_{L_b} \left(\frac{\partial^2 U_y}{\partial X^2} \right)^2 dx \\ &+ \left(\frac{1}{2} \right) (\lambda + 2\mu) I_{YY} \int_{L_b} \left(\frac{\partial^2 U_z}{\partial X^2} \right)^2 dx \\ &+ (\lambda + 2\mu) I_{YZ} \int_{L_b} \left(\frac{\partial^2 U_y}{\partial X^2} \frac{\partial^2 U_z}{\partial X^2} \right) dx \end{aligned} \quad (2.40)$$

with $I_{ZZ} = \int_A Y^2 dA$; $I_{YY} = \int_A Z^2 dA$; $I_{YZ} = \int_A YZ dA$. Substituting the general displacement notation by the selected deflection notation resulting from the modal expansion in Eq. 2.40 we arrive at the following expression:

$$\begin{aligned} PEB_{i_b} &= (\lambda + 2\mu) \frac{I_{ZZ}}{2} \int_{L_b} \left(\frac{\partial^2 W_{i_b}^s}{\partial X^2} \right)^2 dX + (\lambda + 2\mu) \frac{I_{YY}}{2} \int_{L_b} \left(\frac{\partial^2 W_{i_b}^f}{\partial X^2} \right)^2 dX \\ &+ (\lambda + 2\mu) I_{YZ} \int_{L_b} \left(\frac{\partial^2 W_{i_b}^s}{\partial X^2} \frac{\partial^2 W_{i_b}^f}{\partial X^2} \right) dX + \frac{1}{2} \int_L N_0(X, \Omega) \left(\frac{\partial W_{i_b}^s}{\partial X} \right)^2 dX \end{aligned} \quad (2.41)$$

with the centrifugal force function along the blade ([43],[22]): $N_0 = \Omega^2(A\rho) \left((L_b + R_r)^2 - (R_r + X)^2 \right)$. As an approximation, only the spin angular velocity is being considered as the source of centrifugal stiffening. We recognize the terms:

- from deformation strain energy in the principal inertia directions, the first two terms,
- a coupling term,
- the centrifugal stiffness term on the spanwise motion obtained by introducing the centrifugal (inertial, fictitious) force function N_0 .

It is often convenient to substitute the Lamé parameters:

$$\begin{aligned} \lambda &= \frac{E\nu}{(1+\nu)(1-2\nu)} \\ \mu &= \frac{E}{2(1+\nu)}, \end{aligned} \quad (2.42)$$

where E is the corresponding Young modulus and ν is the Poisson ratio.

3.4 Lagrangian and equation of motion

The total Lagrangian of the model can be written in terms of the energies resulting from the previous developments. The Lagrangian is $\mathcal{L} = KE - PE$, which can be broken down as follows $KE = KED + \sum_{i_b} KEB_{i_b}$ of disc and i_b blades; potential energies: $PE = PED + \sum_{i_b} PEB_{i_b}$

$$\begin{aligned} KE &= KED + \sum_{i_b=1}^{N_{blades}} KEB_{i_b} \\ KED &= KED_T + KED_R \\ KEB_{i_b} &= KEBF_{i_b} + KEBS_{i_b} + KEBC_{i_b} \end{aligned} \quad (2.43)$$

where KE is the total kinetic energy, KED is the kinetic energy of the disc with components KED_T associated to the translations and KED_R associated to the angular motion; KEB_{i_b} is the kinetic energy of blade i_b , with components related to the flapwise, spanwise and coupling respectively. Similarly, for the potential energy:

$$\begin{aligned} PE &= PED + \sum_{i_b=1}^{N_{blades}} PEB_{i_b} \\ PED &= PED_T + PED_R + PED_C \\ PEB_{i_b} &= PEBF_{i_b} + PEBS_{i_b} + PEBC_{i_b} + PEBN_{i_b} \end{aligned} \quad (2.44)$$

with PE the total potential energy, PED the disc potential, broken down into the constituents: PED_T for potential associated with translation motion, PED_R associated to the rotation and PED_C for coupling terms; PEB_{i_b} is the total potential of blade i_b with terms in flapwise $PEBF_{i_b}$, spanwise $PEBS_{i_b}$ deformation directions, a coupling term $PEBC_{i_b}$, and a term from the centrifugal effects $PEBN_{i_b}$. This breakdown of terms is useful from a practical perspective, as it allows for the writing of subterms of the Lagrangian, which can then be used to obtain the contribution of each effect to the equation of motion. The Lagrangian can be written then as:

$$\begin{aligned} \mathcal{L} &= KED_T + KED_R + \sum_{i_b=1}^{N_{blades}} (KEBF_{i_b} + KEBS_{i_b} + KEBC_{i_b}) \\ &\quad - ED_T - PED_R - PED_C \\ &\quad - \sum_{i_b=1}^{N_{blades}} (PEBF_{i_b} + PEBS_{i_b} + PEBC_{i_b} + PEBN_{i_b}). \end{aligned} \quad (2.45)$$

The Lagrangian Eq. 2.45 can be supplemented with a dissipation function to take into account this effect. A viscous damping model, for instance, can be treated similarly to the stiffness in the support; some examples are presented in [22] and [39]. A more complex development applies if a corrotational damping term is assumed at the base, which has been the approach of previous investigations in which the bearing interactions are investigated; a detailed discussion is presented in [42]. Similarly, the topic of dissipation mechanisms in the beams requires more in-depth considerations. We have taken a more empirical approach: mild viscous and modal damping terms will be added a posteriori to the equations of motion. Our development, however, is such that these terms can be adjusted, provided the appropriate system characterization of dissipation.

With the Lagrangian Eq. 2.45 available, the Euler-Lagrange equation of the system can be formulated on the generalized coordinates and generalized velocities: $\mathbf{x} = [G_x, G_y, G_z, \theta_1, \theta_2, q_{i_b, j_m}^\bullet]^T$ and $\dot{\mathbf{x}} = [\dot{G}_x, \dot{G}_y, \dot{G}_z, \dot{\theta}_1, \dot{\theta}_2, \dot{q}_{i_b, j_m}^\bullet]^T$:

$$\frac{d}{dt} \left(\frac{\partial}{\partial \dot{x}_i} [\mathcal{L}] \right) = \frac{\partial}{\partial x_i} [\mathcal{L}], i \in [1, \text{DOF}] \quad (2.46)$$

yielding $N = \text{DOF}$ equations describing the dynamics of the system. In practice, Eq. 2.46 can be easily programmed into a computerized algebraic system (CAS) to systematically compute the required operations and group the resulting system of equations into matrix form. This is particularly useful in our case, given the high dimensionality of the systems considered in this work and given the complexity of the expressions involved in these operations. Our developments have been carried out using Wolfram Mathematica 12.1.

The developments established so far have been relatively general, which allows us to obtain different versions of the general model established. In the subsequent chapters, different versions of the model will be applied to examine the desired effects or theories; for instance, the most simple model of interest can be obtained by considering exclusively one translation DOF of the base and one modal response on one blade, resulting in a 2 DOFs system that displays LTP characteristics. Another reduced model is similar to that of [22], in which only planar motion and the corresponding spanwise blade vibration are described; this is: the disc has two translational DOFs, and each blade has two modal DOFs. In the cited work, four blades are used, but we have decided on two blades as they fit our final application better. The largest model employed considers the 5 DOFs of the disc, eight modal variables for each of the two blades, and four modal variables per blade per direction of deformation (spanwise or flapwise); this results in a 21-DOF model. In the sequel, mention will be made of the corresponding version of the model being employed.

To conclude the section, we present a simplified version of the system matrices with only two modes per deformation direction (flapwise or spanwise) to illustrate the features of the system. In the complete 21-DOF case, the corresponding submatrices are simply expanded accordingly. This illustrative model of 13 DOFs has the generalized coordinates $\mathbf{x} = [G_x, G_y, G_z, \theta_1, \theta_2, q_{1,1}^s, q_{1,2}^s, q_{1,1}^f, q_{1,2}^f, q_{2,1}^s, q_{2,2}^s, q_{2,1}^f, q_{2,2}^f]^T$, where for instance $x_7 = q_{1,2}^s$ denotes the spanwise modal variable of the first blade corresponding to the second blade mode shape.

The Stiffness matrix $\mathbf{K}(t)$ can be represented as:

$$\mathbf{K}(t) = \begin{bmatrix} \mathbf{K}^A & \mathbf{K}^B & \mathbf{K}^C \\ 13 \times 5 & 13 \times 4 & 13 \times 4 \end{bmatrix}, \quad (2.47)$$

the submatrix $\mathbf{K}^A_{13 \times 5}$:

$$\mathbf{K}^A_{13 \times 5} = \begin{pmatrix} K_{X,T} & 0 & 0 & 0 & K_{X,R} \\ 0 & K_{Y,T} & 0 & K_{Y,R} & 0 \\ 0 & 0 & K_{Z,T} & 0 & 0 \\ 0 & K_{Y,R} & 0 & K_{\theta_1 \theta_1} \sin^2(t\Omega) + K_{Y,C} & K_{\theta_1 \theta_2} \sin(2t\Omega) \\ K_{X,R} & 0 & 0 & K_{\theta_2 \theta_1} \sin(2t\Omega) & K_{\theta_2 \theta_2} \cos^2(t\Omega) + K_{X,C} \\ 0 & 0 & 0 & 0 & 0 \\ 0 & 0 & 0 & 0 & 0 \\ 0 & 0 & 0 & 0 & 0 \\ 0 & 0 & 0 & 0 & 0 \\ 0 & 0 & 0 & 0 & 0 \\ 0 & 0 & 0 & 0 & 0 \\ 0 & 0 & 0 & 0 & 0 \\ 0 & 0 & 0 & 0 & 0 \end{pmatrix} \quad (2.48)$$

with the following values for the coefficients:

$$\begin{aligned}
K_{X,T} &= K_{X_1} + K_{X_2} \\
K_{Y,T} &= K_{Y_1} + K_{Y_2} \\
K_{Z,T} &= K_{Z_1} + K_{Z_2} \\
K_{Y,R} &= K_{Y_1}L_1 + K_{Y_2}L_2 \\
K_{X,R} &= -K_{X_1}L_1 - K_{X_2}L_2 \\
K_{Y,C} &= K_{Y_1}L_1^2 + K_{Y_2}L_2^2 \\
K_{X,C} &= K_{X_1}L_1^2 + K_{X_2}L_2^2
\end{aligned} \tag{2.49}$$

and:

$$\begin{aligned}
K_{\theta_1\theta_1} &= -\frac{1}{3}2A\rho\Omega^2L_b(3R_rL_b + L_b^2 + 3R_r r^2) \\
K_{\theta_1\theta_2} &= \frac{1}{3}A\rho\Omega^2L_b((3R_r - 1)L_b + 2L_b^2 + 3R_r^2) \\
K_{\theta_2\theta_1} &= \frac{1}{3}A\rho\Omega^2L_b((3R_r - 1)L_b + 2L_b^2 + 3R_r^2) \\
K_{\theta_2\theta_2} &= -\frac{1}{3}2A\rho\Omega^2L_b(3R_rL_b + L_b^2 + 3R_r^2).
\end{aligned} \tag{2.50}$$

The submatrix $\mathbf{K}_{13 \times 4}^B$ is:

$$\mathbf{K}_{13 \times 4}^B = \begin{pmatrix} K_{1,1}^B & K_{1,2}^B & 0 & 0 \\ K_{2,1}^B & K_{2,2}^B & 0 & 0 \\ 0 & 0 & 0 & 0 \\ 0 & 0 & K_{4,3}^B & K_{4,4}^B \\ 0 & 0 & K_{5,3}^B & K_{5,4}^B \\ K_{6,1}^B & K_{6,2}^B & K_{6,3}^B & K_{6,4}^B \\ K_{7,1}^B & K_{7,2}^B & K_{7,3}^B & K_{7,4}^B \\ K_{8,1}^B & K_{8,2}^B & K_{8,3}^B & K_{8,4}^B \\ K_{9,1}^B & K_{9,2}^B & K_{9,3}^B & K_{9,4}^B \\ 0 & 0 & 0 & 0 \\ 0 & 0 & 0 & 0 \\ 0 & 0 & 0 & 0 \\ 0 & 0 & 0 & 0 \end{pmatrix} \tag{2.51}$$

with nonzero elements:

$$\begin{aligned}
K_{1,1}^B &= A\rho\Omega^2 \sin(t\Omega) (\int \varphi_1^s dx) & K_{1,2}^B &= A\rho\Omega^2 \sin(t\Omega) (\int \varphi_2^s dx) & K_{2,1}^B &= -A\rho\Omega^2 \cos(t\Omega) \int \varphi_1^s dx & K_{2,2}^B &= -A\rho\Omega^2 \cos(t\Omega) \int \varphi_2^s dx \\
K_{8,1}^B &= EI_{YZ} \int \varphi_1^{f''} \varphi_1^{s''} dx & K_{8,2}^B &= EI_{YZ} \int \varphi_1^{f''} \varphi_2^{s''} dx & K_{9,1}^B &= EI_{YZ} \int \varphi_1^{s''} \varphi_2^{f''} dx & K_{9,2}^B &= EI_{YZ} \int \varphi_2^{f''} \varphi_2^{s''} dx \\
K_{4,3}^B &= A\rho\Omega^2 \sin(t\Omega) (r \int \varphi_1^f dx + \int x\varphi_1^f dx) & K_{4,4}^B &= A\rho\Omega^2 \sin(t\Omega) (R_r \int \varphi_2^f dx + \int x\varphi_2^f dx) \\
K_{5,3}^B &= -A\rho\Omega^2 \cos(t\Omega) (R_r \int \varphi_1^f dx + \int x\varphi_1^f dx) & K_{5,4}^B &= -A\rho\Omega^2 \cos(t\Omega) (R_r \int \varphi_2^f dx + \int x\varphi_2^f dx) \\
K_{6,3}^B &= EI_{YZ} \int (\varphi_1^f) (\varphi_1^s)'' dx & K_{6,4}^B &= EI_{YZ} \int \varphi_1^{s''} \varphi_2^{f''} dx & K_{7,3}^B &= EI_{YZ} \int \varphi_1^{f''} \varphi_2^{s''} dx & K_{7,4}^B &= EI_{YZ} \int \varphi_2^{f''} \varphi_2^{s''} dx \\
K_{8,3}^B &= EI_{YY} \int \varphi_1^{f''2} dx & K_{8,4}^B &= EI_{YY} \int \varphi_1^{f''} \varphi_2^{f''} dx & K_{9,3}^B &= EI_{YY} \int \varphi_1^{f''} \varphi_2^{f''} dx & K_{9,4}^B &= EI_{YY} \int \varphi_2^{f''2} dx \\
K_{6,1}^B &= 2A\rho R_r \Omega^2 L_b (\int \varphi_1^{s'}(x)^2 dx) + A\rho\Omega^2 L_b^2 (\int \varphi_1^{s'}(x)^2 dx) - 2A\rho R_r \Omega^2 (\int x\varphi_1^{s'}(x)^2 dx) - A\rho\Omega^2 (\int x^2 \varphi_1^{s'}(x)^2 dx) - \\
& A\rho\Omega^2 (\int \varphi_1^{s2} dx) + EI_{ZZ} \int \varphi_1^{s''2} dx
\end{aligned}$$

$$\begin{aligned}
K_{6,2}^B &= 2A\rho R_r \Omega^2 L_b \left(\int \varphi_1^{s'} \varphi_2^{s'} dx \right) + A\rho \Omega^2 L_b^2 \left(\int \varphi_1^{s'} \varphi_2^{s'} dx \right) - 2A\rho R_r \Omega^2 \left(\int x \varphi_1^{s'} \varphi_2^{s'} dx \right) - A\rho \Omega^2 \left(\int x^2 \varphi_1^{s'} \varphi_2^{s'} dx \right) - \\
&A\rho \Omega^2 \left(\int \varphi_1^s \varphi_2^s dx \right) + EI_{ZZ} \int \varphi_1^{s''} \varphi_2^{s''} dx \\
K_{7,1}^B &= 2A\rho R_r \Omega^2 L_b \left(\int \varphi_1^{s'} \varphi_2^{s'} dx \right) + A\rho \Omega^2 L_b^2 \left(\int \varphi_1^{s'} \varphi_2^{s'} dx \right) - 2A\rho R_r \Omega^2 \left(\int x \varphi_1^{s'} \varphi_2^{s'} dx \right) - A\rho \Omega^2 \left(\int x^2 \varphi_1^{s'} \varphi_2^{s'} dx \right) - \\
&A\rho \Omega^2 \left(\int \varphi_1^s \varphi_2^s dx \right) + EI_{ZZ} \int \varphi_1^{s''} \varphi_2^{s''} dx \\
K_{7,2}^B &= 2A\rho R_r \Omega^2 L_b \left(\int \varphi_2^{s'/2} dx \right) + A\rho \Omega^2 L_b^2 \left(\int \varphi_2^{s'/2} dx \right) - 2A\rho R_r \Omega^2 \left(\int x \varphi_2^{s'/2} dx \right) - A\rho \Omega^2 \left(\int x^2 \varphi_2^{s'/2} dx \right) - A\rho \Omega^2 \left(\int \varphi_2^{s/2} dx \right) + \\
&EI_{ZZ} \int \varphi_2^{s''/2} dx,
\end{aligned}$$

and \mathbf{K}^C can be expressed with the same coefficients as \mathbf{K}^B :

$$\mathbf{K}_{13 \times 4}^C = \begin{pmatrix} -K_{1,1}^B & -K_{1,2}^B & 0 & 0 \\ -K_{2,1}^B & -K_{2,2}^B & 0 & 0 \\ 0 & 0 & 0 & 0 \\ 0 & 0 & -K_{4,3}^B & -K_{4,4}^B \\ 0 & 0 & -K_{5,3}^B & -K_{5,4}^B \\ 0 & 0 & 0 & 0 \\ 0 & 0 & 0 & 0 \\ 0 & 0 & 0 & 0 \\ K_{6,1}^B & K_{6,2}^B & K_{6,3}^B & K_{6,4}^B \\ K_{7,1}^B & K_{7,2}^B & K_{7,3}^B & K_{7,4}^B \\ K_{8,1}^B & K_{8,2}^B & K_{8,3}^B & K_{8,4}^B \\ K_{9,1}^B & K_{9,2}^B & K_{9,3}^B & K_{9,4}^B \end{pmatrix}. \quad (2.52)$$

The gyroscopic matrix $\mathbf{G}(t)$ is skew-symmetric, the nonzero elements above the main diagonal are as follows:

$$\begin{aligned}
G_{4,5} &= \frac{1}{3} \Omega (2A\rho L_b^3 + 6A\rho R_r^2 L_b + 6A\rho R_r L_b^2 + 3J_p) & G_{1,6} &= -2A\rho \Omega \cos(t\Omega) \int \varphi_1^s dx \\
G_{1,7} &= -2A\rho \Omega \cos(t\Omega) \int \varphi_2^s dx & G_{1,10} &= 2A\rho \Omega \cos(t\Omega) \int \varphi_1^s dx & G_{1,11} &= 2A\rho \Omega \cos(t\Omega) \int \varphi_2^s dx \\
G_{2,6} &= -2A\rho \Omega \sin(t\Omega) \int \varphi_1^s dx & G_{2,7} &= -2A\rho \Omega \sin(t\Omega) \int \varphi_2^s dx \\
G_{2,10} &= 2A\rho \Omega \sin(t\Omega) \int \varphi_1^s dx & G_{2,11} &= 2A\rho \Omega \sin(t\Omega) \int \varphi_2^s dx
\end{aligned}$$

The mass-inertia matrix $\mathbf{M}(t)$ is symmetric, with the following nonzero elements over the main diagonal:

$$\begin{aligned}
M_{1,1} &= M_{2,2} = M_{3,3} = 2A\rho L_b + M & M_{4,4} &= M_{5,5} = \frac{1}{3} A\rho L_b^3 + A\rho R_r^2 L_b + A\rho R_r L_b^2 + J_d \\
M_{6,6} &= M_{10,10} = A\rho \int \varphi_1^{s/2} dx & M_{6,7} &= M_{10,11} = A\rho \int \varphi_1^s \varphi_2^s dx & M_{7,7} &= M_{11,11} A\rho \int \varphi_2^{s/2} dx \\
M_{8,8} &= M_{12,12} = A\rho \int \varphi_1^{f/2} dx & M_{8,9} &= M_{12,13} = A\rho \int \varphi_1^f \varphi_2^f dx & M_{9,9} &= M_{13,13} = A\rho \int \varphi_1^{f/2} dx \\
M_{1,6} &= -M_{1,10} = -A\rho \sin(t\Omega) \int \varphi_1^s dx & M_{1,7} &= -M_{1,11} = -A\rho \sin(t\Omega) \int \varphi_2^s dx & M_{2,6} &= -M_{2,10} A\rho \cos(t\Omega) \int \varphi_1^s dx \\
M_{2,7} &= -M_{2,11} = A\rho \cos(t\Omega) \int \varphi_2^s dx & M_{3,8} &= M_{3,12} = A\rho \int \varphi_1^f dx & M_{3,9} &= M_{3,13} = A\rho \int \varphi_2^f dx \\
M_{4,8} &= -M_{4,12} = A\rho \sin(t\Omega) (R_r \int \varphi_1^f dx + \int x \varphi_1^f dx) & M_{4,9} &= -M_{4,13} = A\rho \sin(t\Omega) (R_r \int \varphi_2^f dx + \int x \varphi_2^f dx) \\
M_{5,8} &= -M_{5,12} = -A\rho \cos(t\Omega) (R_r \int \varphi_1^f dx + \int x \varphi_1^f dx) & M_{5,9} &= -M_{5,13} = -A\rho \cos(t\Omega) (R_r \int \varphi_2^f dx + \int x \varphi_2^f dx).
\end{aligned}$$

It can be seen that the resulting system of equations is of the form:

$$\mathbf{M}(t) \ddot{\mathbf{x}} + \mathbf{G}(t) \dot{\mathbf{x}} + \mathbf{K}(t) \mathbf{x} = 0, \quad (2.53)$$

that is, the rotor-blade model is indeed LTP. The periodic terms describe time-dependent interactions between the degrees of freedom of the disc and those of the blades. For instance, the term:

$$-A\rho \sin(t\Omega) \left(\int \varphi_{1,1}^s dx \right) \quad (2.54)$$

is a coupling term that reflects the influence of the inertia of blade 1 in its first mode of spanwise motion over the translational motion of the disc, it takes into account the variation in mass distribution as the blade rotates given the spin of the body.

We end the section by enumerating the key features of the model presented:

1. The model includes the axial motion of the rotor and represents the axial-flapwise coupling, with an approach we have not identified in the corresponding literature.
2. The spanwise-flapwise coupling has been included.
3. The rotor or disc has been described using two angular coordinates that are usually neglected in favor of planar motion models.
4. The model can describe the effects of coupling between blade deformation and disc motion, an effect often neglected in the applied literature or taken into account by means of “black-box” approaches (specialized FEM codes for instance).
5. The reduced order provides an ideal dynamical system for the stochastic study by semi-analytical tools, as many of the expressions will be tractable; at the same time, abundant structural and vibratory information remains in the model.

We consider these virtues to be the key innovative aspects of the developments presented in this chapter.

4 Blade modeling and modal discretization

4.1 Modal determination by kinematic methods

This section is devoted to the description of the modal discretization assumed to be available in the previous developments, as stated earlier: the existence of the vector functions $\mathbf{W}_{i_b}(\xi, t) = [\xi, W_{i_b}^s(\xi, t), W_{i_b}^f(\xi, t)]^T$ describing the transverse vibration of the i_b -th blades, in the following the index i_b refers to the blade under consideration; or similarly, the modal representation $W_{i_b}^*(X_b, t) = \sum_j \varphi_{j_m}^*(X_b) q_{i_b, j_m}^*$, where j_m denotes the m -th normal mode of the blade. The general strategy adopted here has been described as the “assumed modes” methods (see: [67] or [22]), while the particular method used to approximate the functions $\varphi_{j_m}^*(X_b)$ is a version of the well-known Rayleigh–Ritz method, a kinematic discretization scheme based in Rayleigh’s principle. In terms of implementation, the main feature of our approach is the capability to update the solution to any variation in the parameters of the blade. The method is also highly adaptable to different orthogonal base functions, although we employ simple polynomial approximation as it proved satisfactory to the problem at hand.

With regards to the Rayleigh–Ritz method, despite being a relatively old technique, it remains a popular choice in mechanical sciences. Reference [59] provides an in-depth discussion of the more modern aspects of the method, including the choice of basis function and penalty methods to increase its applicability. Reference [40] provides an introduction to the method in the context of Finite Element analysis of rotating beams, while [15] utilizes it in the treatment of problems in multi-body dynamics; more recently, it has been applied in uncertain mechanical systems in [27]. Reference [77] provides a literature review of the application of the method in dynamical problems of beams, plates, and shells.

The assumed modes method consists of the following ([67]):

1. an elastic structure is represented by a combination of space-dependent functions multiplied by time-dependent amplitude functions that are considered Lagrangian Generalized coordinates,
2. the space-dependent functions, traditionally selected as a set of orthogonal functions, are selected in such a way that the boundary conditions of the dynamical problem are satisfied,

3. if available, the eigenfunctions (or normal modes) are selected as the space-dependent functions,

in other words, the method makes the assumption that the space-dependent functions approximate the actual eigenfunctions of the system. This translates into:

$$\begin{aligned} f(X_b, t) &= \sum_{j=1}^{\infty} \phi_j(X_b) q_j(t) \\ &\approx \sum_{j=1}^N \phi_j(X_b) q_j(t) \end{aligned} \quad (2.55)$$

so the true mode shapes (or eigenfunctions) of $f(X_b, t)$ are approximated by the ‘‘assumed’’ modes: $\varphi_{j_m}(X_b) \approx \sum_{j=1}^{\infty} C_j \phi_j(X_b)$ with C_j a constant to be determined, and the index j is related to the truncation order of the expansion. With an orthonormal basis of infinite dimension, this is guaranteed. The key difficulty of this approach is the correct choice of mode shapes ϕ_j to ensure a good approximation of φ_{j_m} with as few terms as possible.

We start by writing the energies of the rotating beam, with W^f and W^s the flapwise and spanwise displacement functions of a blade:

$$KE_B^f = \int_0^{L_b} \frac{1}{2} \rho A \left(\frac{\partial W^f}{\partial t} \right)^2 dX + \frac{1}{2} I_p \Omega^2 \quad (2.56)$$

and:

$$KE_B^s = \int_0^{L_b} \frac{1}{2} \rho A \left(\frac{\partial W^s}{\partial t} \right)^2 dX + \frac{1}{2} I_p \Omega^2 + \int_0^{L_b} \rho A X \Omega \left(\frac{\partial W^s}{\partial t} \right) dX \quad (2.57)$$

while the potentials are $PE_B = PE_{\text{elastic}} + PE_{\text{rotation}}$:

$$PE_B^f = \int_0^{L_b} \frac{1}{2} EI_{YY} \left(\frac{\partial^2 W^f}{\partial X^2} \right)^2 dX + \int_0^L \frac{1}{2} \Omega^2 N_0 \left(\frac{\partial W^f}{\partial X} \right)^2 dX \quad (2.58)$$

$$PE_B^s = \int_0^{L_b} \frac{1}{2} EI_{ZZ} \left(\frac{\partial^2 W^s}{\partial X^2} \right)^2 dX + \int_0^{L_b} \frac{1}{2} \Omega^2 N_0 \left(\frac{\partial W^s}{\partial X} \right)^2 dX - \int_0^{L_b} \frac{1}{2} \Omega^2 \rho A W^s{}^2 dX \quad (2.59)$$

now, introducing modal solutions of the form $W^s(X, t) = Q_s(t) \varphi^s(X)$, $W^f(X, t) = Q_f(t) \varphi^f(X)$, where $Q_s(t)$, $Q_f(t)$ have the usual harmonic form $Q_i = \exp[i\omega_i t]$, and using the Euler-Lagrange equations on these new generalized variables, we arrive at a modal form of the equation of motion for each deformation direction:

$$-\omega_f^2 \int_0^{L_b} \rho A (\varphi^f)^2 - EI_{YY} ((\varphi^f)'')^2 - \Omega^2 N_0 ((\varphi^f)')^2 dX = 0 \quad (2.60)$$

$$-(\omega_s^2 + \Omega^2) \int_0^L \rho A (\varphi^s)^2 - EI_{ZZ} ((\varphi^s)'')^2 - \Omega^2 N_0 ((\varphi^s)')^2 dX = 0 \quad (2.61)$$

or, in differential form[43]:

$$-\omega_f^2 \rho A \varphi^f - \frac{d}{dX} \left(N_0(\Omega, X) \frac{d\varphi^f}{dX} \right) + \frac{d^2}{dX^2} \left(EI_{YY} \frac{d^2 \varphi^f}{dX^2} \right) = 0 \quad (2.62)$$

$$-(\omega_s^2 + \Omega^2) \rho A \varphi^s - \frac{d}{dX} \left(N_0(\Omega, X) \frac{d\varphi^s}{dX} \right) + \frac{d^2}{dX^2} \left(EI_{ZZ} \frac{d^2 \varphi^s}{dX^2} \right) = 0. \quad (2.63)$$

To solve the eigenvalue problems in Eq. 2.62 and Eq. 2.63, we apply the Rayleigh–Ritz method: we seek the mode shapes in the form: $\varphi^s(X_b) \approx \sum_{j=1}^N C_j^s \phi_j^s(X_b)$ and $\varphi^f(X_b) \approx \sum_{j=1}^N C_j^f \phi_j^f(X_b)$, where the functions ϕ_j^f and ϕ_j^s chosen as monomial terms satisfying the natural or boundary conditions, in the case of a cantilever beam these are: $\psi^\bullet(0) = 0$ and $(\psi^\bullet)'(0) = 0$. We have:

$$\phi_i^\bullet = \frac{\xi^{i+1}}{L_b^{i+1}} \quad (2.64)$$

now substituting this type of solution into the corresponding energetic expressions we obtain:

$$\begin{aligned} \text{KEB}_{\max} &= \frac{\omega^2}{2} \sum_{i=1}^n \sum_{j=1}^n m_{ij} C_i^\bullet C_j^\bullet \\ \text{PEB}_{\max}^{\text{el}} &= \frac{1}{2} \sum_{i=1}^n \sum_{j=1}^n k_{ij}^{\text{el}} C_i^\bullet C_j^\bullet \\ \text{PEB}_{\max}^{\text{stiffening}} &= \frac{1}{2} \sum_{i=1}^n \sum_{j=1}^n k_{ij}^{\text{stiffening}} C_i^\bullet C_j^\bullet \\ \text{PEB}_{\max}^{\text{softening}} &= -\frac{1}{2} \sum_{i=1}^n \sum_{j=1}^n k_{ij}^{\text{softening}} C_i^\bullet C_j^\bullet \end{aligned} \quad (2.65)$$

here the implied matrices are computed as follows:

$$m_{ij} = \int_0^{L_b} \rho A \left(\frac{\xi}{L_b} \right)^{i+j+2} d\xi = \frac{\rho A L_b}{i+j+3} \quad (2.66)$$

$$k_{ij}^{\text{el}} = \frac{1}{L^4} \int_0^{L_b} EI ((i+1)i(j+1)j \left(\frac{\xi}{L_b} \right)^{i+j-2}) d\xi = \frac{EI}{L_b^3} \frac{ij(i+1)(j+1)}{(i+j-1)} \quad (2.67)$$

$$k_{ij}^{\text{stiffening}} = \int_0^{L_b} N_0(\Omega, \xi) \left(\frac{\xi}{L} \right)^{i+j} d\xi = \Omega^2 \rho A \int_0^L (L^2 + 2R_r L - 2R_r \xi - \xi^2) \left(\frac{\xi}{L} \right)^{i+j} d\xi \quad (2.68)$$

$$k_{ij}^{\text{stiffening}} = \Omega^2 \rho A (i+1)(j+1) \left(L_b \left(\frac{1}{i+j+1} - \frac{1}{i+j+3} \right) + R_r \left(\frac{1}{(i+j+1)L} - \frac{1}{i+j+2} \right) \right) \quad (2.69)$$

$$k_{ij}^{\text{softening}} = \int_0^{L_b} \Omega^2 \rho A \left(\frac{\xi}{L_b} \right)^{i+j+2} d\xi = \frac{\Omega^2 \rho A L}{(i+j+3)} = \Omega^2 m_{ij} \quad (2.70)$$

with $i, j = [1, 2, \dots, N]$ indexes related to the discretization order of the expansion. This leads to the eigenvalue problem:

$$\mathbf{K}\mathbf{C} = \omega^2 \mathbf{M}\mathbf{C} \quad (2.71)$$

where the flapwise version of the problem utilizes: $\mathbf{K} = \mathbf{K}(\Omega) = \mathbf{k}^{\text{el}} + \mathbf{k}^{\text{stiffening}}(\Omega)$, while the spanwise utilizes $\mathbf{K} = \mathbf{K}(\mathbf{M}, \Omega) = \mathbf{k}^{\text{el}} + \mathbf{k}^{\text{stiffening}}(\Omega) - \mathbf{k}^{\text{softening}}(\mathbf{M}, \Omega)$. The solution of this eigenvalue problem yields an approximation of the natural frequencies of the corresponding mode of vibration of the beam: ω_s^k and ω_f^k , and the vector of coefficients \mathbf{C} , with which the mode shape can be reconstructed: $\varphi^s(X_b) \approx \sum_{j=1}^N C_j^s \phi_j^s(X_b)$ and $\varphi^f(X_b) \approx \sum_{j=1}^N C_j^f \phi_j^f(X_b)$ respectively.

This algorithm is implemented in the subroutine *rritz* (Matlab) Alg. 2.1.

Algorithm 2.1 Algorithm *rritz* for rotating beam discretization

1. Initialize beam parameters: I, E, A, ρ, L_b, R_r
 2. Fix angular velocity
 3. Fix polynomial order, monomial family: $\{x^2, x^3, x^4, \dots, x^{\text{Poly}}\}$
 4. Assemble primitive discretized matrices: $\mathbf{M}_0, \mathbf{K}_{E_0}, \mathbf{K}_{S_0}$:
 - (a) $\mathbf{M}_0 = M_{0,(i,j)} = \frac{1}{i+j+3}$
 - (b) $\mathbf{K}_{E_0} = K_{E_0,(i,j)} = \frac{ij(i+1)(j+1)}{(i+j-1)}$
 - (c) $\mathbf{K}_{S_0} = K_{S_0,(i,j)} = (i+1)(j+1) \left(L_b \left(\frac{1}{i+j+1} - \frac{1}{i+j+3} \right) + R_r \left(\frac{1}{(i+j+1)L} - \frac{1}{i+j+2} \right) \right)$
 5. Calculate discretized system matrices with the primitives: $\mathbf{M}^{\text{effective}}, \mathbf{K}^{\text{elastic}}, \mathbf{K}^{\text{stiffening}}, \mathbf{K}^{\text{softening}}$
 - (a) $\mathbf{M}^{\text{effective}} = \rho A L_b \mathbf{M}_0$
 - (b) $\mathbf{K}^{\text{elastic}} = \frac{EI}{L_b^3} \mathbf{K}_{E_0}$
 - (c) $\mathbf{K}^{\text{stiffening}} = \Omega^2 \rho A \mathbf{K}_{S_0}$
 - (d) $\mathbf{K}^{\text{softening}} = \Omega^2 \mathbf{M}_0$
 6. Calculate the effective mass and stiffness matrix for each case (flapwise or spanwise)
 7. Solve the two associated eigenvalue problems, command *Eig*, to obtain beam frequencies and polynomial coefficients
 8. Adjust coefficient scaling from normalization
 9. Returns coefficient array and frequencies of the beam
-

4.2 Load determination in modal basis

We now consider a blade under the effect of a surface external load $L_s(t, X_b)$, for instance, a hydrodynamic load in the case of a tidal turbine. The potential energy injected into the system from this external perturbation can be written utilizing the kinematic description Eq. 2.55:

$$\begin{aligned}
 PE_{ext} &= - \int_S L_s(t, X_b) W_{i_b}^\bullet(X_b, t) dS \\
 &= - \int_S L_s(t, X_b) \sum_{j_m=1}^N \varphi_{j_m}^\bullet(X_b) q_{i_b, j_m}^\bullet(t) dS \\
 &= - \sum_{j_m=1}^N \left(\int_S L_s(t, X_b) \sum_{j_m=1}^{N_{modes}} \varphi_{j_m}^\bullet(X_b) dS \right) q_{i_b, j_m}^\bullet(t), \tag{2.72}
 \end{aligned}$$

where we define the modal projection of the load over the j_m -th mode shape by $L_{\varphi_{j_m}^\bullet}^\bullet(t) = \left(\int_S L_s(t, X_b) \varphi_{j_m}^\bullet(X_b) dS \right)$. Invoking again the Euler-Lagrange equation Eq. 2.46 for this potential alone, we obtain the generalized loads in the modal basis:

$$- \frac{\partial}{\partial x_i} [PE_{ext}] = L_{\varphi_{j_m}^\bullet}^\bullet(t), i \in [1, N] \tag{2.73}$$

for a discretization up to N mode shapes, this yields a load vector of form:

$$\mathbf{L}_{\varphi^\bullet}(t) = \begin{pmatrix} L_{\varphi_1^\bullet}(t) \\ \dots \\ L_{\varphi_N^\bullet}(t) \end{pmatrix}. \tag{2.74}$$

For the discretization scheme developed in this chapter, the modal projections can be written more concretely in terms of the blade parameters:

$$L_{\varphi_{j_m}^\bullet}(t) = \int_0^{L_b} L_s(t, X_b) \varphi_j^\bullet(X_b) dX, \tag{2.75}$$

in this last equation the prismatic nature of the blade has been applied, which permits to reduce the surface integral into a simple integral along the span of the beam.

4.3 Stress determination from modal variables

The Rayleigh–Ritz method, as developed in this section, offers an effective estimation of the bending moment across the blade, which can be utilized to analyze the normal stresses produced in pure or oblique bending in the section of the blade. Provided that the mode shape functions $\varphi_{j_m}^s(X_b)$, $\varphi_{j_m}^f(X_b)$ and modal variables q_{i_b, j_m}^s , q_{i_b, j_m}^f are known, one may write the corresponding bending moments at point $X_b = a$ as:

$$\begin{aligned}
 M_s^a(t) &= EI_{ZZ} \sum_{j_m=1}^{N_{modes}} \varphi_{j_m}^{\prime\prime s}(a) q_{i_b, j_m}^s(t) - EI_{YZ} \sum_{j_m=1}^{N_{modes}} \varphi_j^{\prime\prime f}(a) q_{i_b, j_m}^f(t) \\
 M_f^a(t) &= EI_{YY} \sum_{j_m=1}^{N_{modes}} \varphi_j^{\prime\prime f}(a) q_{i_b, j_m}^f(t) - EI_{YZ} \sum_{j_m=1}^{N_{modes}} \varphi_{j_m}^{\prime\prime s}(a) q_{i_b, j_m}^s(t), \tag{2.76}
 \end{aligned}$$

where $\varphi_{j_m}^{''s}(X_b) = \frac{d}{dX^2} [\varphi_{j_m}^s(X_b)]$ and $\varphi_{j_m}^{''f}(X_b) = \frac{d}{dX^2} [\varphi_{j_m}^f(X_b)]$ are respectively the curvature of the blade in the spanwise and flapwise direction, and $M_s^a(t)$ is the spanwise bending moment in a while $M_f^a(t)$ is the flapwise bending moment in a . If the cross-section of the blade is symmetrical, then $I_{YZ} = 0$. In the cantilever boundary condition selected in our model, the bending moments are maximal at the fixed end $a = 0$. In the corresponding literature, these quantities are termed root bending moment (RBM), and constitute a key design consideration in tidal and wind turbines. In the sequel, we will write $M_s^0(t) = EI_{ZZ} \sum_{j_m=1}^N \varphi_{j_m}^{''s}(0) q_{i_b, j_m}^s(t) - EI_{YZ} \sum_{j_m=1}^{N_{modes}} \varphi_{j_m}^{''f}(0) q_{i_b, j_m}^f(t) = M_s^{RBM}(t)$ and $M_f^0(t) = EI_{YY} \sum_{j_m=1}^N \varphi_{j_m}^{''f}(0) q_{i_b, j_m}^f(t) - EI_{YZ} \sum_{j_m=1}^{N_{modes}} \varphi_{j_m}^{''s}(0) q_{i_b, j_m}^s(t) = M_f^{RBM}(t)$. Additionally, the normal stress due to a given moment component through the cross-section can be expressed as:

$$\begin{aligned}\sigma_x^s(t, Y) &= -\frac{I_{YY}M_s^{RBM}(t) + I_{YZ}M_f^{RBM}(t)}{I_{YY}I_{ZZ} - I_{YZ}^2} Y \\ \sigma_x^f(t, Z) &= -\frac{I_{ZZ}M_f^{RBM}(t) + I_{YZ}M_s^{RBM}(t)}{I_{ZZ}I_{YY} - I_{YZ}^2} Z,\end{aligned}\quad (2.77)$$

where the sign convention entails that a positive moment $M_s^{RBM}(t)$ deforms the blade in compression in the first and second quadrants, and in tension in the third and fourth quadrants, from where the sign of the normal stress follows; similarly, a positive moment $M_f^{RBM}(t)$ results in compression in the second and third quadrants, and tension in the first and fourth quadrants. As usual, the maximal normal stresses in magnitude for each component are attained at the furthest fiber from the neutral plane.

Considering a prismatic, rectangular profile as displayed in Fig. 2.5, we distinguish four critical points where the corresponding maximal normal stresses due to biaxial bending may be present. Since the profile is symmetrical, $I_{YZ} = 0$. This particular section is selected for exposition purposes to ensure the clarity of the developments. When the blade deflects in the positive Y direction, $M_s^{RBM}(t)$ is positive and the fiber $A - B$ is in compression, while the fiber $C - D$ is in tension. Similarly, when the blade deflects in the positive Z direction $M_f^{RBM}(t)$ is positive, the fiber $A - D$ is in tension, while the fiber $B - C$ is in compression. If the coordinates of the critical points are $A = (-\frac{b}{2}, +\frac{h}{2})$, $B = (+\frac{b}{2}, +\frac{h}{2})$, $C = (+\frac{b}{2}, -\frac{h}{2})$, $D = (-\frac{b}{2}, -\frac{h}{2})$ where b is the base and h the height, we may write:

$$\begin{aligned}\sigma_x^A &= -\frac{M_s^{RBM}(t)}{I_{ZZ}} \left(\frac{h}{2}\right) + \frac{M_f^{RBM}(t)}{I_{YY}} \left(\frac{b}{2}\right) + \sigma_x^\Omega \\ \sigma_x^B &= -\frac{M_s^{RBM}(t)}{I_{ZZ}} \left(\frac{h}{2}\right) - \frac{M_f^{RBM}(t)}{I_{YY}} \left(\frac{b}{2}\right) + \sigma_x^\Omega \\ \sigma_x^C &= \frac{M_s^{RBM}(t)}{I_{ZZ}} \left(\frac{h}{2}\right) - \frac{M_f^{RBM}(t)}{I_{YY}} \left(\frac{b}{2}\right) + \sigma_x^\Omega \\ \sigma_x^D &= \frac{M_s^{RBM}(t)}{I_{ZZ}} \left(\frac{h}{2}\right) + \frac{M_f^{RBM}(t)}{I_{YY}} \left(\frac{b}{2}\right) + \sigma_x^\Omega,\end{aligned}\quad (2.78)$$

from where we can conclude that if both moments are positive, the maximum normal stress in compression is attained in B and the maximum normal stress in tension is attained in D , and A and C remain submaximal. The stress σ_x^Ω is due to the centrifugal effect over the blade as it rotates with spin Ω , the axial force at $X = 0$ being $N_0(0) = \Omega^2 b h \rho ((L_b + R_r)^2 - (R_r)^2) = \Omega^2 b h \rho (L_b^2 + 2L_b R_r)$ and introducing the total mass of the blade $m_b = b h \rho L_b$ then $N_0(0) = \Omega^2 (L_b + 2R_r) m_b$, finally:

$$\sigma_x^\Omega = \Omega^2 m_b \frac{(L_b + 2R_r)}{b \times h}.\quad (2.79)$$



Figure 2.5: Blade cross-section

4.4 Numerical implementation: example and comparisons

To conclude the section, we present an example of the implementation of Alg. 2.1 with a comparison to two references from the literature. The same normalization as each respective publication has been utilized to make the comparisons. The offset value is the ratio $\frac{R_c}{L_b}$. In Fig. 2.6 the reference is [149], while in Fig. 2.7 the reference is [108].

5 Numerical example of the dynamical model

To conclude the chapter, we will discuss some numerical aspects of the implementation of the dynamical system, followed by some basic numerical simulations to illustrate the behavior of the system. As the main result of section 3 suggests, the equations of motion will depend on coefficients that are obtained by integrating different quantities involving the mode shapes and their spatial derivatives. These coefficients account for the mass distribution, elastic behavior, centrifugal and geometric effects of the rotation. The practical implementation of Eq. 2.53, along with the matrix quantities established in the previous section, is as follows:

1. The parameters of the system are defined. For the rotor: mass, polar and diametral inertia and radius of the disc, elastic and damping properties of the supports, length of shaft and position of the supports. For the blades: length, elastic moduli, inertia, cross-section and density. Globally: Spin velocity of the system.
2. The modal discretization routine is used to obtain the frequency and mode shape approximations of the corresponding rotating beam problem. The polynomial order of the approximation can be adjusted as required. The frequency values are provided in Tab. 2.3.
3. The subroutine "Shape Form Integrals" uses the polynomial approximations provided by the previous step and the parameters of the system to carry out the corresponding operations of differentiation of shape functions, multiplication by the corresponding factors, and integration along the length of the blade. It returns the required coefficients necessary to express the matrices of the system.
4. The assembly subroutine takes the output of the previous step and the parameters of the system and assembles the mass, gyroscopic, stiffness, and damping matrices into a function dependent on the time

Parameter	Value[units]
M	10000[kg]
J_p	5.5125×10^3 [kgm ²]
J_d	4.0062×10^3 [kgm ²]
R_r	1.05[m]
$K_{X_1}, K_{Y_1}, K_{Z_1}$	[12, 21, 23] $\times 10^7$ [Nm ⁻¹]
$K_{X_2}, K_{Y_2}, K_{Z_2}$	[13, 22, 24] $\times 10^7$ [Nm ⁻¹]

Table 2.1: Disc parameters for simulation

Parameter	Value[units]
ρ	440[kgm ⁻³]
L_b	8.95[m]
A	8.0000×10^{-1} [m ²]
E	25×10^6 [Pa]
I_{ZZ}, I_{YY}	[14, 27.8] [kgm ²]

Table 2.2: Blade parameters for simulation

variable.

The result of this process yield the necessary functions to perform a numerical treatment of Eq. 2.53. As we shall see in the coming chapters, this function can be expressed to first order, or state form. The state form results in a Floquet system, which can be analyzed by time integration or by spectral methods, as Chapter 3 will show. The parameters used for the simulation are shown in Tab. 2.1 for the disc-shaft-support and Tab. 2.2 for the blades. Two blades with eight modes each have been considered, and the angular velocity has been set to $\Omega = 1.5$ [rads⁻¹]. For each case, selected degrees of freedom are visualized, and each case corresponds to an initial excitation on the generalized velocity: $\dot{G}_x = 1$ [ms⁻¹], $\dot{q}_{1,1}^s = 1$ [s⁻¹] and $\dot{\theta}_1 = 0.05$ [rads⁻¹] respectively.

We will briefly comment on the features of each case:

1. In Fig. 2.8 we can see the effects of coupling among the x coordinate and the corresponding angle, and modal coordinates. The impact over the z direction is negligible. The flapwise modal components are more sensitive to the perturbation, and it is observed that the lower modes of each case see a larger magnitude than the higher modes. The x response also features the characteristic modulated behavior of LTP systems, as the next chapter will explore.
2. In Fig. 2.9 we note the effect of the modal variable in the spanwise direction predominantly over the G_x and θ_1 degrees of freedom in the rotor. We also notice that the other modes of the same blade are slightly affected, which is to be expected since a mild coupling among modes has been included in the model. An interesting feature is the influence of the excitation on the same spanwise modes in the other blade.
3. Finally, in Fig. 2.10, a small angular velocity is imposed over the θ_1 degree of freedom. The lower flapwise and spanwise modes of both blades are sensitive to this perturbation, although the same trend

	$\frac{\omega_x^k}{2\pi}$ [Hz]	$\frac{\omega_f^k}{2\pi}$ [Hz]
Mode 1	9.81	6.97
Mode 2	61.52	43.66
Mode 3	172.25	122.24
Mode 4	337.55	239.54

Table 2.3: Blade frequencies from discretization algorithm Alg. 2.1

can be noticed: the higher modes respond in a negligible manner. The effects over the G_x and θ_1 degrees of freedom are the highest, as is expected from the coupling relationships established throughout the chapter.

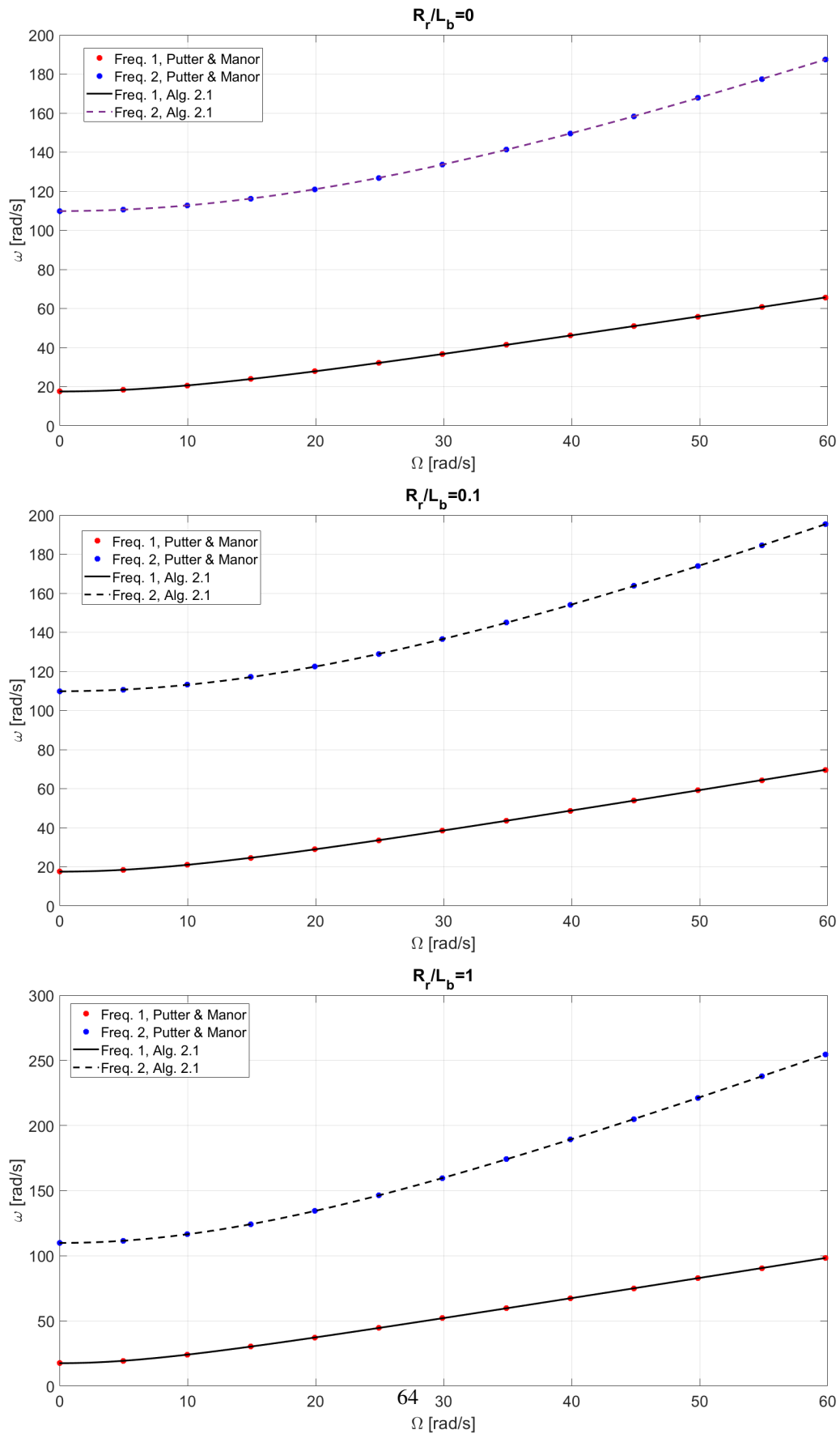


Figure 2.6: Frequencies of rotating beam flapwise vibration, comparison with reference [149] ; offsets 0, 0.1 and 1

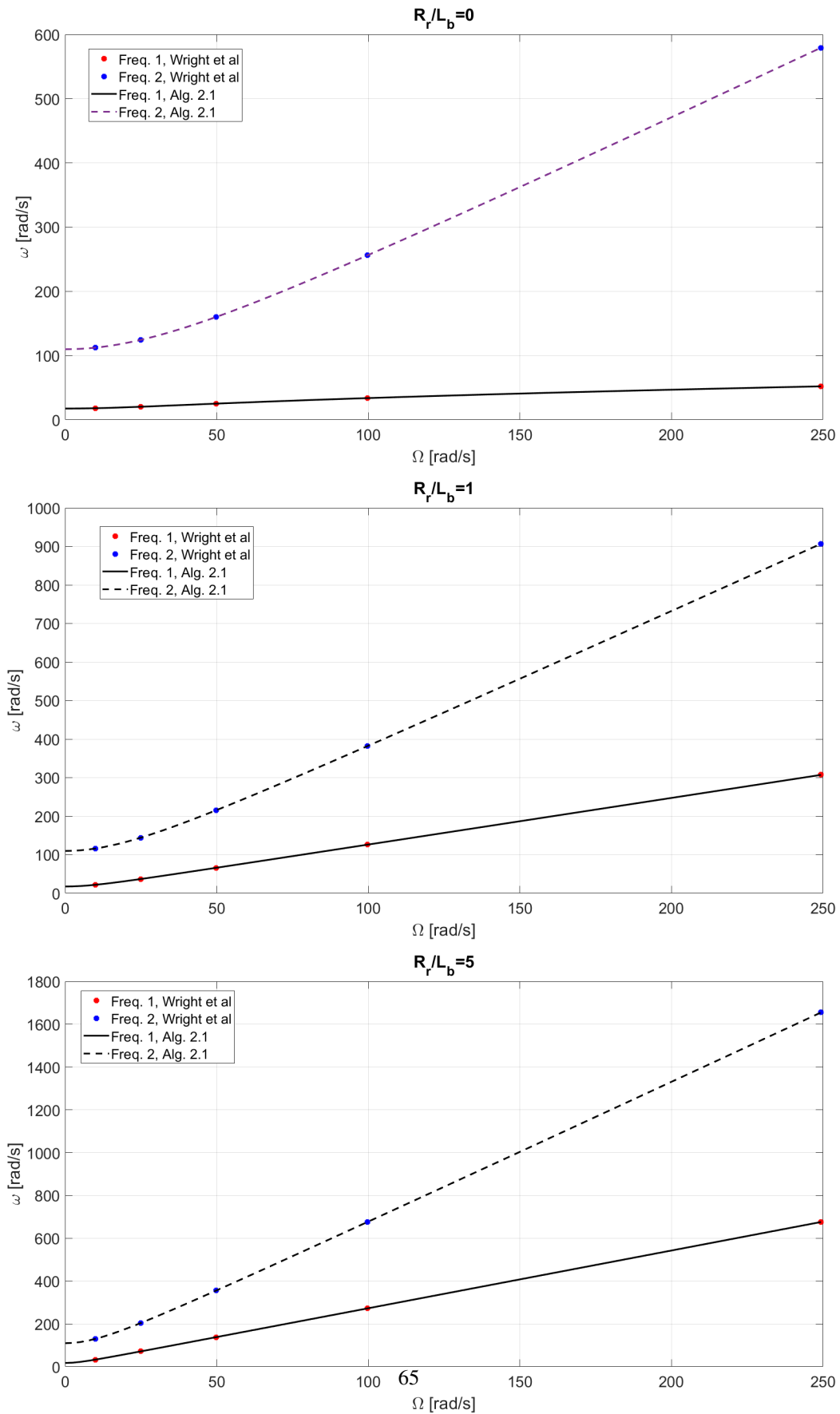


Figure 2.7: Frequencies of rotating beam spanwise vibration, comparison with reference [108] ; offset 0,1 and 5

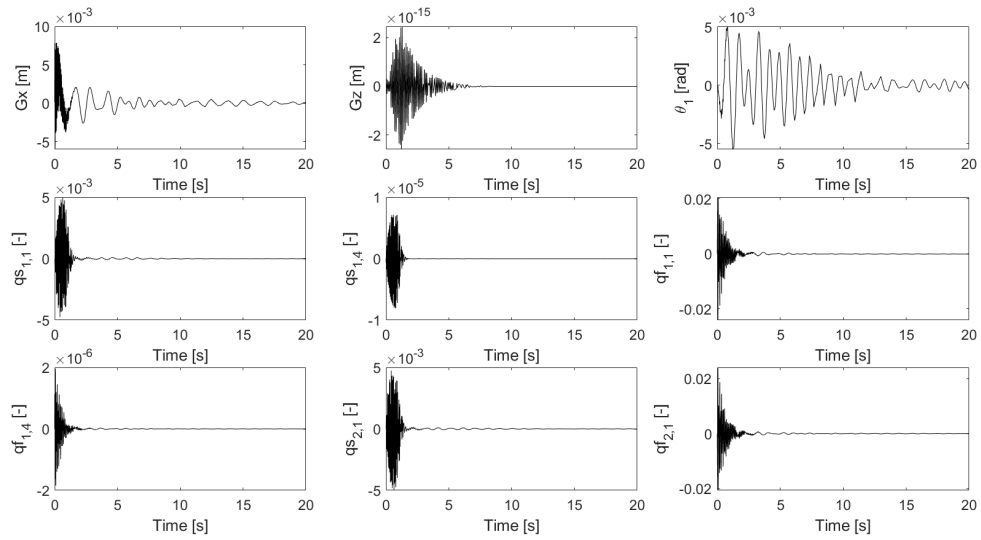


Figure 2.8: Response to initial excitation on $G_x = 1$

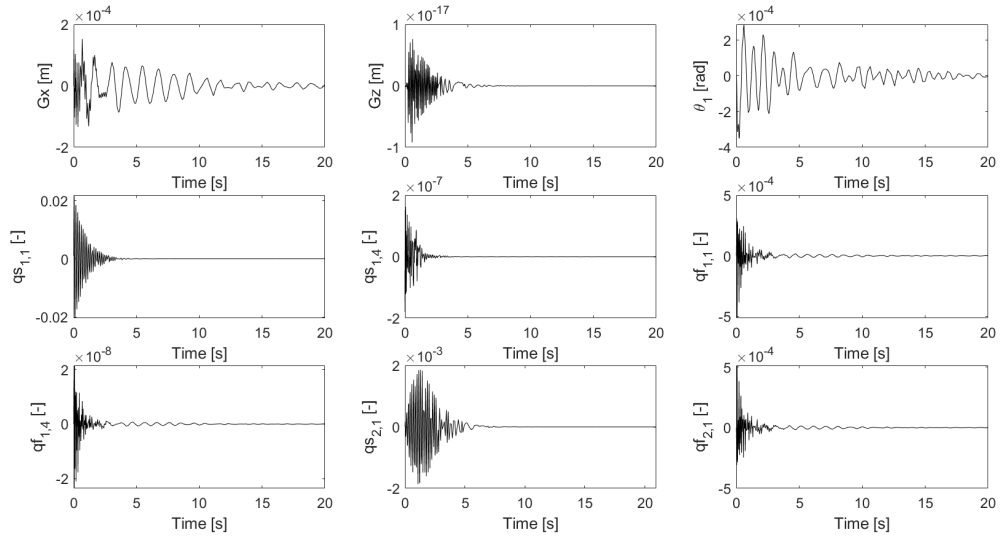


Figure 2.9: Response to initial excitation on $q_{1,1}^s = 1$

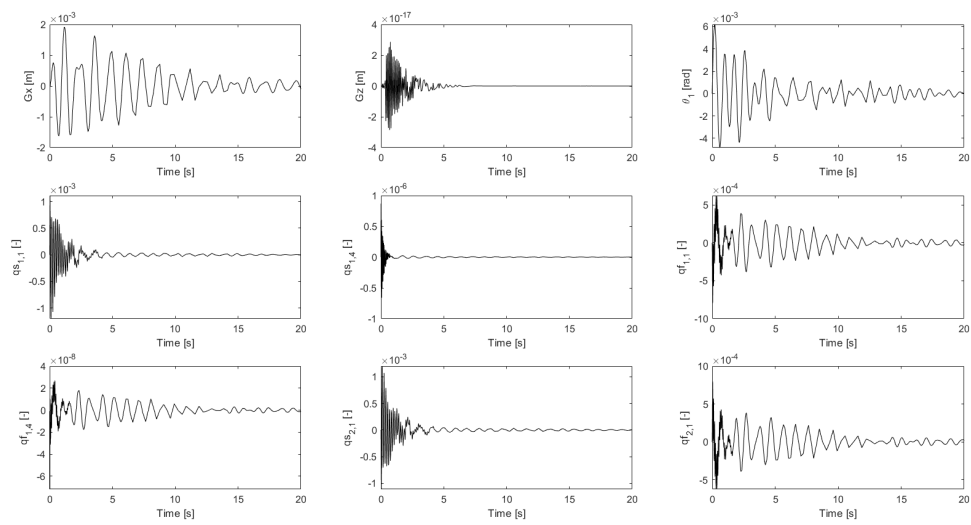


Figure 2.10: Response to initial excitation on $\theta_1 = 0.05$

Chapter 3

Theory of ordinary differential equations with periodic coefficients with applications to deterministic mechanical systems with stochastic input

„Die Devise der Geschichte überhaupt müßte lauten: Eadem, sed aliter. Hat Einer den Herodot gelesen, so hat er, in philosophischer Absicht, schon genug Geschichte studirt. Denn da steht schon Alles, was die folgende Weltgeschichte ausmacht: das Treiben, Thun, Leiden und Schicksal des Menschengeschlechts, wie es aus den besagten Eigenschaften und dem physischen Erdenloose hervorgeht.“

Arthur Schopenhauer, Die Welt als Wille und Vorstellung

The objective of this chapter is to recover the essential results from the theory of ordinary differential equations with periodic coefficients, Floquet theory, and adapt them to the treatment of our subject. The role played by Floquet theory in this sense is an extension of the modal analysis of LTI systems into the LTP domain. Floquet's theorem is the source of what will be called the Floquet modal matrix: a matrix whose columns correspond to Floquet periodic eigenvectors or Floquet periodic modes. Lyapunov's reducibility theorem, connected to Floquet's, is the basis for developing a solution in modal variables. Two parallel but complementary methods are predominant in the study of the free response of LTP systems: a) a class of methods we will refer to as Floquet or Floquet-Lyapunov or direct integration method, which is based in successive integration of the system with appropriate initial conditions to form the state transition matrix, thus characterizing the response of the system; b) a class of methods we will refer to as Hill's, based on developing the periodic matrix of the Floquet system in Fourier series and then formulating an eigenvalue problem that results from the concept of harmonic balance, yielding the Fourier coefficients of the Floquet periodic eigenvectors and by extension the state transition matrix of the system. This chapter will describe both approaches, and their advantages and disadvantages will be contrasted.

Once the modal description of the Floquet system has been established, the goal shifts to the determination of the inhomogeneous or forced response of the Floquet system. Different approaches can be taken to achieve this

goal, and we will explore them in terms of their applicability to the case of stochastic inputs or forces. The convolution solution in the time domain, a viable strategy for LTI systems, will be shown to permit moment propagation when stochastic inputs are considered. Depending on the formulation, the convolution in the Fourier domain will be shown to result in a version of the frequency response or the Power Spectral Density. A third approach will be presented based on recent developments in wavelet analysis and, in many ways, an extension of the Fourier determination of stochastic responses.

First, we will synthesize some key results from deterministic ordinary differential equations as applied to mechanical systems, among these the results concerning the nature of the solution, its modal form, and its behavior. This will allow us to highlight the fundamental differences between linear time-invariant (LTI) systems and linear time-periodic systems (LTP) when the Floquet theory is introduced. We then formulate the characteristics of the solution to a stochastic excitation and discuss the different resolution strategies. The synthesis recovers key results presented in classical works from the literature, such as [87], [105], [44] and [109].

1 Results for LTI systems

The general equation of a forced LTI system is:

$$\mathbf{M}\ddot{\mathbf{x}} + \mathbf{G}\dot{\mathbf{x}} + \mathbf{K}\mathbf{x} = \mathbf{f} \quad (3.1)$$

with $\mathbf{x} = [x_1, x_2, \dots, x_n]^T$, for n Degrees of Freedom (DOF). This equation can be transformed into state form as:

$$\dot{\mathbf{y}} = \mathbf{A}\mathbf{y} + \mathbf{B}\mathbf{f} \quad (3.2)$$

where $\mathbf{y} = [x_1, x_2, \dots, x_n, \dot{x}_1, \dot{x}_2, \dots, \dot{x}_n]^T$ and the reduced order system has dimension $2n$.

Free response When $\mathbf{G} = \mathbf{0}$ and $\mathbf{f} = 0$, the associated free undamped response of Eq. 3.1 can be studied by introducing the assumed form $\mathbf{x} = \Psi^R \exp[st]$, which is nontrivial if [109]:

$$(\mathbf{K} + s^2\mathbf{M})\Psi^R = 0 \quad (3.3)$$

from this eigenvalue problem, one can study the nature of the solutions by analyzing the characteristic equation derived from it:

$$\det[\mathbf{K} + s^2\mathbf{M}] = 0. \quad (3.4)$$

Alternatively, one can formulate a quadratic eigenvalue problem $(s^2\mathbf{M} + s\mathbf{G} + \mathbf{K})\Psi^R = \mathbf{0}$ in the form [44]:

$$\mathbf{U}\Psi^R = \mathbf{V}\Psi^R s \quad \text{or} \quad \mathbf{A}\Psi^R = \Psi^R s \quad (3.5)$$

with $\Psi^R = \begin{bmatrix} \Psi^R \\ \Psi^R s \end{bmatrix}$ and:

$$\mathbf{U} = \begin{bmatrix} \mathbf{0} & \mathbf{K} \\ -\mathbf{K} & -\mathbf{G} \end{bmatrix}; \quad \mathbf{V} = \begin{bmatrix} \mathbf{K} & \mathbf{0} \\ \mathbf{0} & \mathbf{M} \end{bmatrix}; \quad \mathbf{A} = \mathbf{V}^{-1}\mathbf{U}, \quad (3.6)$$

assuming \mathbf{V} is invertible. One arrives at the following characteristic equation:

$$\det[s^2\mathbf{M} + s\mathbf{G} + \mathbf{K}] = 0 \quad (3.7)$$

which gives n pair of poles $s_{[1,2],i} = -\zeta_i\omega_i \pm \sqrt{\zeta_i^2 - 1}\omega_i$, $i \in [1, \dots, n]$ where the ζ_i are the damping factors in the case of a viscous damping model. Stable vibrations are guaranteed if $0 \leq \zeta_i < 1$ and $\omega_i > 0$, in which

case the poles appear in complex conjugate pairs and $\omega_i = |s_i|$, where the ω_i are the natural frequencies¹ of the system.

To each ω_i corresponds an associated right eigenvector Ψ_i^R , and the right modal matrix Ψ^R contains the right eigenvectors as columns. In addition, a set of left eigenvectors Ψ_i^L also corresponds to the same pole s_i , $(\Psi^L)^T (s_i^2 \mathbf{M} + s_i \mathbf{G} + \mathbf{K}) = \mathbf{0}$, leading to the left modal matrix Ψ^L . Then, Ψ^R together with $\Psi^L = \begin{bmatrix} \Psi^L \\ \Psi^L \mathbf{s} \end{bmatrix}$ enabled the diagonalization of \mathbf{A} .

Forced response to an arbitrary excitation The solution of Eq. 3.2 with a general excitation \mathbf{f} can be expressed as:

$$\mathbf{y}(t) = \Phi(t) \mathbf{y}(0) + \int_0^t \Phi(t - \tau) \mathbf{B} \mathbf{f}(\tau) d\tau \quad (3.8)$$

where $\mathbf{y}(0)$ is a vector of initial values (initial conditions), and $\Phi(t)$ is the state transition matrix:

$$\begin{aligned} \Phi(t - \tau) &= \exp[\mathbf{A}(t - \tau)] \\ &= \mathbf{I} + (t - \tau) \mathbf{A} + \frac{(t - \tau)^2}{2!} \mathbf{A}^2 + \dots \end{aligned} \quad (3.9)$$

here $\exp[\mathbf{A}(t - \tau)]$ is to be interpreted as the matrix exponential of the matrix \mathbf{A} . We remark that Eq. 3.8 contains a homogeneous and a particular solution. The homogeneous solution is related to the initial conditions of the problem, while the convolution part of the solution is the forced response:

$$\begin{aligned} \mathbf{y}(t) &= \mathbf{y}_h(t) + \mathbf{y}_f(t) \\ \mathbf{y}_h(t) &= \Phi(t) \mathbf{y}(0) \\ \mathbf{y}_f(t) &= \int_0^t \Phi(t - \tau) \mathbf{B} \mathbf{f}(\tau) d\tau, \end{aligned} \quad (3.10)$$

two additional concepts apply to the characterization of the response of dynamical systems: the transient response and the steady-state response. For a system with damping, the homogeneous response is a part of the transient response and decays to zero as motion evolves. The forced response has transient and steady-state components, the former decaying to zero for damped systems; the steady-state response then is the component that persists from the forced response once the transient part has decayed.

2 Free Response of LTP systems and Floquet modal analysis

We now consider the following equation:

$$\mathbf{M}(t) \ddot{\mathbf{x}} + \mathbf{G}(t) \dot{\mathbf{x}} + \mathbf{K}(t) \mathbf{x} = \mathbf{0} \quad (3.11)$$

where the matrices of the system are such that for a given period T_p : $\mathbf{M}(t + nT_p) = \mathbf{M}(t)$, $n \in \mathbb{Z}$, which can similarly be cast in state form:

$$\dot{\mathbf{y}}(t) = \mathbf{A}(t) \mathbf{y}(t). \quad (3.12)$$

¹Strictly speaking, ω_i is the circular natural frequency; the distinction is important because $f_i = \frac{\omega_i}{2\pi}$ where f_i is an actual frequency: its units are Hertz as opposed to radians per second.

We assume in the sequel that matrix $\mathbf{A}(t)$ has the same period as the matrices of the system. The free response of Eq. 3.12 for an initial condition $\mathbf{y}(0)$ is:

$$\mathbf{y}(t) = \Phi(t, t_0) \mathbf{y}(0) \quad (3.13)$$

where $\Phi(t, \tau)$ is the state transition matrix, now a function of two variables. This solution can be identified as the transient response associated with the initial conditions $\mathbf{y}(0)$.

2.1 Free response and modal analysis: Elements of Floquet theory

The general theory of ordinary differential equations with periodic coefficients is termed Floquet theory. Its subject of study is the following initial value problem (IVP):

$$\dot{\mathbf{y}}(t) = \mathbf{A}(t) \mathbf{y}(t), \mathbf{y}(0) = \mathbf{y}_0, \quad (3.14)$$

where matrix $\mathbf{A}(t)$ is of dimension $n \times n$, it is assumed to be continuous and have minimum period T_p . As in the time-independent case, a solution set of the ODE can be written as the matrix $\mathbf{Y}(t)$ of size $n \times k$ with elements $Y_{i,j}(t)$ $i = 1, \dots, n; j = 1, \dots, k$, every column represents a solution. If $k = n$, then we call $\mathbf{Y}(t)$ a fundamental solution matrix of the ODE. If $\det[\mathbf{Y}(0)] \neq 0$, so the solutions are linearly independent, any other fundamental solution $\mathbf{Y}_1(t)$ can be expressed as a linear combination of the columns of $\mathbf{Y}(t)$: $\mathbf{Y}_1(t) = \mathbf{Y}(t) \mathbf{C}$, with $\mathbf{C} = \mathbf{Y}_1^{-1}(0) \mathbf{Y}(0)$, \mathbf{C} is an $n \times n$ constant matrix; under these conditions we say that $\mathbf{Y}(t)$ constitutes a basis for the vector space of solutions of the ODE.

A particular case of the fundamental solution is one such that $\mathbf{Y}(0) = \mathbf{I}_n$, which we call the Matrizant ([119]) of the system. From this, we can see that using the Matrizant, any fundamental solution matrix can be expressed as: $\mathbf{C} = \mathbf{Y}_1^{-1}(0) \mathbf{Y}(0) = \mathbf{Y}_1^{-1}(0)$, $\mathbf{Y}_1(t) = \mathbf{Y}(t) \mathbf{Y}_1^{-1}(0)$. From the Matrizant, we can obtain any particular solution by applying the initial value: $\mathbf{y}(t) = \mathbf{Y}(t) \mathbf{y}_0$. In a more general sense, we can write the solution in terms of the state transition matrix ([144]), which we note as $\Phi(t, t_0)$, and as with the Matrizant: $\Phi(t_0, t_0) = \mathbf{I}_n$, it also satisfies the differential equation: $\frac{d}{dt} \Phi(t, t_0) = \mathbf{A}(t) \Phi(t, t_0)$. The response of the system with initial condition \mathbf{y}_0 can be written as $\mathbf{y}(t) = \Phi(t, t_0) \mathbf{y}_0$; the state transition matrix merely generalizes the Matrizant in the sense that t_0 is not necessarily 0, although we will adopt this convention throughout the following developments.

The monodromy matrix of the system, in terms of the state transition matrix, is the constant matrix $\Phi(t_0 + T_p, t_0)$; that is, the monodromy matrix is the value of the state transition matrix (or also the Matrizant) at the end of a period. The eigenvalue problem associated with the monodromy matrix:

$$\det[\Phi(t_0 + T_p, t_0) - \mu_n \mathbf{I}_n] = 0 \quad (3.15)$$

yields the n quantities μ_n called Floquet multipliers of the system. The stability of the solutions of the ODE can be established from the analysis of the Floquet multipliers. It's clear from this exposition that the state transition matrix is the key problem in the determination of the solution of the free response of the Floquet system, as it provides access to any particular solution by applying the appropriate initial conditions; the monodromy matrix and with it the Floquet multipliers and the stability of solutions. We will later see how this matrix plays a key role in determining the ODE's forced response.

We now turn to the central results of Floquet theory, which are presented as two separate theorems whose results are complementary to our perspective. The first one, Floquet's theorem, is a statement about the fundamental solution matrices of Floquet systems, and the second one, called Lyapunov reducibility theorem, deals with a change of variable that transforms a Floquet system into an LTI one in new variables.

Floquet's theorem, as stated by [69] reads:

Theorem 2. *Floquet's theorem: Let $\mathbf{Y}(t)$ be a fundamental solution matrix of the Floquet system Eq. 3.14 with period T_Ω , that is, a matrix whose columns are solutions to the system. Then the matrix $\mathbf{Z}(t) = \mathbf{Y}(t + T_p)$ is also a fundamental solution matrix of the Floquet system. There is a function $\mathbf{R}(t)$ of period T_p and a constant matrix $\boldsymbol{\rho}$ such that: $\mathbf{Y}(t) = \mathbf{R}(t) \exp[\boldsymbol{\rho}t]$.*

The Lyapunov reducibility theorem as presented by [119], reads:

Theorem 3. *Lyapunov reducibility theorem: Let $\dot{\mathbf{y}}(t) = \mathbf{A}(t)\mathbf{y}(t)$ be a Floquet system with $\mathbf{A}(t + T_p) = \mathbf{A}(t)$. There exists a non-singular, T_Ω -periodic matrix function $\mathbf{R}(t)$ such that the substitution:*

$$\mathbf{y}(t) = \mathbf{R}(t)\mathbf{q}(t) \quad (3.16)$$

transforms $\dot{\mathbf{y}}(t) = \mathbf{A}(t)\mathbf{y}(t)$ to:

$$\dot{\mathbf{q}}(t) = \boldsymbol{\rho}\mathbf{q}(t), \quad (3.17)$$

where $\boldsymbol{\rho}$ is a constant matrix.

From theorem 2 and with the fact that $\mathbf{y}(t) = \mathbf{Y}(t)\mathbf{y}_0$, we obtain:

$$\begin{aligned} \mathbf{Y}(t) &= \mathbf{R}(t) \exp[\boldsymbol{\rho}t] \\ \mathbf{Y}(t)\mathbf{y}_0 &= \mathbf{R}(t) \exp[\boldsymbol{\rho}t]\mathbf{y}_0 \\ \mathbf{y}(t) &= \mathbf{R}(t) \exp[\boldsymbol{\rho}t]\mathbf{y}_0, \end{aligned} \quad (3.18)$$

to visualize the implication of this result and of theorem 3, let us consider an example. $\mathbf{y}(t) = y_i, i = 1, \dots, n$, the matrix $\mathbf{R}(t) = R_{i,j}, i, j = 1, \dots, n$. Each component of the solution then has the form:

$$y_i(t) = \sum_j R_{i,j}(t) \exp[\boldsymbol{\rho}_j t] y_{0,j} \quad (3.19)$$

in words, each component is a sum of terms modulated by periodic coefficients of the matrix $\mathbf{R}(t)$. The matrix $\mathbf{R}(t)$ is the basis of our extension of LTI modal analysis; we will refer to it as Floquet modal matrix and its columns as Floquet periodic modes or simply Floquet modes. Before focusing on this matrix, we focus first on the expressions $\exp[\boldsymbol{\rho}t]$ and $\boldsymbol{\rho}$ in both preceding theorems.

Matrix Exponential and Jordan Canonical Form The development here synthesizes the result in [69] to adapt it to our situation.

Suppose Φ_0 is a $n \times n$ constant matrix. There is a nonsingular $n \times n$ matrix \mathbf{P} such that $\Phi_0 = \mathbf{P}\boldsymbol{\mu}\mathbf{P}^{-1}$, where $\boldsymbol{\mu}$ is either: a) diagonal if the eigenvalues of Φ_0 are unique, with the eigenvalues in its main diagonal, b) block diagonal if Φ_0 has repeated eigenvalues.

Suppose Φ_0 is a nonsingular $n \times n$ matrix. Then, there is a matrix $\boldsymbol{\rho}$ such that: $\exp[\boldsymbol{\rho}] = \Phi_0$. Here $\boldsymbol{\rho}$ is said to be the matrix logarithm of matrix Φ_0 . We have the following cases:

1. If Φ_0 is diagonal with μ_i distinct elements along the diagonal, then $\rho_{i,i} = \ln[\mu_i]$ and $\rho_{i,j} = 0, i \neq j$, $\exp[\boldsymbol{\rho}] = \Phi_0$
2. If Φ_0 is upper triangular with repeated μ_1 elements along the main diagonal and 1 in the upper entry, then $\rho_{i,i} = \ln[\mu_1]$ and its upper element is $\frac{1}{\mu_1}$, $\exp[\boldsymbol{\rho}] = \Phi_0$
3. If Φ_0 is an arbitrary matrix, then $\Phi_0 = \mathbf{P}\boldsymbol{\mu}\mathbf{P}^{-1}$, and $\boldsymbol{\mu}$ is either diagonal or in Jordan Canonical Form, so the previous two cases apply to $\boldsymbol{\mu}$: $\exp[\boldsymbol{\rho}^*] = \boldsymbol{\mu}$ and ultimately: $\boldsymbol{\rho} = \mathbf{P}\boldsymbol{\rho}^*\mathbf{P}^{-1}$ so $\Phi_0 = \mathbf{P}\exp[\boldsymbol{\rho}^*]\mathbf{P}^{-1}$.

These results can be applied to the main result in theorem 2 as follows: suppose $\Phi(t, t_0)$ is a fundamental solution matrix, then one can express $\Phi(t + T_p, t_0)$ as $\Phi(t + T_p, t_0) = \Phi(t, t_0)\Phi(t_0 + T_p, t_0)$, where $\Phi(t_0 + T_p, t_0)$ is the monodromy matrix, now $\Phi(t_0 + T_p, t_0) = \exp[\boldsymbol{\rho}T_p]$, defining $\mathbf{R}(t) = \Phi(t, t_0)\exp[-\boldsymbol{\rho}t]$ we have: $\Phi(t, t_0) =$

$\Phi(t, t_0) \exp[-\boldsymbol{\rho}t] \exp[\boldsymbol{\rho}t] = \Phi(t, t_0)$. Additionally, since the eigenvalues of $\Phi(t + T_p, t_0)$ are the Floquet multipliers μ_i , we find the following quantities:

$$\begin{aligned}\Phi(t_0 + T_p, t_0) &= \mathbf{R}(0) \exp[\boldsymbol{\rho}T_p] \mathbf{R}^{-1}(0) \\ \rho_i &= \frac{1}{T_p} \ln[\mu_i]\end{aligned}\quad (3.20)$$

these are known as Lyapunov Characteristic exponents. In the following, we will note $\mathbf{R}^{-1}(t) = \mathbf{L}(t)$ as the left periodic modes. Considering now theorem 3: $\mathbf{y}(t) = \mathbf{R}(t) \mathbf{q}(t)$ and

$$\begin{aligned}\dot{\mathbf{y}}(t) &= \dot{\mathbf{R}}(t) \mathbf{q}(t) + \mathbf{R}(t) \dot{\mathbf{q}}(t) \\ \dot{\mathbf{q}}(t) &= (\mathbf{L}(t) \mathbf{A}(t) \mathbf{R}(t) - \mathbf{L}(t) \dot{\mathbf{R}}(t)) \mathbf{q}(t) \\ \dot{\mathbf{q}}(t) &= \boldsymbol{\rho} \mathbf{q}(t)\end{aligned}\quad (3.21)$$

with $\boldsymbol{\rho} = (\mathbf{L}(t) \mathbf{A}(t) \mathbf{R}(t) - \mathbf{L}(t) \dot{\mathbf{R}}(t))$, this is the modal LTI form of the corresponding Floquet system on the new modal variables $\mathbf{q}(t)$. If the monodromy matrix has distinct eigenvalues, that is, if the system has distinct Floquet multipliers, then the Lyapunov transformation not only reduces the system to an LTI one, but $\boldsymbol{\rho}$ is also diagonal so the modal equations are also decoupled.

Some commentary about this development is in place. First, notice that since $\mathbf{R}(t) = \Phi(t, t_0) \exp[-\boldsymbol{\rho}t]$ and the convention has been adopted that $\Phi(t_0, t_0) = \mathbf{I}_n$, it follows that $\mathbf{R}(t_0) = \Phi(t_0, t_0) = \mathbf{I}_n = \mathbf{L}(t_0)$ we adopt as a convention that the Floquet modal matrix of left and right periodic modes reduce to the identity matrix in the extremes of a period $\mathbf{R}(t_0) = \mathbf{R}(t_0 + T_p) = \mathbf{I}_n$, $\mathbf{L}(t_0) = \mathbf{L}(t_0 + T_p) = \mathbf{I}_n$. If this condition is not adopted, then one has: $\Phi(t, t_0) = \mathbf{R}(t) \exp[\boldsymbol{\rho}t] \mathbf{L}(t_0)$, which in t_0 yields $\mathbf{I}_n = \mathbf{R}(t_0) \mathbf{I}_n \mathbf{L}(t_0)$, in other words, the normalization condition for the eigenvectors becomes $\mathbf{R}(t_0) \mathbf{L}(t_0) = \mathbf{I}_n$. This second condition is sometimes more convenient, given the fact that the $\mathbf{R}(t)$, $\mathbf{L}(t)$ pairs are often complex so one need not impose that they are real and unit for conditioning. Second, the Floquet multipliers are not, in general, positive real numbers, so the logarithm involved in the computation of the Characteristic Exponents is a complex function. The complex logarithm is such that:

$$\ln[\mu_i] = \ln|\mu_i| + i(\arg[\mu_i] + 2\pi n), n \in \mathbb{Z}, \mu_i \in \mathbb{C} \quad (3.22)$$

where $|\mu_i|$ is the absolute value of the complex number; so the imaginary part of the logarithm is defined up to an addition of n times the factor 2π . Consequently:

$$\rho_i = \frac{\ln|\mu_i|}{T_p} + i \frac{\arg[\mu_i] + 2\pi n}{T_p}, n \in \mathbb{Z}, \mu_i \in \mathbb{C} \quad (3.23)$$

we will work with the principal value of the logarithm unless otherwise specified, but this ambiguity will be instrumental in the discussion around Hill's method in the next section. Third, a conclusion on the homogeneous solution of the Floquet system under consideration is that the form: $\mathbf{y} = \mathbf{r}(t) \exp[\boldsymbol{\rho}t]$ provides the desired generalization to the LTI methodology, an approach that has been applied effectively in works such as [144],[151] and [22].

The developments in this section suggest a straightforward methodology for the characterization of the homogeneous response of an LTP system:

1. Select n linearly independent initial conditions, such as \mathbf{I}_n .
2. Solve Eq. 3.13 n times, subject to each set of initial conditions on the interval $[0, T_p]$; this can be done using numerical integration for complex systems and is a highly parallelizable process.

3. Form the monodromy matrix from the computed solutions at the end of the interval.
4. Solve the eigenvalue problem associated with the monodromy matrix to find the Floquet multipliers.
5. Use Eq. 3.23 to compute the characteristic exponents.
6. Use $\mathbf{R}(t) = \Phi(t, t_0) \exp[-\boldsymbol{\rho}t]$ and $\mathbf{R}^{-1}(t) = \mathbf{L}(t)$ to compute the periodic eigenvectors.

From this procedure, the stability of the solutions can be assessed, as remarked in Chapter 1; the behavior of the periodic eigenvectors can also be analyzed. An alternative method is widely used for this analysis, introduced in reference [54]. We proceed now to summarize this approach.

2.2 Hill's method for modal analysis of LTP systems

The modern form of Hill's method consists of expanding the system's matrix and modal solutions in Fourier series and then formulating the corresponding eigenvalue problem in terms of the corresponding Fourier coefficients. The coefficients of $\mathbf{A}(t)$ are known quantities, while the unknowns are the characteristic exponents (the eigenvalues) and the Fourier coefficients of the periodic modes. The method circumvents the successive integration step required in the Floquet-Lyapunov approach and provides a spectral description of the periodic eigenvectors. One of the drawbacks comes in the form of the multiplicity of the solutions obtained, which we will show to be related to the apparent ambiguity in the determination of the characteristic exponents described in the previous section. Another limitation comes from the error incurred in the truncation of the infinite Fourier series for the implementation, which can lead to deviations in some sets of the computed exponents. These two problems are subject to active investigation in different domains: different sorting criteria for the eigenvalues and eigenvectors have been proposed [14] and [51] discuss the criteria in the field of tidal turbines, while [7] proposes a sort-free implementation of Hill's approach based on Koopman theory in the context of nonlinear systems, also discussing issues of discretization error and computational cost of this sorting process.

First, $\mathbf{A}(t)$ in Eq. 3.12 is expanded in Fourier series:

$$\mathbf{A}(t) = \sum_{a=-\infty}^{+\infty} \mathbf{A}_a \exp[i(2\pi fa)t], \quad (3.24)$$

where \mathbf{A}_a is a matrix of Fourier coefficients at the harmonic a . Next, a modal fundamental solution is assumed and expressed in terms of Fourier series :

$$\begin{aligned} \mathbf{Y}_k(t) &= \mathbf{R}_k(t) \exp[\rho_k t] \\ \mathbf{R}_k(t) &= \sum_{j=-\infty}^{+\infty} \mathbf{R}_{k,j} \exp[i(2\pi f_j)t] \\ \dot{\mathbf{Y}}_k(t) &= \mathbf{R}_k(t) \frac{d}{dt} [\exp[\rho_k t]] + \dot{\mathbf{R}}_k(t) \exp[\rho_k t] \\ \frac{d}{dt} [\exp[\rho_k t]] &= \rho_k \exp[\rho_k t] \\ \dot{\mathbf{R}}_k(t) &= \left(\sum_{j=-\infty}^{+\infty} (i(2\pi f_j)) \mathbf{R}_{k,j} \exp[i(2\pi f_j)t] \right), \end{aligned} \quad (3.25)$$

where the subindex k denotes the corresponding mode, for instance, $\mathbf{R}_k(t)$ is the k -th column vector of the Floquet modal matrix. This allows the formulation of an eigenproblem on the Fourier coefficients, substituting Eq. 3.24 and Eq. 3.25 in Eq. 3.12:

$$\rho_k \sum_{j=-\infty}^{+\infty} \mathbf{R}_{k,j} + \sum_{j=-\infty}^{+\infty} (i(2\pi f j)) \mathbf{R}_{k,j} - \left(\sum_{a=-\infty}^{+\infty} \mathbf{A}_a \right) \left(\sum_{j=-\infty}^{+\infty} \mathbf{R}_{k,j} \right) = 0, \quad (3.26)$$

here the $\mathbf{R}_k(t)$ are $n \times 1$ vectors, \mathbf{A}_a are $n \times n$ matrices, and the ρ_k are the corresponding characteristic exponents. This can be cast into a hyper-eigenvalue problem of infinite dimension by applying harmonic balance ([151],[22]). In practice, this requires truncation to be applied, which leads to the following expression:

$$(\rho_k \mathbf{I}_n - \mathbf{W}) \mathbf{R}_{k,j} = \mathbf{0}, \quad (3.27)$$

where the matrix \mathbf{W} has the structure (different presentations with similar results in [144],[7], [49] to cite a few):

$$\mathbf{W} = \begin{pmatrix} \dots & \dots & \dots & \dots & \dots & \dots & \dots \\ \dots & \mathbf{A}_0 - i2\pi(2f) \mathbf{I}_n & \mathbf{A}_1 & \mathbf{A}_2 & \mathbf{A}_3 & \mathbf{A}_4 & \dots \\ \dots & \mathbf{A}_{-1} & \mathbf{A}_0 - i2\pi f \mathbf{I}_n & \mathbf{A}_1 & \mathbf{A}_2 & \mathbf{A}_3 & \dots \\ \dots & \mathbf{A}_{-2} & \mathbf{A}_{-1} & \mathbf{A}_0 & \mathbf{A}_1 & \mathbf{A}_2 & \dots \\ \dots & \mathbf{A}_{-3} & \mathbf{A}_{-2} & \mathbf{A}_{-1} & \mathbf{A}_0 + i2\pi f \mathbf{I}_n & \mathbf{A}_1 & \dots \\ \dots & \mathbf{A}_{-4} & \mathbf{A}_{-3} & \mathbf{A}_{-2} & \mathbf{A}_{-1} & \mathbf{A}_0 + i2\pi(2f) \mathbf{I}_n & \dots \\ \dots & \dots & \dots & \dots & \dots & \dots & \dots \end{pmatrix} \quad (3.28)$$

for each eigenvalue ρ_k of $\boldsymbol{\rho}$, there is a modal vector of Fourier coefficients $\mathbf{R}_{k,j}$ from which the modal matrix \mathbf{R}_j can be constructed as $\mathbf{R} = \mathbf{R}_{k,j}$, where j denotes the corresponding Fourier expansion term, and k correspond to the given Floquet periodic mode. The previous approach, when adapted for the initial conditions in the physical system $\mathbf{x}(t_0) = \mathbf{x}_0$ ([151]):

$$\begin{aligned} \mathbf{b}_0 &= \exp[-\boldsymbol{\rho} t_0] \mathbf{L}(t_0) \mathbf{x}_0 \\ \Phi(t, t_0) &= \mathbf{R}(t) \exp[\boldsymbol{\rho} t] \mathbf{L}(t_0) \\ \mathbf{x}(t) &= \mathbf{R}(t) \exp[\boldsymbol{\rho} t] \mathbf{b}_0 \end{aligned} \quad (3.29)$$

provides an expression that allows for the study of the modal behavior of the system.

If $n_j = 2n_H + 1$ terms are considered in the truncated Fourier series, where n_H is the largest harmonic integer, the size of \mathbf{W} in Eq. 3.28 is $(n_H + 1)n \times (n_H + 1)n$, which will result in $(n_H + 1)$ sets of n eigenvalues that approximate the characteristic exponents, and the corresponding sets of eigenvectors. The difference of the eigenvalues between sets is, as expected, in the imaginary part up to an integer multiple of $2\pi k, k \in \mathbb{Z}$. So we will note $\boldsymbol{\Lambda}_l = \{\rho_{k_l}\}$ the set of n characteristic exponents ρ_{k_l} for which the imaginary part is $\rho_k^0 + 2\pi l$, where ρ_k^0 corresponds to the principal value of the corresponding logarithm in Eq. 3.23 as defined in the previous subsection. As discussed in [100], this unintuitive fact about the Hill solution has resulted in some misunderstanding on the interpretation of the Floquet periodic eigenvectors and their associated eigenvalues. All sets are, in principle, equally valid to describe the Floquet modal response (and stability); the main consideration that applies concerns the potential numerical error inherent to the truncation of the associated Fourier series. The choice of $\boldsymbol{\Lambda}_l$ becomes a matter of convenience.

An interesting result from the previous development can be arrived at using Eq. 3.23 and the expression:

$$\mathbf{R}(t) = \Phi(t, t_0) \exp[-\boldsymbol{\rho} t], \quad (3.30)$$

considering the two sets $\boldsymbol{\Lambda}_0$ and $\boldsymbol{\Lambda}_m$ and their associated Floquet modal matrices: $\mathbf{R}^{(0)}$ and $\mathbf{R}^{(m)}$. Rewriting ρ_k in the form $\rho_k = \alpha_k + i\sigma_k$, we arrive at:

$$\begin{aligned}
\rho_{k_0} &= \frac{\ln |\mu_i|}{T_p} + i \frac{\arg [\mu_i]}{T_p} \\
\alpha_{k_0} &= \frac{\ln |\mu_i|}{T_p} \\
\sigma_{k_0} &= \frac{\arg [\mu_i]}{T_p}
\end{aligned} \tag{3.31}$$

for \mathbf{A}_0 , while for \mathbf{A}_m :

$$\begin{aligned}
\rho_{k_m} &= \frac{\ln |\mu_i|}{T_p} + i \frac{\arg [\mu_i] + 2\pi m}{T_p} \\
\alpha_{k_m} &= \frac{\ln |\mu_i|}{T_p} \\
\sigma_{k_m} &= \frac{\arg [\mu_i] + 2\pi m}{T_p}
\end{aligned} \tag{3.32}$$

this implies that $\alpha_{k_0} = \alpha_{k_m}$, and $\sigma_{k_m} = \sigma_{k_0} + \frac{2\pi m}{T_p}$, so we have the exponential expressions:

$$\begin{aligned}
\exp[\rho_0 t] &= \exp[(\alpha_{k_0} + i\sigma_{k_0})t] \\
\exp[\rho_{k_m} t] &= \exp\left[\left(\alpha_{k_0} + i\left(\sigma_{k_0} + \frac{2\pi m}{T_p}\right)\right)t\right] \\
\exp[\rho_{k_m} t] &= \exp[\rho_0 t] \exp\left[i\frac{2\pi m}{T_p}t\right],
\end{aligned} \tag{3.33}$$

this change in phase (or argument) $\Theta(m) = \exp\left[i\frac{2\pi m}{T_p}t\right]$ reflects on the eigenvectors of \mathbf{A}_m :

$$\mathbf{R}^{(m)} = \mathbf{R}^{(0)} \Theta(m), \tag{3.34}$$

higher choices of m lead to higher frequency Floquet modal eigenvectors. This will be illustrated in the examples of this section.

Another aspect of the modal representation of the solution in terms of Fourier series is based on Parseval or Plancherel's theorems, which pertain to the power of the associated eigenvectors. The Floquet modal matrix has the following components:

$$\mathbf{R}(t) = R_{i,j}(t), i, j = 1, \dots, n \tag{3.35}$$

where i describes the corresponding degree of freedom associated, and j describes the corresponding mode. For each of these functions we have:

$$\int_0^{T_p} |R_{i,j}(t)|^2 \approx \sum_{k=-n_H}^{n_H} |R_{(i,j),k}|^2 \tag{3.36}$$

where $R_{(i,j),k}$ is the k -th Fourier coefficient of $R_{i,j}(t)$; this expression describes the power of the component of the modal matrix. Since $\mathbf{R}(t_0) = \mathbf{I}_n$ is a consequence of the initial normalization selected for the state transition matrix, one can think about introducing an initial energy on a given degree of freedom in each mode, in which

case one may think about describing the distribution of this initial energy among the other degrees of freedom in each mode. A participation factor can be introduced as follows:

$$\begin{aligned}\|R_{i,j}\|^2 &\approx \sum_{k=-n_H}^{n_H} |R_{(i,j),k}|^2 \\ D_j &= \sum_i \|R_{i,j}\|^2 \\ \Psi_{i,j} &= \frac{\|R_{i,j}\|^2}{D_j},\end{aligned}\tag{3.37}$$

this factor gives the fraction of energy in the degree of freedom i in mode j from the total energy in the mode D_j . Similarly, one can define the modal participation factor ([100]) :

$$\begin{aligned}E_{i,j} &= \sum_{k=-n_H}^{n_H} |R_{(i,j),k}|^2 \\ \phi_{(i,j),k} &= \frac{|R_{(i,j),k}|^2}{E_{i,j}}\end{aligned}\tag{3.38}$$

which gives the relative magnitude of the k -th harmonic in the expansion of a component $R_{i,j}$.

A major drawback of this formulation can be highlighted if we consider the form of the solution in the state variables \mathbf{y} . As stated earlier:

$$y_i = \sum_j R_{i,j}(t) \exp[\rho_j t] y_{0,j}\tag{3.39}$$

this expression makes it clear that the response of Eq. 3.12 consists of a sum of harmonic terms $\exp[\rho_j t]$ modulated by the periodic functions $R_{i,j}(t)$. This suggests that the y_i are nonstationary signals, and in the stochastic analysis of the system, it will be shown that this feature results in a nonstationary response. The Fourier representation does not provide any information about the time-evolution of the frequency content that characterizes nonstationary signals, and for the stochastic case, one arrives at the necessity of expanding the traditional definitions and descriptions of quantities such as the PSD. Time-frequency representations have been an intense subject of study for both deterministic and stochastic phenomena. References such as [11] provide an in-depth treatment of the classic results in the field from the signal processing perspective, and [116] similarly for nonstationary processes.

An approach that has gained much traction in the treatment of nonstationary signals and processes is based on wavelet analysis. The classic text [95] provides an introduction to wavelet analysis as applied to mechanical vibrations and the family of wavelets introduced by Newland; the Harmonic wavelets have been applied to different classes of problems with great efficacy, for instance, eigenvalue problems of integral equations ([18]) and to transient response determination of time-varying mechanical systems ([150]). In references [129] and [73], the Periodized Generalized Harmonic wavelet (PGHW) is used in the characterization of the response of mechanical systems, linear and nonlinear, respectively, with stochastic inputs. The latter of these references addresses the subject of PSD estimation with this wavelet basis. More recently, in [50] the PGHW has been applied through a Galerkin approach to study the response of rotor-blade systems with nonlinear components and stochastic nongaussian nonstationary inputs.

2.3 PGHW representation of Floquet modes: change of basis approach

The central idea of this subsection is to capitalize on the time-frequency and multi-scale properties of the PGHW basis to analyze the candidate Floquet eigenvectors that emerge in Hill's or Floquet's method. The formulation

of the equivalent eigenvalue problem Eq. 3.27 in the wavelet series expansion is possible but numerically challenging. To address this issue, we rely on a theoretical result from Hilbert bases on a Hilbert space, using the fact that both the Fourier basis and the PGHW basis are Hilbert bases over the vector space of functions defined on $[0, T]$. The PGHW basis vectors have the interesting property of being periodic in the temporal interval over which they have been defined, which is one of the motivations for choosing this particular family of wavelets to study the modal properties of LTP systems given the knowledge that the modes in the sense of Floquet are periodic functions.

Periodic Generalized Harmonic wavelets and time-frequency representation The Periodic Generalized Harmonic wavelet (PGHW) of scale parameter j and translation parameter k in the $[0, T]$ interval is :

$$\begin{aligned}\Psi_{j,k}(t) &= \frac{1}{N_t} \sum_{j=m_j}^{n_j-1} \exp \left[i(2\pi f j) \left(t - \frac{kT}{N_t} \right) \right] \\ &= \frac{1}{N_t} \sum_{j=m_j}^{n_j-1} \exp [i(2\pi f j)t] \exp \left[-i(2\pi f j) \frac{kT}{N_t} \right] \\ &= \frac{1}{N_t} \sum_{j=m_j}^{n_j-1} w_{j,k} \exp [i(2\pi f j)t]\end{aligned}\quad (3.40)$$

where $w_{j,k} = \exp \left[-i(2\pi f j) \frac{kT}{N_t} \right]$ can be interpreted as a weight coefficient (or as a localization window in the time-frequency representation), the sum in j is over a set of integers such that $n_j - m_j = N_t$, where N_t is the corresponding scale number; $f = \frac{2\pi}{T}$; the parameter $k \in [0, 1, \dots, N_t]$; and the following relationship applies: $N = 2N_t N_j$ where N is the number of sampling points in $[0, T]$ and N_t is the bandwidth of each scale (here taken uniform for each scale).

The inner product of a given function $g(t)$ and the PGHW basis can be obtained using the wavelet transform:

$$\begin{aligned}G_{j,k} &= \frac{N_t}{T} \int_0^T g(t) \bar{\Psi}_{j,k}(t) dt \\ &= \langle g(t), \bar{\Psi}_{j,k}(t) \rangle\end{aligned}\quad (3.41)$$

where $G_{j,k}$ is the corresponding wavelet coefficient. This allows the approximation of $g(t)$ through a PGHW-Fourier series of the form:

$$\begin{aligned}g(t) &= \sum_j \sum_k G_{j,k} \Psi_{j,k}(t) + \sum_j \sum_k \tilde{G}_{j,k} \bar{\Psi}_{j,k}(t) \\ &= \sum_j \sum_k (G_{j,k} \Psi_{j,k}(t) + \tilde{G}_{j,k} \bar{\Psi}_{j,k}(t))\end{aligned}\quad (3.42)$$

where $\bar{\Psi}_{j,k}(t)$ stands for the complex conjugate of $\Psi_{j,k}(t)$, and $\tilde{G}_{j,k} = \langle g(t), \Psi_{j,k}(t) \rangle^2$.

The following result can be seen as a corollary to theorem 7.17 in [128].

Theorem 4. *Change of basis on Hilbert spaces.*

Let $\{E_i, i \in \mathbb{Z}\}$ and $\{B_i, i \in \mathbb{Z}\}$ be two orthonormal Hilbert bases on V . For a given $u \in V$, then $u = \sum_{i \in \mathbb{Z}} U_i^E E_i$, and $u = \sum_{i \in \mathbb{Z}} U_i^B B_i$, then:

²Notice that if $g(t)$ is a real function, then $\tilde{G}_{j,k} = \bar{G}_{j,k}$ given the properties of the inner product, but in this investigation, functions with complex values play a key role, and so the distinction will be maintained.

$$U_i^B = \sum_{j \in \mathbb{Z}} F_{i,j} U_j^E \quad (3.43)$$

with $F_{i,j} = \langle E_j, B_i \rangle$.

Proof. First, from (v) in [128] one has: $U_i^B = \langle u, B_i \rangle$. Then, from (vi) :

$$\langle u, B_i \rangle = \sum_{j \in \mathbb{Z}} \langle u, E_j \rangle \langle B_i, E_j \rangle, \quad (3.44)$$

and finally from (v):

$$U_i^E = \langle u, E_i \rangle \quad (3.45)$$

so:

$$\begin{aligned} \langle u, B_i \rangle &= \sum_{j \in \mathbb{Z}} U_j^E \langle B_i, E_j \rangle \\ U_i^B &= \sum_{j \in \mathbb{Z}} U_j^E \langle B_i, E_j \rangle \\ F_{i,j} &= \langle B_i, E_j \rangle. \end{aligned}$$

□

In words, given the series expansion of a function $g(t)$ in a Hilbert basis $\{E_i, i \in \mathbb{Z}\}$ with the associated generalized Fourier coefficient G_i^E given by the inner product $G_i^E = \int_{-\infty}^{\infty} g(t) E_i^* dt$, it is possible to define a change of basis to another Hilbert basis $\{B_i, i \in \mathbb{Z}\}$. This change of basis is equivalent to determining the generalized Fourier coefficients G_i^B in the new basis, which can be achieved through the change of basis matrix $F_{i,j}$.

The previous result allows us to circumvent the formulation and resolution of the eigenvalue problem on the PGHW basis. The classic Hill method is applied to obtain the Floquet periodic eigenvector candidates, and these are projected into the PGHW basis from where a time-frequency representation of each mode can be easily constructed employing the scalogram of the wavelet functions.

Choosing $\{E_i, i \in \mathbb{Z}\}$ as the Fourier basis: $E_n(t) = \exp[i(2\pi fn)t]$ with the inner product:

$$\begin{aligned} \langle g(t), E_n \rangle &= \int_{-\infty}^{\infty} g(t) E_n^* dt \\ &= \int_0^T g(t) E_n^* dt, \end{aligned} \quad (3.46)$$

where $g(t)$ is defined on $[0, T]$ and E_n^* is the complex conjugate of E_n , and we note $G_i^E = \langle g(t), E_i \rangle$. Similarly, choosing $\{B_i, i \in \mathbb{Z}\}$ as the PGHW basis $\Psi_{j,k}(t) = \frac{1}{N_i} \sum_{j=m_j}^{n_j-1} w_{j,k} \exp[i(2\pi f_j)t]$, with inner product:

$$\begin{aligned} \langle g(t), B_n \rangle &= \int_{-\infty}^{\infty} g(t) B_n^* dt \\ &= \int_0^T g(t) B_n^* dt, \end{aligned} \quad (3.47)$$

and $G_i^B = \langle g(t), B_i \rangle$.

For the determination of matrix $F_{i,j}$, we have:

$$\begin{aligned} E_n(t) &= \exp[i(2\pi fn)t] \\ E_{-n}(t) &= \bar{E}_n(t) \end{aligned} \quad (3.48)$$

for Fourier, and:

$$\begin{aligned} B_{p,q}(t) &= \frac{1}{N_t} \sum_{l=m_p}^{n_p-1} w_{l,q} \exp[i(2\pi fl)t] \\ B_{-p,q}(t) &= \bar{B}_{p,q}(t), \end{aligned} \quad (3.49)$$

for the PGHW, the inner products read:

$$F_{i,j,k}^B = \langle E_i(t), B_{j,k}(t) \rangle, \quad (3.50)$$

for instance:

$$\begin{aligned} \langle E_n(t), B_{p,q}(t) \rangle &= \frac{N_t}{T} \int_0^T \exp[i(2\pi fn)t] \bar{\Psi}_{p,q}(t) dt \\ &= \frac{N_t}{T} \int_0^T \exp[i(2\pi fn)t] \frac{1}{N_t} \sum_{l=m_p}^{n_p-1} w_{l,q} \exp[i(2\pi fl)t] dt \\ &= \frac{1}{T} \int_0^T \sum_{l=m_p}^{n_p-1} w_{l,q} \exp[i(2\pi f(l+n))t] dt \end{aligned} \quad (3.51)$$

so we may write:

$$\begin{cases} \langle E_n(t), B_{p,q}(t) \rangle = \frac{1}{T} \sum_{l=m_p}^{n_p-1} w_{l,q} \frac{(\exp[i(2\pi f(n+l))T] - 1)}{i(2\pi f(n+l))} & n+l \neq 0 \\ \langle E_n(t), B_{p,q}(t) \rangle = \frac{1}{T} \sum_{l=m_p}^{n_p-1} w_{l,q} T & n+l = 0 \end{cases} \quad (3.52)$$

from here $F_{i,j,k}^B$ can be assembled.

The development in this subsection then suggests the following method of analysis:

1. Apply Hill's method as described in subsection 2.2, obtaining \mathbf{A}_l sets of eigensolutions.
2. Select the corresponding PGHW parameters to define the associated PGHW basis.
3. Compute the transformation matrix between the Fourier and the PGHW bases $F_{i,j,k}^B$.
4. Transform the Fourier coefficients associated to the \mathbf{A}_l set under analysis into the PGHW coefficients using $F_{i,j,k}^B$.
5. Compute the desired quantities of analysis using the PGHW coefficients: the wavelet scalogram is a time-frequency representation of the power of the modes; the stochastic section will illustrate how this approach can be used to approximate the evolutive PSD of a nonstationary process.

This approach can be, in principle, combined with the idea central to the reference [100] to analyze not only the eigenvectors but the frequency content of the complete solution of the ODE. Additionally, the PGHW coefficients open new approaches to study the forced response of the system, for instance, the wavelet-Galerkin method or the wavelet-transmissibility spectral method explored in reference [31] which extends the LTI concept of transmissibility (and frequency response) to time-varying systems using wavelet transform.

Exponent	Hill	Analytic	Deviation
ρ^{-2}	0.5 - 3.9685i	0.5 - 4i	Re = 0, Im = 3.1499×10^{-2}
ρ^{-1}	0.5 - 2.0002i	0.5 - 2.0000i	Re = 0, Im = 2.4934×10^{-4}
ρ^0	0.5 + 0i	0.5 + 0i	Re = 0, Im = 0
ρ^1	0.5 + 2.0002i	0.5 + 2.0000i	Re = 0, Im = 2.4934×10^{-4}
ρ^2	0.5 + 3.9685i	0.5 + 4i	Re = 0, Im = 3.1499×10^{-2}

Table 3.1: Candidate characteristic exponents by Hill method for example 1

2.4 Selected examples

Example 1 From [69], consider the (scalar) Floquet system :

$$\begin{aligned} \dot{y} &= A(t)y \\ A(t) &= \sin^2[\Omega t] \end{aligned} \quad (3.53)$$

with $\Omega = 1$ and smallest period $T_p = \pi$. The general solution is: $y = c \exp\left[\frac{1}{2}t\right] \exp\left[-\frac{1}{4} \sin[2t]\right]$ where c is an arbitrary constant. By Floquet's theorem, we can see that: $R(t) = c \exp\left[-\frac{1}{4} \sin[2t]\right]$ is a periodic eigenvector. By identification $\exp[\rho t] = \exp\left[\frac{1}{2}t\right]$ so, the characteristic exponent is $\rho^0 = \frac{1}{2}$.

From the developments in this chapter, we have the following:

- with $m = 1$ and $\alpha_1 = \alpha_0 = \frac{1}{2}$, $\sigma_1 = \sigma_0 + \frac{2\pi}{\pi} = 2$ so $\rho^1 = \frac{1}{2} + i2$ is also a Floquet exponent,
- with $m = -1$ and $\alpha_1 = \alpha_0 = \frac{1}{2}$, $\sigma_1 = \sigma_0 - \frac{2\pi}{\pi} = -2$ so $\rho^{-1} = \frac{1}{2} - i2$ is also a Floquet exponent,
- $\Theta(1) = \exp[i2t]$ so $R^{(1)}(t) = c \exp\left[-\frac{1}{4} \sin[2t]\right] \Theta(1)$ is the periodic eigenvector associated to ρ^1 ,
- $\Theta(-1) = \exp[-i2t]$ so $R^{(-1)}(t) = c \exp\left[-\frac{1}{4} \sin[2t]\right] \Theta(-1)$ is the periodic eigenvector associated to ρ^{-1} ,

in each case, the Floquet multiplier is $\mu = \exp\left[\frac{1}{2}\pi\right] \exp\left[-\frac{1}{4} \sin[2\pi]\right] = 4.8105$.

In the Hill method, with $n_H = 4$ and $n_j = 9$, since $n = 1$ the matrix \mathbf{W} of the truncated Hyper-eigenvalue problem is of size 5×5 , so the eigenvalue problem will yield 5 characteristic exponents, which are shown in Tab. 3.1. It is noted that the most "central" characteristic exponent candidates estimated by the method are better approximations of the true characteristic exponents of the system. Finally, in Fig. 3.1, the real and imaginary parts of the periodic eigenvectors associated with ρ^1 and ρ^{-1} , including the analytic expression, the result by Floquet-Lyapunov, and the result from Hill's method.

To conclude the example, in Fig. 3.2, the fraction of power in each harmonic or Fourier term is shown for each periodic eigenvector. For this very simple case, it can be seen that most of the power is concentrated in the harmonic associated with the integer multiple selected for the corresponding characteristic exponent. It has been shown ([100]) that no one harmonic may have over half of the power for a given eigenvector in more realistic cases. The relevance of this type of representation remains in the capability of selecting a convenient set of eigenvectors.

Commentary The previous example highlights several practical considerations concerning Hill's method. The number of Fourier coefficients for the periodic eigenvectors in this method depends on the size of the matrix \mathbf{W} , the truncated hyper-eigenvalue problem, which in turn requires a set number of expansion coefficients of the matrix of the system $\mathbf{A}(t)$. If N_j Fourier terms are desired for the $\mathbf{R}(t)$ vectors, then $2N_j + 1$ coefficients are required in the expansion of $\mathbf{A}(t)$ for the correct formation of \mathbf{W} . This suggests a steep cost in the computation of the associated eigenvalue problem: a higher number of terms to describe $\mathbf{R}(t)$ results in a larger problem

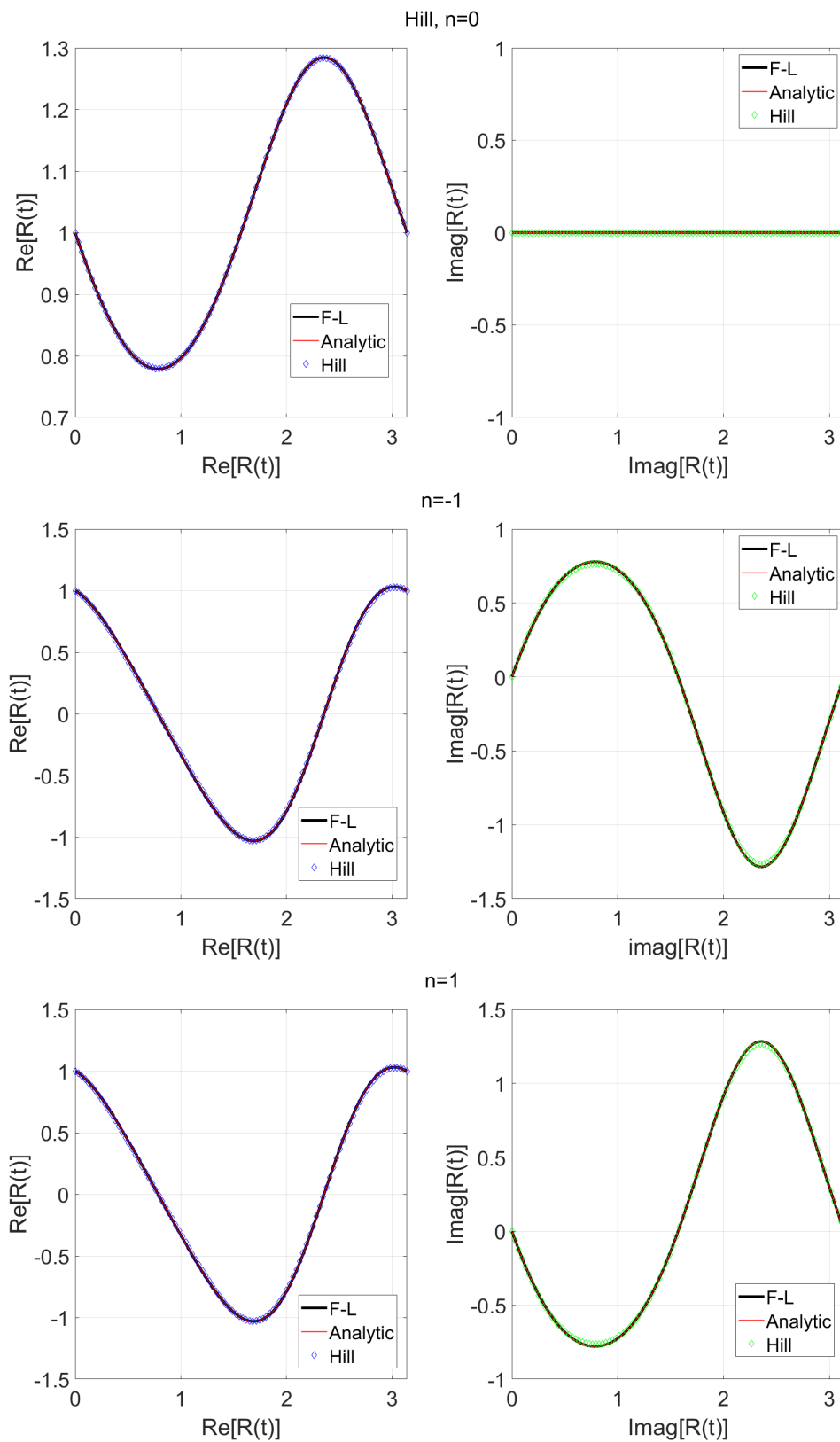


Figure 3.1: Periodic eigenvectors of example 1: top $R^{(0)}$, top center $R^{(-1)}$, bottom $R^{(1)}$, left is the real part, right is the imaginary part

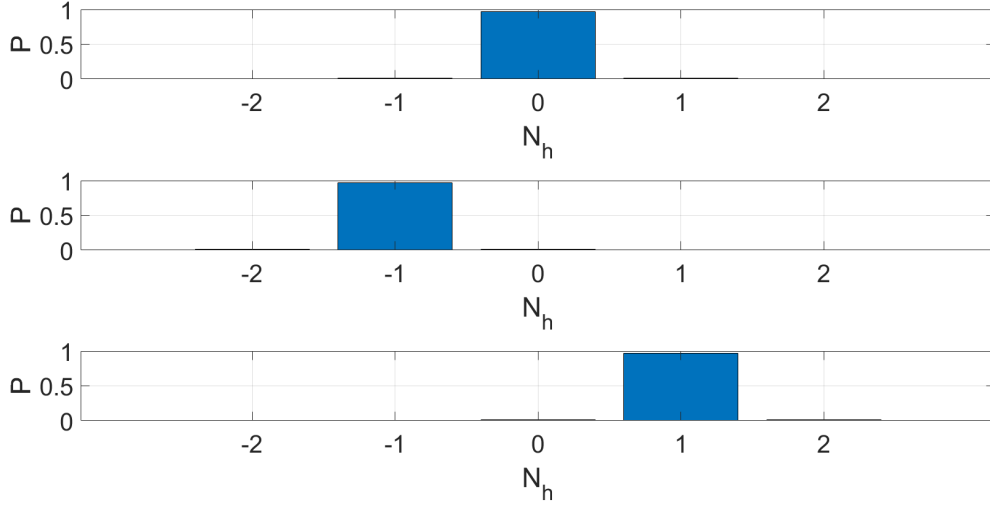


Figure 3.2: Fraction of power on each harmonic component for periodic eigenvectors in example 1: top $R^{(0)}$, top center $R^{(-1)}$, bottom $R^{(1)}$

and increases the number of candidate sets of characteristic exponents. This downside can be mitigated by the application of algorithms that compute, for instance, the k “smallest” eigenvalues and their associated eigenvectors. In many practical situations, however, the terms in the Fourier expansion decay rapidly after a few terms, which means that \mathbf{W} often has a sparse structure dominated by a band centered on its main diagonal.

Example 2 Consider a reduced version of the rotor-blade model introduced in the previous chapter, with 1 DOF describing the lateral motion of the disc and one blade with one modal variable in the spanwise direction for a total of 2 DOF. The equation of motion has the form:

$$\mathbf{M}(t)\ddot{\mathbf{x}} + \mathbf{G}(t)\dot{\mathbf{x}} + \mathbf{K}\mathbf{x} = 0, \quad (3.54)$$

the numerical values of these matrices are:

$$\mathbf{M}(t) = \begin{pmatrix} 12.848 \times 10^3 & -41.791 \sin(\Omega t) \\ -41.791 \sin(\Omega t) & 1 \end{pmatrix}, \quad (3.55)$$

for $\mathbf{G}(t) = \mathbf{G}_G(t) + \mathbf{D}$:

$$\mathbf{G}_G(t) = \Omega \begin{pmatrix} 0 & -41.791 \cos(\Omega t) \\ 41.791 \cos(\Omega t) & 0 \end{pmatrix}, \quad (3.56)$$

and:

$$\mathbf{D} = \begin{pmatrix} 100 & 0 \\ 0 & 0.5 \end{pmatrix}, \quad (3.57)$$

finally for \mathbf{K} :

$$\mathbf{K} = \begin{pmatrix} 2 \times 10^5 & 0 \\ 0 & 7.0181 \times 10^2 \end{pmatrix}. \quad (3.58)$$

Quantity	Value(Units)
M	10^4 [kg]
K_X	2×10^5 [Nm ⁻¹]
D_X	1×10^2 [Nsm ⁻¹]
D_{s1}	0.5
E	25×10^6 [Pa]
I	4.7[kgm]
L	9[m]
ρ	211[kgm ⁻³]
A	1.5[m ²]
R_r	1[m]
Ω	1.15[rads ⁻¹]

Table 3.2: Parameters of the system in example 2

The physical parameters can be found in Tab. 3.2. For the modal analysis, we will neglect the damping of the system, setting the corresponding parameters to zero.

In state form, the system is:

$$\dot{\mathbf{y}} = \mathbf{A}(t)\mathbf{y}, \quad (3.59)$$

with the usual substitution: $\mathbf{y} = [\mathbf{x}, \dot{\mathbf{x}}]^T$ and $\mathbf{A}(t) = \begin{pmatrix} \mathbf{0}_2 & \mathbf{I}_2 \\ -\mathbf{M}^{-1}\mathbf{K} & -\mathbf{M}^{-1}\mathbf{G} \end{pmatrix}$, with $\mathbf{A}(t) = \mathbf{A}(t + nT_p)$, $n \in \mathbb{Z}$, $\mathbf{A}(t)$ is of size 4×4 . Since $\Omega = 1.15 \frac{rad}{s}$, we have $T_p = 5.4636s$. For this system, $\mathbf{A}(t)$ can be written as:

$$\mathbf{A}(t) = \begin{pmatrix} 0 & 0 & 1 & 0 \\ 0 & 0 & 0 & 1 \\ \frac{k_{11}}{m_{11} - m_1^2 \sin^2(t\Omega)} - \frac{k_{12}m_1 \sin(t\Omega)}{m_{11} - m_1^2 \sin^2(t\Omega)} & D_{11} & \frac{m_1^2 \Omega \sin(t\Omega) \cos(t\Omega)}{m_{11} - m_1^2 \sin^2(t\Omega)} \\ \frac{k_{21}m_1 \sin(t\Omega)}{m_{11} - m_1^2 \sin^2(t\Omega)} & \frac{k_{22}m_{11}}{m_{11} - m_1^2 \sin^2(t\Omega)} - \frac{m_1^2 \Omega \sin(t\Omega) \cos(t\Omega)}{m_{11} - m_1^2 \sin^2(t\Omega)} & D_{22} \end{pmatrix}. \quad (3.60)$$

Solving the system with the 4 initial conditions $\mathbf{y}_0^{(1)} = [1 \ 0 \ 0 \ 0]^T$, $\mathbf{y}_0^{(2)} = [0 \ 1 \ 0 \ 0]^T$, $\mathbf{y}_0^{(3)} = [0 \ 0 \ 1 \ 0]^T$, $\mathbf{y}_0^{(4)} = [0 \ 0 \ 0 \ 1]^T$ we obtain a monodromy matrix:

$$\Phi(T_p, t_0) = \begin{pmatrix} -0.88102 & 4.1768 \times 10^{-5} & 0.10798 & 6.0981 \times 10^{-6} \\ 0.1123 & 0.1878 & 0.07166 & -0.00493 \\ -1.6806 & -0.00018 & -0.88187 & 1.0553 \times 10^{-5} \\ 0.047259 & 3.4567 & 0.22584 & 0.19025 \end{pmatrix} \quad (3.61)$$

and the Floquet multipliers are then: $\mu_1 = -0.88144 + 0.426i$, $\mu_2 = -0.88144 - 0.426i$, $\mu_3 = 0.18902 + 0.13048i$, $\mu_4 = 0.18902 - 0.13048i$. The exponents will have the form:

$$\begin{aligned} \rho_{k_m} &= \frac{\ln |\mu_i|}{T_p} + i \frac{\arg[\mu_i] + 2\pi m}{T_p} \\ &= \frac{\ln |\mu_i|}{T_p} + i \left(\frac{\arg[\mu_i]}{T_p} + 1.15m \right) \end{aligned} \quad (3.62)$$

for instance, the characteristic exponents for $m = 0$ are: $\rho_1^0 = -0.00389 + 0.49260i$, $\rho_2^0 = -0.00389 + 0.49260i$, $\rho_3^0 = -0.26924 + 0.11058i$, $\rho_4^0 = -0.26924 - 0.11058i$, the Floquet eigenvectors associated to these exponents are shown in Fig. 3.4.

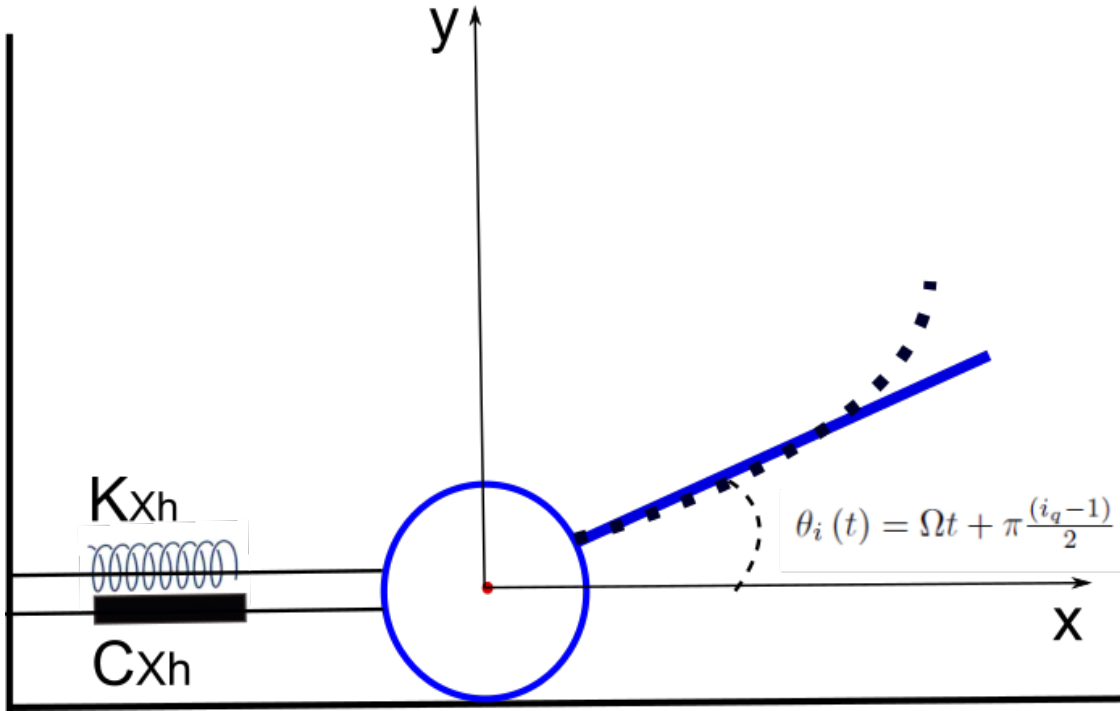


Figure 3.3: Diagram of the 2DOF rotor-blade system

The Hill method can be equally applied. Choosing $N_j = 9$, there will be 9 sets of candidate characteristic exponents. We have selected the following set to display the characteristics of the eigenvectors: $\rho_1^0 = -0.00389 - 0.49260i$, $\rho_2^0 = -0.00389 + 0.4926i$, $\rho_3^* = -0.26924 + 27.489i$, $\rho_4^* = -0.26924 - 27.489i$, notice that this is a mixed set: the first two characteristic exponents correspond to $m = 0$, while the other two correspond to the added multiple $m = 24$ approximately. The eigenvectors are shown in Fig. 3.5.

Commentary The physical interpretation of these eigenvectors requires some consideration. While the Floquet system under analysis has 4 DOF, the associated mechanical system has 2, so two modes are associated with the physical displacement variables of the system. At the same time, the other two are, in fact, a description of the generalized velocity variables introduced in the state reduction. In both eigenvector sets, one can distinguish two modes dominated by the fourth DOF while the rest remain almost constant. In comparison, the other two modes contain fairly mixed activation among all degrees of freedom. The fourth degree of freedom is the generalized velocity of the blade modal variable. In the same vein, the physical interpretation of the unit initial condition imposed to find the fundamental matrix of the system imposes an impulse-like initial condition that affects all the generalized variables and highlights the coupling effects that can be seen in the equation of motion.

Each mode has been characterized by the DOF participation and the harmonic participation per mode, as displayed in Fig. 3.6. In terms of DOF participation, the two modes dominated by the velocity of the blade modal variable can be easily identified, whereas the other two modes reveal the activation of the disc translation and blade deformation; this permits a more quantitative interpretation of the preceding graphics. The harmonic importance factor shows that the central frequencies provide the majority of the power in each mode, a behavior that justifies early truncation in the Fourier expansion.

Parametric study of Floquet exponents with respect to the pumping frequency To conclude the study of the free system with 2 DOFs, we present two additional analytical tools that result from our developments on

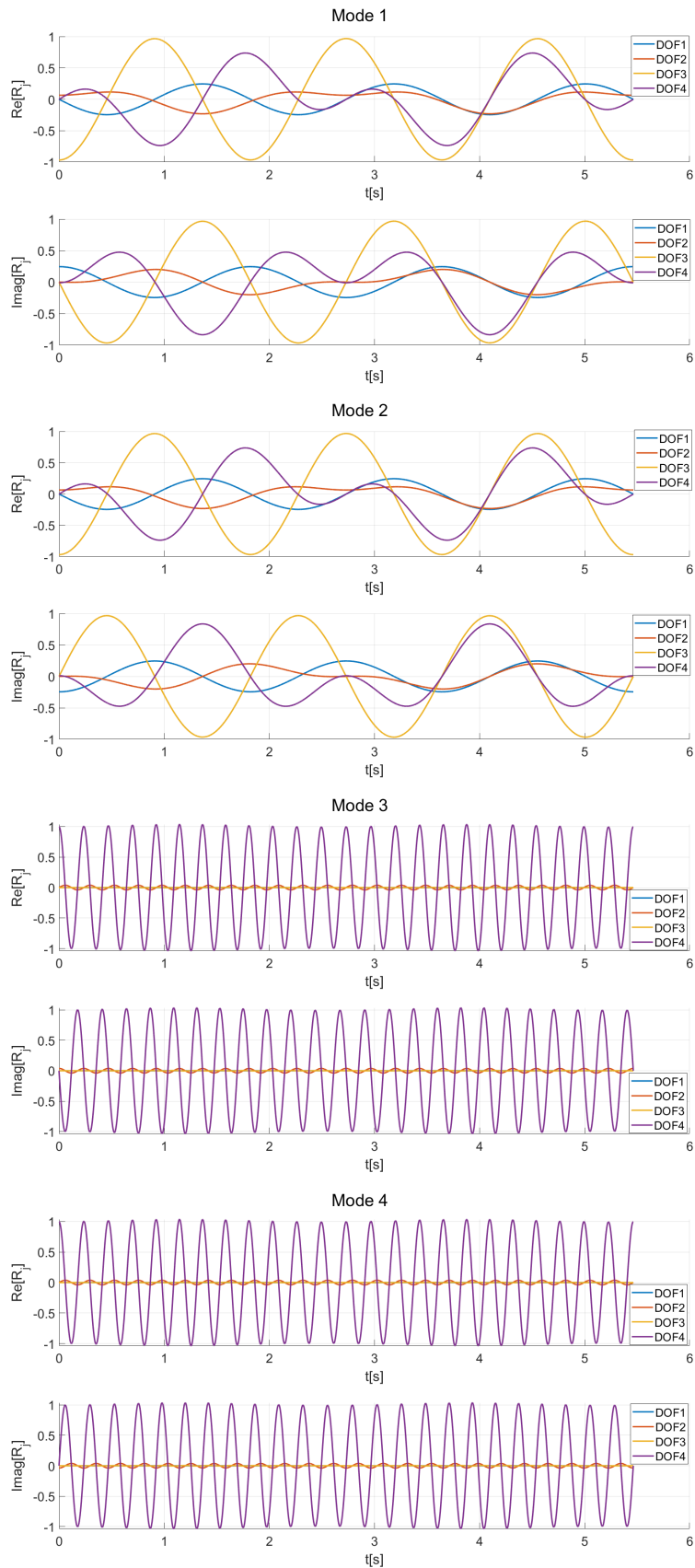


Figure 3.4: Floquet eigenvectors for the ρ_i^0 exponents, example 2, Floquet-Lyapunov method

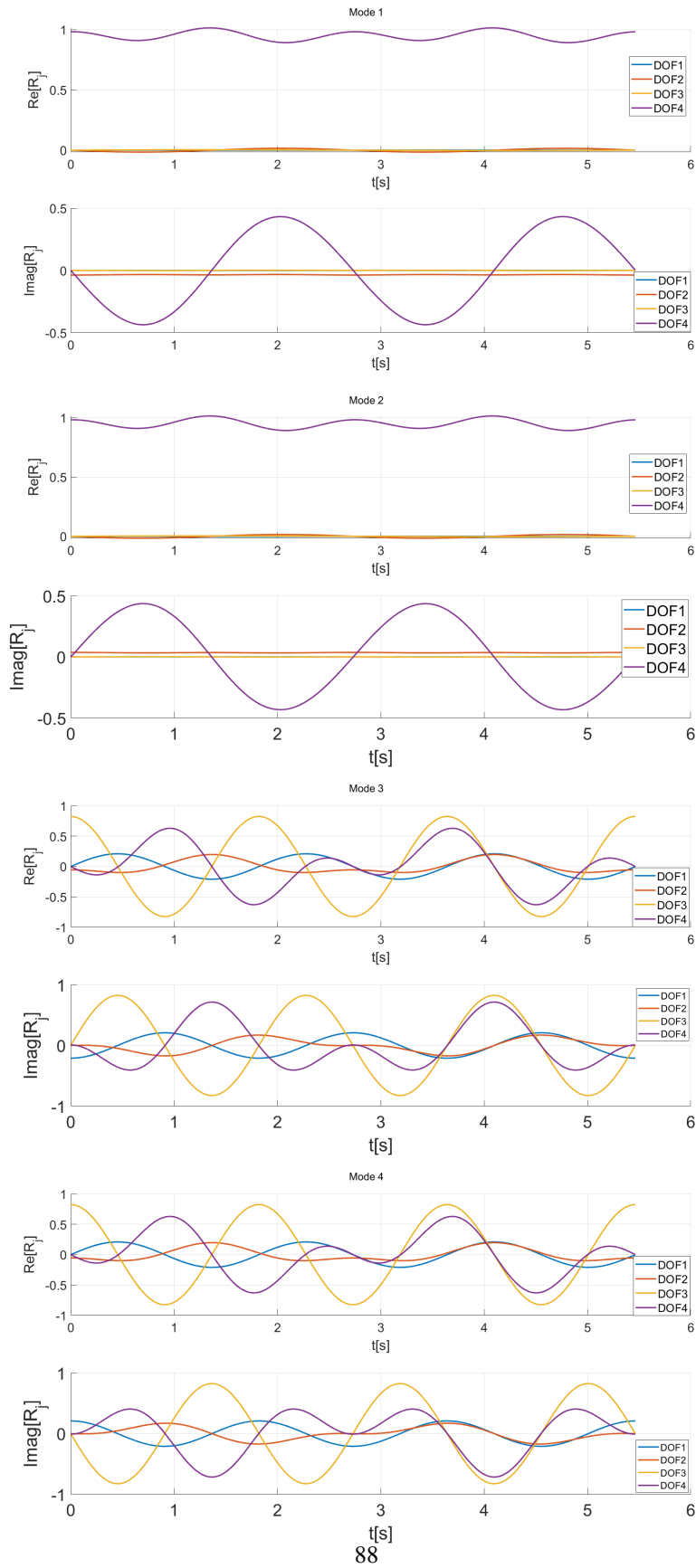


Figure 3.5: Floquet eigenvectors for the ρ_i mixed exponents, example 2, Hill method

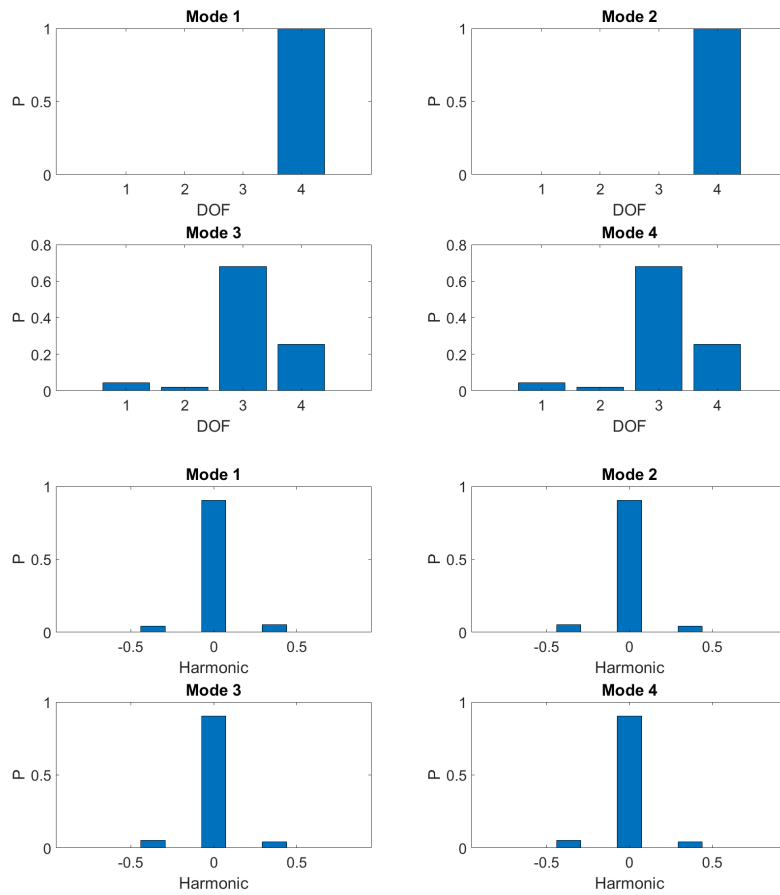


Figure 3.6: Participation factors in Floquet modes, a) DOF participation per mode, b) Harmonic importance per mode

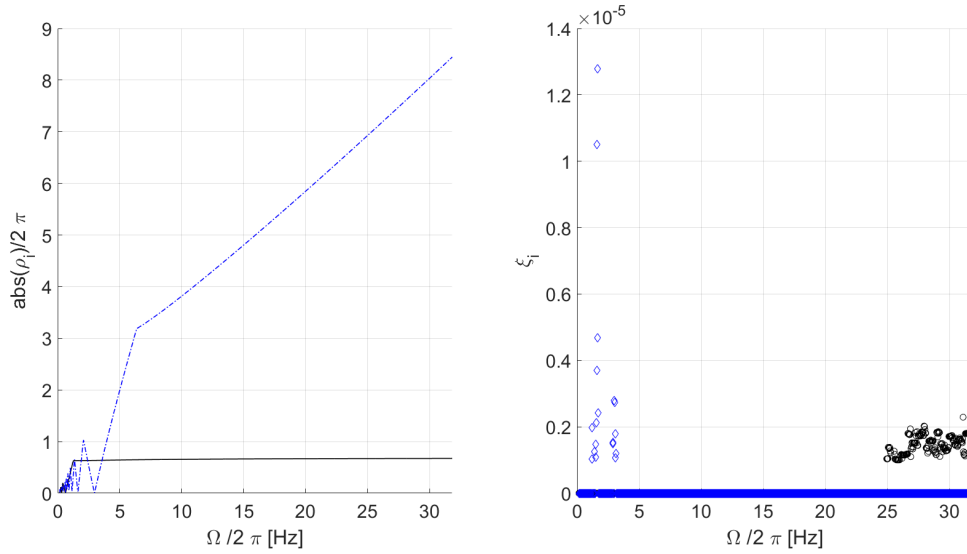


Figure 3.7: Lyapunov-Campbell and stability plots

Floquet exponents and stability. The objective is to show the parametric dependence of the Floquet exponents of the system with respect to the periodicity of the properties of the system; more specifically, the parameter Ω or $f_p = \frac{\Omega}{2\pi}$ from where the period of the system is derived by $T_p = \frac{1}{f_p}$. The quantity f_p is sometimes referred to in the literature as pumping frequency. The first diagram resembles the Campbell diagram described in section section 1 of chapter 2, with the distinction that the natural frequencies are replaced by the magnitude of the characteristic exponents $\|\rho_i\|$. Such graphical representation would be meaningless if the stability properties of the solution as predicted by the real part of the Floquet exponents were left out, so a simple indicator is developed to accompany the diagram: $\xi_i = -\frac{\text{Re}(\rho_i)}{\|\rho_i\|}$, knowing that the stability criteria in terms of the characteristic exponents require $\text{Re}(\rho_k) \leq 0$ so the sign of ξ_i provides the equivalent information to the modal damping factor in an LTI analogy.

The Lyapunov-Campbell and stability diagrams of system Eq. 3.54 with $\mathbf{D} = \mathbf{0}$ is presented in Fig. 3.7. Due to their conjugate nature, only two characteristic exponents of the Floquet system are included. Given that the undamped version of the system is studied, the amount of unstable solutions is expected. The low-frequency exponents show high oscillation until the pumping frequency $f_p = 2.08\text{Hz}$ is reached; after this frequency, the exponents increase monotonically for the rest of the study. Although this result shows high sensitivity of the exponents to the pumping frequency in the low regime, further investigation is necessary since, as shown in Eq. 3.39, the Floquet eigenvectors modulate the modal response and thus introduce an additional frequency component into the physical or state solution.

For reference, in the case of $\Omega = 0$, the blade frequency from the discretization scheme is $f_{blade} = 4.2094\text{Hz}$, and frequencies of the disc-blade assembly are respectively $f_1^{sys} = 0.6279\text{Hz}$ and $f_2^{sys} = 4.2096\text{Hz}$; for $\Omega = 60$ at the end of the represented interval, the blade frequency from the discretization scheme is $f_{blade} = 6.8143\text{Hz}$. These values allow us to assign some correspondence to the quantities in Fig. 3.7: the lower frequency component in black corresponds to the base DOF, whereas the higher frequency component in blue corresponds to the blade modal DOF. As Ω is increased, the first frequency (black) oscillates with an upward trend until it reaches the vicinity of the non-rotating frequency of the base DOF, $f_1^{sys} = 0.6279\text{Hz}$ at approximately $f_p = 1.3435\text{Hz}$, and then slowly increases in monotonic fashion. The second frequency shows a similar monotonic increase after $f_p = 2.9978\text{Hz}$, although its value lags the equivalent frequency for the rotating blade problem.

3 Forced response of LTP systems

We now consider the following equation:

$$\mathbf{M}(t)\ddot{\mathbf{x}} + \mathbf{G}(t)\dot{\mathbf{x}} + \mathbf{K}(t)\mathbf{x} = \mathbf{f}(t), \quad (3.63)$$

where the matrices of the system are such that for a given period T_p : $\mathbf{M}(t + T_p) = \mathbf{M}(t)$, which can similarly be cast in state form:

$$\dot{\mathbf{y}}(t) = \mathbf{A}(t)\mathbf{y}(t) + \mathbf{B}(t)\mathbf{f}(t), \quad (3.64)$$

which is a forced Floquet system, and matrix $\mathbf{B}(t) = \begin{bmatrix} \mathbf{0} \\ \mathbf{M}^{-1}(t) \end{bmatrix}$. Having established the modal analysis foundation and the characterization of the state transition matrix for the Floquet system in the previous section, we now turn to the study of the forced or steady-state response. The deterministic methods presented here will enable, in the next chapter, the moment propagation of LTP systems; some of the spectral results can be applied to estimate the PSD in stochastic situations.

Provided the state transition matrix of the Floquet system $\Phi(t, t_0)$, the total solution of Eq. 3.64 can be expressed as follows([144]):

$$\mathbf{y}(t) = \Phi(t, t_0)\mathbf{y}(0) + \int_{t_0}^t \Phi(t, \tau)\mathbf{B}(\tau)\mathbf{f}(\tau) d\tau, \quad (3.65)$$

where $\Phi(t, \tau)$ is again the state transition matrix (as in Eq. 3.8), each term can be recognized as a homogeneous solution related to the initial conditions $\mathbf{y}_h = \Phi(t, t_0)\mathbf{y}(0)$, and a forced response associated with the load $\mathbf{y}_f = \int_{t_0}^t \Phi(t, \tau)\mathbf{B}(\tau)\mathbf{f}(\tau) d\tau$. As seen in the previous section, the substitution $\mathbf{y}(t) = \mathbf{R}(t)\mathbf{q}(t)$ transforms system Eq. 3.64 into the LTI system in modal variables $\mathbf{q}(t)$. One resolution strategy is to solve the forced LTI problem in the modal variables $\mathbf{q}(t)$ subject to the corresponding adapted force:

$$\dot{\mathbf{q}}(t) = \boldsymbol{\rho}\mathbf{q}(t) + \mathbf{p}(t), \quad (3.66)$$

where we have introduced the adapted force $\mathbf{p}(t) = \mathbf{L}(t)\mathbf{B}(t)\mathbf{f}(t)$. Once the modal response is found, the return to the state or physical variables is straightforward. Another alternative is the passage to the frequency domain or some other representation basis associated with a convenient integral transform, such as the traditional Fourier transform approach or a wavelet treatment. In each case, the convenience of the method comes from the improved efficiency in operations such as the convolution in Eq. 3.65.

3.1 Time-domain resolution in modal variable

The goal is to find:

$$\mathbf{y}_f(t) = \int_{t_0}^t \Phi(t, \tau)\mathbf{B}(\tau)\mathbf{f}(\tau) d\tau \quad (3.67)$$

where the subindex stands for steady-state. Admitting the previous development we have:

$$\dot{\mathbf{q}}(t) = \boldsymbol{\rho}\mathbf{q}(t) + \mathbf{p}(t), \quad (3.68)$$

where the system is LTI and $\boldsymbol{\rho}$ is a constant, diagonal matrix. The forced response of Eq. 3.68 is well known in vibration theory ([111],[104],[85]); given the impulse response $\mathbf{h}(t)$ of the system, one obtains:

$$\mathbf{q}(t) = \int_{-\infty}^{\infty} \mathbf{h}(t - \tau)\mathbf{p}(\tau) d\tau = \int_{-\infty}^{\infty} \mathbf{h}(\tau)\mathbf{p}(t - \tau) d\tau, \quad (3.69)$$

since Eq. 3.68 is a first-order system, its impulse response is : $\mathbf{h}(t) = \exp[\boldsymbol{\rho}t]$; we also know that the system is causal, so the integration limits can be adjusted since $\mathbf{h}(t) = 0, t < 0$. This results in:

$$\mathbf{q}(t) = \int_0^{\infty} \mathbf{h}(\tau) \mathbf{p}(t - \tau) d\tau = \int_0^{\infty} \exp[\boldsymbol{\rho}(t - \tau)] \mathbf{p}(\tau) d\tau, \quad (3.70)$$

with $\mathbf{h}(\tau) = \exp[\boldsymbol{\rho}\tau]$ and we remark that as before $\exp[\boldsymbol{\rho}t]$ is a matrix exponential. This last expression, provided that the characteristic exponents $\boldsymbol{\rho}$ are known, can be integrated numerically to obtain $\mathbf{q}(t)$ and ultimately $\mathbf{y}(t) = \mathbf{R}(t) \mathbf{q}(t)$:

$$\begin{aligned} \mathbf{q}(t) &= \int_0^{\infty} \mathbf{h}(\tau) \mathbf{p}(t - \tau) d\tau \\ \mathbf{y}(t) &= \mathbf{R}(t) \mathbf{q}(t) \\ &= \mathbf{R}(t) \int_0^{\infty} \mathbf{h}(\tau) \mathbf{p}(t - \tau) d\tau. \end{aligned} \quad (3.71)$$

3.2 Spectral approach

A class of spectral methods based on the Fourier transform have wide application in LTI dynamics, taking advantage of the fact that convolutions in the time-domain transform into a simple product in the spectral (Fourier) domain. The monograph by Bentvelsen [8] provides a detailed exposition of spectral approaches in the aeroelastic domain under forced conditions, with the main application being in a Ziegler column. The approach taken in this section is similar to that in [151], although this will be revisited in chapter 5 to yield the stochastic quantities of interest. The main limitation of the deterministic approaches found in the literature is the fact that they are focused on the spectrum, yet from a stochastic perspective, the second-order quantities, particularly the PSD, are more descriptive.

We start from the relationship 3.68 first, focusing on the description of the adapted excitation $\mathbf{p}(t) = \mathbf{L}(t) \mathbf{B}(t) \mathbf{f}(t)$.

Recalling that $\mathbf{B}(t) = \begin{bmatrix} \mathbf{0} \\ \mathbf{M}^{-1}(t) \end{bmatrix}$, we write the Fourier expansion as:

$$\begin{aligned} \mathbf{B}(t) &= \sum_{b=-\infty}^{+\infty} \mathbf{B}_b \exp \left[i \left(\frac{2\pi}{T_p} b \right) t \right] \\ &\approx \sum_{b=-n_H}^{+n_H} \mathbf{B}_b \exp \left[i \left(\frac{2\pi}{T_p} b \right) t \right], \end{aligned} \quad (3.72)$$

where each coefficient matrix \mathbf{B}_b has dimension $[2n \times n]$ and . Next, we proceed similarly with the left modal matrix:

$$\begin{aligned} \mathbf{L}(t) &= \sum_{l=-\infty}^{+\infty} \mathbf{L}_l \exp \left[i \left(\frac{2\pi}{T_p} l \right) t \right] \\ &\approx \sum_{l=-n_H}^{+n_H} \mathbf{L}_l \exp \left[i \left(\frac{2\pi}{T_p} l \right) t \right], \end{aligned} \quad (3.73)$$

which yields the following truncated representation of $\mathbf{p}(t)$:

$$\begin{aligned} \mathbf{p}(t) &= \mathbf{L}(t) \mathbf{B}(t) \mathbf{f}(t) \\ &\approx \left(\sum_{l=-n_H}^{+n_H} \mathbf{L}_l \exp \left[i \left(\frac{2\pi}{T_p} l \right) t \right] \right) \left(\sum_{b=-n_H}^{+n_H} \mathbf{B}_b \exp \left[i \left(\frac{2\pi}{T_p} b \right) t \right] \right) \mathbf{f}(t). \end{aligned} \quad (3.74)$$

Next, we proceed with the modal representation of the response $\mathbf{y}(t) = \mathbf{R}(t) \mathbf{q}(t)$, as before the right modal matrix is:

$$\begin{aligned} \mathbf{R}(t) &= \sum_{q=-\infty}^{+\infty} \mathbf{R}_q \exp \left[i \left(\frac{2\pi}{T_p} q \right) t \right] \\ &\approx \sum_{q=-n_H}^{n_H} \mathbf{R}_q \exp \left[i \left(\frac{2\pi}{T_p} q \right) t \right] \end{aligned} \quad (3.75)$$

and by substitution:

$$\begin{aligned} \mathbf{y}(t) &= \mathbf{R}(t) \mathbf{q}(t) \\ &\approx \left(\sum_{q=-n_H}^{n_H} \mathbf{R}_q \exp \left[i \left(\frac{2\pi}{T_p} q \right) t \right] \right) \mathbf{q}(t) \end{aligned} \quad (3.76)$$

and more specifically, the convolution solution $\mathbf{y} = \mathbf{R}(t) \left(-\int_0^\infty \exp[\boldsymbol{\rho}(t-\tau)] \mathbf{p}(\tau) d\tau \right)$:

$$\mathbf{y}(t) = \left(\sum_{q=-n_H}^{n_H} \mathbf{R}_q \exp \left[i \left(\frac{2\pi}{T_p} q \right) t \right] \right) \left(-\int_0^\infty \exp[\boldsymbol{\rho}(t-\tau)] \mathbf{p}(\tau) d\tau \right). \quad (3.77)$$

Substituting the adapted force representation then:

$$\begin{aligned} \mathbf{y}(t) &= \left(\sum_{q=-n_H}^{n_H} \mathbf{R}_q \exp \left[i \left(\frac{2\pi}{T_p} q \right) t \right] \right) \\ &\quad \left(-\int_0^\infty \exp[\boldsymbol{\rho}(t-\tau)] \left(\sum_{l=-n_H}^{+n_H} \mathbf{L}_l \exp \left[i \left(\frac{2\pi}{T_p} l \right) \tau \right] \right) \left(\sum_{b=-n_H}^{+n_H} \mathbf{B}_b \exp \left[i \left(\frac{2\pi}{T_p} b \right) \tau \right] \right) \mathbf{f}(\tau) d\tau \right) \end{aligned} \quad (3.78)$$

rearranging terms and grouping the Fourier kernels:

$$\mathbf{y}(t) = \sum_{q=-n_H}^{n_H} \sum_{l=-n_H}^{+n_H} \sum_{b=-n_H}^{+n_H} \mathbf{R}_q \left(-\int_0^\infty \exp \left[\boldsymbol{\rho}(t-\tau) + i \left(\frac{2\pi}{T_p} (b+l) \right) \tau \right] \mathbf{L}_l \mathbf{B}_b \mathbf{f}(\tau) d\tau \right) \exp \left[i \left(\frac{2\pi}{T_p} q \right) t \right], \quad (3.79)$$

the Fourier transform of $\mathbf{f}(t)$ if it exists is:

$$\mathbf{F}(f) = \int_{-\infty}^{\infty} \mathbf{f}(t) \exp[-i2\pi ft] dt, \quad (3.80)$$

Applying Fourier transform over the entire expression Eq. 3.79:

$$\begin{aligned} \mathbf{Y}(f) &= \sum_{q=-n_H}^{n_H} \sum_{l=-n_H}^{+n_H} \sum_{b=-n_H}^{+n_H} \mathbf{R}_q \int_{-\infty}^{\infty} \left\{ \left(-\int_0^\infty \exp \left[\boldsymbol{\rho}(t-\tau) + i \left(\frac{2\pi}{T_p} (b+l) \right) \tau \right] \mathbf{L}_l \mathbf{B}_b \mathbf{f}(\tau) d\tau \right) \right. \\ &\quad \left. \exp \left[-i2\pi \left(f - \frac{q}{T_p} \right) t \right] \right\} dt, \end{aligned} \quad (3.81)$$

the Fourier transform of this convolution results in:

$$\mathbf{Y}(f) = \sum_{q=-n_H}^{n_H} \sum_{l=-n_H}^{+n_H} \sum_{b=-n_H}^{+n_H} \mathbf{R}_q \mathbf{\Lambda}(f) \mathbf{L}_l \mathbf{B}_b \mathbf{F}(v(f)) \quad (3.82)$$

where $\mathbf{F}(v(f))$ is the Fourier transform of the force, but with a shifted frequency argument $v(f) = v(f, T_p, l, b, q) = f + \frac{(q+l+b)}{T_p}$, that is: $\mathbf{F}(v(f)) := \mathbf{F}\left(f + \frac{(q+l+b)}{T_p}\right)$, and the matrix $\mathbf{\Lambda}(f) = \Lambda_{i,j}(f, T_p, l, b, \boldsymbol{\rho})$ is diagonal with terms:

$$\Lambda_{i,j}(f, T_p, l, b, \boldsymbol{\rho}) = \begin{cases} \frac{1}{i2\pi\left(f + \frac{(l+b)}{T_p}\right) - \rho_i}, & i = j \\ 0 & i \neq j \end{cases}, \quad (3.83)$$

this last expression warrants some exposition. First, $\mathbf{\Lambda}$ is a function of the independent frequency variable f . Second, in the main diagonal, the ρ_i terms in the denominator are the characteristic exponents of the system; for each value of q, l, b in the triple sum, a diagonal matrix function is defined, with each of the multipliers in the main diagonal. Third, it is clear that this expression allows us to diagnose the occurrence of peaks in amplitude and that these peaks will arrive not only when $i2\pi f - \rho_i$ is close to zero, which is the behavior of natural systems, but also at the additional instances in which $i2\pi\left(f + \frac{(l+b)}{T_p}\right) - \rho_i$ approach zero. This type of behavior is characteristic of forced LTP systems.

Example 3 To illustrate the spectral developments, we consider the same Floquet system described in 2.4 with the Floquet exponents and periodic eigenvectors obtained from Hill's method and subjected to the simple external load:

$$\mathbf{f}(t) = \begin{pmatrix} c_1 \sin(2\pi f_f t) \\ c_2 \sin(2\pi f_f t) \end{pmatrix} \quad (3.84)$$

with $c_1 = 10^3$, $c_2 = 10^4$ and $f_f = 5\text{Hz}$. The relevant quantities in the frequency domain are available from the modal study performed on the system, these quantities are the Fourier coefficients \mathbf{R}_q , \mathbf{L}_l , \mathbf{B}_b , and the characteristic exponents $\rho_1^0 = -0.00389 - 0.49260i$, $\rho_2^0 = -0.00389 + 0.49260i$, $\rho_3^* = -0.26924 + 27.489i$, $\rho_4^* = -0.26924 - 27.489i$. We also recall that the Fourier expansion consists of 9 terms with integers $-4, -3, -2, -1, 0, 1, 2, 3, 4$, and with T_p : the base period in the expansion is selected as the fundamental period of the Floquet system. Invoking 3.83 we obtain:

$$\mathbf{\Lambda}(f) = \begin{pmatrix} \frac{1}{i2\pi\left(f + \frac{(l+b)}{T_p}\right) - \rho_1^0} & 0 & 0 & 0 \\ 0 & \frac{1}{i2\pi\left(f + \frac{(l+b)}{T_p}\right) - \rho_2^0} & 0 & 0 \\ 0 & 0 & \frac{1}{i2\pi\left(f + \frac{(l+b)}{T_p}\right) - \rho_3^*} & 0 \\ 0 & 0 & 0 & \frac{1}{i2\pi\left(f + \frac{(l+b)}{T_p}\right) - \rho_4^*} \end{pmatrix}, \quad (3.85)$$

and after applying Eq. 3.82 the response in frequency $\mathbf{Y}(f)$ is obtained, the four components are shown in Fig. 3.8.

Taking the first component of $\mathbf{Y}(f)$ for analysis purposes, in Fig. 3.9, we can identify the location of the main peaks in amplitude as they relate to the Floquet exponents and the pumping period. Writing the imaginary part of the characteristic exponents in Hertz we have the following system frequencies: $f_1^{\text{sys}} = 4.38\text{Hz}$, $f_2^{\text{sys}} = -4.38\text{Hz}$, $f_3^{\text{sys}} = 0.08\text{Hz}$, $f_4^{\text{sys}} = -0.08\text{Hz}$, and taking into account the integer multiples of the pumping period we further obtain $f_n^{\text{pump}} = \frac{n}{T_p} = 0.18 \times n$, with n an integer in $[-4, 4]$. We say, for instance, that a frequency $f_1^{\text{sys}} + f_n^{\text{pump}}$ is a harmonic of f_1^{sys} . There are 36 base frequency harmonics to consider, and these are shown in Tab. 3.3. Given the structure of $\mathbf{\Lambda}(f)$ and $v(f)$, we find derived frequencies as a result of the combination of the various integer

Hz	$n = -4$	$n = -3$	$n = -2$	$n = -1$	$n = 0$	$n = 1$	$n = 2$	$n = 3$	$n = 4$
f_1^{sys}	3.64	3.83	4.01	4.19	4.38	4.56	4.74	4.92	5.11
f_2^{sys}	-5.11	-4.92	-4.74	-4.56	-4.38	-4.19	-4.01	-3.83	-3.64
f_3^{sys}	-0.65	-0.47	-0.29	-0.10	0.08	0.26	0.44	0.63	0.81
f_4^{sys}	-0.81	-0.63	-0.44	-0.26	-0.08	0.10	0.29	0.47	0.65

Table 3.3: Harmonics of base system frequencies

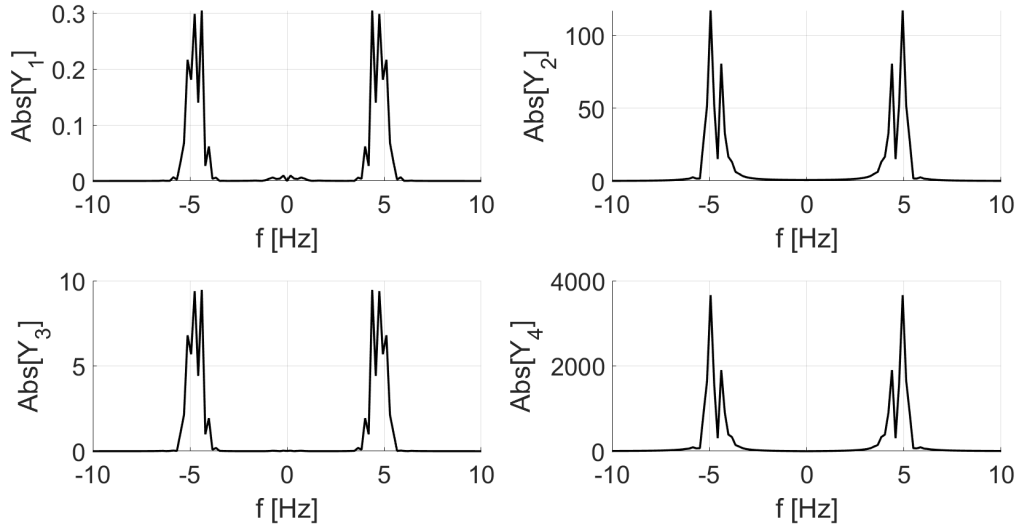


Figure 3.8: Response $\mathbf{Y}(f)$ in frequency domain

indexes, for instance, the peaks near 5.85Hz and -5.85Hz , which result from $f_1^{\text{sys}} + 0.18 \times n$ with $n = 8$ and $f_2^{\text{sys}} + 0.18 \times n$ with $n = -8$ respectively. One final frequency peak location is evident in Fig. 3.9: that of the pumping frequency itself 0.18Hz and its multiples, among which the predominant is 0.54Hz.

To conclude the example, we show in Fig. 3.10 the time-domain reconstruction of the state variables $y_1(t)$ and $y_2(t)$ by making use of the inverse Fourier Transform. The solution in Fig. 3.10 represents the steady-state regime of the forced response.

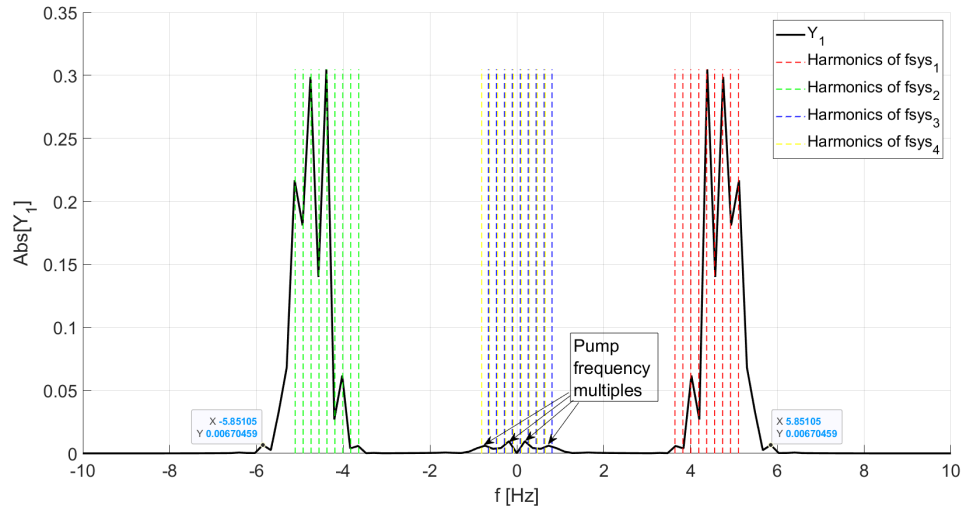


Figure 3.9: Component $Y_1(f)$ of the response with harmonic peaks

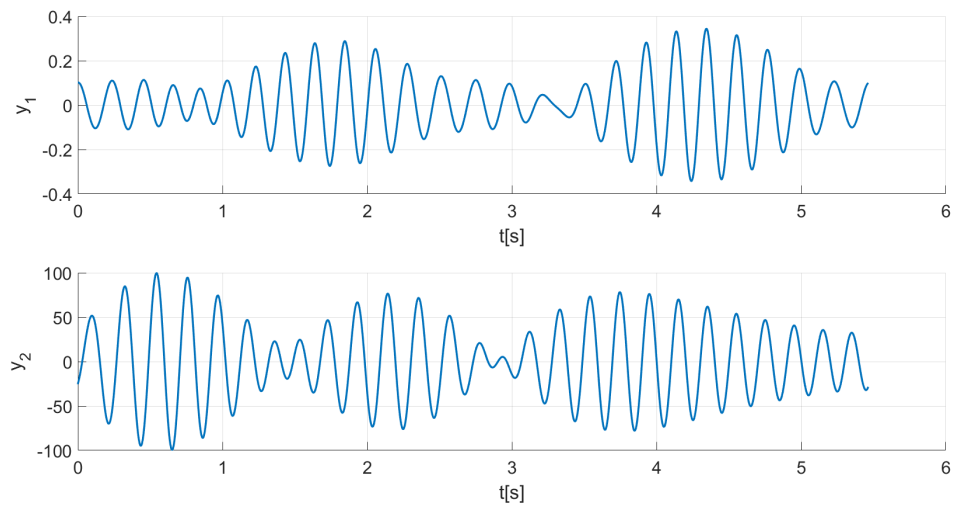


Figure 3.10: Time-domain reconstruction of y_1 and y_2

Chapter 4

Load description and moment propagation with PDF estimation

“To ensure maximum readability, we have omitted all unnecessary mathematical formalisms and set-theoretical jargon (epsilonics), and have, instead, chosen an informal style (à la Lagrange!) that stresses physical concepts and ideas; and a notation in line with the best classical traditions of the subject...”

John G. Papastavridis, A panoramic overview of the principles and equations of motion of advanced engineering dynamics

This chapter details the load description in stochastic terms and introduces the techniques of moment propagation and PDF reconstruction from propagated moments. The goal is to introduce the necessary mathematical developments to describe stochastic quantities and the methods and results obtained by moment propagation. To this end, we will first introduce the relevant definitions and concepts formulated in the notation introduced by Suptille in [134]. Much of our treatment of stochastic processes and fields follows the methods and results in this thesis. However, we will adapt them to the particularities of our problem and extend those results. We will then proceed to develop moment propagation relationships for stochastic processes and fields and provide particular results for the Gaussian case. The problem of moment-based PDF reconstruction is addressed. In this chapter, the proposed examples are primarily related to the Morison force on a rigid pile; the next chapter will combine these results with the Floquet description of LTP systems established earlier.

Before the first section, we will discuss the motivations for the approach and the methods involved. The global strategy adopted can be summarized as follows:

1. Characterize the deterministic response of the system under study.
2. Model the input forces: moments, spectral characteristics, distribution.
3. Apply the characterization of the response with the moments of the force as inputs, obtaining the moments of the response.
4. Reconstruct any stochastic quantity of interest of the response using the moments.
5. Apply analysis criteria and inference.

Once a modeling decision has been made, this strategy capitalizes on the moments of processes and fields being usually available in the sense that they are easy to compute. Since the moments are deterministic functions, one can treat them as inputs to compute the moments of the response. We call this broad procedure *moment propagation*. The limitations of the approach are manifold: first, a distribution may have an infinite number of moments, which from a numerical perspective requires a form of truncation in the computation of the moments propagated; second, the computational cost of calculating moments grows rapidly with order, a fact that is particularly pronounced in the case of inter-instant moment quantities such as the bi-covariance and tri-covariance; third, as commented in the introduction, moments alone do not fully describe any arbitrary distribution, which highlights the fact that these probabilistic descriptors offer valuable but limited information about the response; fourth, and in connection to the previous point, quantities such as the PDF or CDF are not as easy to propagate to the response, and reconstruction of these based on propagated moments is challenging in the most general case.

An alternative approach to moment propagation is the broad class of Monte-Carlo methods. In this approach, the input process is simulated, usually in the time domain, and the system's response to each process realization is computed as in the deterministic case. The statistics of this ensemble of responses estimate the true stochastic response. This approach is widely regarded as the most general. Yet, it is not without limitations: first, while the simulation of stationary Gaussian processes and fields is relatively simple and computationally efficient, the simulation of more general processes such as nongaussian and nonstationary ones is still a challenging task; second, the validity of the statistical inference of the ensemble response depends on the number of samples or realizations that have been generated, this puts a potentially prohibitive computational cost on a reliable estimate, for instance in large complex systems whose resolution per iteration demands an important resolution time.

Many of the developments in this section will be compared against an MCS benchmark, and some convergence measures will be applied to this Monte-Carlo estimate. Relatively simple force models will be utilized in this section. However, the final chapter will illustrate that realistic force models often can not be easily treated analytically, so the "input-output" flow must go through a computational "black box" that applies some numerical estimation of the load model.

1 Notation

1.1 Generalities

Throughout this chapter, unless otherwise specified, random variables will be noted as upper case letters such as X , processes as upper case with an explicit time dependence such as $X(t)$, while fields will be noted in calligraphic script such as $\mathcal{X}(\mathbf{x}, t)$. Let us consider first the simple scalar temporal random process $X(t)$, where t denotes the time. This section's basic definitions and results can be consulted in texts such as [98] or [104]. At a fixed time t , its instantaneous n -th probabilistic moment with respect to the origin, which is also called ordinary moment, is defined as:

$$\mathrm{E}[X^n(t)] = \int_{\mathbb{R}} x^n f(x, t) dx \quad (4.1)$$

where $\mathrm{E}[\bullet]$ denotes the expectation operator, x covers the range of the possible values of the process and $f_x(x, t)$ is its marginal probability density function (PDF). We note this n -th probabilistic moment by $\mu_{X^n}(t)$. Hence:

$$\mu_{X^n}(t) = \mathrm{E}[X^n(t)] \quad (4.2)$$

and we further write $\mu_{X^n} = \mu_{X \times X \dots \times X}$ (n times). For instance, the quantity $\mu_{X^2}(t)$ is equivalent to the quantity $\mu_{XX}(t)$, $\mu_{X^3}(t) = \mu_{XXX}(t)$ and so on. With this proposed notation, we have encoded the information about the kernel, *i.e.*, the operand, of the expectation operator in the index of the moment symbol. Moreover, when stationary processes are of interest, instantaneous moments read:

$$\mu_{X^n} = \mathrm{E}[X^n(t)]. \quad (4.3)$$

A first result, easy to read with this notation, comes while considering another process $W(t)$, called the output, defined in terms of a transformation of this initial process $X(t)$, viewed as an input process. As an example, let us consider the case $W(t) = X^2(t)$ from a simple but nonlinear model. This type of transformation is extensively used, for instance, in offshore engineering in the modeling of wave forces that are defined as a function of a velocity field in the oceanic medium (see, for instance, [13, 93]). The first moments of the input stationary process are written:

$$\begin{aligned}
\mu_X(t) &= E[X(t)] \\
\mu_{XX}(t) &= E[X^2(t)] \\
\mu_{XXX}(t) &= E[X^3(t)] \\
&\vdots \\
\mu_{XXXXXXXX}(t) &= E[X^8(t)] \\
&\vdots
\end{aligned} \tag{4.4}$$

and now, turning to the first four output moments, we get:

$$\begin{aligned}
\mu_W(t) &= E[W(t)] = E[X^2(t)] = \mu_{XX}(t) = \mu_{X^2}(t) \\
\mu_{WW}(t) &= E[W^2(t)] = E[X^4(t)] = \mu_{XXXX}(t) = \mu_{X^4}(t) \\
\mu_{WWW}(t) &= E[W^3(t)] = E[X^6(t)] = \mu_{XXXXXX}(t) = \mu_{X^6}(t) \\
\mu_{WWWW}(t) &= E[W^4(t)] = E[X^8(t)] = \mu_{XXXXXXXX}(t) = \mu_{X^8}(t)
\end{aligned} \tag{4.5}$$

which is a very simple result to derive with the proposed notation. This example makes it clear that the proposed notation is convenient for establishing and programming general relationships for output processes defined from a known model. A first useful application of the notation lies in the computation of output moments, given that the moments of $X(t)$ are known quantities since they are part of the description of an input of the problem.

Again, considering the random process $X(t)$, the instantaneous $n - th$ probabilistic moment with respect to the mean, the so-called central moment, is defined as:

$$E[(X(t) - E[X(t)])^n] = \int_{\mathbb{R}} (x - \mu_X(t))^n f(x, t) dx \tag{4.6}$$

in which case the proposed notation is:

$$\begin{aligned}
E[(X(t) - E[X(t)])^n] &= E[(X(t) - E[X(t)]) \times (X(t) - E[X(t)]) \times \dots \times (X(t) - E[X(t)])] \\
&= \sigma_{X \times X \dots (n \text{ times})}
\end{aligned} \tag{4.7}$$

with the observation that for this central moment, the equivalence in the subscript notation can not be preserved, for example, $\sigma_{X^2X}(t) \neq \sigma_{XXX}(t)$. However, useful relationships exist between the central moments and those centered in the origin. Indeed, since $(X(t) - \mu_X)^n = \sum_{k=0}^n \binom{n}{k} X^{n-k}(t) (-\mu_X)^k$, if we drop the writing of the time dependence of the moments for easier reading of the current developments, we can then apply the expectation operator to obtain an explicit expression thanks to the proposed notation:

$$\begin{aligned}
\sigma_{X \times X \dots (n \text{ times})} &= E \left[\sum_{k=0}^n \binom{n}{k} X^{n-k}(t) (-\mu_X)^k \right] \\
&= \sum_{k=0}^n \binom{n}{k} \mu_{X^{n-k}} (-\mu_X)^k
\end{aligned} \tag{4.8}$$

where $\binom{n}{k}$ denotes the binomial coefficient or each arrangement of k elements taken from n . As expected, when $n = 2$, we obtain the well-known relationship for the variance: $\sigma_{XX}(t) = \mu_{XX}(t) - \mu_X^2(t)$. Thus, the above expression Eq. 4.8 establishes a link between the central moment of any order and the moments with respect to the origin.

Furthermore, Eq. 4.8 can be inverted to express the moments with respect to the origin in terms of the mean and central moments. To do this, we introduce the random process:

$$V(t) = X(t) - \mu_X(t). \quad (4.9)$$

By definition (relation Eq. 4.2): $\mu_{X^n}(t) = E[(V(t) + \mu_X(t))^n]$ for $n \geq 1$, so knowing that $(V(t) + \mu_X)^n = \sum_{k=0}^n \binom{n}{k} V^{n-k}(t) (\mu_X)^k$, we find:

$$\begin{aligned} \mu_{X^n} &= E \left[\sum_{k=0}^n \binom{n}{k} V^{n-k}(t) (\mu_X)^k \right] \\ &= \sum_{k=0}^n \binom{n}{k} E[V^{n-k}(t)] (\mu_X)^k \\ &= \sum_{k=0}^n \binom{n}{k} \mu_{V^{n-k}} (\mu_X)^k. \end{aligned} \quad (4.10)$$

Another important aspect of the proposed notation is that it allows the handling of probabilistic information among different processes in a compact form. This can be easily seen when considering the simplest case of two input processes, $X(t)$ and $Y(t)$. As an example, we define the output with a third process from a simple weighted linear model:

$$W(t) = aX(t) + bY(t). \quad (4.11)$$

This type of expression arises if, for instance, the input processes model different ambient forces acting on a structure, so the output process is simply the resulting force. The instantaneous moments of the output can be written:

$$\begin{aligned} \mu_W(t) &= E[W(t)] \\ \mu_{WW}(t) &= E[W^2(t)] \\ \mu_{WWW}(t) &= E[W^3(t)] \\ \mu_{WWWW}(t) &= E[W^4(t)] \\ &\vdots \end{aligned} \quad (4.12)$$

and using the definition Eq. 4.11, these expressions can be developed as:

$$\begin{aligned} \mu_W(t) &= E[W(t)] = E[aX(t) + bY(t)] = a\mu_X(t) + b\mu_Y(t) \\ \mu_{WW}(t) &= E[W^2(t)] = E[(aX(t) + bY(t))^2] \\ &= a^2\mu_{XX}(t) + 2ab\mu_{XY}(t) + b^2\mu_{YY}(t) \\ \mu_{WWW}(t) &= E[W^3(t)] \\ &= a^3\mu_{XXX}(t) + 3a^2b\mu_{XXY}(t) + 3ab^2\mu_{XYY}(t) + b^3\mu_{YYY}(t) \\ \mu_{WWWW}(t) &= E[W^4(t)] \\ &= a^4\mu_{XXXX}(t) + 4a^3b\mu_{XXX Y}(t) + 6a^2b^2\mu_{XXYY}(t) + 4ab^3\mu_{XYYY}(t) + b^4\mu_{YYYY}(t) \end{aligned} \quad (4.13)$$

where cross moments between the processes $X(t)$ and $Y(t)$ have been introduced. For the second moment of $W(t)$, the quantity $\mu_{XY}(t) = E[X(t)Y(t)]$ is a second-order cross moment, and it contains probabilistic information about the correlation of the two processes $X(t)$ and $Y(t)$. Besides, we can note that $\mu_{XY}(t) = \mu_{YX}(t)$: subscript commutativity of ordinary cross moments. For higher moments of $W(t)$, higher crossed moments appear in the resulting expressions.

The instantaneous moments discussed previously are evaluated at the same instant in the time variable. These can be generalized to describe probabilistic relationships between the random variables at different times of a given process and/or among different processes, and the proposed notation can be extended to these generalizations of the moments in a very similar way. Let us consider first the random process $X(t)$. It can be interpreted as a set of random variables indexed by the variable t . From this, it is known that the auto-correlation function $R_{XX}(t_1, t_2)$ of the process $X(t)$, being the correlation of a process with itself, is a generalization of the moments around the origin, describing the behavior between any two of the underlying random variables as:

$$R_{XX}(t_1, t_2) = E[X(t_1)X(t_2)]. \quad (4.14)$$

Thus, if $t_1 = t_2 = t$, the auto-correlation function yields: $R_{XX}(t, t) = E[X(t)X(t)] = \mu_{XX}(t)$ in the proposed notation.

Furthermore, the auto-correlation function can describe more complex information among the different points in time or equivalently among different random variables, and we propose to write the n -th order auto-correlation as:

$$R_{X^n}(t_1, t_2, \dots, t_n) = E \left[\prod_{i=1}^n X(t_i) \right], \quad (4.15)$$

and similar relationships exist between these higher-order correlations and the conventional moments around the origin: $R_{X^n}(t, t, \dots) = \mu_{X^n}(t)$.

Next, the central moments can be generalized using the auto-covariance function:

$$\Sigma_{XX}(t_1, t_2) = E[(X(t_1) - E[X(t_1)])(X(t_2) - E[X(t_2)])], \quad (4.16)$$

and similar relationships are valid between the auto-covariance function and the central moments. For example, if $t_1 = t_2 = t$, $\Sigma_{XX}(t_1, t_2) = \Sigma_{XX}(t, t) = \sigma_{XX}$ using the proposed notation. Another useful result is the known relationship between covariance and correlation functions of order two:

$$\begin{aligned} \Sigma_{XX}(t_1, t_2) &= E[(X(t_1) - E[X(t_1)])(X(t_2) - E[X(t_2)])] \\ &= E[X(t_1)X(t_2) - \mu_X(t_1)\mu_X(t_2)] \\ &= R_{XX}(t_1, t_2) - \mu_X(t_1)\mu_X(t_2). \end{aligned} \quad (4.17)$$

It is also possible to generalize the covariance function to higher orders, giving rise to the bi-covariance and tri-covariance functions, and further. As before, we can write:

$$\Sigma_{X^n}(t_1, t_2, \dots, t_n) = E \left[\prod_{i=1}^n (X(t_i) - E[X(t_i)]) \right]. \quad (4.18)$$

As with the two types of moments evaluated at the same point in time, centered around the origin and centered around the mean, we state that it is possible to establish a general relationship between the covariances and the correlation functions analogous to the expression Eq. 4.8. This result can be demonstrated with the proposed notation. First, the expression inside the expectation operator of the definition Eq. 4.18 can be developed using the multi-binomial theorem:

$$\begin{aligned} \prod_{i=1}^n (X(t_i) - E[X(t_i)]) &= \prod_{i=1}^n (X(t_i) + (-\mu_X(t_i))) \\ &= \sum_{I \subseteq \{1, \dots, n\}} \prod_{i \in I} X(t_i) \prod_{i \in \{1, \dots, n\} \setminus I} (-\mu_X(t_i)). \end{aligned} \quad (4.19)$$

Applying the expectation:

$$\begin{aligned} \mathbb{E} \left[\prod_{i=1}^n (X(t_i) - \mathbb{E}[X(t_i)]) \right] &= \mathbb{E} \left[\sum_{I \subseteq \{1, \dots, n\}} \prod_{i \in I} X(t_i) \prod_{i \in \{1, \dots, n\} \setminus I} (-\mu_X(t_i)) \right] \\ &= \sum_{I \subseteq \{1, \dots, n\}} \mathbb{E} \left[\prod_{i \in I} X(t_i) \right] \prod_{i \in \{1, \dots, n\} \setminus I} (-\mu_X(t_i)) \end{aligned} \quad (4.20)$$

where we recognize the term $\mathbb{E}[\prod_{i \in I} X(t_i)]$ as a moment with respect to the origin, its order determined by the index of the product I . From this, we can finally express the general useful result as:

$$\Sigma_{X^n}(t_1, t_2, \dots, t_n) = \sum_{I \subseteq S} R_{X^k}(t_1, t_2, \dots, t_k) \prod_{i \in S \setminus I} (-\mu_X(t_i)) \quad (4.21)$$

where S is the partition of $\{1, 2, \dots, n\}$ with the inclusion of the null set, that is, the set of all groupings of elements such that each element is in one and only one grouping or subset; $k = \text{card}(I)$ is the cardinality of I ; I is a subset of S , and $S \setminus I$ refers to the elements of S excluding those of the current I .

As an example, we take $n = 2$ for the covariance function $\Sigma_{XX}(t_1, t_2)$. In this case, $S = \{\emptyset, \{1\}, \{2\}, \{1, 2\}\}$. The sum takes place over these four I with cardinalities 0, 1, 1, 2 respectively. The correlation term is 1 for $k = 0$, reduces to $\mu_X(t_i)$ for $k = 1$, and is a correlation function $R_{X^2}(t_i, t_j)$ for $k = 2$. This yields:

$$\begin{aligned} \Sigma_{XX}(t_1, t_2) &= \sum_{I \subseteq S} R_{X^k}(t_1, t_2, \dots, t_k) \prod_{i \in S \setminus I} (-\mu_X(t_i)) \\ &= 1 \times (-\mu_X(t_1))(-\mu_X(t_2)) + \mu_X(t_1)(-\mu_X(t_2)) + \mu_X(t_2)(-\mu_X(t_1)) + R_{X^2}(t_1, t_2) \\ &= R_{X^2}(t_1, t_2) - \mu_X(t_1)\mu_X(t_2) \end{aligned} \quad (4.22)$$

which is consistent with the known relationship Eq. 4.17. Another interesting example is the bi-covariance function $\Sigma_{XXX}(t_1, t_2, t_3)$, for which $n = 3$, that gives:

$$\begin{aligned} \Sigma_{XXX}(t_1, t_2, t_3) &= R_{X^3}(t_1, t_2, t_3) + 2\mu_X(t_1)\mu_X(t_2)\mu_X(t_3) \\ &\quad - (\mu_X(t_1)R_{X^2}(t_2, t_3) + \mu_X(t_2)R_{X^2}(t_1, t_3) + \mu_X(t_3)R_{X^2}(t_1, t_2)) \end{aligned} \quad (4.23)$$

In addition, we can also demonstrate and propose a writing for the relationship between the correlation functions and the covariances functions. Introducing again the process $V(t) = X(t) - \mu_X(t)$ which verifies:

- $\mu_V(t) = 0$ and $\mu_{VV}(t) = \sigma_{XX}(t)$, or in general $\mu_{V^n}(t) = \sigma_{X^n}(t)$,
- $\mu_X(t) = \mathbb{E}[V(t) + \mu_X]$ or $\mu_{X^n}(t) = \mathbb{E}[(V(t) + \mu_X(t))^n]$,
- $R_{X^n}(t_1, \dots, t_n) = \mathbb{E} \left[\prod_{i=1}^n (V(t_i) + \mu_X(t_i)) \right]$,
- $R_{V^n}(t_1, \dots, t_n) = \Sigma_{X^n}(t_1, \dots, t_n)$.

Knowing these relations, we proceed as before by expressing first:

$$\begin{aligned} \prod_{i=1}^n (V(t_i) + \mathbb{E}[X(t_i)]) &= \prod_{i=1}^n (V(t_i) + \mu_X(t_i)) \\ &= \sum_{I \subseteq \{1, \dots, n\}} \prod_{i \in I} V(t_i) \prod_{i \in \{1, \dots, n\} \setminus I} \mu_X(t_i), \end{aligned} \quad (4.24)$$

then we write the correlation functions as:

$$\begin{aligned}
R_{X^n}(t_1, t_2, \dots, t_n) &= \mathbb{E} \left[\prod_{i=1}^n (V(t_i) + \mu_X(t_i)) \right] \\
&= \mathbb{E} \left[\sum_{I \subseteq \{1, \dots, n\}} \prod_{i \in I} V(t_i) \prod_{i \in \{1, \dots, n\} \setminus I} \mu_X(t_i) \right] \\
&= \sum_{I \subseteq \{1, \dots, n\}} \mathbb{E} \left[\prod_{i \in I} V(t_i) \right] \prod_{i \in \{1, \dots, n\} \setminus I} \mu_X(t_i) \\
&= \sum_{I \subseteq \{1, \dots, n\}} R_{V^k}(t_1, t_2, \dots, t_k) \prod_{i \in \{1, \dots, n\} \setminus I} \mu_X(t_i)
\end{aligned} \tag{4.25}$$

to finally get the following result:

$$R_{X^n}(t_1, t_2, \dots, t_n) = \sum_{I \subseteq \{1, \dots, n\}} \Sigma_{X^k}(t_1, t_2, \dots, t_k) \prod_{i \in \{1, \dots, n\} \setminus I} \mu_X(t_i). \tag{4.26}$$

Note that, to obtain this result, we have recognized that the term $\mathbb{E}[\prod_{i \in I} V(t_i)]$ is a correlation function whose order will depend on I , as seen before, with respect to the origin of $V(t)$, which by construction corresponds to the covariance of analogous order of $X(t)$.

1.2 Extension to vector processes

Consider now a random vector $\mathbf{X}(t) = [X_1(t), X_2(t), \dots, X_n(t)]^T$ where each component is a stochastic process. The first non-central moment is:

$$\boldsymbol{\mu}_X(t) = \mathbb{E}[\mathbf{X}(t)], \tag{4.27}$$

which is a column vector of the same dimension as $\mathbf{X}(t)$, and by extension of the notation, we can write, for instance $\mu_{X_i}(t) = \mathbb{E}[X_i(t)]$ to denote the mean of a particular component. The second moment is:

$$\boldsymbol{\mu}_{\mathbf{X}\mathbf{X}}(t) = \mathbb{E}[\mathbf{X}(t)\mathbf{X}^T(t)], \tag{4.28}$$

where the matrix of moments $\boldsymbol{\mu}_{\mathbf{X}\mathbf{X}}(t)$ has dimension $n \times n$: the diagonal elements are the second moments of each component, while the off-diagonal elements are the cross-moments between different components:

$$\mu_{X_i X_j}(t) = \mathbb{E}[X_i(t)X_j(t)], \tag{4.29}$$

in the case of instantaneous moments $\mu_{X_i X_j}(t) = \mu_{X_j X_i}(t)$, and $\boldsymbol{\mu}_{\mathbf{X}\mathbf{X}}(t)$ is symmetric. The higher-order moments involve high dimensional arrays, which can be described by components. There are $N \times N \times N$ third-order moments:

$$\mu_{X_i X_j X_k}(t) = \mathbb{E}[X_i(t)X_j(t)X_k(t)], i, j, k \in [1, 2, \dots, N], \tag{4.30}$$

and similarly for the fourth moment, with $N \times N \times N \times N$ components:

$$\mu_{X_i X_j X_k X_l}(t) = \mathbb{E}[X_i(t)X_j(t)X_k(t)X_l(t)], i, j, k, l \in [1, 2, \dots, N], \tag{4.31}$$

in general, one may write of the k -th non-central moment:

$$\mu_{X_i \dots X_k}(t) = \mathbb{E}[X_i(t) \times \dots \times X_k(t)], i, \dots, k \in [1, 2, \dots, N], \tag{4.32}$$

with N^k components. The central moments admit a similar representation; for instance, the variance is:

$$\boldsymbol{\sigma}_{\mathbf{X}\mathbf{X}}(t) = \mathbb{E} \left[(\mathbf{X}(t) - \boldsymbol{\mu}_{\mathbf{X}}(t)) (\mathbf{X}(t) - \boldsymbol{\mu}_{\mathbf{X}}(t))^{\mathbf{T}} \right], \quad (4.33)$$

with a similar interpretation: the diagonal terms contain the variance of components and off-diagonal terms contains cross-variance terms. In general, one has:

$$\sigma_{X_i \dots X_k}(t) = \mathbb{E} \left[(X_i(t) - \mu_{X_i}(t)) \times \dots \times (X_k(t) - \mu_{X_k}(t)) \right], i, \dots, k \in [1, 2, \dots, N]. \quad (4.34)$$

The first inter-instant moments, or the correlation and covariance functions, are expressed as:

$$\begin{aligned} \mathbf{R}_{\mathbf{X}\mathbf{X}}(t_1, t_2) &= \mathbb{E} \left[\mathbf{X}(t_1) \mathbf{X}^{\mathbf{T}}(t_2) \right] \\ \boldsymbol{\Sigma}_{\mathbf{X}\mathbf{X}}(t_1, t_2) &= \mathbb{E} \left[(\mathbf{X}(t_1) - \boldsymbol{\mu}_{\mathbf{X}}(t_1)) (\mathbf{X}(t_2) - \boldsymbol{\mu}_{\mathbf{X}}(t_2))^{\mathbf{T}} \right], \end{aligned} \quad (4.35)$$

or by component:

$$\begin{aligned} R_{X_i X_j}(t_1, t_2) &= \mathbb{E} [X_i(t_1) X_j(t_2)] \\ \sigma_{X_i X_j}(t_1, t_2) &= \mathbb{E} \left[(X_i(t_1) - \mu_{X_i}(t_1)) (X_j(t_2) - \mu_{X_j}(t_2)) \right], \end{aligned} \quad (4.36)$$

and the $k - th$ order inter-instant moments have the general representation:

$$\begin{aligned} R_{X_i \dots X_k}(t_1, \dots, t_k) &= \mathbb{E} [X_i(t_1) \times \dots \times X_k(t_k)], i, \dots, k \in [1, 2, \dots, N] \\ \Sigma_{X_i \dots X_k}(t_1, \dots, t_k) &= \mathbb{E} \left[(X_i(t_1) - \mu_{X_i}(t_1)) \times \dots \times (X_k(t_k) - \mu_{X_k}(t_k)) \right], i, \dots, k \in [1, 2, \dots, N]. \end{aligned} \quad (4.37)$$

An important practical remark is that for cross-correlation and cross-covariance terms in nonstationary processes, symmetry is not preserved, in general:

$$R_{X_i X_j}(t_1, t_2) \neq R_{X_j X_i}(t_1, t_2); i \neq j, \quad (4.38)$$

the symmetry is achieved if index and time are permuted:

$$R_{X_i X_j}(t_1, t_2) = R_{X_j X_i}(t_2, t_1); i \neq j. \quad (4.39)$$

In the case of a random vector with complex values $\mathbf{X}(t) = [X_1(t), X_2(t), \dots, X_n(t)]^{\mathbf{T}}$, $X_i(t) \in \mathbb{C}$, once has the following expressions for the second order probabilistic moments([98]):

$$\begin{aligned} \boldsymbol{\mu}_{\mathbf{X}\mathbf{X}}(t) &= \mathbb{E} \left[\mathbf{X}(t) \mathbf{X}^{\mathbf{H}}(t) \right] \\ \boldsymbol{\sigma}_{\mathbf{X}\mathbf{X}}(t) &= \mathbb{E} \left[(\mathbf{X}(t) - \boldsymbol{\mu}_{\mathbf{X}}(t)) (\mathbf{X}(t) - \boldsymbol{\mu}_{\mathbf{X}}(t))^{\mathbf{H}} \right] \\ \mathbf{R}_{\mathbf{X}\mathbf{X}}(t_1, t_2) &= \mathbb{E} \left[\mathbf{X}(t_1) \mathbf{X}^{\mathbf{H}}(t_2) \right] \\ \boldsymbol{\Sigma}_{\mathbf{X}\mathbf{X}}(t_1, t_2) &= \mathbb{E} \left[(\mathbf{X}(t_1) - \boldsymbol{\mu}_{\mathbf{X}}(t_1)) (\mathbf{X}(t_2) - \boldsymbol{\mu}_{\mathbf{X}}(t_2))^{\mathbf{H}} \right], \end{aligned} \quad (4.40)$$

where $\mathbf{X}^{\mathbf{H}}(t)$ is the conjugate transpose of $\mathbf{X}(t)$.

1.3 Extension to fields

We now consider spatio-temporal random fields of the form $\mathcal{X}(\mathbf{x}, t)$, which depend on 3D space with coordinates \mathbf{x} and time t . Then, thinking first of a notation for ordinary moments of the second order, we propose to write:

$$\mu_{\mathcal{X}(\mathbf{x}_1)\mathcal{X}(\mathbf{x}_2)}(t) = \mathbb{E}[\mathcal{X}(\mathbf{x}_1, t)\mathcal{X}(\mathbf{x}_2, t)] \quad (4.41)$$

which allows us to extend the results obtained when stochastic processes are considered into results for stochastic fields directly. The moments of the stochastic field $\mathcal{X}(\mathbf{x}, t)$ for $1, \dots, n$ coordinates are noted as follow:

$$\mu_{\mathcal{X}(\mathbf{x}_1)\dots\mathcal{X}(\mathbf{x}_n)}(t) = \mathbb{E}[\mathcal{X}(\mathbf{x}_1, t)\dots\mathcal{X}(\mathbf{x}_n, t)], \quad (4.42)$$

$$\sigma_{\mathcal{X}(\mathbf{x}_1)\dots\mathcal{X}(\mathbf{x}_n)}(t) = \mathbb{E}[(\mathcal{X}(\mathbf{x}_1, t) - \mathbb{E}[\mathcal{X}(\mathbf{x}_1, t)])\dots(\mathcal{X}(\mathbf{x}_n, t) - \mathbb{E}[\mathcal{X}(\mathbf{x}_n, t)])] \quad (4.43)$$

$$R_{\mathcal{X}(\mathbf{x}_1)\dots\mathcal{X}(\mathbf{x}_n)}(t_1, \dots, t_n) = \mathbb{E}[\mathcal{X}(\mathbf{x}_1, t_1)\dots\mathcal{X}(\mathbf{x}_n, t_n)] \quad (4.44)$$

$$\Sigma_{\mathcal{X}(\mathbf{x}_1)\dots\mathcal{X}(\mathbf{x}_n)}(t_1, \dots, t_n) = \mathbb{E}[(\mathcal{X}(\mathbf{x}_1, t_1) - \mathbb{E}[\mathcal{X}(\mathbf{x}_1, t_1)])\dots(\mathcal{X}(\mathbf{x}_n, t_n) - \mathbb{E}[\mathcal{X}(\mathbf{x}_n, t_n)])]. \quad (4.45)$$

When two stochastic fields $\mathcal{X}_1(\mathbf{x}, t)$ and $\mathcal{X}_2(\mathbf{x}, t)$ are considered, moments are written:

$$\mu_{\mathcal{X}_1(\mathbf{x}_1)\mathcal{X}_2(\mathbf{x}_2)}(t) = \mathbb{E}[\mathcal{X}_1(\mathbf{x}_1, t)\mathcal{X}_2(\mathbf{x}_2, t)], \quad (4.46)$$

the extension to several stochastic fields $\mathcal{X}_j(\mathbf{x}, t)$ for $j = 1, \dots, n$ is written:

$$\mu_{\mathcal{X}_1(\mathbf{x}_1)\dots\mathcal{X}_n(\mathbf{x}_n)}(t) = \mathbb{E}[\mathcal{X}_1(\mathbf{x}_1, t)\dots\mathcal{X}_n(\mathbf{x}_n, t)], \quad (4.47)$$

$$\sigma_{\mathcal{X}_1(\mathbf{x}_1)\dots\mathcal{X}_n(\mathbf{x}_n)}(t) = \mathbb{E}[(\mathcal{X}_1(\mathbf{x}_1, t) - \mathbb{E}[\mathcal{X}_1(\mathbf{x}_1, t)])\dots(\mathcal{X}_n(\mathbf{x}_n, t) - \mathbb{E}[\mathcal{X}_n(\mathbf{x}_n, t)])]. \quad (4.48)$$

$$R_{\mathcal{X}_1(\mathbf{x}_1)\dots\mathcal{X}_n(\mathbf{x}_n)}(t_1, \dots, t_n) = \mathbb{E}[\mathcal{X}_1(\mathbf{x}_1, t_1)\dots\mathcal{X}_n(\mathbf{x}_n, t_n)] \quad (4.49)$$

$$\Sigma_{\mathcal{X}_1(\mathbf{x}_1)\dots\mathcal{X}_n(\mathbf{x}_n)}(t_1, \dots, t_n) = \mathbb{E}[(\mathcal{X}_1(\mathbf{x}_1, t_1) - \mathbb{E}[\mathcal{X}_1(\mathbf{x}_1, t_1)])\dots(\mathcal{X}_n(\mathbf{x}_n, t_n) - \mathbb{E}[\mathcal{X}_n(\mathbf{x}_n, t_n)])]. \quad (4.50)$$

This covers the main features of the notation and the key idea behind moment propagation as we will apply it. In the following sections, concrete examples will be developed and compared with results from the literature. The main advantage of this notation and the inherent propagation technique lies in its practicality to applied mechanical problems. It also permits a very intuitive numerical implementation of the developed expressions.

2 Morison force in offshore engineering

The Morison force describes the interaction between the oceanic wave-induced flow and a submerged cylindrical structure. Under certain conditions and after a transformation of variables, the equation can be expressed as $W(t) = a_{20}X_1^2(t) + a_{01}X_2(t)$, where $X_1(t)$ is a particle velocity, and $X_2(t)$ is an acceleration, the time derivative of $X_1(t)$: $X_2(t) = \frac{dX_1(t)}{dt} = \dot{X}_1(t)$. These random processes are assumed to be differentiable and to have a finite variance. The description of the statistical properties of $W(t)$ is important in the design of offshore structures and machines. Based on widely general assumptions in this field on that which relates to the characteristics of the velocity field as well as the response of the structure, the essential statistical descriptors are the first two moments of the response and its correlation or covariance function. These assumptions include the stationarity of the input process and the linearity of the response to the input.

We first develop the general results of interest by a direct application of the obtained formulas, thus demonstrating the ease inherent to the proposed notation and concepts. Then, to go further, assuming a Gaussian process hypothesis for $X_1(t)$, we theoretically show that some terms in the covariance function can vanish. In addition, analytically, it is shown how the higher-order moments can be related to the first two moments when this assumption is taken into account. Although these additional developments are not necessary for a numerical application of the obtained results, they allow us to compare our proposed results with the literature results provided in references [47] and [12].

2.1 General results

For the first moment of the output $W(t)$, we get:

$$\mu_W = a_{20}\mu_{X_1X_1} + a_{01}\mu_{X_2} \quad (4.51)$$

where $\mu_{X_1^2} = \mu_{X_1X_1} = \sigma_{X_1X_1} + \mu_{X_1}^2$. Then, for the second moment with respect to the origin, we have:

$$\begin{aligned} \mu_{WW} &= a_{20}^2\mu_{X_1^2X_1^2} + a_{01}^2\mu_{X_2X_2} + a_{20}a_{01}\mu_{X_1^2X_2} + a_{20}a_{01}\mu_{X_2X_1^2} \\ &= a_{20}^2\mu_{X_1X_1X_1X_1} + a_{01}^2\mu_{X_2X_2} + 2a_{20}a_{01}\mu_{X_1^2X_2} \end{aligned} \quad (4.52)$$

and we have for the variance :

$$\sigma_{WW} = a_{20}^2\sigma_{X_1^2X_1^2} + a_{01}^2\sigma_{X_2X_2} + a_{20}a_{01}\sigma_{X_2X_1^2} + a_{20}a_{01}\sigma_{X_1^2X_2}. \quad (4.53)$$

For the auto-correlation and auto-covariance functions we have:

$$R_{WW}(t_1, t_2) = a_{20}^2R_{X_1^2X_1^2}(t_1, t_2) + a_{01}^2R_{X_2X_2}(t_1, t_2) + a_{20}a_{01}\left(R_{X_2X_1^2}(t_1, t_2) + R_{X_1^2X_2}(t_1, t_2)\right) \quad (4.54)$$

$$\Sigma_{WW}(t_1, t_2) = a_{20}^2\Sigma_{X_1^2X_1^2}(t_1, t_2) + a_{01}^2\Sigma_{X_2X_2}(t_1, t_2) + a_{20}a_{01}\left(\Sigma_{X_2X_1^2}(t_1, t_2) + \Sigma_{X_1^2X_2}(t_1, t_2)\right). \quad (4.55)$$

2.2 Covariance result for a stationary Gaussian process input

If we assume that $X_1(t)$ is a stationary Gaussian process, it can be shown that the term $\Sigma_{X_2X_1^2}(t_1, t_2) + \Sigma_{X_1^2X_2}(t_1, t_2)$ in equation Eq. 4.55 vanishes, while the term $\Sigma_{X_1^2X_1^2}(t_1, t_2)$ can be expressed as $\Sigma_{X_1^2X_1^2}(\tau)$ with $\tau = t_2 - t_1$, from stationarity, and it can be related to $\Sigma_{X_1X_1}(\tau)$ and μ_{X_1} since Gaussian processes are completely defined by their two moments only.

Indeed, first, we note that:

$$\Sigma_{X_1^2X_2}(\tau) = \Sigma_{X_1^2X_1}(t_1, t_2) = \frac{\partial}{\partial t_2}\left(\Sigma_{X_1^2X_1}(t_1, t_2)\right) \quad (4.56)$$

where the following equality has been used: $\Sigma_{X_1^2X_1}(t_1, t_2) = 2\mu_{X_1}\Sigma_{X_1X_1}(t_1, t_2) = 2\mu_{X_1}\Sigma_{X_1X_1}(\tau)$; thus:

$$\Sigma_{X_1^2X_2}(\tau) = 2\mu_{X_1}\frac{\partial}{\partial t_2}\left(\Sigma_{X_1X_1}(t_1, t_2)\right) = 2\mu_{X_1}\frac{\partial}{\partial \tau}\left(\Sigma_{X_1X_1}(\tau)\right) = 2\mu_{X_1}\dot{\Sigma}_{X_1X_1}(\tau). \quad (4.57)$$

Then, from another side, we have:

$$\Sigma_{X_2X_1^2}(\tau) = \Sigma_{X_1X_1^2}(t_1, t_2) = \frac{\partial}{\partial t_1}\left(\Sigma_{X_1X_1^2}(t_1, t_2)\right) \quad (4.58)$$

by using $\Sigma_{X_1X_1^2}(t_1, t_2) = 2\mu_{X_1}\Sigma_{X_1X_1}(t_1, t_2) = 2\mu_{X_1}\Sigma_{X_1X_1}(\tau)$; it follows that:

$$\Sigma_{X_2X_1^2}(\tau) = 2\mu_{X_1}\frac{\partial}{\partial t_1}\left(\Sigma_{X_1X_1}(t_1, t_2)\right) = -2\mu_{X_1}\frac{\partial}{\partial \tau}\left(\Sigma_{X_1X_1}(\tau)\right) = -2\mu_{X_1}\dot{\Sigma}_{X_1X_1}(\tau). \quad (4.59)$$

As a consequence, it is deduced that $\Sigma_{X_2X_1^2}(\tau) + \Sigma_{X_1^2X_2}(\tau) = 0$ from relations Eq. 4.57 and Eq. 4.59, and equation Eq. 4.55 simplifies to:

$$\Sigma_{WW}(t_1, t_2) = a_{20}^2\Sigma_{X_1^2X_1^2}(t_1, t_2) + a_{01}^2\Sigma_{X_2X_2}(t_1, t_2) \quad (4.60)$$

where $\Sigma_{X_1^2X_1^2}(\tau) = R_{X_1^2X_1^2}(t_1, t_2) - \mu_{X_1}^2\mu_{X_1}^2$. From the application of the result by [148], we deduce that:

$$R_{X_1^2X_1^2}(t_1, t_2) = \mu_{X_1}^2\mu_{X_1}^2 + 2\Sigma_{X_1X_1}^2(t_1, t_2) + 4\mu_{X_1}\mu_{X_1}\Sigma_{X_1X_1}(t_1, t_2) \quad (4.61)$$

thus:

$$\Sigma_{X_1^2 X_1^2}(\tau) = 2\Sigma_{X_1 X_1}^2(\tau) + 4\mu_{X_1} \mu_{X_1} \Sigma_{X_1 X_1}(\tau) \quad (4.62)$$

and finally we can express the covariance of the output purely in terms of the covariance of the input as:

$$\Sigma_{WW}(\tau) = a_{20}^2 (2\Sigma_{X_1 X_1}^2(\tau) + 4\mu_{X_1} \mu_{X_1} \Sigma_{X_1 X_1}(\tau)) + a_{01}^2 \Sigma_{X_2 X_2}(t_1, t_2). \quad (4.63)$$

2.3 Comparison with two existing results in the literature

Results of reference [47] In reference [47], a method is proposed to study of the extremes of the Morison force, for which some statistical characteristics are necessary. The proposed method is applicable beyond the case without current, a condition that limited many of the results available at the time. Using an analytical approach consisting of normalization of the input processes, the results presented with respect to dimensionless parameters and under the assumption of Gaussianity and stationarity are:

$$\begin{aligned} m_W &= \xi y_0^2 \\ s_W^2 &= (\zeta^2 + \beta^2) y_0^4 \end{aligned} \quad (4.64)$$

where the notation used is m_W for the mean of the response process $W(t)$, s_W^2 for the variance of this response, y_0 for the mean of the input velocity $X_1(t)$, being the current velocity, and ξ, ζ, β are dimensionless variables related to the statistical properties of the inputs adjusted by some scale measure:

$$\xi = \frac{m_1}{y_0^2}, \zeta = \frac{s_1}{y_0^2}, \beta = \frac{\alpha s_{X_2}}{y_0^2}, \alpha = \frac{s_{X_1}}{y_0^2} \quad (4.65)$$

where m_1 and s_1 are the mean and standard deviation of $X_1^2(t)$, s_{X_1} is the standard deviation of $X_1(t)$, s_{X_2} is the standard deviation of the acceleration $X_2(t)$. In this development, the Gaussianity of the velocity implies the decorrelation between velocity and acceleration when evaluated at the same time.

Coming back to our formulation and making $a_{20} = 1$ in expression Eq. 4.51, we get the expression for the first moment, introducing the zero mean of the acceleration $\mu_{X_2} = 0$:

$$\begin{aligned} \mu_W &= \mu_{X_1 X_1} + a_{01} \mu_{X_2} \\ &= \mu_{X_1 X_1} \end{aligned} \quad (4.66)$$

while, for the variance, taking the result Eq. 4.53 and introducing $\mu_{X_1^2 X_2} = 0$ (decorrelation among the variables):

$$\begin{aligned} \sigma_{WW} &= \sigma_{X_1^2 X_1^2} + a_{01} \sigma_{X_2 X_2} \\ &= (\mu_{X_1 X_1 X_1 X_1} - \mu_{X_1 X_1}^2) + a_{01} \mu_{X_2 X_2} \end{aligned} \quad (4.67)$$

since the process $X_2(t)$ has zero mean from which it follows that $\mu_{X_2 X_2} = \sigma_{X_2 X_2}$. Hence, we can notice the consistency of the results with those in the reference by studying the substitutions:

$$\begin{aligned} m_W &= \frac{m_1}{y_0^2} y_0^2 = m_1 \\ s_W^2 &= \left(\left(\frac{s_1}{y_0^2} \right)^2 + \left(\frac{\alpha s_{X_2}}{y_0^2} \right)^2 \right) y_0^4 = s_1^2 + \alpha^2 s_{X_2}^2 \end{aligned} \quad (4.68)$$

Thus, for a normalized process where $a_{20} = 1$, it is possible to recognize the similarity between these two results. The mean of the response m_1 is the mean of $X_1^2(t)$, and the variance of the response is a combination of the variances of $X_1^2(t)$ and $X_2(t)$. However, the comparison is not direct at first reading, given the successive normalization and approximation or assumption taken in the reference [47]. In practice, as seen in the first developments, our proposed notation allows us to easily consider the parameters' general values without normalization to see how they propagate into the results with no more development steps.

	Monte-Carlo	Borgman [12]	Proposed
μ_W [Nm]	5.213×10^4	5.213×10^4	5.213×10^4
μ_{W^2} [N ² m ²]	3.291×10^9	3.287×10^9	3.291×10^9

Table 4.1: Results comparison with Monte-Carlo simulation, reference [12], and proposed formulas

Results of reference [12] In reference [12], another analytical approach is used to characterize the output process $W(t)$ of a Morison force. These results are valid for an input Gaussian process $X_1(t)$. The following expressions are presented in the theorem 4.4 of [12]:

$$\begin{aligned}\mu_W &= \frac{[\gamma \mathcal{Z}(\gamma) + (\gamma^2 + 1) \mathcal{P}(\gamma)]}{\alpha} \\ \mu_{W^2} &= \frac{[\gamma^4 + 6\gamma^2 + 3]}{4\alpha^2 + 1}\end{aligned}\quad (4.69)$$

where $\alpha = \frac{\rho k}{2cs^2}$ and $\gamma = \frac{m}{s}$ for $m = \mu_{X_1}$, $\mathcal{Z}(x) = (2\pi)^{-\frac{1}{2}} \exp\left[-\frac{x^2}{2}\right]$, and $\mathcal{P}(x) = \int_0^x \mathcal{Z}(y) dy$, while s is the standard deviation of the velocity, ρ is the standard deviation of the acceleration; $c = a_{20}$, $k = a_{01}$ are the Morison constants, and m is the mean velocity. Compared to already established expressions Eq. 4.51 and Eq. 4.52 obtained in the proposed notation, we get a more readable result. Moreover, we remark that, while very precise in numerical terms, the initial expressions for $\mathcal{P}(x)$ and $\mathcal{Z}(x)$ functions require a non-trivial computational effort in their evaluations.

A numerical comparison in Tab. 4.1 is presented with the results for the first two non-central moments calculated by a Monte-Carlo simulation, the results from Borgman, reference [12], and the equations obtained using the proposed notation. The values of the coefficients are $c = 2.7038 \times 10^4$; $k = 2.9729 \times 10^5$; the processes have: $\sigma_{X_1 X_1} = 0.0873$; $\sigma_{X_2 X_2} = 0.0010$ and $\mu_{X_1} = 1.3568$; $\mu_{X_2} = 0$. For the Monte-Carlo simulation, the computational procedure detailed in reference [135]¹ is used to simulate 10,000 samples of $X_1(t)$ and $X_2(t)$, and the empirical statistics obtained are averaged over one hundred runs. Tab. 4.1 demonstrates the consistency among these results.

For the correlation function, Borgman demonstrates the following expression in theorem 5.1:

$$\begin{aligned}R_{WW}(t_1, t_2) &= c^2 s_1^2 s_2^2 G(r_{vv}) + k^2 \rho_1 \rho_2 r_{aa} \\ &\quad + ck \left(\frac{8}{\pi}\right)^{\frac{1}{2}} (\rho_2 s_1^2 r_{va} + \rho_1 s_2^2 r_{av})\end{aligned}\quad (4.70)$$

with:

$$G(r) = \frac{\left[(2 + 4r^2) \arcsin r + 6r(1 - r^2)^{\frac{1}{2}} \right]}{\pi}\quad (4.71)$$

where s_1, s_2 are the standard deviations of the velocity at times t_1, t_2 , ρ_1, ρ_2 are the standard deviations of the acceleration, $r_{vv}, r_{aa}, r_{av}, r_{va}$ are the correlation coefficients of the corresponding processes. Noticing that $s_1^2 s_2^2 G(r_{vv}) = R_{X_1^2 X_1^2}(t_1, t_2)$ is a result derived from the properties of Gaussian processes, $\rho_1 \rho_2 r_{aa} = R_{X_2 X_2}(t_1, t_2)$ and $\left(\frac{8}{\pi}\right)^{\frac{1}{2}} (\rho_2 s_1^2 r_{va} + \rho_1 s_2^2 r_{av}) = R_{X_2 X_1^2}(t_1, t_2) + R_{X_1^2 X_2}(t_1, t_2)$, the correspondence between the expressions Eq. 4.70 and Eq. 4.54 can be checked.

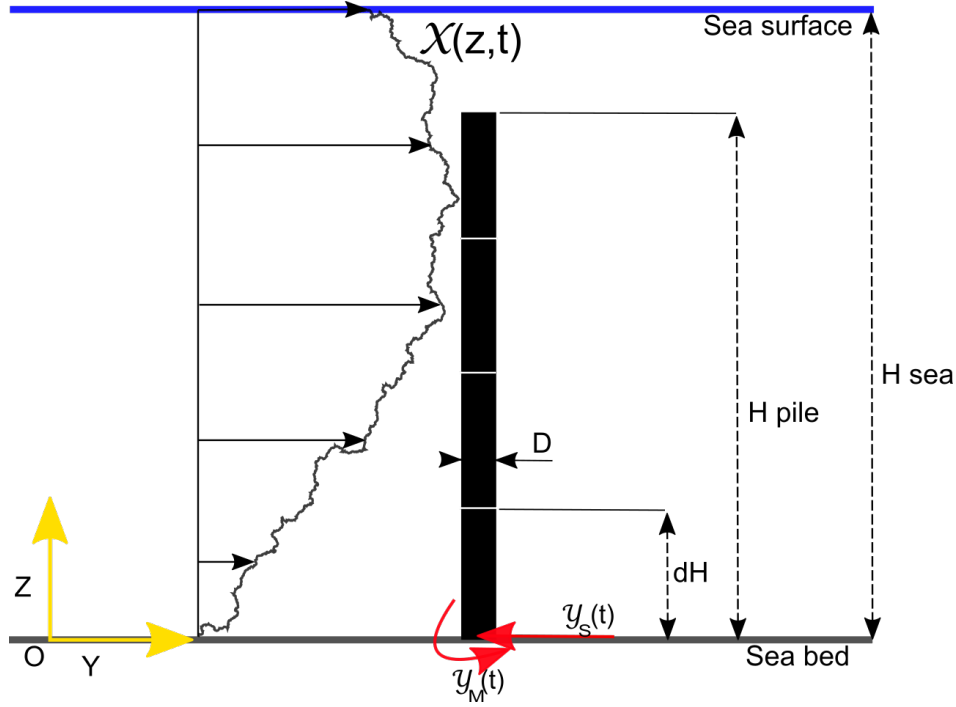


Figure 4.1: Diagram of the problem

3 Morison load with stochastic field input and PDF reconstruction

3.1 System description and input field

This application concerns the probabilistic characterization of the mechanical moment² that results from a flow that acts on a submerged pile, assuming it is a rigid cylinder of height H_{pile} and diameter D_{pile} . The flow is assumed to be aligned along the y -direction, without diffraction effects, and modeled by $\mathcal{X}_1(\mathbf{x}, t)$, a stochastic field describing the velocity of a turbulent flow that depends on the depth which is aligned with the z -coordinate. This stochastic field is assumed to be differentiable and to have a finite variance.

The bending moment can be expressed as:

$$Z(t) = \int_{\mathbb{V}} \mathbf{a}_{220}(\mathbf{x}) \mathcal{X}_1^2(\mathbf{x}, t) + \mathbf{a}_{201}(\mathbf{x}) \mathcal{X}_2(\mathbf{x}, t) d\mathbf{x} \quad j = 1, 2 \quad (4.72)$$

where $\mathcal{X}_2(\mathbf{x}, t) = \frac{d}{dt} [\mathcal{X}_1(\mathbf{x}, t)]$, $\mathbf{a}_{120}(\mathbf{x}) = k_{\text{drag}}$, $\mathbf{a}_{101}(\mathbf{x}) = k_{\text{inertia}}$, $\mathbf{a}_{220}(\mathbf{x}) = k_{\text{drag}}z$, $\mathbf{a}_{201}(\mathbf{x}) = k_{\text{inertia}}z$, $k_d = \frac{1}{2}\rho_f C_{\text{drag}} D_{\text{pile}}$, $k_{\text{inertia}} = \frac{\pi}{4}\rho_f C_{\text{inertia}} D_{\text{pile}}^2$ for ρ_f the fluid density, C_{drag} the drag coefficient, C_{inertia} the inertia coefficient, and \mathbb{V} the support of $\mathbf{x} = [x, y, z]^T$. Expression Eq. 4.72 comes from the Morison formula [90] when $\mathcal{X}_1(\mathbf{x}, t) > 0 \forall t$.

Classical assumptions for the statistical characterization of the input stochastic field are stationarity over a given period of time and Gaussianity. Consequently, it can be described by only its mean $\mu_{\mathcal{X}_1(\mathbf{x})}$, which models the physical current, and its covariance function to model the physical turbulence. For this application, the covariance function is assumed to be of the following form:

¹Annex D contains a synthetic overview of this and other procedures to simulate stochastic processes

²At this stage, we inevitably find ourselves referring to two entirely different quantities as moments: probabilistic moments and mechanical moments. We will insist on the distinction to prevent confusion.

$$\Sigma_{\mathcal{X}_1(\mathbf{x}_1)\mathcal{X}_1(\mathbf{x}_2)}(\tau) = \rho_{\mathcal{X}_1(\mathbf{x}_1)\mathcal{X}_1(\mathbf{x}_2)}(\tau) \sqrt{\sigma_{\mathcal{X}_1(\mathbf{x}_1)\mathcal{X}_1(\mathbf{x}_1)} \sigma_{\mathcal{X}_1(\mathbf{x}_2)\mathcal{X}_1(\mathbf{x}_2)}} \quad (4.73)$$

where $\tau = t_2 - t_1$ and $\rho_{\mathcal{X}_1(\mathbf{x}_1)\mathcal{X}_1(\mathbf{x}_2)}(\tau)$ is the covariance coefficient of the stochastic field, decomposed into a spatial $\rho_{\mathcal{X}_1(\mathbf{x}_1)\mathcal{X}_1(\mathbf{x}_2)}^{\text{space}}$ and a temporal function $\rho^{\text{time}}(\tau)$ as:

$$\rho_{\mathcal{X}_1(\mathbf{x}_1)\mathcal{X}_1(\mathbf{x}_2)}(\tau) = \rho_{\mathcal{X}_1(\mathbf{x}_1)\mathcal{X}_1(\mathbf{x}_2)}^{\text{space}} \rho^{\text{time}}(\tau). \quad (4.74)$$

Moreover, from the Gaussianity assumption, it is known that:

$$\Sigma_{\mathcal{X}_1^2(\mathbf{x}_1)\mathcal{X}_1^2(\mathbf{x}_2)}(\tau) = 2\Sigma_{\mathcal{X}_1(\mathbf{x}_1)\mathcal{X}_1(\mathbf{x}_2)}^2(\tau) + 4\mu_{\mathcal{X}_1(\mathbf{x}_1)}\mu_{\mathcal{X}_1(\mathbf{x}_2)}\Sigma_{\mathcal{X}_1(\mathbf{x}_1)\mathcal{X}_1(\mathbf{x}_2)}(\tau) \quad (4.75)$$

$$\begin{aligned} \Sigma_{\mathcal{X}_1^2(\mathbf{x}_1)\mathcal{X}_1^2(\mathbf{x}_2)\mathcal{X}_1^2(\mathbf{x}_3)}(\tau_1, \tau_2) = & 8 [\mu_{\mathcal{X}_1(\mathbf{x}_1)}\mu_{\mathcal{X}_1(\mathbf{x}_2)}\Sigma_{\mathcal{X}_1(\mathbf{x}_1)\mathcal{X}_1(\mathbf{x}_3)}(\tau_2 - \tau_1)\Sigma_{\mathcal{X}_1(\mathbf{x}_2)\mathcal{X}_1(\mathbf{x}_3)}(\tau_2) \\ & + \mu_{\mathcal{X}_1(\mathbf{x}_2)}\mu_{\mathcal{X}_1(\mathbf{x}_3)}\Sigma_{\mathcal{X}_1(\mathbf{x}_1)\mathcal{X}_1(\mathbf{x}_2)}(\tau_1)\Sigma_{\mathcal{X}_1(\mathbf{x}_1)\mathcal{X}_1(\mathbf{x}_3)}(\tau_2 - \tau_1) \\ & + \mu_{\mathcal{X}_1(\mathbf{x}_1)}\mu_{\mathcal{X}_1(\mathbf{x}_3)}\Sigma_{\mathcal{X}_1(\mathbf{x}_1)\mathcal{X}_1(\mathbf{x}_2)}(\tau_1)\Sigma_{\mathcal{X}_1(\mathbf{x}_2)\mathcal{X}_1(\mathbf{x}_3)}(\tau_2) \\ & + \Sigma_{\mathcal{X}_1(\mathbf{x}_1)\mathcal{X}_1(\mathbf{x}_2)}(\tau_1)\Sigma_{\mathcal{X}_1(\mathbf{x}_1)\mathcal{X}_1(\mathbf{x}_3)}(\tau_2 - \tau_1)\Sigma_{\mathcal{X}_1(\mathbf{x}_2)\mathcal{X}_1(\mathbf{x}_3)}(\tau_2)] \end{aligned} \quad (4.76)$$

Tab. 4.2 shows the parameters used for the numerical implementation. In addition, the mean velocity is expressed as a polynomial of the fourth degree in order to fit measured data presented in reference [79] :

$$\mu_{\mathcal{X}_1(\mathbf{x})} = -4.414 \times 10^{-6} z^4 + 3.312 \times 10^{-4} z^3 - 8.350 \times 10^{-3} z^2 + 9.700 \times 10^{-2} z + 9.215 \times 10^{-1} [\text{m/s}] \quad (4.77)$$

and the variance is expressed as:

$$\sigma_{\mathcal{X}_1(\mathbf{x})\mathcal{X}_1(\mathbf{x})} = (TI)^2 \mu_{\mathcal{X}_1(\mathbf{x})}^2 \left(\frac{z}{H_{\text{sea}}} \right)^{\frac{1}{\alpha}} \quad (4.78)$$

where TI is the turbulence index of the flow and α is identified from measurements [79]. The correlation function is modeled by:

$$\begin{aligned} \rho_{\mathcal{X}_1(\mathbf{x}_1)\mathcal{X}_1(\mathbf{x}_2)}^{\text{space}} &= \left(1 - \left(\frac{z_2 - z_1}{L} \right)^2 \right) \exp \left(- \left(\frac{z_2 - z_1}{L} \right)^2 \right) && \text{Spatial correlation} \\ \rho^{\text{time}}(\tau) &= \text{FT}^{-1}[S(f)] && \text{Temporal correlation} \end{aligned} \quad (4.79)$$

where L is the correlation length, $\text{FT}[\bullet]$ is the Fourier Transform operator and f is the frequency, while $S(f)$ is expressed by (see Fig. 4.2):

$$S(f) = \frac{1}{f^4} \exp \left(- \frac{8 \times 10^{-4}}{f^{\frac{5}{3}}} \right) \left[\frac{\text{m}^2}{\text{s}^2} \text{Hz}^{-1} \right] \quad (4.80)$$

to fit the experimental data presented in reference [137].

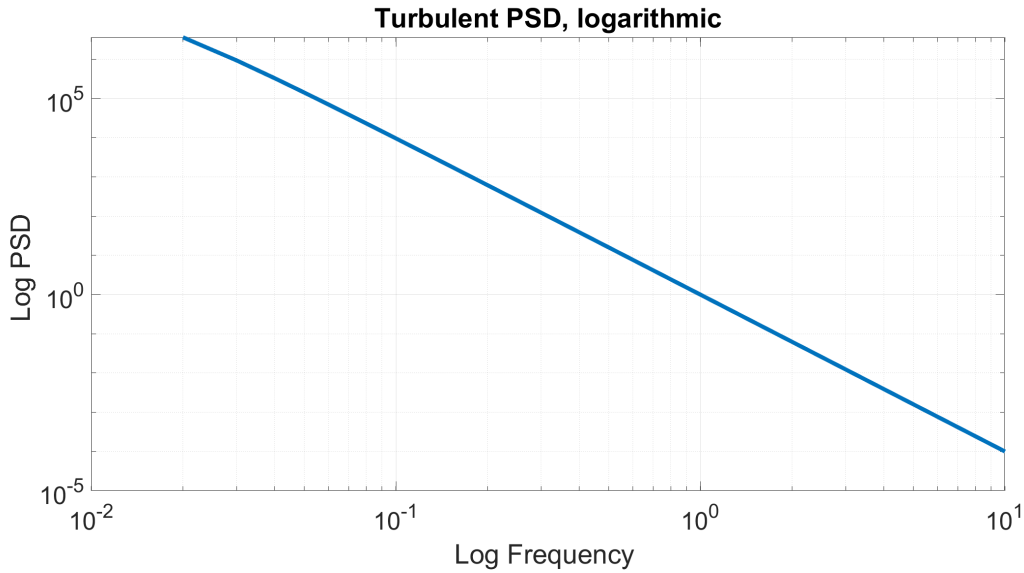


Figure 4.2: Power Spectral Density (PSD) function S of the velocity field

Property	Value
ρ_f	1030 [kgm^{-3}]
D	3.5 [m]
C_{drag}	1.15
C_{inertia}	2
H_{sea}	40 [m]
H_{pile}	30 [m]
α	7.1
TI	$\frac{25}{100}$
L_ρ	$\frac{H_{\text{sea}}}{3}$ [m]

Table 4.2: Physical properties of the submerged pile application

3.2 PDF reconstruction from moments

Maximum entropy distribution The maximum entropy (ME) principle is used to fit a probability density function (PDF) given a number of constraints in the centered or non-centered moments of the underlying random variable. The advantage of this method is that the least number of assumptions about the distribution needs to be made. Among the limitations of this approach, the most concerning one is that the process of finding the associated coefficients (or Lagrange multipliers) involves the resolution of a system of nonlinear equations, which is a problem that has a heavy sensitivity to the choice of the initial point from a numerical perspective.

The maximum entropy problem can be written as [5, 136]:

$$\begin{aligned}
 \int_S h_i(x) f(x) dx &= \alpha_i \\
 H[f(x)] &= \int_S f(x) \log(f(x)) dx \\
 f(x) &= \exp[\lambda_0 + \sum_{i=1}^{\infty} \lambda_i h_i(x)]
 \end{aligned} \tag{4.81}$$

where $H[f(x)]$ is the entropy functional $f(x)$ is the PDF of a random variable X , x are realizations of said random variable, S is the support of X , α_i are the moments of $f(x)$ and the functions $h_i(x)$ allow us to define these moments. For instance, with non-centered moments, one has $h_i(x) = x^i; i = 1, 2, \dots$. In practice, the previous expression is truncated to a finite number of terms. Notice that $f(x)$, as defined in the previous equation, is the solution to the variational problem defined before. Since $f(x)$ is the PDF that maximizes the entropy functional,

the problem is reduced to finding the corresponding λ_i . The system of equations that needs to be solved, given a truncated summation, is the following :

$$\begin{aligned} \int_S f(x) dx &= 1 \\ \int_S h_1(x) f(x) dx &= \alpha_1 \\ \int_S h_2(x) f(x) dx &= \alpha_2 \\ \int_S h_3(x) f(x) dx &= \alpha_3 \\ \int_S h_4(x) f(x) dx &= \alpha_4 \end{aligned} \quad (4.82)$$

which can be rearranged, introducing $\hat{f}(x) = \exp[\lambda_o + \sum_{i=1}^4 \lambda_i h_i(x)]$, and defining the objective vector function:

$$\mathbf{G}(\lambda_i) = \begin{bmatrix} 1 - \int_S \hat{f}(x) dx \\ \alpha_1 - \int_S x \hat{f}(x) dx \\ \alpha_2 - \int_S x^2 \hat{f}(x) dx \\ \alpha_3 - \int_S x^3 \hat{f}(x) dx \\ \alpha_4 - \int_S x^4 \hat{f}(x) dx \end{bmatrix}, \quad (4.83)$$

so the optimization problem can be formulated as:

$$\underset{\lambda_i}{\text{minimize}} [\mathbf{G}(\lambda_i)] \quad (4.84)$$

in other words, we seek the λ_i that solve the previous system of equations within certain numerical tolerance.

Addressing sensitivity to initial conditions The problem defined in Eq. 4.84 is very sensitive to the choice of initial λ_i selected to search for the solution. Two steps are sketched to address this issue from a practical perspective:

1. The maximum entropy distribution with two moments results in the PDF of a Gaussian process. By comparing the ME PDF and the standard PDF of a Gaussian random variable, one can deduce an initial point very close to the solution.
2. From empirical observations, the PDF with four moments has the shape of a Gaussian with some minor “perturbations” applied to it. So, given four statistical moments, we solve the ME problem for the first two moments using the relationships mentioned in the previous point. Then, the ME problem is formulated with four moments, and as starting point, we pick the solution of the Gaussian case. The two new multipliers are initially set to zero.

The relationships for the Gaussian approximation are:

$$\begin{aligned} \lambda_0 &= \ln \sigma \sqrt{2\pi} + \frac{1}{2} \left(\frac{\mu}{\sigma} \right)^2 \\ \lambda_1 &= -\frac{\mu}{\sigma^2} \\ \lambda_2 &= \frac{1}{2\sigma^2} \end{aligned} \quad (4.85)$$

where we have committed the sub-indexes in the mean and variance, given the clarity of the context.

3.3 Results

Probabilistic moments of the response Recasting Eq. 4.72 as:

$$\mathbf{Z}(t) = \int_V \mathbf{a}(z) \mathcal{X}(z, t) + \mathbf{b}(z) \mathcal{Y}(z, t) dz, \quad (4.86)$$

notice the fact that this transforms the sum of two fields into a stochastic process, in the case at hand the mechanical or “overturning” moment at the base of the pile. As $Z(t)$ is a process, it can be treated with our previous developments concerning PDF reconstruction. The general relationships for the first four non-central moments are as follows:

$$\mu_Z = \int_L a\mu_{\mathcal{X}(z)\mathcal{X}(z)} + b\mu_{\mathcal{Y}(z)} dz, \quad (4.87)$$

$$\mu_{ZZ} = \int_L \int_L a^2\mu_{\mathcal{X}^2(z_1)\mathcal{X}^2(z_2)} + b^2\mu_{\mathcal{Y}(z_1)\mathcal{Y}(z_2)} + 2ab\mu_{\mathcal{X}^2(z_1)\mathcal{Y}(z_2)} dz_1 dz_2, \quad (4.88)$$

the third moment reads:

$$\begin{aligned} \mu_{ZZZ} = & \int_L \int_L \int_L a^3\mu_{\mathcal{X}^2(z_1)\mathcal{X}^2(z_2)\mathcal{X}^2(z_3)} + b^3\mu_{\mathcal{Y}(z_1)\mathcal{Y}(z_2)\mathcal{Y}(z_3)} \\ & + 3a^2b\mu_{\mathcal{X}^2(z_1)\mathcal{X}^2(z_2)\mathcal{Y}(z_3)} + 3ab^2\mu_{\mathcal{X}^2(z_1)\mathcal{Y}(z_2)\mathcal{Y}(z_3)} dz_1 dz_2 dz_3, \end{aligned} \quad (4.89)$$

the fourth:

$$\begin{aligned} \mu_{Z^4} = & \int_L \int_L \int_L \int_L a^4\mu_{\mathcal{X}^2(z_1)\mathcal{X}^2(z_2)\mathcal{X}^2(z_3)\mathcal{X}^2(z_4)} \\ & + b^4\mu_{\mathcal{Y}(z_1)\mathcal{Y}(z_2)\mathcal{Y}(z_3)\mathcal{Y}(z_4)} + 4a^3b\mu_{\mathcal{X}^2(z_1)\mathcal{X}^2(z_2)\mathcal{X}^2(z_3)\mathcal{Y}(z_4)} \\ & + 6a^2b^2\mu_{\mathcal{X}^2(z_1)\mathcal{X}^2(z_2)\mathcal{Y}(z_3)\mathcal{Y}(z_4)} \\ & + 4ab^3\mu_{\mathcal{X}^3(z_1)\mathcal{Y}(z_2)\mathcal{Y}(z_3)\mathcal{Y}(z_4)} dz_1 dz_2 dz_3 dz_4, \end{aligned} \quad (4.90)$$

and the variance:

$$\sigma_{ZZ} = \int_L \int_L a^2\sigma_{\mathcal{X}^2(z_1)\mathcal{X}^2(z_2)} + b^2\sigma_{\mathcal{Y}(z_1)\mathcal{Y}(z_2)} + dz_1 dz_2, \quad (4.91)$$

and in a similar manner the inter-temporal moments can be obtained, for instance the covariance:

$$\begin{aligned} \Sigma_{ZZ}(t_1, t_2) = & \int_{L^2} a^2\Sigma_{\mathcal{X}^2(z_1)\mathcal{X}^2(z_2)}(t_1, t_2) dz_1 dz_2 \\ & + \int_{L^2} b^2\Sigma_{\mathcal{Y}(z_1)\mathcal{Y}(z_2)}(t_1, t_2) dz_1 dz_2 \\ & + \int_{L^2} ab\Sigma_{\mathcal{X}^2(z_1)\mathcal{Y}(z_2)}(t_1, t_2) dz_1 dz_2 \\ & + \int_{L^2} ab\Sigma_{\mathcal{Y}(z_1)\mathcal{X}^2(z_2)}(t_1, t_2) dz_1 dz_2. \end{aligned} \quad (4.92)$$

			Transformation	Empirical(MC)	Equation
$E[Z]$	$\times 10^6$	$[Nm]$	6.8318	6.8313	Eq. 4.87
$E[Z^2]$	$\times 10^{13}$	$[N^2m^2]$	5.1697	5.1670	Eq. 4.88
$E[Z^3]$	$\times 10^{20}$	$[N^3m^3]$	4.2693	4.2692	Eq. 4.89
$E[Z^4]$	$\times 10^{27}$	$[N^4m^4]$	3.8153	3.8151	Eq. 4.90
$Var[Z]$	$\times 10^{12}$	$[N^2m^2]$	5.0240	5.0036	Eq. 4.91

Table 4.3: Moments of the response, integral transformation formula vs empirical (MC)

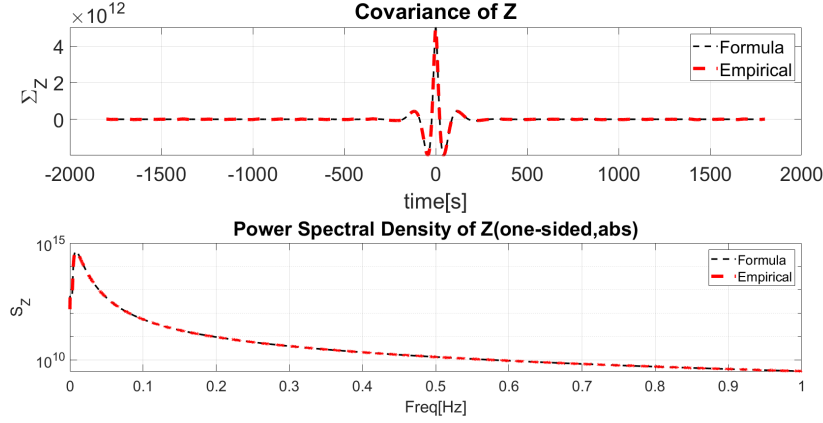


Figure 4.3: Covariance of Z and one-sided PSD, Transformation (4.92) vs empirical (MC)

These developments are broadly general, at least within the confines of the input processes considered in application. These expressions simplify considerably when the Gaussian hypothesis is introduced, as previously stated; for instance, considering a Gaussian $X(t_1)$ and $Y(t_1) = \dot{X}(t_1)$, these two processes are independent, hence decorrelated, and their inter-covariance is zero. It is worth noting that, by means of Wiener's theorem, this moment description also yields the PSD of the response: $S_{ZZ}(f) = TF[\Sigma_{ZZ}(t_1, t_2)]$, which is the basis of the spectral characterization of the response process.

The results of implementing these equations have been compared with the corresponding MC simulation, as shown in Tab. 4.3 and Fig. 4.3. The way in which the computations have been made is as follows:

- The MCS has been carried out by spatial and temporal discretization of the field as vector processes. The number of processes has been selected by testing the convergence in mean and variance, with 20 processes being employed at convergence and for comparison.
- The transformation equations are computed numerically, first expressing the required input probabilistic moments as functions and then evaluating the corresponding integrals by adaptive quadrature integration. The implementation has been done in the Matlab framework.
- In terms of ensemble convergence, 1×10^4 realizations have been selected, with similar criteria over mean and variance convergence.

PDF reconstruction and EVD We use the results in the preceding sections to calculate the ME estimator of the response PDF. The problem specifications remain the same as before, while the comparison is among a Monte-Carlo simulation with an empirical PDF commercial subroutine, an ME fit with two specified moments (ME-2M), and an ME fit with four specified moments (ME-4M). It can be shown that the maximum entropy

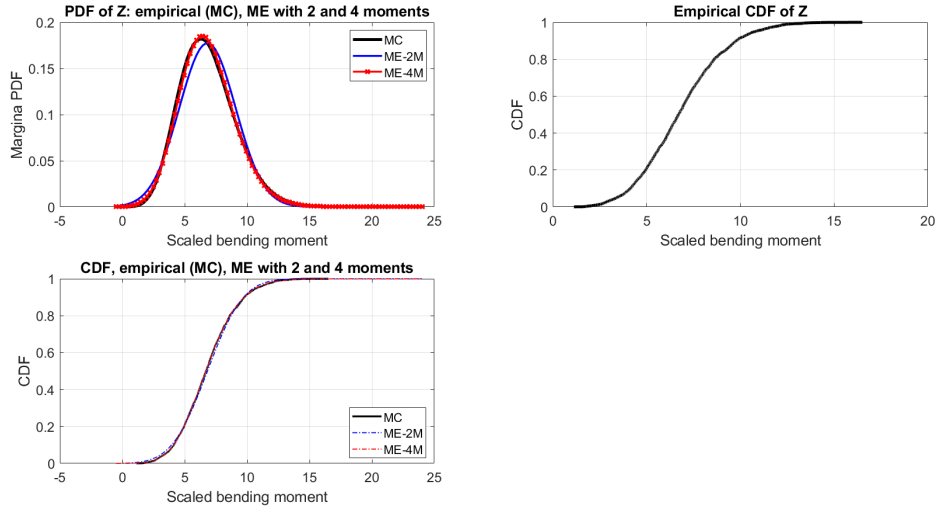


Figure 4.4: PDF and CDF of Z: empirical (MC) and ME distribution (2 and 4 moments)

PDF with two moments is equivalent to that of a Gaussian distribution, and so the non-Gaussianity of the response becomes evident from the comparison in Fig. 4.4. It must be noted that the flexibility of the approach presented is one of its main advantages. The shape of the PDF will be heavily reliant on the ratio of the drag component to the inertia component; for instance, [2] defines $K = \frac{2C_D\sigma_{XX}}{\pi C_M D \sqrt{\sigma_{YY}}}$, and the response tends to the Gaussian as $K \rightarrow 0$, and its non-Gaussianity is more prominent as $K \rightarrow \infty$. The case under study corresponds to $K \approx 0.25$. The sensitivity of the PDF on this parameter is clear, given how close to the extreme of Gaussianity it is while producing a PDF that has considerable asymmetry. For situations in which K is higher, additional moments may be warranted to ensure an accurate fit of the maximum entropy to the resulting PDF.

The ME PDF is integrated to obtain the ME CDF, with which an isoprobabilistic transformation can be established such that the non-gaussian process $Z(t)$ can be simulated by Gaussian Translation ([65]). In particular, by sampling a Gaussian parent process, the mean number of upcrossings λ_Z^+ of $Z(t)$ can be estimated, and under the Poisson hypotheses Eq. 1.25 yields the estimated EVD: the ME+TGP+Poisson estimation of the EVD. The results obtained from this methodology are compared with two MCMs: 1) directly counting the upcrossings of the 1×10^4 samples of process $Z(t)$ to obtain an empirical mean number of upcrossings λ_Z^+ in combination with Eq. 1.25 to obtain the Counting+Poisson estimation of the EVD, 2) using a commercial subroutine to find the maximum value of each of the 1×10^4 samples of process $Z(t)$, to then find the CDF of this sample of extreme values to obtain what we term MC empirical estimation of the EVD. Finally, the statistical method, usually referred to as the Square Root of the Sum of Squares (SRSS), is also used for comparison, the motivation being the widespread usage of this technique as a first-resolution attempt in various practical domains.

The results for the EVD are shown in Fig. 4.5; the most remarkable feature is also the most expected: the SRSS, despite its practicality, behaves poorly for random quantities that are not uncorrelated. While the ME+TGP+Poisson estimation is close to the empirical MCS, a significant deviation exists. These deviations can not be attributed to the Poisson assumption in the modeling of the extremes, as the direct counting method relies on the same choice and yet results in a much closer fit. The logical conclusion is a deficient estimation of λ_Z^+ by the TGP method.

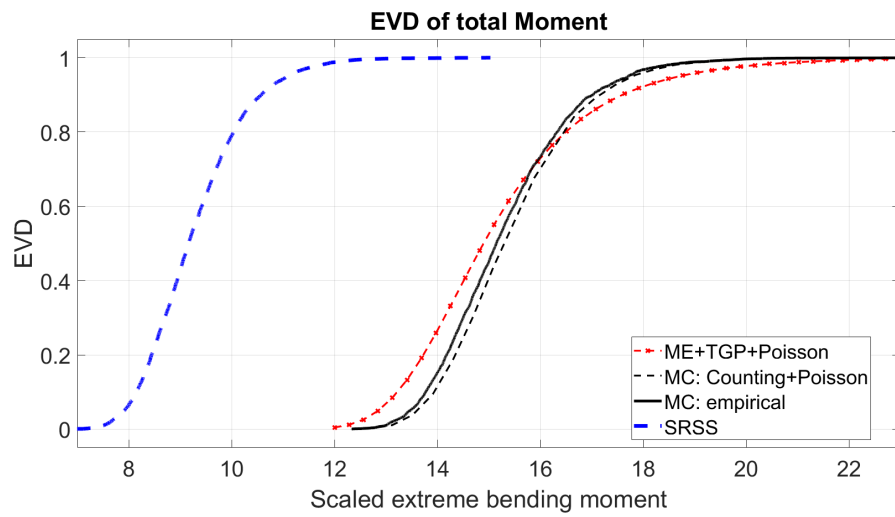


Figure 4.5: Extreme value distribution: Empirical (black), Direct upcrossing counting (dashed black), SRSS (blue), and proposed (red)

Chapter 5

Moment propagation in LTP systems with periodic modal representation

“This is exactly the sort of thing that happens when you recklessly try to have fun without taking the time to analyze your situation mathematically.”

Hannah Fry, *The Indisputable Existence of Santa Claus: The Mathematics of Christmas*

This chapter combines the key results in Floquet theory and moment propagation to produce a systematic treatment of Floquet systems under stochastic excitation. The first section extends the methods developed in the previous chapter to a basic cyclic process, taking a concrete but typical example that will allow us to establish some features of this type of transformation. The second section utilizes the same technique and shows how it combines with extreme value methods pertaining to Gaussian processes; it includes an analysis of the variance of this type of process as related to the mean upcrossing rate to a certain level. The third section picks up from the deterministic results in Chapter 3 to establish moment propagation relationships, constructing a Floquet-based moment propagation technique.

1 Moment transformation of nonstationary processes

1.1 Cyclic Gaussian scalar process

The development that follows is based on a concrete and simple example. The motivation for this approach is twofold: on the one hand, it illustrates the moment propagation approach described in the previous chapter as it is extended seamlessly to this class of nonstationary process; on the other hand, the example considered can be thought of as a building block of the type of processes that will be considered during the rest of the chapter, some features can be discerned with clarity and can then be identified in the more complex cases. The features identified for the cyclic Gaussian case will then be referenced as necessary throughout the chapter.

We seek to obtain the probabilistic moments of the cyclic process $Y(t) = \sin[\Omega t] X(t)$, where $X(t)$ is a narrow band stationary Gaussian process, defined from its mean $\mu_X = 10$ and its covariance function:

$$\Sigma_{XX}(\tau) = \frac{f_2 \operatorname{sinc}(2f_2 \tau) - f_1 \operatorname{sinc}(2f_1 \tau)}{f_2 - f_1} \quad (5.1)$$

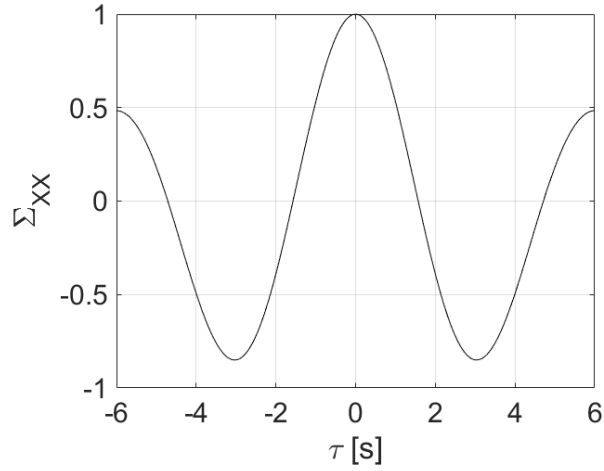


Figure 5.1: Covariance function of the stationary process $X(t)$

with $\tau = t_2 - t_1$, $f_{1,2} = f_0 \mp \delta/2$, $f_0 = \frac{1}{2\pi}$ Hz, $\delta = 0.1$ Hz. Then, $X(t)$ is such that $\sigma_{XX} = 1$, and its first four moments with respect to the origin are: $\mu_X = 10$; $\mu_{XX} = 101$; $\mu_{XXX} = 1030$; $\mu_{XXXX} = 10603$. These can be obtained either by using the equations deduced from the Moment Generating function (see subsection 1.2) or by applying Withers' theorem at the same time instant (see subsection 1.2). The covariance function can be seen in Fig. 5.1. To complete the description of $X(t)$, we recall that $R_{XX}(\tau) = \Sigma_{XX}(\tau) + \mu_X^2$ and, from the Withers' theorem:

$$R_{XXX}(t_1, t_2, t_3) = \mu_X (\Sigma_{XX}(t_2, t_3) + \Sigma_{XX}(t_1, t_3) + \Sigma_{XX}(t_1, t_2) + \mu_X^2). \quad (5.2)$$

The process $Y(t)$ is typical of a Gaussian force acting on a rotating system with angular velocity Ω .

Using the definition of the central moments with respect to the origin and the framework detailed in Chapter 4, we can write the first four moments of $Y(t)$:

$$\begin{aligned} \mu_Y(t) &= \sin[\Omega t] \mu_X \\ \mu_{YY}(t) &= \sin^2[\Omega t] \mu_{XX} \\ \mu_{YYY}(t) &= \sin^3[\Omega t] \mu_{XXX} \\ \mu_{YYYY}(t) &= \sin^4[\Omega t] \mu_{XXXX} \end{aligned} \quad (5.3)$$

and we can further establish that the variance is $\sigma_{YY}(t) = \sin^2[\Omega t] \sigma_{XX}$. Taking $\Omega = 1$, a comparison of these formulas with a Monte-Carlo simulation with empirical statistics is shown in Fig. 5.2-Fig. 5.3. The simulation has been carried out on a time interval of $T = [0, 2\pi]$, over 10,000 realizations. In Fig. 5.2, we particularly highlight the values at $t = \pi/2s$ where $\sin[\Omega t] = 1$, $\mu_Y = \mu_X$, $\mu_{YY} = \mu_{XX}$, $\mu_{YYY} = \mu_{XXX}$, $\mu_{YYYY} = \mu_{XXXX}$. The Fig. 5.3 shows a contrast between the stationary covariance function of the input $X(t)$ and the cyclic covariance function of process $Y(t)$ obtained from MCS. Empirical statistics for thirty runs of the MCS are displayed in this figure, using the computational procedure detailed in reference [135] to simulate the stationary Gaussian process $X(t)$. These figures evidence the consistency of the results obtained.

Some observations from these results will be useful for later cases. First, the mean of the output preserves the same periodicity as the modulating function. Second, from Eq. 5.3, Fig. 5.2 and Fig. 5.3, we notice that second-order moments have a fundamental period that is half of the original, the source being the squaring of the modulating sinusoidal function. We will refer to this as period halving, and we take the opportunity to stress that the original period of the modulating function is still a period of the second-order moments, just not the fundamental period.

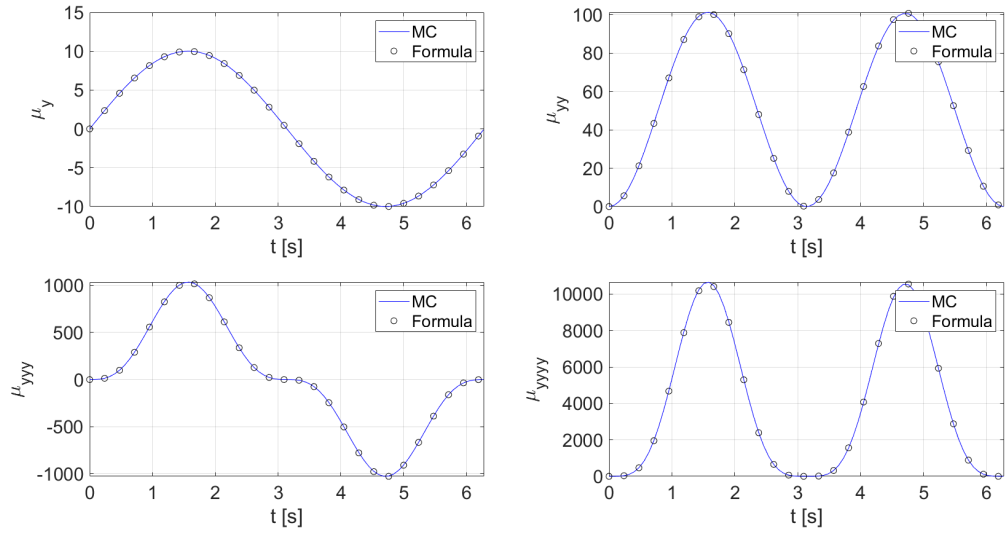


Figure 5.2: First four moments with respect to the origin of $Y(t)$: one typical Monte-Carlo simulation vs. formula

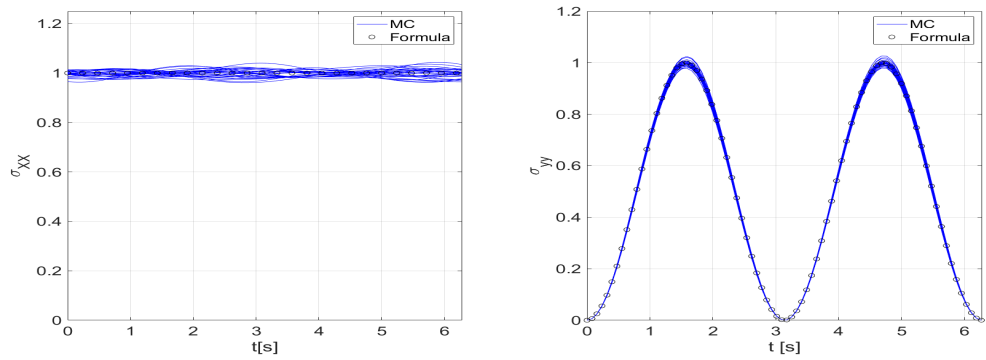


Figure 5.3: Variance of $Y(t)$: thirty runs of Monte-Carlo simulation vs. formula

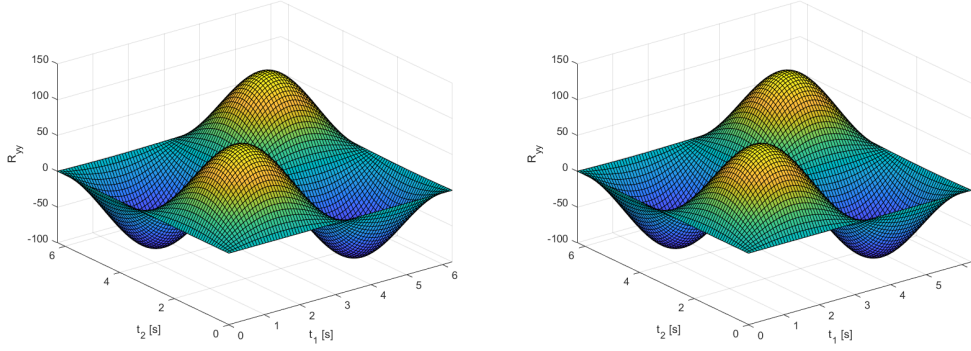


Figure 5.4: Correlation functions of $Y(t)$: one typical Monte-Carlo simulation (left) vs. formula (right)

A similar procedure can be applied to determine relationships among $X(t)$ and $Y(t)$ for the covariance function, correlation function, and their higher-order equivalents. We find:

$$\begin{aligned} R_{YY}(t_1, t_2) &= \sin[\Omega t_1] \sin[\Omega t_2] R_{XX}(t_1, t_2) \\ \Sigma_{YY}(t_1, t_2) &= \sin[\Omega t_1] \sin[\Omega t_2] \Sigma_{XX}(t_1, t_2) \end{aligned} \quad (5.4)$$

and since $Y(t)$ is not stationary, the equivalence between its correlation function and covariance function must be expressed as $\Sigma_{YY}(t_1, t_2) = R_{YY}(t_1, t_2) - \mu_Y(t_1) \mu_Y(t_2)$. Before testing these expressions numerically, we proceed to enunciate a conjecture concerning this nonstationary process and Withers' theorem:

Withers' theorem can be extended to cyclic processes generated from a Gaussian stationary process.

Therefore, if we consider the bi-correlation function, the following expression holds for the cyclic process $Y(t)$:

$$\begin{aligned} E[Y(t_1)Y(t_2)Y(t_3)] &= R_{YYY}(t_1, t_2, t_3) \\ &= \mu_Y(t_1) \mu_Y(t_2) \mu_Y(t_3) + \mu_Y(t_1) \Sigma_{YY}(t_2, t_3) \\ &\quad + \mu_Y(t_2) \Sigma_{YY}(t_1, t_3) + \mu_Y(t_3) \Sigma_{YY}(t_1, t_2). \end{aligned} \quad (5.5)$$

In Fig. 5.4 and Fig. 5.5, we compare the empirical statistics from a typical Monte-Carlo simulation with results from Eq. 5.4. Then, we put the conjecture to test. In Fig. 5.6, we compare a slice of the bi-correlation of $Y(t)$ at $t_3 = \pi/2s$. The graph on the left of the figure is from the conjecture Eq. 5.5 using the covariance function of $Y(t)$, while the one on the right is generated from:

$$R_{YYY}(t_1, t_2, t_3) = \sin[\Omega t_1] \sin[\Omega t_2] \sin[\Omega t_3] R_{XXX}(t_1, t_2, t_3) \quad (5.6)$$

using Eq. 5.2. All these results support the validity of the proposed approach and the correctness of the conjecture for this problem.

For this application, it is particularly noticeable that a benefit of the proposed notation resides in that it provides a systematic encoding of probabilistic information that is particularly suitable for computer implementation, making it unnecessary to develop, for example, the handwritten expression of the bi-covariance function of the nonstationary process $Y(t)$ from that of the Gaussian process $X(t)$. This may also be true for the evaluation of the higher-order statistics of the Gaussian process $X(t)$ from Withers' results in the form we give in subsection 1.2.

1.2 On Withers' theorem and Gaussian moments

In reference [148], Withers' theorem for multivariate Gaussian random variables is stated as follows: let $\mathbf{X} = [X_1, X_2, \dots, X_p]^T$ be a p -dimensional joint Gaussian vector with known mean $\boldsymbol{\mu}_X$ and covariance $\boldsymbol{\Sigma} = \{\sigma_{ij}\}$.

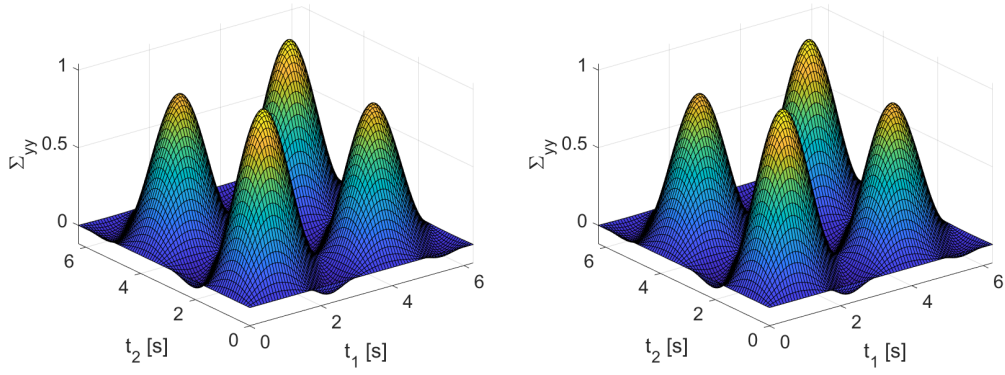


Figure 5.5: Covariance functions of $Y(t)$: one typical Monte-Carlo simulation (left) vs. formula (right)

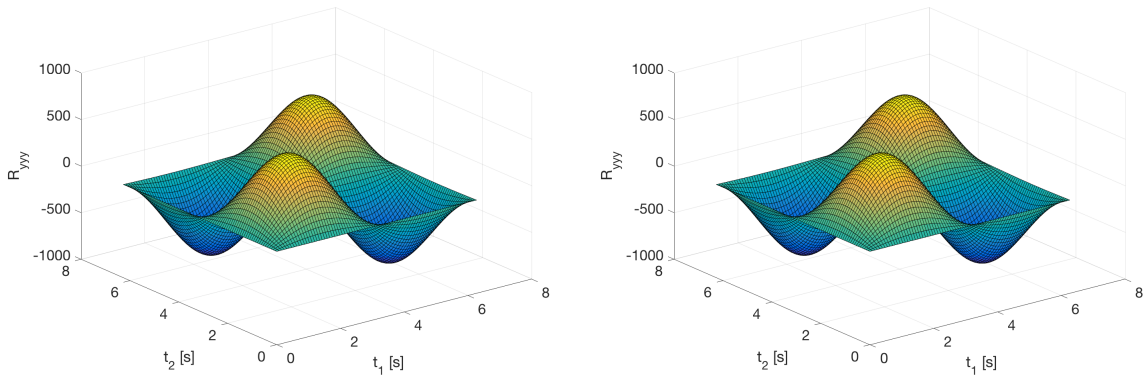


Figure 5.6: Bi-covariance functions of $Y(t)$ for $t_3 = \pi/2s$ from relations 5.5 (left) and 5.6 (right)

Then, for $\{\alpha_1, \alpha_2, \dots, \alpha_r\}$ in $\{1, 2, \dots, p\}$:

$$E[X_{\alpha_1} \dots X_{\alpha_r}] = \sum_{l+2k=r} \sum^m \mu_{a_1} \dots \mu_{a_l} \sigma_{b_1 b_2} \dots \sigma_{b_{2k-1} b_{2k}} \quad (5.7)$$

where the second summation takes places over m permutations $m = \frac{r!}{l!2^k k!}$ of the $\{a_1 \dots a_l b_1 b_2 \dots b_{2k}\}$ in $\{\alpha_1 \alpha_2 \dots \alpha_r\}$. This subsection expands on the technical aspects of the application of this result, particularly when the expression is generalized to Gaussian stochastic processes.

First, assuming stationary Gaussian random processes, for instance, $X_1(t)$ and $X_2(t)$, this theorem provides a direct form of computing the noncentral cross moment. The result is also valid for the cross moment among different random variables that constitute a given process as defined, for instance, the cross moments among $X_1(t_1)$ and $X_1(t_2)$. The result is valid for nonnull mean Gaussian variables, which is its main advantage over the analogous Isserlis' theorem exposed in the reference [61], in the sense that it provides a clear identification of the effects of the mean value when these moments are used on the moment propagation expressions used in this work.

As expressed at the start, we have:

$$\mu_{X_{\alpha_1} \dots X_{\alpha_r}} = E[X(t)_{\alpha_1} \dots X(t)_{\alpha_r}]. \quad (5.8)$$

The script r indicated the number of variables involved in the product or the order of the moment. The script l is associated with the noncentral moments involved, and the k is associated with the central moments or variances. The procedure to apply this result is:

1. Establish the order of the cross moment and the variables involved, r and $\{\alpha_1 \alpha_2 \dots \alpha_r\}$, for example, if $\mathbf{X} = (X_1, X_2, X_3, X_4)$, we can write $\mu_{X_1 X_1 X_2} = \mu_{X_1^2 X_2}$ with $\{\alpha_1 \alpha_2 \alpha_3\}$ and $\alpha_1 = \alpha_2 = 1$, the α_i need not be different, and clearly $r = 3$, so this expresses a cross moment or order 3.
2. Solve $l + 2k = r$ for positive integer (and zero) values of l and k and the given r . For $r = 3$, ($l = 1, k = 1$) and ($l = 3, k = 0$), two solutions.
3. For each solution in the previous step, determine the permutations with $m = \frac{r!}{l!2^k k!}$, $m_1 = \frac{3!}{1!2^1 1!} = 3$ and $m_2 = \frac{3!}{3!2^0 0!} = 1$, these permutations can be expressed as $\{a_1 b_2 b_3\}, \{a_2 b_1 b_3\}, \{a_3 b_2 b_1\}$ (one index for μ because $l = 1$ and two for σ because $2k = 2$) for m_1 and $\{a_1 a_2 a_3\}$ for m_2 (no index for σ because $2k = 0$, and three for μ because $l = 3$).
4. Finally we develop these sums with the information established:

$$\begin{aligned} \mu_{X_1 X_2 X_3} &= \sum^1 \mu_{a_1} \dots \mu_{a_l} \sigma_{b_1 b_2} \dots \sigma_{b_{2k-1} b_{2k}} + \sum^3 \mu_{a_1} \dots \mu_{a_l} \sigma_{b_1 b_2} \dots \sigma_{b_{2k-1} b_{2k}} \\ &= \mu_{a_1} \mu_{a_2} \mu_{a_3} + \mu_{a_1} \sigma_{b_2 b_3} + \mu_{a_2} \sigma_{b_1 b_3} + \mu_{a_3} \sigma_{b_2 b_1} \end{aligned} \quad (5.9)$$

which can be written as:

$$\mu_{X_1 X_2 X_3} = \mu_{X_1} \mu_{X_2} \mu_{X_3} + \mu_{X_1} \sigma_{X_2 X_3} + \mu_{X_2} \sigma_{X_1 X_3} + \mu_{X_3} \sigma_{X_2 X_1}. \quad (5.10)$$

For the product:

$$\mu_{X_1 X_2 X_3 X_4} = E[X_1(t) X_2(t) X_3(t) X_4(t)] \quad (5.11)$$

we have the following results:

1. Order 4, $r = 4$.
2. Solutions: ($l = 4, k = 0$), ($l = 2, k = 1$), ($l = 0, k = 2$).

3. Permutations are $m_1 = \frac{4!}{4!1} = 1$, $m_2 = \frac{4!}{2!2 \times 1} = 6$, $m_3 = \frac{4!}{12^2 2!} = 3$.
4. The permutations are, for m_1 : $\{a_1 a_2 a_3 a_4\}$, for m_2 and m_3 respectively:

$$m_2 : \{a_1 a_2 b_3 b_4\}, \{a_1 a_3 b_2 b_4\}$$

$$\{a_1 a_4 b_2 b_3\}, \{a_2 a_3 b_1 b_4\}$$

$$\{a_2 a_4 b_1 b_3\}, \{a_3 a_4 b_1 b_2\}$$

$$m_3 : \{b_1 b_2 b_3 b_4\}$$

$$\{b_1 b_3 b_2 b_4\}$$

$$\{b_1 b_4 b_2 b_3\}.$$

5. The sum gives

$$\begin{aligned} \mu_{X_1 X_2 X_3 X_4} &= \mu_{X_1} \mu_{X_2} \mu_{X_3} \mu_{X_4} \\ &+ \mu_{X_1} \mu_{X_2} \sigma_{X_3 X_4} + \mu_{X_1} \mu_{X_3} \sigma_{X_2 X_4} \\ &+ \mu_{X_1} \mu_{X_4} \sigma_{X_2 X_3} + \mu_{X_2} \mu_{X_3} \sigma_{X_1 X_4} \\ &+ \mu_{X_2} \mu_{X_4} \sigma_{X_1 X_3} + \mu_{X_3} \mu_{X_4} \sigma_{X_1 X_2} \\ &+ \sigma_{X_1 X_2} \sigma_{X_3 X_4} + \sigma_{X_1 X_3} \sigma_{X_2 X_4} \\ &+ \sigma_{X_1 X_4} \sigma_{X_2 X_3}. \end{aligned} \quad (5.12)$$

We now present an argument for the application of this theorem for the computation of the moment generalizations between points in time, more precisely, the correlation function and its generalizations. We can interpret a random process as a set of random variables indexed by a so-called time parameter. A Gaussian random process is such that any two of its component random variables are jointly Gaussian. In the discrete case, this condition fits the assumptions under which Withers' theorem has been proved. The discrete case is precisely the case of interest when it comes to numerical simulations of the process: a time discretization is performed, and the relevant quantities are calculated at those discrete points. Thus, when applying the theorem, it suffices to replace $\Sigma = \{\sigma_{ij}\}$, by the covariance function evaluated at the relevant points in time: $\Sigma_{XX}(t_1, t_2)$.

To illustrate the previous argument, we consider the Gaussian random process $X(t)$ with mean function $\mu_X(t)$ and correlation function $\Sigma_{XX}(t_1, t_2)$. The bi-correlation function reads:

$$E[X(t_1)X(t_2)X(t_3)] = R_{XXX}(t_1, t_2, t_3) \quad (5.13)$$

where:

$$\begin{aligned} R_{XXX}(t_1, t_2, t_3) &= \mu_X(t_1) \mu_X(t_2) \mu_X(t_3) + \\ &\mu_X(t_1) \Sigma_{XX}(t_2, t_3) + \mu_X(t_2) \Sigma_{XX}(t_1, t_3) + \mu_X(t_3) \Sigma_{XX}(t_1, t_2) \end{aligned} \quad (5.14)$$

and if the process under consideration is stationary, then $\mu_X(t) = \mu_X = \text{constant}; \forall t$, $\Sigma_{XX}(t_1, t_2) = \Sigma(\tau); \tau = t_2 - t_1$, and we can write:

$$R_{XXX}(\tau_1, \tau_2) = \mu_X \mu_X \mu_X + \mu_X (\Sigma_{XX}(\tau_1) + \Sigma_{XX}(\tau_2) + \Sigma_{XX}(\tau_2 - \tau_1)) \quad (5.15)$$

with $\tau_1 = t_2 - t_1; \tau_2 = t_3 - t_1; \tau_2 - \tau_1 = t_3 - t_2$.

MGF of Gaussian variables A Gaussian random variable is fully determined by its first two moments. Conventionally, this information about a Gaussian random variable is presented in terms of its first-order moment with respect to the origin, its mean, and its second-order moment with respect to the mean, its variance. Every

Moment	Formula
μ_X	μ_X
μ_{XX}	$\mu_X^2 + \sigma_{XX}$
μ_{XXX}	$\mu_X^3 + 3\mu_X\sigma_{XX}$
$\mu_{X^{(4)}}$	$\mu_X^4 + 6\mu_X^2\sigma_{XX} + 3\sigma_{XX}^2$
$\mu_{X^{(5)}}$	$\mu_X^5 + 10\mu_X^3\sigma_{XX} + 15\mu_X\sigma_{XX}^2$
$\mu_{X^{(6)}}$	$\mu_X^6 + 15\mu_X^4\sigma_{XX} + 45\mu_X^2\sigma_{XX}^2 + 15\sigma_{XX}^3$
$\mu_{X^{(7)}}$	$\mu_X^7 + 21\mu_X^5\sigma_{XX} + 105\mu_X^3\sigma_{XX}^2 + 105\mu_X\sigma_{XX}^3$
$\mu_{X^{(8)}}$	$\mu_X^8 + 28\mu_X^6\sigma_{XX} + 210\mu_X^4\sigma_{XX}^2 + 420\mu_X^2\sigma_{XX}^3 + 105\sigma_{XX}^4$

Table 5.1: First eight moments of a Gaussian random variable in terms of mean and variance

other moment can be expressed in terms of these two. A convenient way of expressing these moments is by using the Moment Generating Function (MGF) of the Gaussian random variable:

$$m_X(s) = \exp[s\mu_X + \frac{1}{2}\sigma_{XX}s^2] \quad (5.16)$$

where μ_X is the mean and σ_{XX} is the variance of the Gaussian random variable X . The n -th moment of X with respect to the origin can be obtained by differentiation of the MGF and the evaluation of this derivative at $s = 0$, that is:

$$\mu_{X^{(n)}} = \left. \frac{d^{(n)}}{ds^{(n)}} [m_X(s)] \right|_{s=0} \quad (5.17)$$

so using this expression, all the moments of the variable X can be obtained, and the analytic expressions of the first eight ones are given in Tab. 5.1. Moreover, it is noticed that odd moments will be null when $\mu_X = 0$.

Commentary In principle, the approach taken in this development is equally valid for the more general case $Y(t) = a(t, \Omega)X(t)$ where the modulation function $a(t, \Omega)$ is periodic on $T_p = \frac{2\pi}{\Omega}$, but not necessarily as selected in the example of subsection 1.1. The motivation of this example is precisely the fact that the Floquet periodic modes act as time modulators in the passage from the Floquet modal variables to the state variables. Indeed, from the results in chapter 3, we write:

$$\begin{aligned} \mathbf{y}(t) &= \mathbf{R}(t)\mathbf{q}(t) \\ \dot{\mathbf{q}}(t) &= \boldsymbol{\rho}\mathbf{q}(t) + \mathbf{p}(t) \\ \mathbf{p}(t) &= \mathbf{L}(t)\mathbf{B}(t)\mathbf{f}, \end{aligned} \quad (5.18)$$

the forced response in the modal variables is:

$$\mathbf{q}_f(t) = \int_{-\infty}^{\infty} \mathbf{h}(t-\tau)\mathbf{p}(\tau)d\tau \quad (5.19)$$

so considering the modal solution $\mathbf{q}_f(t)$ as a stochastic variable, the return to the state variable is:

$$\mathbf{y}_f(t) = \mathbf{R}(t)\mathbf{q}_f(t) \quad (5.20)$$

where we know that $\mathbf{R}(t)$ is periodic; in this case, $\mathbf{R}(t)$ replaces $a(t, \Omega)$. Taking the first DOF of $\mathbf{y}_f(t)$, for instance, one has:

$$y_f^{(1)} = \sum_{j=1}^N R_{1,j}(t) q_f^{(j)}, \quad (5.21)$$

with N the number of modes; this suggests the application of the previous development to sums of periodic terms of the form:

$$Y(t) = a_1(t, \Omega) X_1(t) + a_2(t, \Omega) X_2(t) + \dots + a_N(t, \Omega) X_N(t), \quad (5.22)$$

for which the notation and methodology introduced in the previous chapter is particularly well-suited to handle. It is worth highlighting that the moment equations obtained are not limited to the Gaussian case; if the input moments can be computed, these relationships can be equally applied. Input moments of unknown distributions, such as those emerging by complex transformations of an underlying field, can be computed by MCS sampling.

2 Extreme value distribution of periodic zero-mean nonstationary processes

Building on the previous method, we turn to the problem of estimating the CDF of the extreme values of a nonstationary Gaussian stochastic process generated by applying a periodic modulation to a weakly stationary underlying or antecedent Gaussian stochastic process. Concretely, we study the following class of stochastic processes:

$$Y(t) = a(t, \Omega) X(t), \quad (5.23)$$

where $X(t)$ is a Gaussian stationary process with finite variance $|\sigma_{XX}(t)| < \infty, \forall t$, and $a(t, \Omega)$ is periodic on $T_p = \frac{2\pi}{\Omega}$, a deterministic modulating function. In this case, $Y(t)$ is nonstationary and Gaussian. For simplicity, we assume $X(t) \rightarrow \mathcal{N}(0, \Sigma_{XX}(\tau))$: the underlying Gaussian is centered. The mean of $Y(t)$ is:

$$\mu_Y = a(t, \Omega) \mu_X = 0, \quad (5.24)$$

the covariance function of $Y(t)$ will coincide with its correlation:

$$\begin{aligned} E[Y(t_1) Y(t_2)] &= E[a(t_1, \Omega) X(t_1) a(t_2, \Omega) X(t_2)] \\ R_{YY}(t_1, t_2) &= a(t_1, \Omega) a(t_2, \Omega) R_{XX}(t_1, t_2) \\ \Sigma_{YY}(t_1, t_2) &= R_{YY}(t_1, t_2). \end{aligned} \quad (5.25)$$

The periodicity of $a(t, \Omega)$ implies that $a(t_1, \Omega) = a(t_1 + nT_p, \Omega)$ where T_p is the period, and $n \in \mathbb{Z}$. Since the stationarity of $X(t)$ implies $R_{XX}(t_1, t_2) = R_{XX}(\tau)$ with $\tau = t_2 - t_1$, we have:

$$\mu_Y(t) = \mu_Y(t + nT_p) = 0, \forall t \in [0, T] \quad (5.26)$$

and:

$$\begin{aligned} R_{YY}(t_1, t_2) &= a(t_1, \Omega) a(t_2, \Omega) R_{XX}(t_1, t_2) \\ R_{YY}(t_1 + nT_p, t_2 + nT_p) &= a(t_1 + nT_p, \Omega) a(t_2 + nT_p, \Omega) R_{XX}(t_1 + nT_p, t_2 + nT_p) \end{aligned} \quad (5.27)$$

from the modulating functions: $a(t_1 + nT_p, \Omega) = a(t_1, \Omega)$; $a(t_2 + nT_p, \Omega) = a(t_2, \Omega)$. From the correlation $\tau = t_2 - t_1$, $(t_2 + nT_p) - (t_1 + nT_p) = t_2 - t_1 = \tau$, $R_{XX}(t_1 + nT_p, t_2 + nT_p) = R_{XX}(\tau) = R_{XX}(t_1, t_2)$, so:

$$R_{YY}(t_1 + nT_p, t_2 + nT_p) = R_{YY}(t_1, t_2) \quad (5.28)$$

a centered stationary stochastic process modulated by a periodic function is a wide-sense cyclostationary ([110]) stochastic process.

Given the probabilistic descriptors of $X(t)$ one can establish transformation relationships for $Y(t)$, as we have done in the previous development. Our interest is to use these probabilistic descriptors to obtain the extremes of $Y(t)$. Different formulations of the extremes of $Y(t)$ are interconnected. On the interval $[0, T]$, one can define the random variable: $M_Y = \max[Y(t)]$, $0 \leq t \leq T$. We call the CDF of M_Y the Extreme Value Distribution (EVD) of $Y(t)$. An associated problem is the first-passage probability: $\mathbb{P}[\exists t \in [0, T] : Y(t) \geq u]$. Both problems are related to the upcrossing (or outcrossing) rate at which the stochastic process surpasses a threshold u in $[0, T]$, indeed as shown in Eq. 1.24 and Eq. 1.25, knowledge of the mean number of upcrossings $\lambda_X^+(u)$ is instrumental in the determination of Poisson-type EVD. The relevance of Eq. 1.22 is precisely the fact that it provides the crossing intensity that enables the obtention of $\lambda_X^+(u)$, but it can be seen that the Rice formula requires information about the derivative of the process under analysis. We now proceed to extend the analysis to consider the moment propagation of the derivative process.

2.1 Moment propagation of derivative process

We consider again the transformation:

$$Y(t) = a(t, \Omega)X(t), \quad (5.29)$$

where the stationary input $X(t)$ has mean $\mu_X = 0$, variance $\sigma_{XX} = \mu_{XX}$, correlation function $R_{XX}(t_1, t_2) = \Sigma_{XX}(t_1, t_2)$; we further define the derivative of $X(t)$ as $\dot{X}(t) = \frac{d}{dt}[X(t)]$ which has mean $\mu_{\dot{X}} = 0$, variance $\sigma_{\dot{X}\dot{X}} = \mu_{\dot{X}\dot{X}}$, and correlation function $R_{\dot{X}\dot{X}}(t_1, t_2) = \Sigma_{\dot{X}\dot{X}}(t_1, t_2)$. Further, the correlation function of $\dot{X}(t)$ can be obtained from the correlation function of $X(t)$: $R_{\dot{X}\dot{X}}(t_1, t_2) = \frac{\partial}{\partial t_1 \partial t_2}[R_{XX}(t_1, t_2)]$. The stationarity of $X(t)$ implies $\mu_{X\dot{X}} = \sigma_{X\dot{X}} = 0$, or the process is orthogonal to its derivative. It follows that:

$$\begin{aligned} \mu_Y(t) &= a(t, \Omega) \mu_X = 0 \\ \mu_{\dot{Y}}(t) &= \dot{a}(t, \Omega) \mu_X + a(t, \Omega) \mu_{\dot{X}} = 0 \\ \sigma_{YY}(t) &= a^2(t, \Omega) \sigma_{XX} \\ \sigma_{\dot{Y}\dot{Y}}(t) &= \dot{a}^2(t, \Omega) \sigma_{XX} + a^2(t, \Omega) \sigma_{\dot{X}\dot{X}} \\ \sigma_{Y\dot{Y}}(t) &= a(t, \Omega) \dot{a}(t, \Omega) \sigma_{XX} \\ \mu_{\dot{Y}} &= \ddot{a}(t, \Omega) \mu_X + 2\dot{a}(t, \Omega) \mu_{\dot{X}} + a(t, \Omega) \mu_{\ddot{X}} = 0 \\ \mu_{Y\dot{Y}} &= a(t, \Omega) \ddot{a}(t, \Omega) \mu_{XX} + a^2(t, \Omega) \mu_{X\dot{X}}, \end{aligned} \quad (5.30)$$

we introduce the relationship $\mu_{X\dot{X}} = -\mu_{\dot{X}X} = -\sigma_{\dot{X}X}$, resulting in:

$$\mu_{Y\dot{Y}} = a(t, \Omega) \ddot{a}(t, \Omega) \sigma_{XX} - a^2(t, \Omega) \sigma_{\dot{X}X}. \quad (5.31)$$

Additionally, from the relationship between mean, variance, and second-order moment, we can establish $\sigma_{Y\dot{Y}} = \mu_{Y\dot{Y}} - \mu_Y \mu_{\dot{Y}}$, which results in:

$$\sigma_{Y\dot{Y}}(t) = a(t, \Omega) \ddot{a}(t, \Omega) \sigma_{XX} - a^2(t, \Omega) \sigma_{\dot{X}X}. \quad (5.32)$$

These relationships characterize the first two moments (mean and variance) of the output process and its derivative.

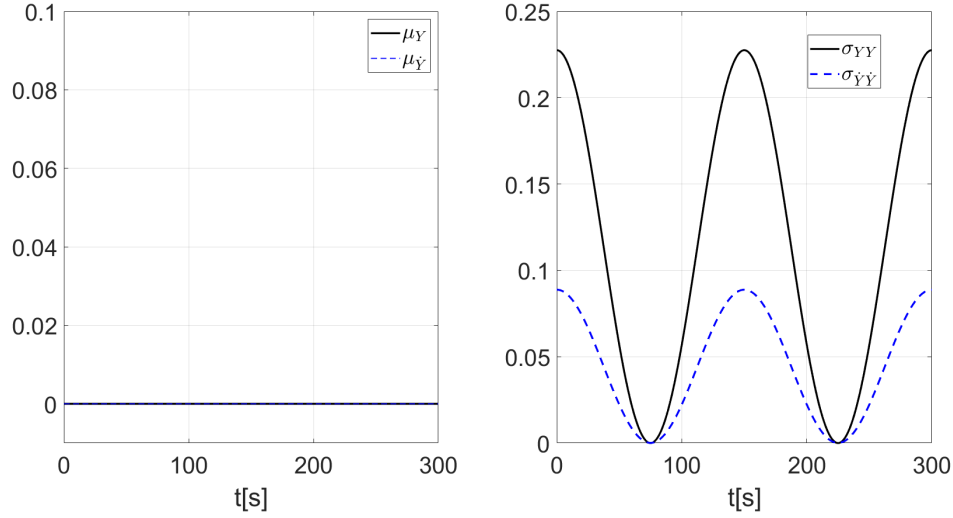


Figure 5.7: Mean and variance of modulated Gaussian process and its derivative

3 Analyzing upcrossings of Gaussian periodically modulated processes

This section analyzes the link between upcrossing and peak variance in periodically modulated Gaussian processes. The result is a methodology to estimate the upcrossing and EVD of periodic Gaussian processes. We consider a process of the form:

$$Y(t) = \cos(\Omega t) X(t), \quad (5.33)$$

where $X(t)$ is a stationary, zero-mean Gaussian process with $\mu_X = 0$ and $\sigma_{XX} = \mu_{XX} = 0.2275$, for the modulation function $\Omega = 0.0209$. Using the relationships in Eq. 5.31, we can propagate moments towards the output $Y(t)$ and its derivative $\dot{Y}(t)$. The moments obtained from the established equations are shown in Fig. 5.7. We now proceed to the upcrossings analysis and EVD determination.

3.1 Preliminaries

We start with the formula for the expected number of upcrossings:

$$\lambda_X^+ = E[N(u_i, 0, T)] = \int_0^T v_X^+(u_i, t) dt, \quad (5.34)$$

for the stationary Gaussian process $X(t)$, the closed-form solution exists in the following form:

$$\lambda_X^+ = E[N(u_i, 0, T)] = \frac{T}{\sqrt{2\pi}} \sqrt{\frac{\sigma_{\dot{X}\dot{X}}}{\sigma_{XX}}} \exp\left[-\frac{u_i^2}{2\sigma_{XX}}\right]. \quad (5.35)$$

The formula in Eq. 5.35 can be interpreted as the integral in Eq. 5.34 for the Gaussian stationary case on the interval $[0, T]$. Our aim is to try to approximate the λ_Y^+ of the nonstationary Gaussian process $Y(t)$ by finding appropriate equivalent stationary Gaussian processes such as $X(t)$, defined on a given subinterval of $[0, T]$, and applying Eq. 5.35.

To gain some insight into the relationship between the variance of the nonstationary process and the expected number of upcrossings, we construct the following visualization in Fig. 5.8, where we count the exceedances of level u within a given time interval, and compare it to the time evolution of the variance. The values selected as

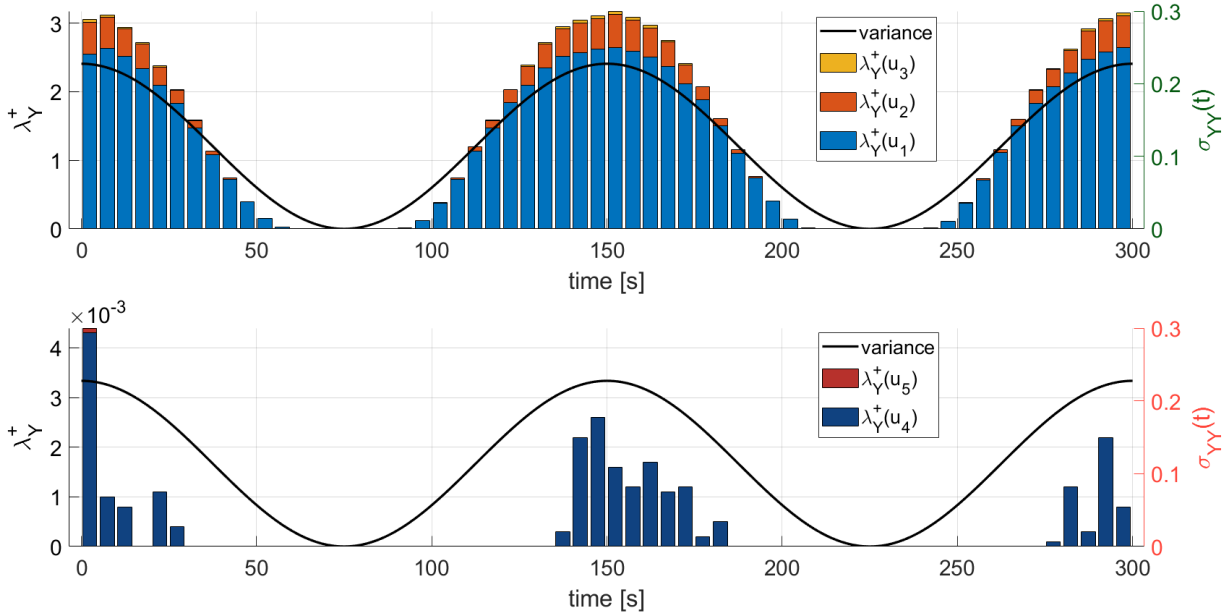


Figure 5.8: Mean number of upcrossings λ_Y^+ for five levels u_i on discretized time bins vs. variance

u_i are $u_1 = 0.5437$, $u_2 = 0.9536$, $u_3 = 1.3634$, $u_4 = 1.7733$ and $u_5 = 2.1831$. The test is performed over 10,000 realizations of the modulated Gaussian process introduced in Eq. 5.33.

The interpretation of Fig. 5.8 is the following: lower values of the threshold u_i are more likely to be reached, so we see the highest λ_Y^+ in blue for $u_1 = 0.5437$; the bars are stacked to facilitate visualization, for instance, the occurrence of u_1 is many times the occurrence of $u_2 = 0.9536$; for the highest thresholds, a separate plot is made since these are completely overshadowed by the larger scale of the first three u_i ; the second vertical axis shows the value of $\sigma_{YY}(t)$ as it evolves in time; finally, as expected, the upcrossing occurrence is concentrated in the regions of high variance, a region that narrows significantly as u_i increases.

The occurrence of upcrossings is concentrated on the intervals of high variance, as has been noted in the literature, particularly clear in [72] but in terms of the covariance function.

3.2 Method of interval approximation

Based on the preliminaries, the general idea of the proposed method is to approximate the expected number of upcrossings of periodically modulated processes in a piece-wise fashion using the stationary result on each subinterval of high variance (Alg. 5.1). For the example on which Fig. 5.8 is based, we take $N_{SC} = 3$, with $T_1 = [0, 50]$; $T_2 = [125, 175]$; $T_3 = [250, 300]$; the intervals have the same length $\Delta t = 50s$. The mid-point variances are shown in Tab. 5.2. Formula Eq. 5.35 is applied using Tab. 5.2 and replacing T with $\Delta t = 50$; this yields the “partial” CDF in Fig. 5.9. Finally, we compare the method with:

- an empirical CDF obtained with a Matlab routine over the 10,000 realizations of the process,
- direct count of the upcrossings of the realizations to calculate the mean number of upcrossings,

the results are shown in Fig. 5.10. While the method provides a very satisfactory result for a Gaussian process, the ultimate goal would be to extend this idea to more general distributions. Indeed, the main challenge, as already outlined, consists in the reconstruction of the joint PDF of the propagated moments for general distributions.

Algorithm 5.1 Interval approximation method

1. Select a number of time subintervals N_{sc} of high variance: $T_1, T_2 \dots T_{N_{sc}}$, and compute their length Δt .
 2. Approximate the mean number of upcrossings for each subinterval. This is done using the stationary formula: the time-varying process is approximated as a stationary process in that subinterval. The variance of Y and \dot{Y} in each interval are chosen as that of the mid-point in that interval, although it is worth evaluating different choices.
 3. Each subinterval produces its contribution to the total estimated CDF: $P_{Y_m}^1(u) = \exp[-\lambda_1]; P_{Y_m}^2(u) = \exp[-\lambda_2]; \dots P_{Y_m}^{N_{sc}}(u) = \exp[-\lambda_{N_{sc}}]$.
 4. The total CDF of Y_m is $P_{Y_m}(u) = P_{Y_m}^1(u) \times P_{Y_m}^2(u) \times \dots \times P_{Y_m}^{N_{sc}}(u)$.
-

Variance	t_1	t_2	t_3
σ_{YY}	0.1706	0.2274	0.1706
$\sigma_{\dot{Y}\dot{Y}}$	0.0666	0.0888	0.0666

Table 5.2: Interval variance approximation at mid-point

Finally, this method has been developed for the simplified case of a zero-mean process. For processes with non-zero mean, adjustments must be made in Eq. 5.35 to account for the mean value, and the choice of interval will also require the consideration of the mean. These adjustments will be exemplified in section 5 of Chapter 6. The key idea of the method, however, remains the same: the periodic process can be analyzed by temporal intervals in which the intervening moments result in a high likelihood of threshold crossing, and each contributing interval can be combined to yield the estimated EVD. In this sense, for a zero-mean process, peak variance is the main consideration; conversely, a process with low variance with respect to its mean value would be more likely to realize a crossing at peak mean points.

4 Floquet moment transformation

The goal of this section is to use the results from the Floquet modal theory to establish moment propagation relationships between input and output variables. Unlike the results established so far, which fall into the category of memoryless transformations (See: [134] or [104]), the input-output relationship of a dynamical system belongs to the class of memory transformations. We will proceed as in Chapter 3, from the modal representation of the forced response. The key distinction is that now the inputs are considered as stochastic processes.

Consider the LTP system:

$$\mathbf{M}(t)\ddot{\mathbf{x}} + \mathbf{G}(t)\dot{\mathbf{x}} + \mathbf{K}(t)\mathbf{x} = \mathbf{f}(t), \quad (5.36)$$

with period T_p such that $\mathbf{M}(t+nT_p) = \mathbf{M}(t), n \in \mathbb{Z}$ and equally for $\mathbf{G}(t)$ and $\mathbf{K}(t)$; where $\mathbf{f}(t)$ is a stochastic vector of loads. The system can be cast into state form with the substitutions $\mathbf{y} = \begin{bmatrix} \mathbf{x} \\ \dot{\mathbf{x}} \end{bmatrix}$, $\mathbf{A}(t) = \begin{bmatrix} \mathbf{0} & \mathbf{I} \\ \mathbf{M}^{-1}\mathbf{K} & \mathbf{M}^{-1}\mathbf{G} \end{bmatrix}$,

$$\mathbf{B}(t) = \begin{bmatrix} \mathbf{0} \\ \mathbf{M}^{-1} \end{bmatrix}:$$

$$\dot{\mathbf{y}} = \mathbf{A}(t)\mathbf{y} + \mathbf{B}(t)\mathbf{f}(t), \quad (5.37)$$

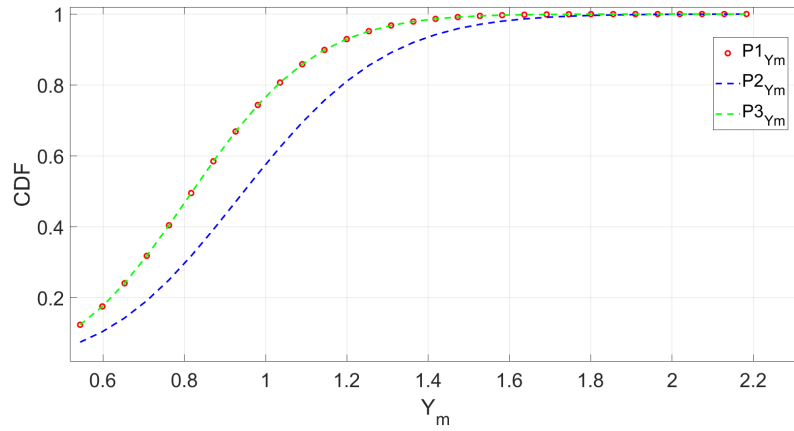


Figure 5.9: Partial CDF with $N_{SC} = 3$ and mid-point variance

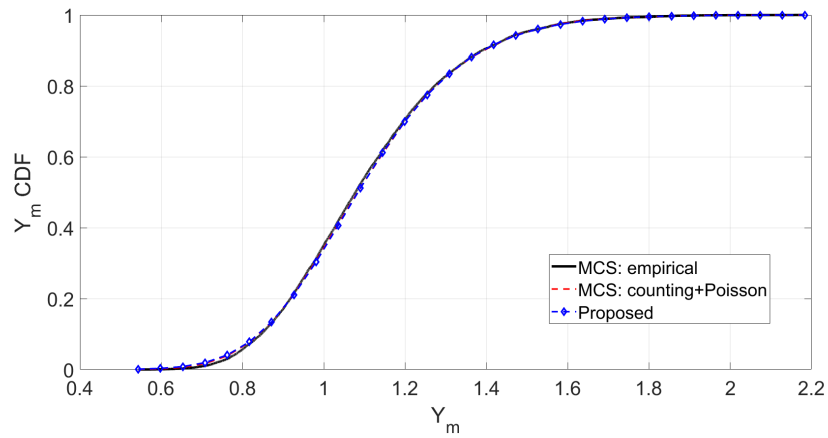


Figure 5.10: Estimated CDF by proposed method compared to 2 other approaches for $T = 300s$

which is a forced Floquet system. The original or physical system has dimension N_{dim} , or N_{dim} DOFs, whereas the state form has $2N_{\text{dim}}$ DOFs. The pumping frequency of the system is $f_p = \frac{1}{T_p}$. The Lyapunov substitution $\mathbf{y}(t) = \mathbf{R}(t) \mathbf{q}(t)$ leads to the modal LTI system:

$$\dot{\mathbf{q}}(t) = \boldsymbol{\rho} \mathbf{q}(t) + \mathbf{p}(t), \quad (5.38)$$

where the $\mathbf{q}(t)$ are the new modal variables, $\mathbf{R}(t)$ is the right modal matrix of periodic eigenvectors, $\boldsymbol{\rho}$ is a diagonal matrix containing the characteristic exponents of the system, and the adapted load $\mathbf{p}(t) = \mathbf{L}(t) \mathbf{B}(t) \mathbf{f}(t)$, where $\mathbf{L}(t) = \mathbf{R}^{-1}(t)$ is the left modal matrix, in practice the inverse of the right modal matrix. In general, the periodic eigenvectors in $\mathbf{R}(t)$ and $\mathbf{L}(t)$ are functions of complex values, the implication being that the adapted excitation $\mathbf{p}(t) = \mathbf{L}(t) \mathbf{B}(t) \mathbf{f}(t)$ is a complex function, and the modal variables $\mathbf{q}(t)$ are equally complex. This fact requires some care in the computation of the corresponding moments of both $\mathbf{p}(t)$ and $\mathbf{q}(t)$. We recall the relationships established in Chapter 4 for random vector processes with complex values, in particular $\mathbf{p}(t) = [p_i(t)]$, $p_i(t) \in \mathbb{C}$, the second moments are:

$$\mu_{p_i p_j}(t) = \mathbb{E} [p_i(t) p_j^*(t)] \quad (5.39)$$

where $p_j^*(t)$ is the complex conjugate of component j in the complex random vector $\mathbf{p}(t)$. During the section, the complex conjugate transpose of a matrix, say $\mathbf{h}(t)$, will be expressed as $\mathbf{h}^H(t)$.

4.1 Convolution relationships

Consider the LTI system in Eq. 5.38, with $\boldsymbol{\rho} \in \mathbb{C}^{2N_{\text{dim}} \times 2N_{\text{dim}}}$ a constant diagonal matrix, and $\mathbf{q}(t), \dot{\mathbf{q}}(t), \mathbf{p}(t) \in \mathbb{C}^{2N_{\text{dim}}}$. Assuming the system at rest before a certain initial time of interest, by convention set to $t_0 = 0$, and provided an initial condition in such a state: $\mathbf{q}(0) = \mathbf{q}_0$, the general solution of this equation is:

$$\mathbf{q}(t) = \exp[\boldsymbol{\rho}(t)] \mathbf{q}_0 + \int_0^t \exp[\boldsymbol{\rho}(t - \tau)] \mathbf{p}(\tau) d\tau, \quad (5.40)$$

where $\mathbf{q}_h(t) = \exp[\boldsymbol{\rho}(t)] \mathbf{q}_0$ is called the homogeneous response, and $\mathbf{q}_f(t) = \int_0^t \exp[\boldsymbol{\rho}(t - \tau)] \mathbf{p}(\tau) d\tau$ is the forced response. It is convenient to introduce the impulse response function, the following matrix quantity:

$$\mathbf{h}(t) = \exp[\boldsymbol{\rho}t], \quad (5.41)$$

from where it can be seen that $\mathbf{q}_h(t) = \mathbf{h}(t) \mathbf{h}^{-1}(0) \mathbf{q}_0$; the forced response is then:

$$\mathbf{q}_f(t) = \int_0^t \mathbf{h}(t - \tau) \mathbf{p}(\tau) d\tau, \quad (5.42)$$

a convolution equation often termed Duhamel integral. Based on our developments in Chapter 3, it is apparent that $\mathbf{h}(t)$ is a fundamental solution of the system, and the origin of the convolution solution can be traced to the variation of constants method for inhomogeneous ODEs.

A different classification of the response is useful when damping is involved: a part of the response, said to be transient, decays with time; another part of the response, said to be steady-state, is persistent so long as $\mathbf{p}(t)$ is acting on the system. The homogeneous response $\mathbf{q}_h(t)$ in damped systems is transient, whereas the forced response $\mathbf{q}_f(t)$ has a transient component and a steady-state component:

$$\begin{aligned} \mathbf{q}_f(t) &= \mathbf{q}_f^{(tr)}(t) + \mathbf{q}_f^{(ss)}(t) \\ \mathbf{q}_f^{(tr)}(t) &\xrightarrow{t \rightarrow \infty} 0 \\ \mathbf{q}_f(t) &\xrightarrow{t \rightarrow \infty} \mathbf{q}_f^{(ss)}(t). \end{aligned} \quad (5.43)$$

In the sequel, we focus on the forced response $\mathbf{q}_f(t)$, which is to say $\mathbf{q}_0 = \mathbf{0}$, and hence the subscript in $\mathbf{q}_f(t)$ is dropped for convenience.

Consider again the convolution equation:

$$\mathbf{q}(t) = \int_0^t \mathbf{h}(t-\tau) \mathbf{p}(\tau) d\tau \quad t > 0, \quad (5.44)$$

in the developments that will follow from this expression, it is equally assumed that $t > 0$; we may introduce the change of variable $\tau_1(\tau) = t - \tau$, $d\tau_1 = -d\tau$, $\tau_1(0) = t$, $\tau_1(t) = 0$, which results in:

$$\begin{aligned} \mathbf{q}(t) &= \int_0^t \mathbf{h}(t-\tau) \mathbf{p}(\tau) d\tau \\ &= \int_t^0 \mathbf{h}(\tau_1) \mathbf{p}(t-\tau_1) (-d\tau_1) \\ &= \int_0^t \mathbf{h}(\tau_1) \mathbf{p}(t-\tau_1) d\tau_1, \end{aligned} \quad (5.45)$$

the passage from the penultimate to the last equality being a direct consequence of the fundamental theorem of calculus, and the result shows that this convolution equation is commutative. It is also important to remark on the implicit initial condition inherent to the convolution equation: the system starts at rest in $t_0 = 0$, and the perturbation $\mathbf{p}(t)$ begins to act over the system at this instant. The complex, periodically modulated stochastic input $\mathbf{p}(t)$ is indeed defined in $-\infty < t < \infty$, implicit in the convolution equation is the fact that the input begins its action at the initial time of interest.

We may convert back to the state variables with:

$$\begin{aligned} \mathbf{y}(t) &= \mathbf{R}(t) \mathbf{q}(t) \\ &= \mathbf{R}(t) \int_0^t \mathbf{h}(t-\tau) \mathbf{p}(\tau) d\tau. \end{aligned} \quad (5.46)$$

In the modal variables, we can apply the expectation to obtain:

$$\begin{aligned} E[\mathbf{q}(t)] &= E \left[\int_0^t \mathbf{h}(t-\tau) \mathbf{p}(\tau) d\tau \right] \\ \boldsymbol{\mu}_q(t) &= \int_0^t \mathbf{h}(t-\tau) \boldsymbol{\mu}_p(\tau) d\tau \end{aligned} \quad (5.47)$$

giving the mean between adapted input and modal output. Introducing now $\mathbf{V} = \mathbf{q}(t) - \boldsymbol{\mu}_q(t)$ and computing $E[\mathbf{V}\mathbf{V}^H]$:

$$\begin{aligned} \mathbf{V} &= \mathbf{q}(t) - \boldsymbol{\mu}_q(t) \\ \mathbf{V}^H &= \mathbf{q}^H(t) - \boldsymbol{\mu}_q^H(t) \\ \mathbf{V}\mathbf{V}^H &= \mathbf{q}(t) \mathbf{q}^H(t) - \mathbf{q}(t) \boldsymbol{\mu}_q^H(t) - \boldsymbol{\mu}_q(t) \mathbf{q}^H(t) + \boldsymbol{\mu}_q(t) \boldsymbol{\mu}_q^H(t) \\ E[\mathbf{V}\mathbf{V}^H] &= \boldsymbol{\mu}_{qq}(t) - \boldsymbol{\mu}_q(t) \boldsymbol{\mu}_q^H(t), \end{aligned} \quad (5.48)$$

so the variance is:

$$\boldsymbol{\sigma}_{qq}(t) = \boldsymbol{\mu}_{qq}(t) - \boldsymbol{\mu}_q(t) \boldsymbol{\mu}_q^H(t), \quad (5.49)$$

the second moment with respect to the origin $\boldsymbol{\mu}_{qq}(t) = \mathbb{E}[\mathbf{q}(t)\mathbf{q}^H(t)]$ is:

$$\begin{aligned}
\boldsymbol{\mu}_{qq}(t) &= \mathbb{E} \left[\int_0^t \mathbf{h}(t-\tau_1) \mathbf{p}(\tau_1) d\tau_1 \left(\int_0^t \mathbf{h}(t-\tau_2) \mathbf{p}(\tau_2) d\tau_2 \right)^H \right] \\
&= \mathbb{E} \left[\int_0^t \mathbf{h}(t-\tau_1) \mathbf{p}(\tau_1) d\tau_1 \left(\int_0^t \mathbf{p}^H(\tau_2) \mathbf{h}(t-\tau_2)^H d\tau_2 \right) \right] \\
&= \mathbb{E} \left[\int_0^t \int_0^t \mathbf{h}(t-\tau_1) \mathbf{p}(\tau_1) \mathbf{p}^H(\tau_2) \mathbf{h}(t-\tau_2)^H d\tau_1 d\tau_2 \right] \\
&= \int_0^t \int_0^t \mathbf{h}(t-\tau_1) \mathbb{E}[\mathbf{p}(\tau_1) \mathbf{p}^H(\tau_2)] (\tau_2) \mathbf{h}(t-\tau_2)^H d\tau_1 d\tau_2 \\
&= \int_0^t \int_0^t \mathbf{h}(t-\tau_1) \mathbf{R}_{pp}(\tau_1, \tau_2) \mathbf{h}(t-\tau_2)^H d\tau_1 d\tau_2.
\end{aligned} \tag{5.50}$$

In the same way, the inter-instant moments can be obtained, for instance, the correlation function is obtained as $\mathbf{R}_{qq}(t_1, t_2) = \mathbb{E}[\mathbf{q}(t_1)\mathbf{q}^H(t_2)]$:

$$\begin{aligned}
\mathbf{R}_{qq}(t_1, t_2) &= \mathbb{E}[\mathbf{q}(t_1)\mathbf{q}^H(t_2)] \\
&= \mathbb{E} \left[\left(\int_0^{t_1} \mathbf{h}(t_1-\tau_1) \mathbf{p}(\tau_1) d\tau_1 \right) \left(\int_0^{t_2} \mathbf{h}(t_2-\tau_2) \mathbf{p}(\tau_2) d\tau_2 \right)^H \right] \\
&= \mathbb{E} \left[\int_0^{t_2} \int_0^{t_1} \mathbf{h}(t_1-\tau_1) \mathbf{p}(\tau_1) \mathbf{p}^H(\tau_2) \mathbf{h}(t_2-\tau_2)^H d\tau_1 d\tau_2 \right] \\
&= \int_0^{t_2} \int_0^{t_1} \mathbf{h}(t_1-\tau_1) \mathbb{E}[\mathbf{p}(\tau_1) \mathbf{p}^H(\tau_2)] \mathbf{h}(t_2-\tau_2)^H d\tau_1 d\tau_2 \\
&= \int_0^{t_2} \int_0^{t_1} \mathbf{h}(t_1-\tau_1) \mathbf{R}_{pp}(\tau_1, \tau_2) \mathbf{h}(t_2-\tau_2)^H d\tau_1 d\tau_2,
\end{aligned} \tag{5.51}$$

and the covariance function can be deduced from correlation and mean $\boldsymbol{\Sigma}_{qq}(t_1, t_2) = \mathbb{E}[(\mathbf{q}(t_1) - \boldsymbol{\mu}_q(t_1))(\mathbf{q}(t_2) - \boldsymbol{\mu}_q(t_2))^H]$:

$$\boldsymbol{\Sigma}_{qq}(t_1, t_2) = \mathbf{R}_{qq}(t_1, t_2) - \boldsymbol{\mu}_q(t_1) \boldsymbol{\mu}_q^H(t_2), \tag{5.52}$$

or directly from the covariance function of the adapted load:

$$\begin{aligned}
\boldsymbol{\Sigma}_{qq}(t_1, t_2) &= \mathbb{E} \left[(\mathbf{q}(t_1) - \boldsymbol{\mu}_q(t_1)) (\mathbf{q}(t_2) - \boldsymbol{\mu}_q(t_2))^H \right] \\
&= \mathbb{E} \left[\left(\int_0^{t_2} \int_0^{t_1} \mathbf{h}(t_1-\tau_1) \mathbf{p}(\tau_1) \mathbf{p}^H(\tau_2) \mathbf{h}^H(t_2-\tau_2) d\tau_1 d\tau_2 - \int_0^{t_2} \int_0^{t_1} \mathbf{h}(t_1-\tau_1) \boldsymbol{\mu}_p(\tau_1) \mathbf{p}^H(\tau_2) \mathbf{h}^H(t_2-\tau_2) d\tau_1 d\tau_2 \right) \right] \\
&= \int_0^{t_2} \int_0^{t_1} \mathbf{h}(t_1-\tau_1) \mathbf{R}_{pp}(\tau_1, \tau_2) \mathbf{h}^H(t_2-\tau_2) d\tau_1 d\tau_2 - \int_0^{t_2} \int_0^{t_1} \mathbf{h}(t_1-\tau_1) \boldsymbol{\mu}_p(\tau_1) \boldsymbol{\mu}_p^H(\tau_2) \mathbf{h}^H(t_2-\tau_2) d\tau_1 d\tau_2 \\
&= \int_0^{t_2} \int_0^{t_1} \mathbf{h}(t_1-\tau_1) (\mathbf{R}_{pp}(\tau_1, \tau_2) - \boldsymbol{\mu}_p(\tau_1) \boldsymbol{\mu}_p^H(\tau_2)) \mathbf{h}^H(t_2-\tau_2) d\tau_1 d\tau_2 \\
&= \int_0^{t_2} \int_0^{t_1} \mathbf{h}(t_1-\tau_1) \boldsymbol{\Sigma}_{pp}(\tau_1, \tau_2) \mathbf{h}^H(t_2-\tau_2) d\tau_1 d\tau_2
\end{aligned} \tag{5.53}$$

For a system with N degrees of freedom, $\boldsymbol{\mu}_q(t)$ is a vector with N components; $\boldsymbol{\mu}_{qq}(t)$, $\boldsymbol{\sigma}_{qq}(t)$, $\mathbf{R}_{qq}(t_1, t_2)$ and $\boldsymbol{\Sigma}_{qq}(t_1, t_2)$ are matrices of dimension $N \times N$. The higher order moments require a tensor description, as

they are expressed by multi-index arrays; for instance the third moment with respect to the origin $\boldsymbol{\mu}_{qqq}(t)$ has dimension $N \times N \times N$ and the fourth $\boldsymbol{\mu}_{qqqq}(t)$ has $N \times N \times N \times N$. Generally, $\boldsymbol{\mu}_{q^k}(t)$ will have N^k components, from a computational perspective this imposes a high memory demand even for relatively low order systems, a limitation remarked before in the literature, for instance [158] for nonlinear systems.

Working by components, we note $\mu_{qqq}^{i,j,k}(t) = \mathbb{E} [q_i(t) q_j^*(t) q_k(t)]$, $i, j, k \in N$, where $q_i(t)$ is the i -th component of \mathbf{q} ; introducing $h_{i,j}(t) = \exp[\rho_{i,j}(t - \tau)]$ the indicial representation of the components of $\mathbf{h}(t)$, we write:

$$q_i(t) = \sum_j \left(\int_0^t h_{i,j}(t) p_j(\tau) d\tau \right) \quad (5.54)$$

where p_j is the j -th component of the adapted load vector. With this approach, we can write:

$$\begin{aligned} \mu_{qqq}^{i,j,k}(t) &= \mathbb{E} \left[\sum_l \left(\int_0^t h_{i,l}(t) p_l(\tau_1) d\tau_1 \right) \sum_m \left(\int_0^t h_{i,m}^*(t) p_m^*(\tau_2) d\tau_2 \right) \sum_n \left(\int_0^t h_{i,n}(t) p_n(\tau_3) d\tau_3 \right) \right] \\ &= \sum_n \sum_m \sum_l \left(\int_0^t \int_0^t \int_0^t h_{i,n}(t) h_{i,m}^*(t) h_{i,l}(t) R_{ppp}^{l,m,n}(\tau_1, \tau_2, \tau_3) d\tau_1 d\tau_2 d\tau_3 \right), \end{aligned} \quad (5.55)$$

and similarly for the fourth order moment:

$$\mu_{qqqq}^{i,j,k,l}(t) = \sum_n \sum_m \sum_o \sum_s \left(\int_0^t \int_0^t \int_0^t \int_0^t h_{i,n}(t) h_{i,m}^*(t) h_{i,o}(t) h_{i,s}^*(t) R_{pppp}^{n,m,o,s}(\tau_1, \tau_2, \tau_3, \tau_4) d\tau_1 d\tau_2 d\tau_3 d\tau_4 \right). \quad (5.56)$$

These expressions can serve as the basis of frequency-domain descriptors, for instance the PSD $\mathbf{S}_{qq}(f_1, f_2) = \text{FT}[\boldsymbol{\Sigma}_{qq}(t_1, t_2)]$:

$$\mathbf{S}_{qq}(f_1, f_2) = \int_{-\infty}^{\infty} \int_{-\infty}^{\infty} \boldsymbol{\Sigma}_{qq}(t_1, t_2) \exp[-i2\pi(f_1 t_1 + f_2 t_2)] dt_1 dt_2, \quad (5.57)$$

the main limitation of this definition of the PSD is that it does not provide a temporal description of the time evolution of the frequency content. Several contending definitions of the nonstationary PSD exist, for instance, the Wigner spectrum ([116],[11]):

$$\mathbf{S}_{qq}^W(t, f) = \int_{-\infty}^{\infty} \boldsymbol{\Sigma}_{qq}(t, \tau) \exp[-i2\pi f \tau] d\tau \quad (5.58)$$

where $\boldsymbol{\Sigma}_{qq}(t, \tau)$ is the instantaneous covariance function, the following adjustment has been made on the covariance function: $\boldsymbol{\Sigma}_{qq}(t, \tau) = \boldsymbol{\Sigma}_{qq}(t + \frac{\tau}{2}, t - \frac{\tau}{2})$. More broadly, time-varying processes can be treated from a signal analysis perspective with tools from time-frequency analysis, as remarked in [120]:

- Wavelet basis with the associated Wavelet Transforms: Wavelets provide time-frequency representation as well as multi-resolution characteristics;
- Short-Time Fourier Transform (STFT): it offers a localized distribution of the energy with time-frequency resolution;
- Wigner-Ville Distribution: it provides a time-frequency representation with many additional properties useful to stochastic analysis.

Inspired by the results in [120], some preliminary results about the application of time-frequency representations to LTP systems with stochastic inputs have been explored in [64], where one of the simplest LTP systems is considered and the PGHW, STFT, Wigner-Ville and Fourier representations are tested.

Another relevant proposal for nonstationary PSD is the Priestley spectrum ([106],[107]):

$$\mathbf{S}_{qq}^{Priestley}(t, f) = |\tilde{\mathbf{A}}(t, f)|^2 \mathbf{S}_{qq}^s(f) \quad (5.59)$$

where the underlying nonstationary process has been represented in terms of the slowly varying modulating function $\tilde{\mathbf{A}}(t, f)$, and $\mathbf{S}_{qq}^s(f)$ corresponds to a stationary PSD [104]:

$$\mathbf{q}(t) = \int_{-\infty}^{\infty} \tilde{\mathbf{A}}(t, f) dZ(f) \quad (5.60)$$

where $Z(t)$ is an independent increment process. A technique that has seen much attention in the last decade is the Harmonic Wavelet estimation of Eq. 5.59, as seen in [32], [73], [130], and [129]. In fact, the slowly varying modulating function $\tilde{\mathbf{A}}(t, f)$ in the previous expression is not unique, and several families of functions fulfill the requirements, resulting in different versions of the evolutionary PSD. Reference [56] recontextualizes the main results from Priestley's proposal, arguing that it is equivalent to a Short-Time Fourier Transform (STFT) where the family of functions $\tilde{\mathbf{A}}(t, f)$ acts as a temporal window that localizes the energy decomposition of the EPSD. In this framework, the Harmonic Wavelet estimation consists of projecting the solution in the corresponding Wavelet basis, which amounts to selecting a temporal window associated with the corresponding family of Wavelets. In [129], we have, for a stochastic process $X(t)$:

$$S_{XX}(f_i, t_k) = \frac{T_0}{n-m} \mathbb{E} \left[|W_{i,k}^X|^2 \right] \quad (5.61)$$

where $W_{i,k}^X$ is the Wavelet coefficient of the i -th scale and k -th translation of $X(t)$, T_0 is the final time of the observation of the signal or process, $n-m$ is the bandwidth of a given scale (traditionally selected as uniform), and: $m_i \Delta f \leq f_i < n_i \Delta f$, $k \frac{T_0}{n-m} \leq t_k < (k+1) \frac{T_0}{n-m}$ define the frequency and time intervals in which a given coefficient is localized.

State variable relationships Having established the convolution expressions for moment propagation in modal variables for the forced response, we now propagate the moments to the state variables. From $\mathbf{y}(t) = \mathbf{R}(t) \mathbf{q}(t)$, we have the following relationships:

$$\boldsymbol{\mu}_y(t) = \mathbf{R}(t) \boldsymbol{\mu}_q(t), \quad (5.62)$$

for the first moment, for the second moment $\boldsymbol{\mu}_{yy}(t) = \mathbb{E}[\mathbf{y}(t) \mathbf{y}^H(t)]$:

$$\boldsymbol{\mu}_{yy}(t) = \mathbf{R}(t) \boldsymbol{\mu}_{qq}(t) \mathbf{R}^H(t), \quad (5.63)$$

and the correlation and covariance functions, respectively:

$$\begin{aligned} \mathbf{R}_{yy}(t_1, t_2) &= \mathbf{R}(t_1) \mathbf{R}_{qq}(t_1, t_2) \mathbf{R}^H(t_2) \\ \boldsymbol{\Sigma}_{yy}(t_1, t_2) &= \mathbf{R}(t_1) \boldsymbol{\Sigma}_{qq}(t_1, t_2) \mathbf{R}^H(t_2). \end{aligned} \quad (5.64)$$

The higher-order instantaneous moments can be transformed as:

$$\begin{aligned} \mu_{yyy}^{i,j,k}(t) &= \sum_n \sum_m \sum_l R_{i,n}(t) R_{j,m}^*(t) R_{k,l}(t) \mu_{qqq}^{n,m,l}(t) \\ \mu_{yyyy}^{i,j,k,l}(t) &= \sum_n \sum_m \sum_o \sum_s R_{i,n}(t) R_{j,m}^*(t) R_{k,o}(t) R_{l,s}^*(t) \mu_{qqqq}^{n,m,o,s}(t), \end{aligned} \quad (5.65)$$

some care is required in the interpretation of these expressions, as $\mathbf{R}(t)$ without index stands for the modal matrix from the Floquet representation, with components $R_{i,j}(t); i, j \in N$; while $\mathbf{R}_{qq}(t_1, t_2)$, with stochastic variable index stands for the correlation function of the corresponding stochastic quantity.

4.2 Transformations of the adapted excitation

We now apply moment propagation to the adapted excitation $\mathbf{p}(t) = \mathbf{L}(t)\mathbf{B}(t)\mathbf{f}(t)$ from the physical excitation $\mathbf{f}(t)$, which we will assume to be nonstationary. We recall the fact that $\mathbf{L}(t)$ and $\mathbf{B}(t)$ are periodic with the same period of the system. First, the mean is:

$$\begin{aligned} \mathbb{E}[\mathbf{p}(t)] &= \boldsymbol{\mu}_p(t) \\ \boldsymbol{\mu}_p(t) &= \mathbb{E}[\mathbf{L}(t)\mathbf{B}(t)\mathbf{f}(t)] \\ \boldsymbol{\mu}_p(t) &= \mathbf{L}(t)\mathbf{B}(t)\boldsymbol{\mu}_f(t), \end{aligned} \quad (5.66)$$

the second moment is:

$$\begin{aligned} \mathbb{E}[\mathbf{p}(t)\mathbf{p}^H(t)] &= \boldsymbol{\mu}_{pp}(t) \\ \boldsymbol{\mu}_{pp}(t) &= \mathbf{L}(t)\mathbf{B}(t)\boldsymbol{\mu}_{ff}(t)\mathbf{B}^H(t)\mathbf{L}^H(t), \end{aligned} \quad (5.67)$$

the correlation function:

$$\begin{aligned} \mathbb{E}[\mathbf{p}(t_1)\mathbf{p}^H(t_2)] &= \mathbf{R}_{pp}(t_1, t_2) \\ \mathbf{R}_{pp}(t_1, t_2) &= \mathbf{L}(t_1)\mathbf{B}(t_1)\mathbf{R}_{ff}(t_1, t_2)\mathbf{B}^H(t_2)\mathbf{L}^H(t_2) \end{aligned} \quad (5.68)$$

and the covariance function:

$$\boldsymbol{\Sigma}_{pp}(t_1, t_2) = \mathbf{L}(t_1)\mathbf{B}(t_1)\boldsymbol{\Sigma}_{ff}(t_1, t_2)\mathbf{B}^H(t_2)\mathbf{L}^H(t_2). \quad (5.69)$$

Some peculiar facts emerge from this development concerning the adapted excitation. Let us assume that the physical excitation has the form:

$$\mathbf{f}(t) = \begin{pmatrix} a_1(t, \Omega) f_1(t) \\ a_2(t, \Omega) f_2(t) \\ \dots \\ a_N(t, \Omega) f_N(t) \end{pmatrix}, \quad (5.70)$$

where the $a_i(t, \Omega)$ are deterministic modulating function, and each $f_i(t)$ is a stationary stochastic process. We note:

- If $a_i(t, \Omega) = a_i$ is a constant, the excitation is stationary, the adapted excitation $\mathbf{p}(t) = \mathbf{L}(t)\mathbf{B}(t)\mathbf{f}(t)$ will be periodic with the same periodicity of the system.
- If $a_i(t + nT_f, \Omega) = a_i(t, \Omega)$ is periodic with period T_f , the adapted excitation may or may not be periodic, depending on the relationship between the period T_f and the period of the system T_p , that is their commensurability.
- Since $\mathbf{L}(t)$ is, in general, a matrix function with complex values, the adapted excitation is usually complex, too.

- From a stochastic perspective, the adapted excitation will be a mixture of several input processes.
- As discussed in Chapter 3, the periodic eigenvectors are not unique, and the choice of integer in the imaginary part that determines the characteristic exponent from the Floquet multipliers has an effect on the shape of the eigenvector. This choice will impact the shape of the adapted excitation, which suggests that for the study of the forced response through convolutional relationships, certain sets \mathbf{A}_m formed by the characteristic exponents $\rho_k = \alpha_k + i\sigma_k$ and their associated periodic eigenvectors may be preferred from a computational perspective. As shown in the example of Chapter 3, certain eigenvectors may have a high-frequency oscillatory behavior as opposed to their counterparts from an alternative \mathbf{A}_m , a behavior that makes the evaluation of the corresponding convolution computations substantially more challenging.

Example Consider the following excitation over a 4-DOF Floquet system:

$$\mathbf{B}(t)\mathbf{f}(t) = \begin{pmatrix} 0 \\ 0 \\ a_1(t, \Omega) f_1(t) \\ a_2(t, \Omega) f_2(t) \end{pmatrix}, \quad (5.71)$$

where, for exposition purposes, $\mathbf{B}(t) = \begin{bmatrix} \mathbf{0} \\ \text{diag}[\mathbf{M}^{-1}] \end{bmatrix}$ and the time-varying terms have been assimilated into $a_1(t, \Omega)$ and $a_2(t, \Omega)$; the adapted excitation has the form:

$$\begin{aligned} \mathbf{p}(t) &= a_1(t, \Omega) \begin{pmatrix} f_1 L_{13}(t) \\ f_1 L_{23}(t) \\ f_1 L_{33}(t) \\ f_1 L_{43}(t) \end{pmatrix} + a_2(t, \Omega) \begin{pmatrix} f_2 L_{14}(t) \\ f_2 L_{24}(t) \\ f_2 L_{34}(t) \\ f_2 L_{44}(t) \end{pmatrix} \\ &= a_1(t, \Omega) f_1 \mathbf{L}_{i,3}(t) + a_2(t, \Omega) f_2 \mathbf{L}_{i,4}(t), \end{aligned} \quad (5.72)$$

where $\mathbf{L}_{i,3}(t)$ is the third column of $\mathbf{L}(t)$ corresponding to the third periodic mode. Considering $\mathbf{h}(t)$:

$$\mathbf{h}(t) = \begin{pmatrix} \exp[\rho_1 t] & 0 & 0 & 0 \\ 0 & \exp[\rho_2 t] & 0 & 0 \\ 0 & 0 & \exp[\rho_3 t] & 0 \\ 0 & 0 & 0 & \exp[\rho_4 t] \end{pmatrix}, \quad (5.73)$$

we can apply the previous developments, for instance considering the first moment of the adapted excitation:

$$\boldsymbol{\mu}_p(t) = \begin{pmatrix} \mu_{p_1}(t) \\ \mu_{p_2}(t) \\ \mu_{p_3}(t) \\ \mu_{p_4}(t) \end{pmatrix}, \quad (5.74)$$

the four convolution expressions to evaluate to obtain the modal forced response are:

$$\begin{aligned} \mu_{q_1}(t) &= \int_0^t h_{1,1}(t-\tau) \mu_{p_1}(\tau) d\tau \\ \mu_{q_2}(t) &= \int_0^t h_{2,2}(t-\tau) \mu_{p_2}(\tau) d\tau \\ \mu_{q_3}(t) &= \int_0^t h_{3,3}(t-\tau) \mu_{p_3}(\tau) d\tau \\ \mu_{q_4}(t) &= \int_0^t h_{4,4}(t-\tau) \mu_{p_4}(\tau) d\tau, \end{aligned} \quad (5.75)$$

the second moments of the adapted excitation are:

$$\boldsymbol{\mu}_{pp}(t) = \begin{pmatrix} \mu_{p_1 p_1}(t) & \mu_{p_1 p_2}(t) & \mu_{p_1 p_3}(t) & \mu_{p_1 p_4}(t) \\ \mu_{p_2 p_1}(t) & \mu_{p_2 p_2}(t) & \mu_{p_2 p_3}(t) & \mu_{p_2 p_4}(t) \\ \mu_{p_3 p_1}(t) & \mu_{p_3 p_2}(t) & \mu_{p_3 p_3}(t) & \mu_{p_3 p_4}(t) \\ \mu_{p_4 p_1}(t) & \mu_{p_4 p_2}(t) & \mu_{p_4 p_3}(t) & \mu_{p_4 p_4}(t) \end{pmatrix}, \quad (5.76)$$

where: $\mu_{p_i p_j}(t) = \mathbb{E}[p_i(t) p_j^*(t)]$, $\mu_{p_j p_i}(t) = \mathbb{E}[p_j(t) p_i^*(t)]$, letting $p_i(t) = p_i^{Re}(t) + i p_i^{Im}(t)$, and $p_j(t) = p_j^{Re}(t) + i p_j^{Im}(t)$ we have:

$$\begin{aligned} \mu_{p_i p_j}(t) &= \mathbb{E}[p_i(t) p_j^*(t)] \\ &= \mathbb{E}[(p_i^{Re}(t) p_j^{Re}(t) + p_i^{Im}(t) p_j^{Im}(t)) + i(p_j^{Re}(t) p_i^{Im}(t) - p_i^{Re}(t) p_j^{Im}(t))] \\ \mu_{p_j p_i}(t) &= \mathbb{E}[p_j(t) p_i^*(t)] \\ &= \mathbb{E}[(p_i^{Re}(t) p_j^{Re}(t) + p_i^{Im}(t) p_j^{Im}(t)) + i(p_i^{Re}(t) p_j^{Im}(t) - p_j^{Re}(t) p_i^{Im}(t))] \\ \mu_{p_j p_i}^*(t) &= \mathbb{E}[(p_i^{Re}(t) p_j^{Re}(t) + p_i^{Im}(t) p_j^{Im}(t)) + i(p_j^{Re}(t) p_i^{Im}(t) - p_i^{Re}(t) p_j^{Im}(t))] \\ \mu_{p_j p_i}^*(t) &= \mu_{p_i p_j}(t), \end{aligned} \quad (5.77)$$

or $\boldsymbol{\mu}_{pp}(t)$ is a hermitian matrix. The second moments of the modal forced response are obtained through the following expression:

$$\boldsymbol{\mu}_{qq}(t) = \int_0^t \int_0^t \begin{pmatrix} h_{1,1}(t-\tau_1) h_{1,1}^*(t-\tau_2) R_{p_1 p_1}(\tau_1, \tau_2) & h_{1,1}(t-\tau_1) h_{2,2}^*(t-\tau_2) R_{p_1 p_2}(\tau_1, \tau_2) \\ h_{2,2}(t-\tau_1) h_{1,1}^*(t-\tau_2) R_{p_2 p_1}(\tau_1, \tau_2) & h_{2,2}(t-\tau_1) h_{2,2}^*(t-\tau_2) R_{p_2 p_2}(\tau_1, \tau_2) \\ h_{3,3}(t-\tau_1) h_{1,1}^*(t-\tau_2) R_{p_3 p_1}(\tau_1, \tau_2) & h_{3,3}(t-\tau_1) h_{2,2}^*(t-\tau_2) R_{p_3 p_2}(\tau_1, \tau_2) \\ h_{4,4}(t-\tau_1) h_{1,1}^*(t-\tau_2) R_{p_4 p_1}(\tau_1, \tau_2) & h_{4,4}(t-\tau_1) h_{2,2}^*(t-\tau_2) R_{p_4 p_2}(\tau_1, \tau_2) \\ h_{1,1}(t-\tau_1) h_{3,3}^*(t-\tau_2) R_{p_1 p_3}(\tau_1, \tau_2) & h_{1,1}(t-\tau_1) h_{4,4}^*(t-\tau_2) R_{p_1 p_4}(\tau_1, \tau_2) \\ h_{2,2}(t-\tau_1) h_{3,3}^*(t-\tau_2) R_{p_2 p_3}(\tau_1, \tau_2) & h_{2,2}(t-\tau_1) h_{4,4}^*(t-\tau_2) R_{p_2 p_4}(\tau_1, \tau_2) \\ h_{3,3}(t-\tau_1) h_{3,3}^*(t-\tau_2) R_{p_3 p_3}(\tau_1, \tau_2) & h_{3,3}(t-\tau_1) h_{4,4}^*(t-\tau_2) R_{p_3 p_4}(\tau_1, \tau_2) \\ h_{4,4}(t-\tau_1) h_{3,3}^*(t-\tau_2) R_{p_4 p_3}(\tau_1, \tau_2) & h_{4,4}(t-\tau_1) h_{4,4}^*(t-\tau_2) R_{p_4 p_4}(\tau_1, \tau_2) \end{pmatrix} d\tau_1 d\tau_2, \quad (5.78)$$

another way of writing this result is by introducing the following matrix:

$$\begin{aligned} \mathbf{h}_2(t_1, t_2) &= \begin{pmatrix} h_{1,1}(t_1) h_{1,1}^*(t_2) & h_{1,1}(t_1) h_{2,2}^*(t_2) & h_{1,1}(t_1) h_{3,3}^*(t_2) & h_{1,1}(t_1) h_{4,4}^*(t_2) \\ h_{2,2}(t_1) h_{1,1}^*(t_2) & h_{2,2}(t_1) h_{2,2}^*(t_2) & h_{2,2}(t_1) h_{3,3}^*(t_2) & h_{2,2}(t_1) h_{4,4}^*(t_2) \\ h_{3,3}(t_1) h_{1,1}^*(t_2) & h_{3,3}(t_1) h_{2,2}^*(t_2) & h_{3,3}(t_1) h_{3,3}^*(t_2) & h_{3,3}(t_1) h_{4,4}^*(t_2) \\ h_{4,4}(t_1) h_{1,1}^*(t_2) & h_{4,4}(t_1) h_{2,2}^*(t_2) & h_{4,4}(t_1) h_{3,3}^*(t_2) & h_{4,4}(t_1) h_{4,4}^*(t_2) \end{pmatrix} \\ &= \begin{pmatrix} \exp[\rho_1 t_1 + \rho_1^* t_2] & \exp[\rho_1 t_1 + \rho_2^* t_2] & \exp[\rho_1 t_1 + \rho_3^* t_2] & \exp[\rho_1 t_1 + \rho_4^* t_2] \\ \exp[\rho_2 t_1 + \rho_1^* t_2] & \exp[\rho_2 t_1 + \rho_2^* t_2] & \exp[\rho_2 t_1 + \rho_3^* t_2] & \exp[\rho_2 t_1 + \rho_4^* t_2] \\ \exp[\rho_3 t_1 + \rho_1^* t_2] & \exp[\rho_3 t_1 + \rho_2^* t_2] & \exp[\rho_3 t_1 + \rho_3^* t_2] & \exp[\rho_3 t_1 + \rho_4^* t_2] \\ \exp[\rho_4 t_1 + \rho_1^* t_2] & \exp[\rho_4 t_1 + \rho_2^* t_2] & \exp[\rho_4 t_1 + \rho_3^* t_2] & \exp[\rho_4 t_1 + \rho_4^* t_2] \end{pmatrix} \end{aligned} \quad (5.79)$$

and making use of the Shur or element-wise product $\mathbf{R}_{pp}(t_1, t_2) \odot \mathbf{h}_2(t_1, t_2)$, then:

$$\boldsymbol{\mu}_{qq}(t) = \int_0^t \int_0^t \mathbf{R}_{pp}(\tau_1, \tau_2) \odot \mathbf{h}_2(t-\tau_1, t-\tau_2) d\tau_1 d\tau_2. \quad (5.80)$$

A similar expression applies to the covariance function, for instance:

$$\Sigma_{q_1 q_1}(t_1, t_2) = \int_0^{t_1} \int_0^{t_2} h_{1,1}(t_1 - \tau_1) h_{1,1}^*(t_2 - \tau_2) \Sigma_{p_1 p_1}(\tau_1, \tau_2) d\tau_1 d\tau_2, \quad (5.81)$$

with $\Sigma_{p_1 p_1}(\tau_1, \tau_2)$ the auto-covariance function of the first entry of the adapted excitation. As before, using $\mathbf{h}_2(t_1, t_2)$ we obtain:

$$\Sigma_{qq}(t_1, t_2) = \int_0^{t_1} \int_0^{t_2} \Sigma_{pp}(\tau_1, \tau_2) \odot \mathbf{h}_2(t_1 - \tau_1, t_2 - \tau_2) d\tau_1 d\tau_2. \quad (5.82)$$

The matrix function $\mathbf{h}_2(t_1, t_2)$ expresses the interactions between all possible combinations of impulse response components in the Floquet modal variable. It is analogous to the quadratic impulse response function found in the corresponding literature pertaining to nonlinear systems, for instance, in [53] and [153]. A remarkable conclusion from the preceding development is that the stochastic characterization of higher moments involves higher-order generalizations of this function. From the example at hand, for instance, the third-order impulse response will have the form:

$$h_{q_1 q_2 q_3}(t_1, t_2, t_3) = \exp[(\rho_1 t_1 + \rho_2^* t_2 + \rho_3 t_3)] \quad (5.83)$$

where the quantity at hand is a third order tensor with $4 \times 4 \times 4 = 64$ components.

5 Illustrative example

We now test the Floquet modal transformation approach developed in this chapter with a concrete example. The Floquet system employed is the 2-DOF simplified system introduced in Chapter 3, with the \mathbf{A}_0 modal representation consisting of the characteristic exponents: $\rho_1 = -0.0038 + i0.4926$, $\rho_2 = -0.0038 - i0.4926$, $\rho_3 = -0.26924 + i0.11058$, $\rho_4 = -0.26924 - i0.11058$, and the corresponding periodic eigenvectors. For this system, we remark that using the previously introduced extension to the critical damping ratio $\xi_i = -\frac{\text{Re}(\rho_i)}{\|\rho_i\|}$, we have $\xi_{[1,2]} = 0.0079$ and $\xi_{[3,4]} = 0.9250$. We subject the system to a Gaussian excitation vector constructed by modulation of a stationary process. We will propagate the moments to define the input from this antecedent Gaussian vector, apply the relationships established to describe the adapted load, and finally apply the convolution relationships to obtain the moments. Finally, we will use the PGHW representation to extract the EPSPD of the response.

5.1 Load description

Input load We consider the following input process on the interval $[0, 3T_p]$ with $T_p = 5.4636s$:

$$\mathbf{f}(t) = \begin{pmatrix} f_1(t) \\ f_2(t) \end{pmatrix}, \quad (5.84)$$

the process $f_1(t)$ is Gaussian and stationary:

$$f_1(t) \rightarrow \begin{cases} \mu_{f_1} = 5000 \\ \mu_{f_1 f_1} = 2.5 \times 10^7 \end{cases} \quad (5.85)$$

and the process $f_2(t)$ is obtained from modulation of another Gaussian stationary process, the first two moments have the following form:

$$f_2(t) \rightarrow \begin{cases} \mu_{f_2}(t) = 5000 \cos(1.15t) \\ \mu_{f_2 f_2}(t) = 2.5 \times 10^7 \cos^2(1.15t) \end{cases} \quad (5.86)$$

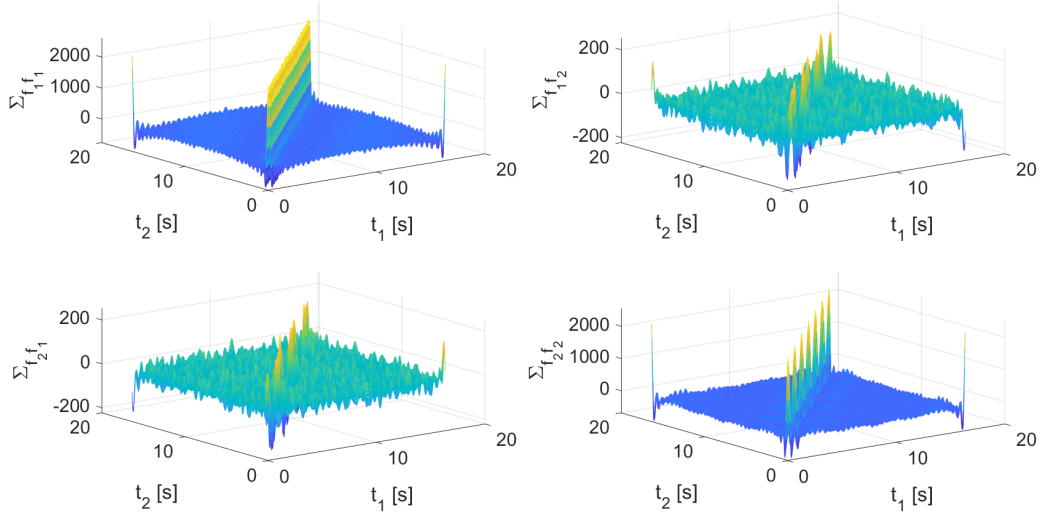


Figure 5.11: Components of the covariance functions of input load

The second-order cross moments are $\mu_{f_1 f_2}(t) = \mu_{f_2 f_1}(t) = 2.5 \times 10^7 \cos(1.15t)$. The components of the covariance function are shown in Fig. 5.11.

We highlight the fact that the auto-covariance function of the first process is stationary, while the auto-covariance function of the second, as expected, is similar to the modulated processes described at the beginning of this chapter, a feature that propagates to the cross-covariance functions. The first moment of $\mathbf{f}(t)$ is thus:

$$\boldsymbol{\mu}_f(t) = \begin{pmatrix} \mu_{f_1} \\ \mu_{f_2}(t) \end{pmatrix}, \quad (5.87)$$

and the second moments are:

$$\boldsymbol{\mu}_{ff}(t) = \begin{pmatrix} \mu_{f_1 f_1} & \mu_{f_1 f_2}(t) \\ \mu_{f_1 f_2}(t) & \mu_{f_2 f_2}(t) \end{pmatrix}, \quad (5.88)$$

the variances can be easily obtained from the covariance function as $\sigma_{f_i f_j}(t) = \Sigma_{f_i f_j}(t, t)$, or using the following expressions:

$$\begin{aligned} \sigma_{f_1 f_1} &= \mu_{f_1 f_1} - \mu_{f_1}^2 \\ \sigma_{f_2 f_2}(t) &= \mu_{f_2 f_2}(t) - \mu_{f_2}^2(t) \\ \sigma_{f_1 f_2}(t) &= \mu_{f_1 f_2}(t) - \mu_{f_1} \mu_{f_2}(t). \end{aligned} \quad (5.89)$$

Adapted load Applying the modal transformations on the load expressions Eq. 5.66 and Eq. 5.68, we obtain the moments of the adapted excitation seen in Fig. 5.12 for the mean and Fig. 5.13 for the auto-correlation components of the correlation matrix. As remarked previously, these probabilistic descriptors are now complex quantities. The mean function of each pair of adapted load components μ_{p_1} , μ_{p_2} and μ_{p_3} , μ_{p_4} differ in their imaginary part: one of the pair is the conjugate of the other; we can also notice a higher frequency of oscillation in mean function for μ_{p_3} and μ_{p_4} , with a well-defined envelope.

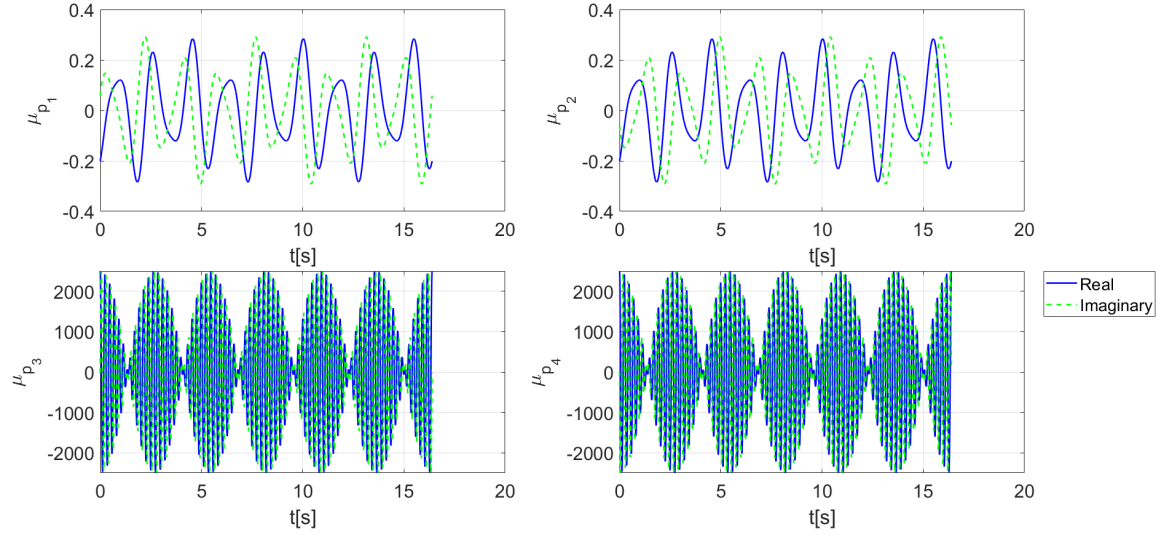


Figure 5.12: Mean of adapted excitation

5.2 Response and analysis

Two resolution methods have been used to determine the response of the system to the excitation:

1. MCS, in which the prescribed input process has been simulated, and the equation of motion has been solved numerically for each realization, producing an ensemble of solutions from which statistical approximations of the response can be drawn. For this application, 10,000 samples have been generated in the $[0, 3T_p]$ interval, with null initial conditions. The numerical algorithm for the resolution is Matlab's ODE113, which is an implementation of the Adams-Bashforth-Moulton method of order 1–13.
2. The convolution solution is obtained by applying formulas Eq. 5.47, Eq. 5.50, Eq. 5.52, and Eq. 5.51 to the previously described adapted excitation and with the corresponding impulse response depending on the characteristic exponents of the system.

We use the MCS as a reference to test the consistency of the convolution relationships established earlier. The choice of 10,000 samples has been made under stochastic convergence and computational resources considerations; the mean and variance obtained from increasing samples are shown in Fig. 5.14. One of the advantages of the convolution approach relates to the computational cost incurred with respect to MCS. To offer some perspective, the total time required to complete the MCS resolution with 10,000 samples was $t_{comp,MCS} = 461.76s$ with 14 parallel cores, without accounting for the time incurred in computing the statistics of the ensemble. The convolution response required $t_{comp,conv} = 239.68s$ accounting for load adaptation 134.31s and proper convolution time 105.37s. In addition to this significant time saving, additional advantages can be noted: no convergence considerations are required for the convolution method, as the moments are propagated directly from the inputs and not from an ensemble, whereas $t_{comp,MCS}$ scales with the number of samples; $t_{comp,MCS}$ is very sensitive to the integration length $[0, 3T_p]$, if a long observation time is required then the MCS time becomes prohibitive, while the convolution computation also scales with the length of the signals involved, this scaling is less pronounced.

From Fig. 5.15, we can draw several important conclusions about the behavior of the system and the particularities of each solution. The mean functions are not periodic on T_p due to the presence of transient components of the solution, however some trends are apparent. Consider the temporal average of the mean function in the observed interval, that is: $\bar{\mu}_x = \frac{1}{3T_p} \int_0^{3T_p} \mu_x(t) dt$, which is approximately 0.0247, and it represents a constant

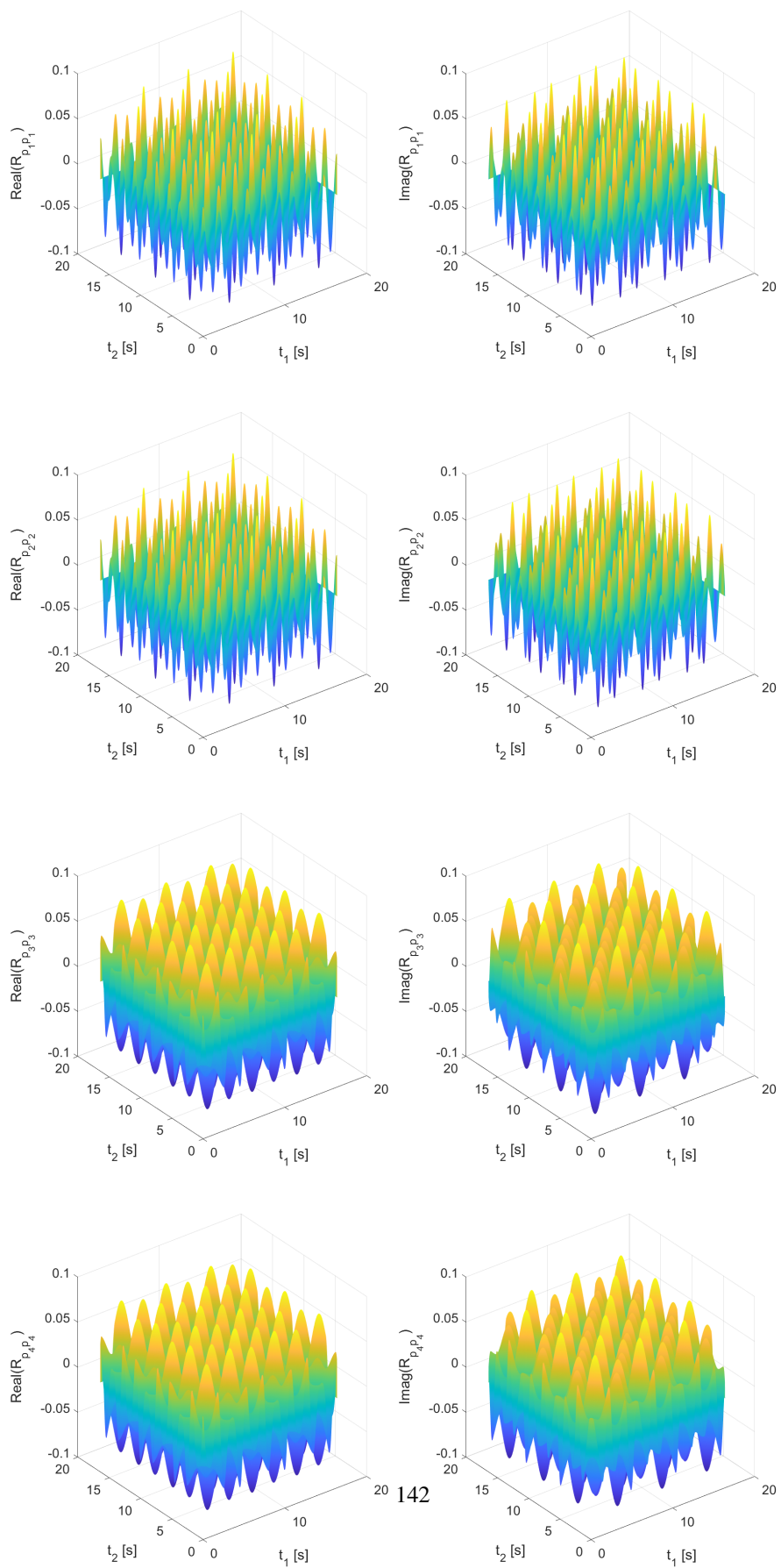


Figure 5.13: Auto-correlation functions of adapted excitation

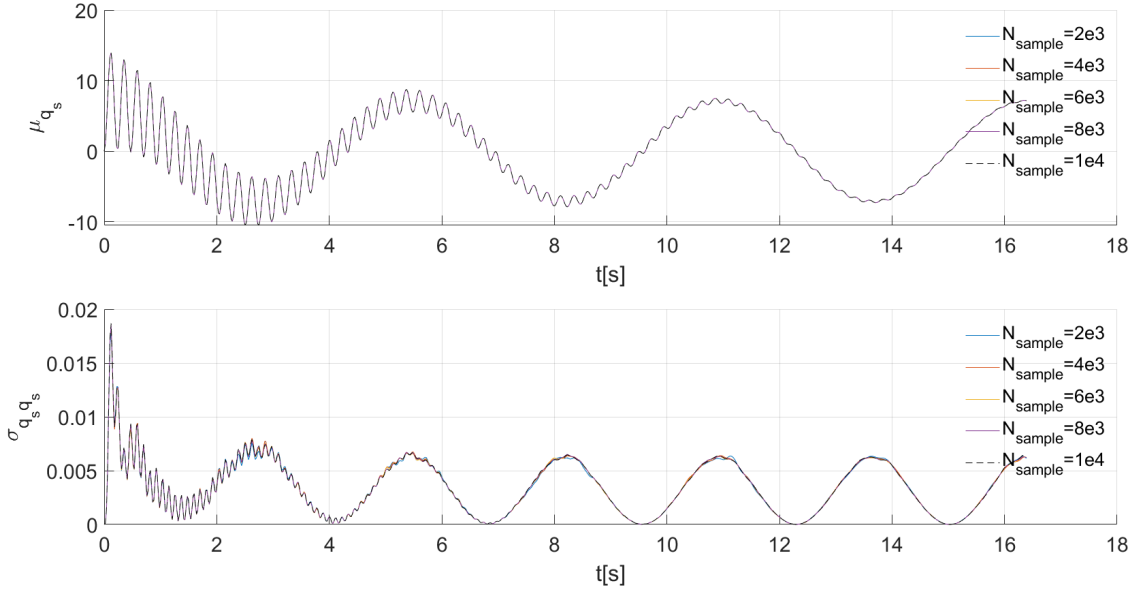


Figure 5.14: Convergence in mean and variance

value around which the mean $\mu_x(t)$ oscillates; conversely, $\mu_{q_s}(t)$ does not show a similar oscillation around a constant value, but it features a moving average over which smaller oscillations occur. This behavior is a manifestation of the fact that the DOF x is perturbed by a stationary process, while q_s is perturbed by a cyclic process; in fact, the moving average of $\mu_{q_s}(t)$ is approximately $\bar{\mu}_{q_s}(t) = 7 \cos(1.15t)$, the same shape as the mean excitation with an adjusted magnitude that reflects the amplitude of the response of the system. These quantities can be visualized in Fig. 5.16.

The second moments in Fig. 5.17 show a similar pattern: transient components at the beginning of motion, which subside as time progresses; the second moments also display similar behavior to the one studied in Fig. 5.2 concerning the halving of periods. As explored in the first section of the chapter, this halving of the period has its origins in the products of sinusoidal periodic terms involved in the moments of second order (central and non-central). From Fig. 5.18, the halving of the period can be seen in the variance of q_s , but not in the variance of x ; in fact, $\sigma_{xx}(t)$ displays a behavior that is analogous to the rise of variance in LTI stochastic processes ([85], [104]) and has been noticed in LTP systems in previous works¹ ([131]).

The rise of variance, along with the decrease of the mean, can be explained in terms of the characteristic exponents of the system and the transient-steady-state formulation of the response introduced in Eq. 5.43. The total stochastic response is:

$$\mathbf{x}_{total}(t) = \mathbf{x}_h(t) + \mathbf{x}_f(t) = \mathbf{x}_h(t) + \mathbf{x}_f^{(tr)}(t) + \mathbf{x}_f^{(ss)}(t), \quad (5.90)$$

from where we can see that the total transient response is $\mathbf{x}_{total}^{(tr)}(t) = \mathbf{x}_h(t) + \mathbf{x}_f^{(tr)}(t)$. The part of the response $\mathbf{x}_h(t)$ depends on the initial conditions of the dynamical problem, and so by making $\mathbf{x}(t_0) = \mathbf{0}$ one has $\mathbf{x}_h(t) = \mathbf{0}$, leaving $\mathbf{x}_{total}^{(tr)}(t) = \mathbf{x}_f^{(tr)}(t)$. As motion evolves, $\mathbf{x}_{total}^{(tr)}(t) \rightarrow \mathbf{0}$ through dissipation mechanisms in the system. In stochastic terms, the mean of the response decreases with time because the transient component goes to zero; it is a deterministic behavior that is preserved in the stochastic case. This reasoning can be justified further by considering that for linear systems, the mean of the response ensemble to an ensemble of realizations of a load is equal to the response of the system to the mean function of the load. The rate at which $\mathbf{x}_{total}^{(tr)}(t)$ decays is

¹In the work of Spires and Sinha, a zero-mean load is considered, so $\sigma_{xx}(t) = \mu_{xx}(t)$.

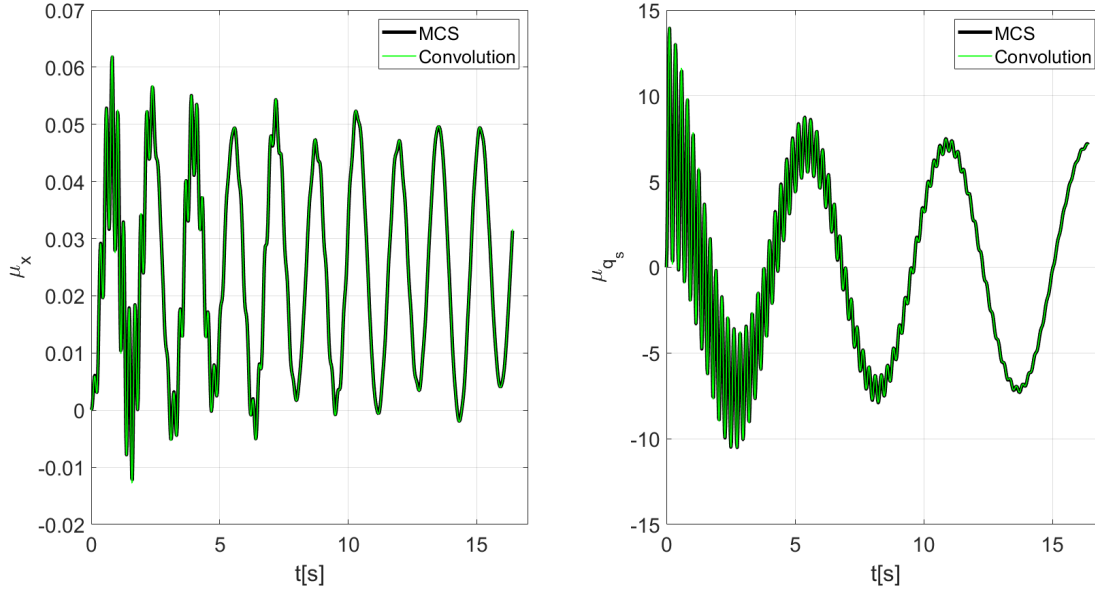


Figure 5.15: Mean response, MCS vs. Convolution

directly linked to the quantity $\xi_i = -\frac{\text{Re}(\rho_i)}{\|\rho_i\|}$: as this quantity increases, so does the rate at which $\mathbf{x}_{total}^{(tr)}(t)$ decays, and the steady-state regime is approached faster.

In the case of the rise of variance, at t_0 , the system is fixed in the configuration $\mathbf{x}(t_0) = \mathbf{x}_0$, so in t_0 , there is no randomness and consequently no variance. As motion evolves, the variability in each realization of the load manifests in the response, causing the variance to increase. As $\mathbf{x}_{total}^{(tr)}(t)$ goes to zero, the variance decreases in magnitude again until it stabilizes when the steady state is reached. In Fig. 5.18, $\sigma_{q_s q_s}(t)$ reaches a peak at around $t = 0.12s$ and then decreases, converging on the halved period pattern observed in the early example Fig. 5.3, this fast arrival at the steady-state comes from the fact that $\xi_{[3,4]} = 0.9250$. In the case of $\sigma_{xx}(t)$, the variance is increasing during the entire observation time; the steady-state is far from being reached given that $\xi_{[1,2]} = 0.0079$.

The understanding of the stochastic response in the terms established in this subsection has far-reaching implications from an analysis and design perspective (problems of type A and type B). Considering the link between mean, variance, and the occurrence of extreme events, this development suggests the existence of two regimes of interest: a transient regime, early in the time-evolution of the system where mean and variance undergo peak values, resulting in high probabilities of threshold crossings; and a steady-state regime that is more representative of the long-term response of the system and features considerably lower values for mean and variance.

The correlation functions of both methods are compared in Fig. 5.19, with good agreement between both solutions. The correlation of the base variable shows a structure similar to the ones exemplified at the start of the chapter, while the blade variable contains an additional modulation that is more clearly visualized in Fig. 5.17 since:

$$\mu_{q_s q_s}(t) = R_{q_s q_s}(t, t), \tag{5.91}$$

so looking at the second moment is equivalent to looking at a slice of $R_{q_s q_s}(t, t)$ along the $t_1 = t_2 = t$ line.

In terms of applications, consider the blade modal variable $q_s = q_1^s$: we can write the mechanical moment at the root of the blade adapting Eq. 2.76 with $N_{modes} = 1, I_{YZ} = 0$: $M_s^{RBM}(t) = -EI_{ZZ} \varphi_1^{l_s}(0) q_1^s(t)$, the probabilistic moments of this key design variable are readily available from the results established by simple arithmetic operations. The response stochastic process $M_s^{RBM}(t)$ can then be treated for design or analysis purposes using

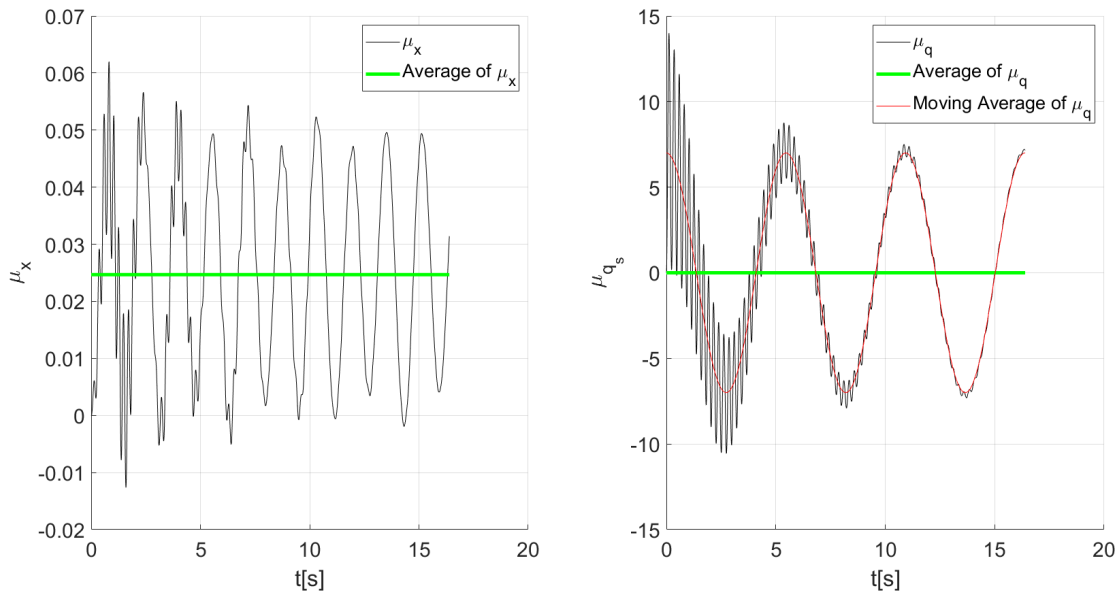


Figure 5.16: Mean functions, average and moving average

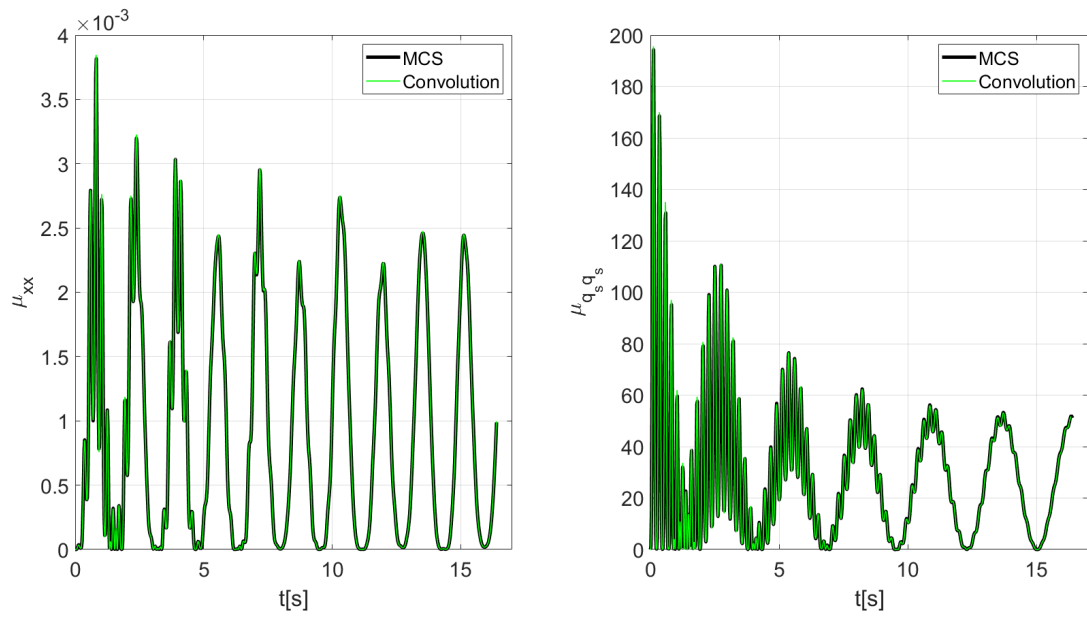


Figure 5.17: Second moments of response, MCS vs. Convolution

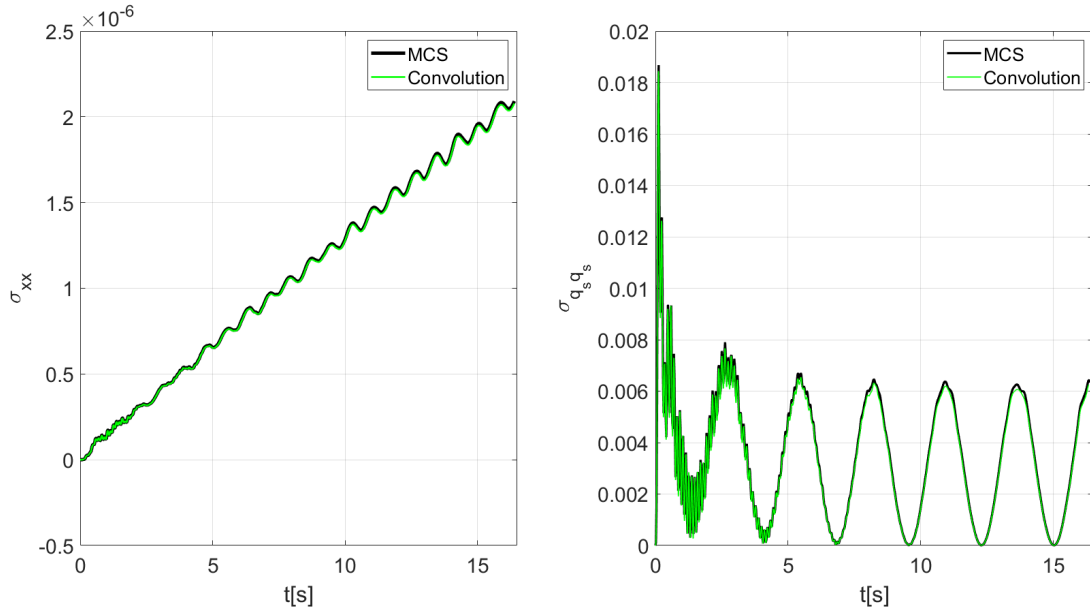


Figure 5.18: Variances of response, MCS vs. Convolution

the established convolution relationships. In fact, the transformation expressions introduced in Chapter 4 reveal that, for this simplified example, the moments of $M_s^{RBM}(t)$ differ from those of q_1^s by a multiplicative constant. This approach will be used later in the modeling of a more realistic system.

PGHW analysis and EPSD To conclude the example, we will make use of the sampled transient response to obtain the EPSD with the PGHW family of Wavelets as expressed in Eq. 5.61. The procedure consists of projecting each realization of the response in the PGHW basis, obtaining the corresponding wavelet coefficients, at which point the Wavelet coefficients are treated as random variables: the expected value of the square of their absolute value results in a local description of the PSD, an EPSD, for the corresponding time and frequency intervals of a particular coefficient. The PGHW parameters are collected in Tab. 5.3; these have been chosen in such a way that: 1) each realization is well described in the associated Wavelet series; 2) a reasonable time-frequency resolution is obtained.

An important aspect of the technique used to estimate the EPSD using PGHW is ensuring that the wavelet parameters selected result in a family of basis functions that accurately approximate each sample of the studied stochastic variable. A concrete way of verifying this requirement is by applying the wavelet reconstruction formula Eq. 3.42 and comparing the reconstructed response with the original. Formula Eq. 3.42 and the traditional PGHW formulation is applicable to zero-mean² functions, so the function is transformed to zero-mean before applying the corresponding wavelet integral transform. We will proceed in the traditional form since our goal is PSD estimation, which, by virtue of its relationship with the covariance function, traditionally ignores mean components on signals. It is important to highlight that it is possible to modify formula Eq. 3.42 to include a so-called constant level Wavelet coefficient that accounts for the mean component of the signal. Indeed, the classic text of Newland [95], as well as more recent publications such as [18], integrate this constant level coefficient for HW and PHW families, respectively. In Fig. 5.20, we present the comparison between one realization of the solution to the example under study and the respective PGHW reconstruction. The close agreement between function and reconstruction shows that the parameters selected are adequate and further illustrate that the calculated Wavelet coefficients used to approximate the EPSD capture the key information in the processes they

²Here, zero-mean is used in the signal or functional sense, not in the stochastic sense.

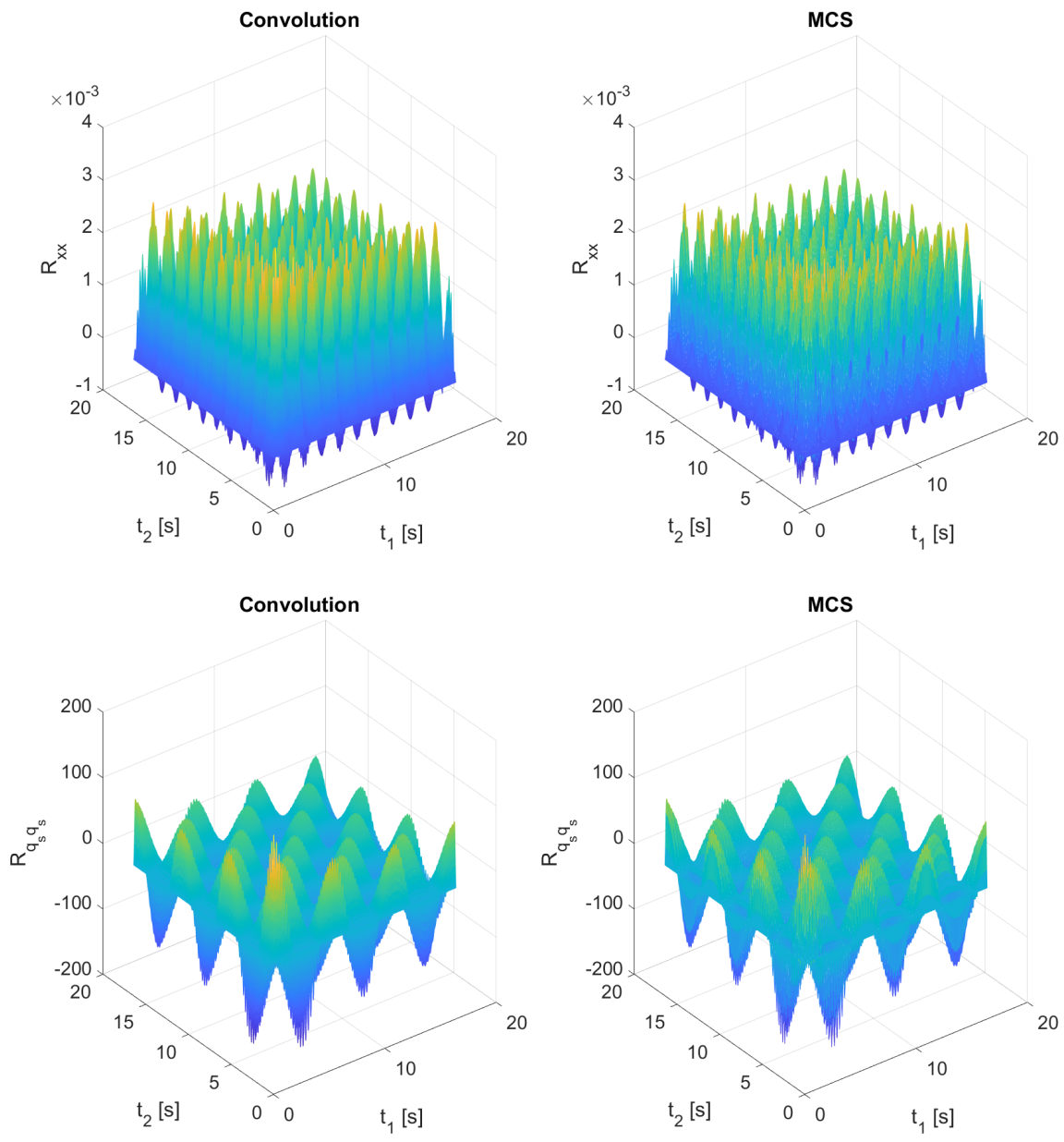


Figure 5.19: Auto-Correlations of response, MCS vs. Convolution

Parameter	Value
N_t	10
N_f	125
T_0	$3T_\Omega$

Table 5.3: PGHW parameters for EPSD estimation

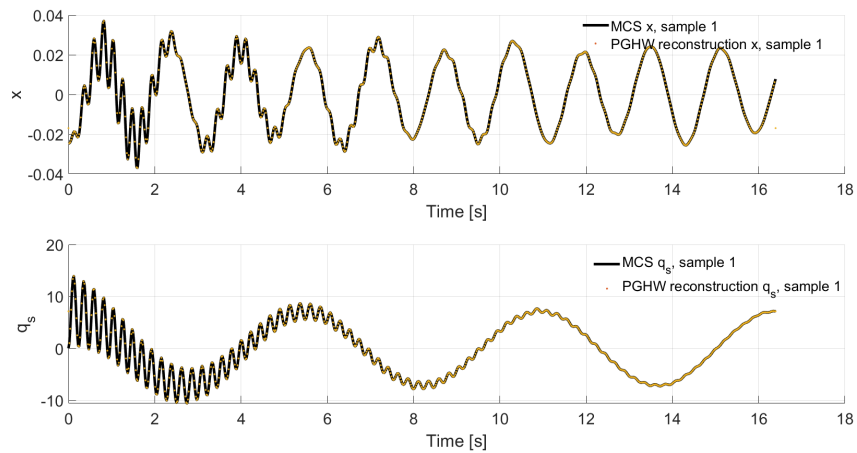


Figure 5.20: PGHW reconstruction for the selected realization of the response

represent.

In Fig. 5.21, the EPSD of the selected DOFs are displayed. The base DOF features an almost constant PSD in time, except for the rapidly decaying frequency component close to the 0.5Hz mark. On the other hand, the blade DOF has an oscillating amplitude in the 0.30Hz, which goes from 0.82 to 0.85, and a rapidly decaying frequency component in the 4 – 5Hz frequency band.

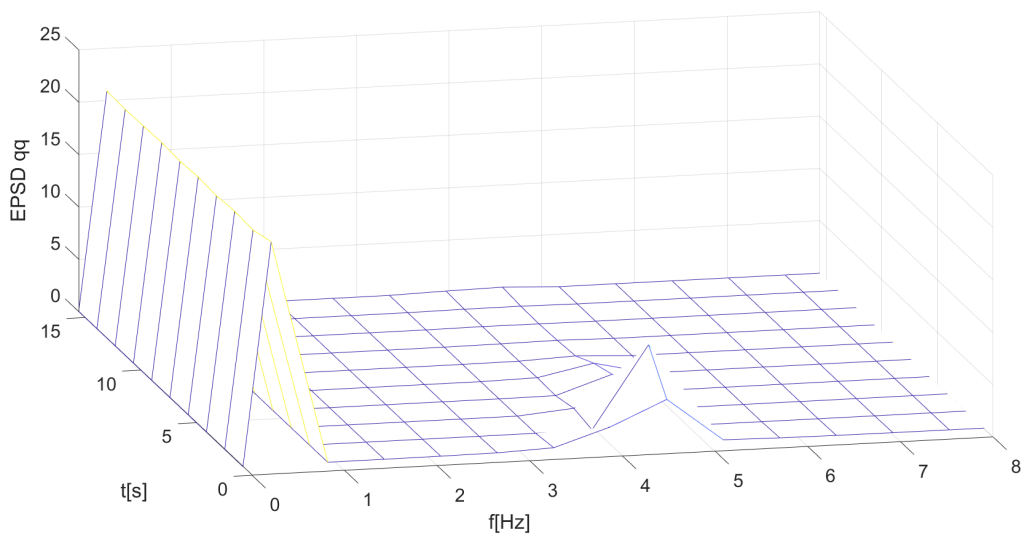
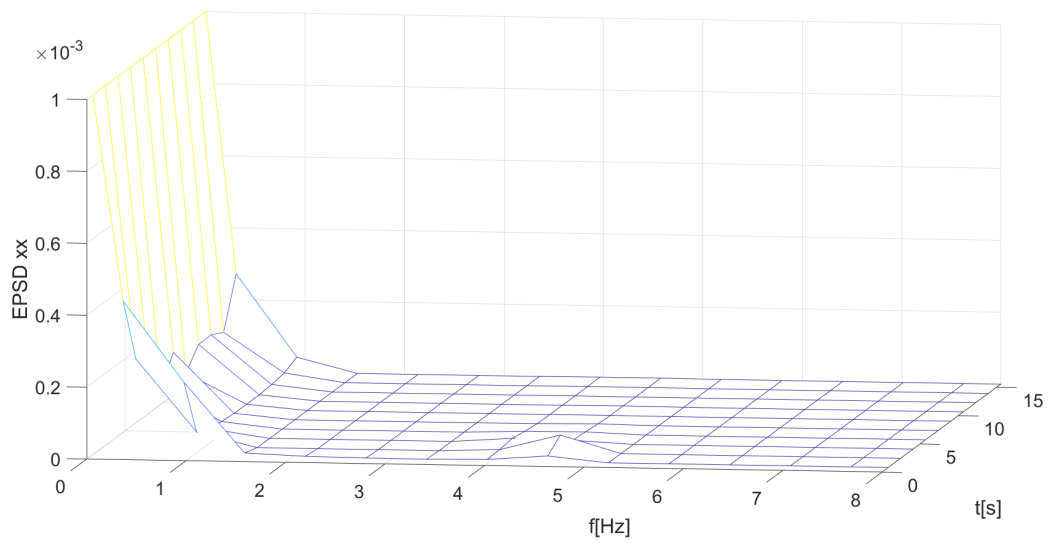


Figure 5.21: Transient EPSD by PGHW

Chapter 6

Application: reliability of a tidal turbine model

“Without the Principia, for example, measurements made with the Atwood machine would have meant nothing at all.”

Thomas S. Kuhn, *The Structure of Scientific
Revolutions*

This chapter applies the results obtained throughout this work to the concrete problem of studying the reliability of a tidal turbine subjected to hydrodynamic force driven by wave, current, and ambient turbulence. First, some perspective of the tidal turbine domain is provided in the first section. The reliability problem is also formulated, and the main concepts at play are introduced. Second, the dynamical model developed in Chapter 2 is parametrized to describe an arbitrary tidal turbine, and its Floquet modal representation is obtained. The third section describes the underlying velocity field’s modeling particulars that induce the hydrodynamic force. Finally, section four compiles the relevant results: moment propagation in Floquet modal form, time-domain ODE-based MCS, Floquet-based spectral MCS for the steady-state regime, the corresponding EVD estimation by each method with the associated reliability prediction, and the PGHW estimation of the EPSD of the design variable in the transient regime.

1 Background

1.1 Tidal stream turbines

The demand for renewable and reliable energy sources has led to major research efforts on tidal stream power. Tidal stream turbines are subjected to very complex loads given their environment of operation, involving such effects as waves, tidal cycles, and turbulent flow, a complexity that warrants the application of stochastic tools to describe the intricacies of these phenomena. The feasibility of this ongoing development rests upon the available energy potential and the reliable operation of the generators in terms of efficiency and integrity. These facts underscore the relevance of developing advanced tools to apply in the design process of tidal stream turbines, such as stochastic descriptions of the oceanic medium and reliability-based methodologies that permit a more robust design.

As discussed in [140], major failure modes in technology deployments are those of blades and supporting structure. In recent years, important research efforts have gone into developing a more detailed understanding of the different loads involved during the operation of tidal stream turbines in terms of extreme loads and

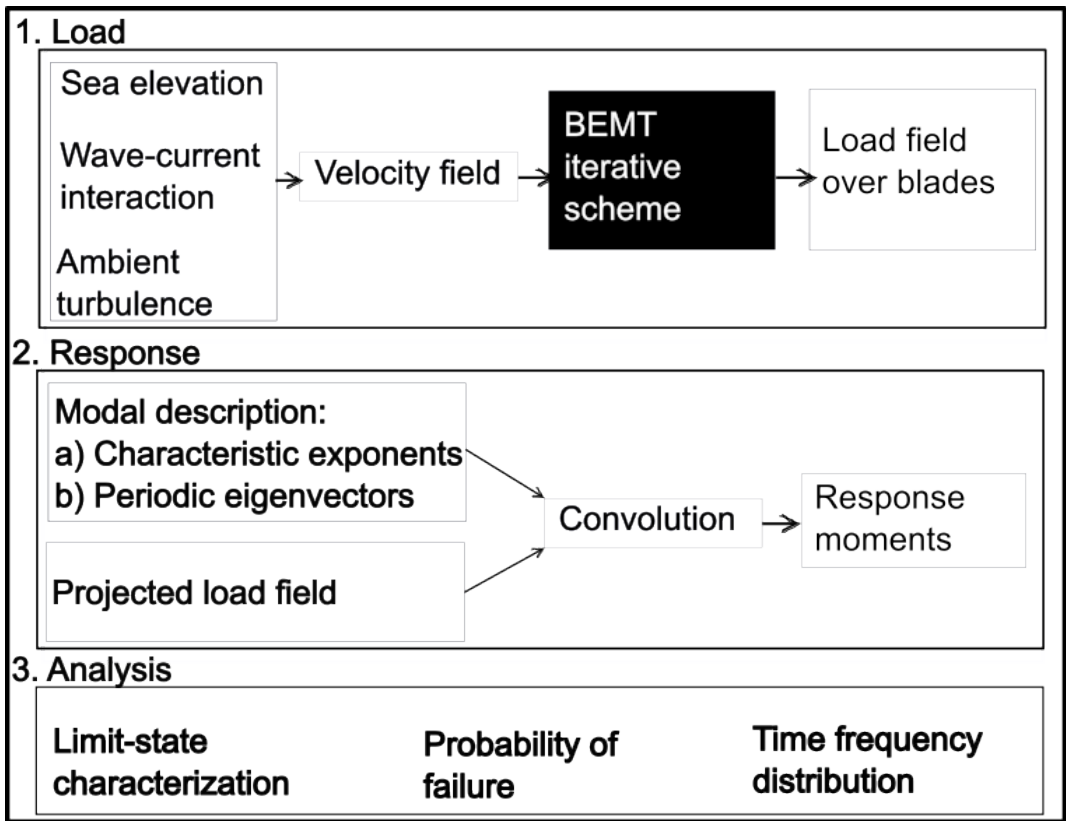


Figure 6.1: Methodology of the application

fatigue. These investigations include scaled experimental tests as well as computational simulations. We now turn to some key results from the recent literature to provide context. In [29], an experimental investigation is carried out on a scaled tidal turbine to assess the extreme loads of the structure produced by waves. The NewWave group methodology is utilized to produce the most probable extreme wave associated with a given elevation spectra, and the quantities analyzed include the power, root-bending moment (RBM), thrust, and overturning moments at the base of the supporting structure. The results show an important effect of waves on the extreme loads on both blade and support. The wave-current-turbulence effect on thrust, power, and RBM is investigated in [80] using numerical simulation, and it is demonstrated that neglecting this interaction leads to important discrepancies between the predicted values and the observed ones. It is found that the current-turbulence interaction can not be neglected and that turbulence plays a major role in the loading of the structure. These results are consistent with the finding in [126], where experimental tests are performed on three scaled prototypes to establish the effects of turbulence on turbine loads, and it is found that increased turbulence is a major driver of load fluctuation; more broadly, an earlier experimental investigation presented in [41] demonstrates how wave effects are a major driver of fatigue over the blades, while also highlighting the fact that the main effect of current-wave interaction is found in the variance of the response. In [55], three approaches are contrasted: CFD simulation, the traditional BEM method, and experimental results from which the simulation conditions were established. Three wave types were analyzed. While the results again show the effects of waves on fatigue considerations found in later works mentioned before, this particular work highlights the steep computational cost of performing detailed simulations, as various simplifying assumptions had to be applied to reduce computation time. More recent studies, such as [117], have shed more light on the complex effects of realistic flow conditions on the loading over blades, including not only wave and high ranges of turbulence but also flow misalignment with the turbine; in [26], the effects of blade deformation on the hydrodynamic characteristics are analyzed, showing an effect on performance, and in loads affecting the blades. These results demonstrate 1) the necessity for schemes that permit a complex description of the flow, including wave, current, and turbulence contributions; 2) the importance of taking into account deformations on blades.

In addition to the previous advances, some efforts have been focused on the study of the reliability of the blades of tidal or hydrokinetic turbines: [58] studies the reliability of composite blades of a hydrokinetic turbine using sampling techniques and finite element analysis to determine the response, the randomness of the river flow and material properties are considered, and Stochastic Polynomial Chaos is used to construct a surrogate model to then apply the time-dependent reliability analysis on the output of this surrogate. In [139], a probabilistic model is constructed to model the reliability of pitch-controlled tidal turbines considering turbulence. The failure mode under consideration is the extreme bending moment in the flapping direction.

1.2 Time-dependent reliability

A time-dependent reliability problem has the form:

$$G(t) = R(t) - S(t), \quad (6.1)$$

where $G(t)$ is termed limit-state or performance function, $R(t)$ is the available resistance, and $S(t)$ is the response, or design variable; the safety region corresponds to $G(t) > 0$. The failure criteria are described using the performance function, with the condition $G(t) \leq 0$, so the probability of failure in the observed time interval $[0, T]$ is:

$$P_f(0, T) = \mathbb{P}[G(t) \leq 0, t \in [0, T]]. \quad (6.2)$$

If the Extreme Value Distribution (EVD) of $S(t)$ is known or can be estimated, $S_M = \text{Max}_{[0, T]}[S(t)]$, P_{S_M} is the CDF of the random variable S_M , then:

$$\begin{aligned} P_f(0, T) &= 1 - P_{S_M}(\varpi) \\ P_s(0, T) &= P_{S_M}(\varpi) \end{aligned} \quad (6.3)$$

is an alternative formulation of the desired probability, where P_s is the reliability and $\varpi \in \Omega$ is the set of events such that S_M does not surpass the set threshold or available resistance $R(t)$. Assuming that the occurrence of the extreme sea state is a rare event over the design life of the system and making use of their statistical independence, one can further describe the reliability of the system in its total expected service life:

$$P_s^* = (P_{S_M}(f))^\alpha \quad (6.4)$$

with α the total number of occurrences of the specified state during operation life. Traditionally, $R(t)$ is used in reliability analysis to describe material degradation over time through mechanisms such as corrosion. This is the most common source of time-dependent reliability found in the literature. Conversely, $S(t)$ describes the response and is often taken as a random variable.

Adapting Eq. 6.1 to our problem entails:

$$G(t) = R - S(t), \quad (6.5)$$

where:

- The maximum available stress R is constant, given that no material degradation is considered.
- The response $S(t)$ is a nonstationary non-Gaussian stochastic process. The nonstationarity is a consequence of it being a linear combination of the response of an LTP system and also because of the nonstationarity of the load vector, which will be expanded on in the next section; the non-Gaussianity is a consequence of the non-Gaussian load vector, a consequence of the nonlinear load models at play to describe the fluid-structure interactions, as shown in Chapters 4 and 5 for the Morison model.

The challenge of solving the reliability problem is accurately evaluating Eq. 6.2 from the available response variable characterization $S(t)$. The main difficulties arise from the nonstationary and non-Gaussian nature of the response.

More broadly, time-dependent reliability analysis has seen much attention in the past decade. We briefly remark on some related developments:

- In [58], a simulation approach is taken to assess the reliability of a hydrokinetic turbine. The failure mode considered is the Tsai–Hill criterion for fatigue on composite blades. The challenges of nonstationarity from a computational perspective are discussed. The FORM method is applied to the simulation results. A major conclusion is the importance of the environmental load description (the river variability in their case study) to correctly assess the reliability indicator.
- In [57], the JUR/FORM method is introduced, standing for Joint Upcrossing Rate/First-Order Reliability Method; the method extends the FORM approach to a broad class of time-dependent limit-state functions.
- In [139], a problem close to ours is considered; the approach consists of a logarithmic fitting of the bending moment of the blade to the flow input velocity. The flapwise direction is considered, and the results apply to pitch-controlled turbines. Only turbulence is considered in this case.
- In [45], the NEWREL procedure is introduced and contrasted with two broadly used methods: direct MCS and the PHI2+ ([133]). Roughly speaking, this methodology approximates the response process as a series of random variables at discrete time instants, and the limit-state function is evaluated for each instant in time. The total limit-state is obtained by considering each discrete limit-state as a series reliability system.

Parameter	Value	Parameter	Value	Parameter	Value
K_{x_1}	$1.2 \times 10^7 [\text{Nm}^{-1}]$	K_{y_1}	$2.1 \times 10^7 [\text{Nm}^{-1}]$	K_{z_1}	$2.3 \times 10^7 [\text{Nm}^{-1}]$
K_{x_2}	$1.3 \times 10^7 [\text{Nm}^{-1}]$	K_{y_2}	$2.2 \times 10^7 [\text{Nm}^{-1}]$	K_{z_2}	$2.4 \times 10^7 [\text{Nm}^{-1}]$
L_1	0.5[m]	L_2	1[m]	R_r	1[m]
M_r	10000[kg]	J_p	$5 \times 10^3 [\text{kgm}^2]$	J_d	$3.75 \times 10^3 [\text{kgm}^2]$

Table 6.1: Disc-shaft parameters

Parameter	Value[units]
N blades	2
$A\rho$	$352 [\text{kgm}^{-1}]$
EI_{ZZ}	$3.5 \times 10^8 [\text{Nm}^2]$
EI_{YY}	$6.95 \times 10^8 [\text{Nm}^2]$
L_b	9[m]

Table 6.2: Blade parameters

2 System description

2.1 Dynamical model

The dynamical model used in this section has been described in Chapter 2, consisting of 21 DOF: 5 DOF corresponding to the disc-shaft, three translations, and two tilt or angular variables; 2 blades deforming in spanwise and flapwise direction, each discretized with four mode shapes per blade per direction. The system is lightly damped, and the spin is constant, set at $\Omega = 1.5 \left[\frac{\text{rad}}{\text{s}} \right]$. The resulting equation of motion of this system corresponds to an LTP system of form:

$$\mathbf{M}(t)\ddot{\mathbf{x}} + \mathbf{G}(t)\dot{\mathbf{x}} + \mathbf{K}(t)\mathbf{x} = \mathbf{f}(\mathbf{x}, t), \quad (6.6)$$

where the corresponding matrices are such that $\mathbf{M}(t) = \mathbf{M}(t + nT_p)$, $n \in \mathbb{N}$, and similarly for $\mathbf{G}(t)$ and $\mathbf{K}(t)$, and $\mathbf{f}(\mathbf{x}, t)$ is a nonstationary non-Gaussian stochastic vector of loads. This class of model emerges in the description of physical systems combining rotors and continuum media undergoing vibrations, as is the case of the rotor-blade model in which a disc or hub rotates with large angles around a main spin axis, with blades attached radially, the latter being described as beams or plates that vibrate in the two transverse directions.

The detailed structure of the matrices in Eq. 6.6 is provided in Annex A; we will briefly comment on some aspects of the parameter selection. The disc-shaft and support parameters are displayed in Tab. 6.1, where the base stiffnesses have been chosen so that the underlying rotor is anisotropic, implying that there will be angular coupling on the equivalent stiffness matrix. The total turbine rotor diameter is 20m, with a disc diameter of 2m and a blade length of 9m. The blade parameters are presented in Tab. 6.2. The parameter selection is a simplification of the profile studied in [10], adapted to our dynamical model and blade discretization scheme; unlike this reference, the profile is assumed to be uniform and rectangular, and the material behavior is assumed to be isotropic. In our case, the quantity $A\rho$ is equivalent to the mass per unit of length used in the reference, for one blade: $A\rho L_b = 3168 [\text{Kg}]$ is its total mass. Similarly, with the equivalent properties $E = 10 [\text{GPa}]$ and $I_{YY} = 6.67 [m^4]$, $I_{ZZ} = 3.36 [m^4]$, the prescribed products $EI_{YY} = 6.95 \times 10^8 [\text{Nm}^2]$ and $EI_{ZZ} = 3.5 \times 10^8 [\text{Nm}^2]$ are satisfied.

A simple diagonal damping matrix has been considered for the application, ensuring light damping of each degree of freedom. For the disc, the damping parameters are of the order of 10^3Nsm^{-1} , and for the blades of 10^1Nsm^{-1} . General damping values for this application are not widely found in the literature but provide an adequate characterization; for instance, in the case of an experimental prototype, these values can be easily integrated into the model. In this sense, the model presented here should be interpreted as describing a generic tidal turbine, and it can be adapted to more concrete studies that provide adequate characterization.

Two other known fluid-structure interaction effects have been ignored in our model: the added mass and hydrodynamic damping. The added mass effect results from the volume of fluid displaced by the structure under accelerated motion, and it manifests in an additional unsteady load component that can be expressed as an additional mass contribution. This effect results in a higher effective mass parameter and consequently tends to reduce the response frequency of the blades ([155]). Hydrodynamic damping results from the fluid's viscous properties being displaced by the structure. It can be described as an additional term on the velocity-dependent system matrix; it tends to extract energy from the system just like conventional structural damping. The added mass and hydrodynamic damping effects are sensitive to the amplitude of the motion that displaces the corresponding fluid volume. Consequently, these effects are particularly pronounced in floating horizontal axis tidal turbines since this type of support results in important structure displacements due to surge motion in the free surface. Considering these two effects requires the coupling between the fluid dynamic equations in the vicinity of the structure and the dynamic equations of the structure, which results in a steep computational expense. Recent investigations in the literature have aimed their efforts at estimating these effects by deducing compensatory added mass and hydrodynamic damping matrices that modify the value of the structural matrices and circumvent the need for coupled resolution; these results, however, are highly dependent on the prescribed displacement motion (See for instance: [97] and [23]). Our choice to ignore these effects is based on two main considerations: first, as previously argued, we aim to describe a generic situation and leave the study of more specialized conditions to further studies; second, the small displacement regime under which our case study evolves warrants the assumption that these effects will be negligible. One final and obvious simplification in our model is the neglect of the gravitational force over the turbine, the reasoning being the counteracting static lift force exerted by the fluid.

System Eq. 6.6 can be cast into state form:

$$\begin{aligned}\dot{\mathbf{y}} &= \mathbf{A}(t)\mathbf{y} + \mathbf{B}(t)\mathbf{f}(t) \\ \mathbf{A}(t) &= \begin{bmatrix} \mathbf{0} & \mathbf{I} \\ \mathbf{M}^{-1}\mathbf{K} & \mathbf{M}^{-1}\mathbf{G} \end{bmatrix} \\ \mathbf{B}(t) &= \begin{bmatrix} \mathbf{0} \\ \mathbf{M}^{-1} \end{bmatrix},\end{aligned}\tag{6.7}$$

which will serve as the basis of our analysis: on the one hand, this system can be integrated numerically to provide the Floquet modal characterization of the system using the methods presented in Chapter 3; on the other hand, direct integration can be used in a MCS approach to obtain samples of the solution in state variables. The Eq. 6.6 can be supplemented with an observability matrix \mathbf{C} which allows the recovery of mechanical quantities of interest in design and analysis:

$$\mathbf{S}(t) = \mathbf{C}\mathbf{y}(t),\tag{6.8}$$

where $\mathbf{S}(t)$ is the response in Eq. 6.5, in reliability terms it is the response, in a dynamics and control sense it is an observed quantity, and in an applied sense it is a design variable. For simplicity, we will consider a single design variable: $\mathbf{S}(t) = \begin{pmatrix} S^1(t) \\ 0 \end{pmatrix}$. Following the developments in subsection 4.3 of Chapter 2, the selected design variable in this chapter is the magnitude of the maximal normal stress due to the combined effects of spanwise and flapwise root bending moment:

$$\begin{aligned}S^1(t) &= \sigma_x^{RBM}(t) \\ &= \frac{|M_s^{RBM}(t)|}{I_{ZZ}} \left(\frac{h}{2}\right) + \frac{|M_f^{RBM}(t)|}{I_{YY}} \left(\frac{b}{2}\right),\end{aligned}\tag{6.9}$$

where 2.78 is being utilized, the blade cross-section is symmetric ($I_{ZY} \approx 0$), and given the slow spin velocity of this type of system, the centrifugal axial stress is neglected.

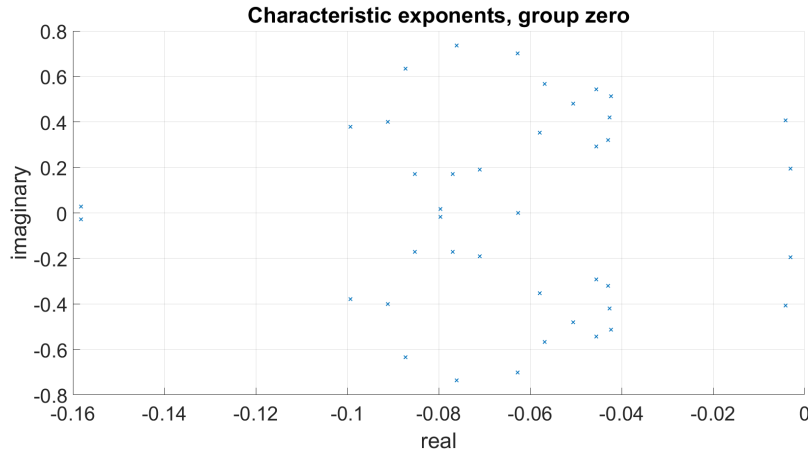


Figure 6.2: Characteristic exponents with integer multiple of imaginary part zero (group zero)

Exponents	$\frac{\ \rho_i\ }{2\pi}$ [Hz]	$-\frac{\text{Re}[\rho_i]}{\ \rho_i\ }$	Exponents	$\frac{\ \rho_i\ }{2\pi}$ [Hz]	$-\frac{\text{Re}[\rho_i]}{\ \rho_i\ }$	Exponents	$\frac{\ \rho_i\ }{2\pi}$ [Hz]	$-\frac{\text{Re}[\rho_i]}{\ \rho_i\ }$
1, 2	0.0310	0.0157	15,16	0.0868	0.0835	29,30	0.0673	0.1007
3,4	0.0647	0.0103	17,18	0.0908	0.0996	31,32	0.0256	0.9847
5,6	0.0821	0.0821	19,20	0.0470	0.1542	33,34	0.0297	0.412
7,8	0.0770	0.1046	21,22	0.0515	0.1328	35,36	0.0325	0.3478
9,10	0.1020	0.1361	23,24	0.0623	0.2539	37,38	0.01	1
11,12	0.1120	0.0892	25,26	0.0571	0.1613	39,40	0.0129	0.9796
13,14	0.1177	0.1029	27,28	0.0654	0.2219	41,42	0.0306	0.4439

Table 6.3: Frequency and damping ratio associated with each conjugate pair of characteristic exponents in set zero

2.2 Modal analysis

The Floquet-Lyapunov approach has been applied to the system, providing the characteristic exponents for group zero, the state transition matrix, and the corresponding periodic modes of the system. The set \mathbf{A}_0 of characteristic exponents is shown in Fig. 6.2 on the real-imaginary plane. Additionally, in Tab. 6.3, the frequencies and associated damping factors are shown for every conjugate pair of characteristic exponents of the set. The system is stable as every real part of every exponent is on the left half of the plane; that is, every characteristic exponent has a negative real part.

Some visualization and simplification will be imposed to analyze the periodic modes. For each selected mode, the real and imaginary part of each degree of freedom is illustrated for one period. The imaginary part is always shown right underneath the corresponding real part. For each mode, the displacement degrees of freedom are displayed; moreover, the representations have been divided: the DOF associated to the disc-shaft are shown in the top left-most square; followed by the spanwise and flapwise modal DOF of the first blade; in the following row, the spanwise and flapwise DOF of the second blade are displayed. The legend provides some reference for which quantities are in display: $q_{1,2}^s$ denotes the spanwise variable of the first blade, second mode shape, for instance. Given the large size of the system and the fact that many modes display similar behavior, the analysis presented is restrained to one representative mode for each type of behavior.

1. The first mode, Fig. 6.3, shows the participation of translational and rotational DOF in the disc except for G_z , as well as the lower flapwise and spanwise mode shapes of the blades.
2. The sixth mode, Fig. 6.4, is dominated by the spanwise blade motion, although the translational DOF of

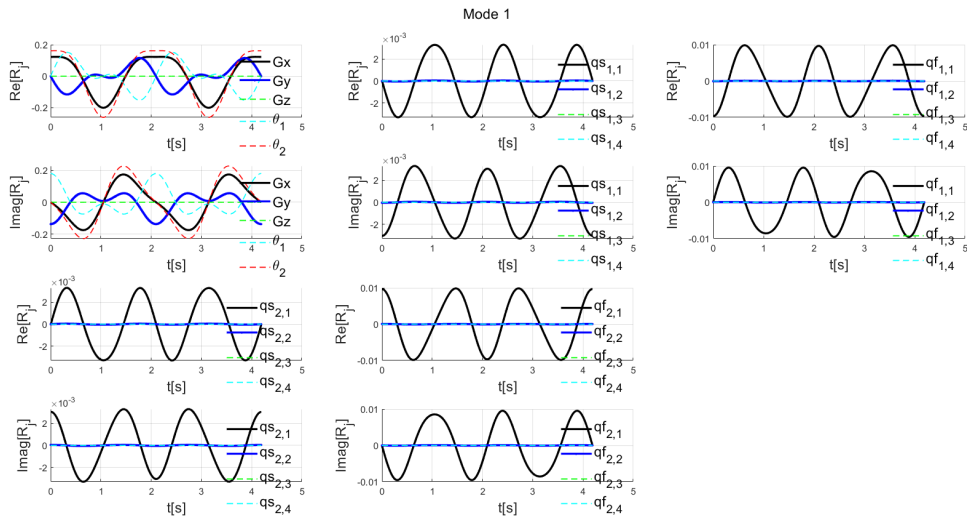


Figure 6.3: First periodic mode

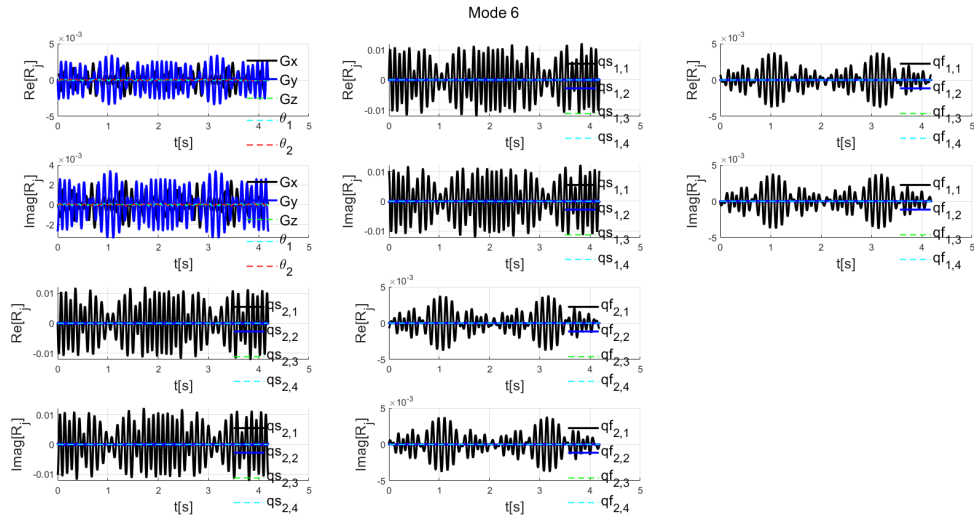


Figure 6.4: Sixth periodic mode

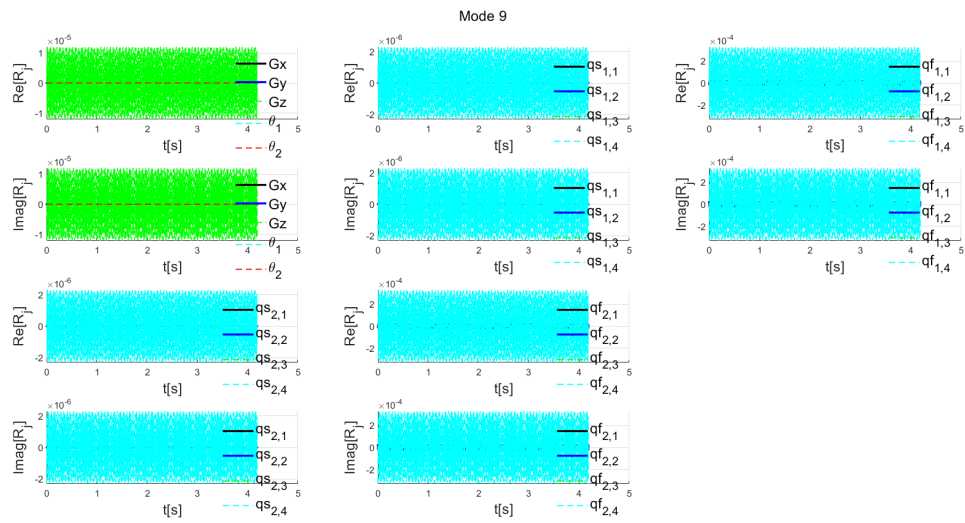


Figure 6.5: Ninth periodic mode

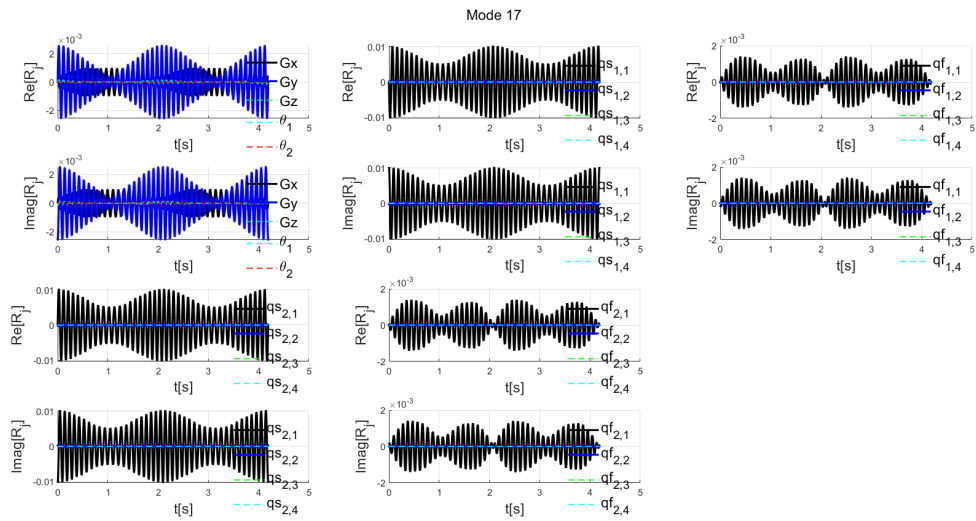


Figure 6.6: Seventeenth periodic mode

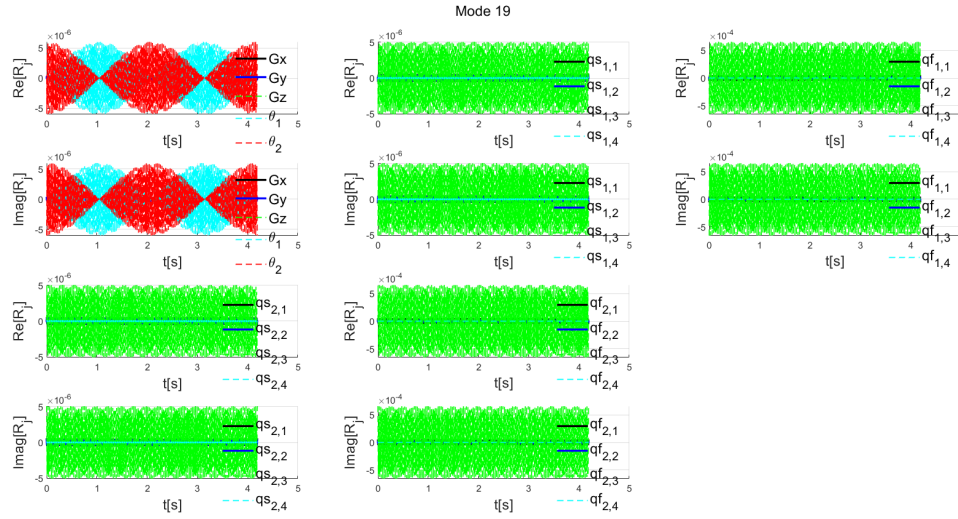


Figure 6.7: Nineteenth periodic mode

the disc and the lower flapwise mode shapes of the blades show some motion; this mode resembles the planar motion of this type of system.

3. The ninth mode, Fig. 6.5, is a coupled flapwise and G_z mode, with some spanwise motion present in the higher mode shapes; a remarkable feature is the high oscillation frequency.
4. The seventeenth mode, Fig. 6.6, is another form of coupled motion dominated by the translation of the disc and the lower mode shapes of each blade; a distinguishing feature is the well-defined envelope on each active DOF.
5. The nineteenth mode, Fig. 6.7, is a form of coupled motion involving predominantly the angular DOF of the disc and some of the higher mode shapes of the blades in spanwise and flapwise directions; the angular DOFs seem to have a $\frac{1}{4}$ delay with respect to one another.

More broadly, some general behaviors seem to hold: modes dominated by DOF with lower frequencies, such as the translational DOF of the base, oscillate with low frequencies regardless of the observed DOF; those dominated by higher frequency DOFs contain some combination of fast fluctuation and modulated behavior across active DOFs.

Another important observation about the modal analysis of the system concerns the nature of the periodic modes. Broadly accepted interpretations of LTI modes involve the ratio of amplitudes among the DOF remaining constant, for instance [111], or that of synchronous motion patterns such as [87] or [43]. In the case of periodic modes, the previous interpretation does not hold, and as seen in Chapter 3, the relationship between the frequency content among the modes seems more relevant.

3 Load modeling and simulation

3.1 Preliminaries

The load acting over a tidal turbine arises from the interaction of the structure with the fluid flow of the oceanic medium, a complex phenomenon to which several environmental events can substantially contribute to 1) the

surface elevation of the ocean in which waves are propagating, 2) submarine current, 3) turbulent flow patterns that can be the result of different conditions, for instance the flow disruption by the interaction of other structures, as is the case in tidal farms where several devices are installed. The determination of the loads over the structure then requires the description of these quantities and their interactions. The complexity and variability of some of these quantities make the choice of a stochastic description fit, provided that enough information about these processes is available. Once the effective velocity perceived by the structure has been determined, the following expression provides the hydrodynamic load [115]¹:

$$\mathbf{F}(X_b, t) = \frac{1}{2} \rho_w c(X_b) \mathbf{V}_{rel}^2(\mathbf{X}, t) \mathbf{C}(X_b) \quad (6.10)$$

where ρ_w is the density of the fluid, $c(X_b)$ is the local cord, $\mathbf{C}(X_b)$ contains the local lift and drag coefficients that are empirical descriptors of a given hydrodynamic profile, and $\mathbf{V}_{rel}(\mathbf{X}, t)$ is the relative velocity of the flow with respect to the point of interest over the blade X_b . $\mathbf{F}(X_b, t)$ is the distributed load in the lift and drag directions. Notice here that $\mathbf{V}_{rel}(\mathbf{X}, t)$ is the relative velocity of the flow with respect to the rotating structure.

We will briefly inspect the construction of $\mathbf{V}_{rel}(\mathbf{X}, t)$ from the perceived velocity field $\mathbf{V}(\mathbf{X}, t)$. Let $\mathbf{V}(\mathbf{X}, t)$ be a spatio-temporal stochastic field on $\{\Omega, \mathcal{F}, P\}$ describing the velocity of the fluid flow on the ocean environment. We make the following hypotheses about this field:

- The field is unidirectional: $\mathbf{V}(\mathbf{X}, t) = \begin{bmatrix} 0 \\ 0 \\ V_z \end{bmatrix}; \forall(t, \mathbf{X})$.
- The field has finite moments $E[\mathbf{V}(\mathbf{X}, t)^n] = \mu_{\mathcal{V}^n(\mathbf{X})} < \infty$.
- It is a Gaussian, stationary field $E[\mathbf{V}(\mathbf{X}, t)] = \mu_{\mathcal{V}(\mathbf{X}, t)} = \mu_{\mathcal{V}(\mathbf{X})}; \text{Var}[\mathbf{V}(\mathbf{X}, t)] = \sigma_{\mathcal{V}(\mathbf{X}, t)\mathcal{V}(\mathbf{X}, t)} = \sigma_{\mathcal{V}(\mathbf{X})\mathcal{V}(\mathbf{X})}$.
- The field is homogeneous in the X and Z directions, so $\mathcal{V}(\mathbf{X}, t) = \mathcal{V}(Y, t)$.
- A diagram of the velocity field under these assumptions and in the inertial reference frame of the rotor-blade system is shown in Fig. 6.8 for various time instants of an arbitrary realization of the stochastic field.

The unperturbed velocity of the fluid is $\mathbf{V}(\mathbf{X}, t) = \begin{bmatrix} 0 \\ 0 \\ -V_z \end{bmatrix}$ in the inertial referential, with norm $\|\mathbf{V}(\mathbf{X}, t)\| = \sqrt{V_z^2}$. From the Blade Element Momentum theory, this velocity becomes:

$$\begin{aligned} \mathbf{V}(\mathbf{X}, t) &= \begin{bmatrix} 0 \\ 0 \\ -(1 - a_z(X_b)) V_z \end{bmatrix} + \begin{bmatrix} -a_x(X_b) \Omega (R_r + X_b) \\ 0 \\ 0 \end{bmatrix} \\ &= \begin{bmatrix} -a_x(X_b) \Omega (R_r + X_b) \sin(\Omega t) \\ 0 \\ -(1 - a_z(X_b)) V_z \end{bmatrix}, \end{aligned} \quad (6.11)$$

the corresponding induction factors that account for the changes in momentum on the flow: $a_x(X_b)$, $a_z(X_b)$; now taking into account the velocity $\dot{\mathbf{P}}_O$ of a point on the blade in the inertial referential:

$$\dot{\mathbf{P}}_O = \Omega \begin{bmatrix} -(R_r + X_b) \sin(\Omega t) \\ (R_r + X_b) \cos(\Omega t) \\ 0 \end{bmatrix}, \quad (6.12)$$

¹ the following equation is the vector form of the couple of equivalent relations used, for instance, in lift and drag components

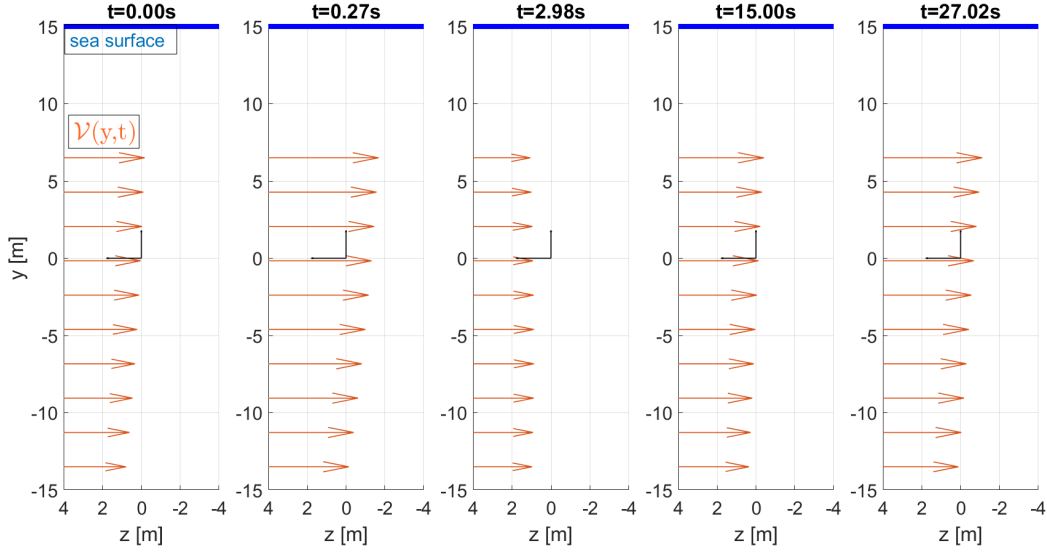


Figure 6.8: Visual representation of velocity field with inertial reference

we compute the relative velocity as follows $\mathbf{V}_{rel}(\mathbf{X}, t) = \mathbf{V}(\mathbf{X}, t) - \dot{\mathbf{P}}_O$:

$$\mathbf{V}_{rel}(\mathbf{X}, t) = \begin{pmatrix} -(a_X(X_b) + 1)\Omega(R_r + X_b)\sin(\Omega t) \\ -\Omega(R_r + X_b)\cos(\Omega t) \\ -(1 - a_Z(X_b))V_z \end{pmatrix}, \quad (6.13)$$

since Eq. 6.10 requires the square of the velocity, we have:

$$\begin{aligned} \mathbf{V}_{rel}^2(\mathbf{X}, t) = & \frac{1}{8} (8\Omega^2 a_x^2 (X_b + R_r)^2 \sin^2(t\Omega) + 16\Omega^2 a_x (X_b + R_r)^2 \sin^2(t\Omega) + 8V_z^2 a_z^2 \\ & - 16V_z^2 a_z - 8R_r \Omega^2 X_b \cos(2t\Omega) - 2R_r \Omega^2 X_b \cos(4t\Omega) \\ & + 10R_r \Omega^2 X_b - 4\Omega^2 X_b^2 \cos(2t\Omega) - \Omega^2 X_b^2 \cos(4t\Omega) + 5\Omega^2 X_b^2 \\ & - 4R_r^2 \Omega^2 \cos(2t\Omega) - R_r^2 \Omega^2 \cos(4t\Omega) + 5R_r^2 \Omega^2 + 8V_z^2), \quad (6.14) \end{aligned}$$

this shows that $\mathbf{V}_{rel}^2(\mathbf{X}, t)$ will not, in general, be a stationary field, even if $\mathbf{V}(\mathbf{X}, t)$ is stationary; the nonstationarity of the load emerges, as in the previous chapter, from the relative motion of the rotating system.

The resolution of Eq. 6.13 involves an iterative procedure that amounts to enforcing momentum equilibrium over some idealized ring elements representing the rotor. This approach is based on considering a turbine fixed in space and with rigid blades. Before discussing the modeling of the velocity field $\mathbf{V}(\mathbf{X}, t)$ from its antecedents, some thought should be placed in the justification of our approximation of the loads given that our model is not fixed in space and the blades do undergo deformation. The system occupies the following positions:

$$\mathbf{x}(t_i), t_i = t_{i-1} + \Delta t, (t, t_i) \in [T_0, T_f], \quad (6.15)$$

but the positions depend on the forces induced by the velocity $\mathbf{x}(t_i) = \mathbf{f}(\mathbf{V}(\mathbf{x}(t_i), t_i), t_i)$, and since the $\mathbf{x}(t_i)$ are the unknowns of our problem, this couples the simulation and resolution steps of the procedure. Some simplifications are imposed to escape this limitation:

1. The resolution of Eq. 6.13 is carried out assuming a fixed, rigid rotor with a similar geometry to the one described by the dynamical system.
2. With the solution from the previous step, Eq. 6.10 is applied to compute the loads acting at discrete points over the rigid rotor, providing a field of hydrodynamic forces.
3. The hydrodynamic force field is used as the load vector of our dynamical system.

This approach is akin to approximating the deformable system as rigid for load determination. The accuracy of this approach will be determined by the amplitude of the displacements $\mathbf{x}(t_i)$ and the correlation and continuity properties of $\mathbf{V}(\mathbf{X}, t)$. To see this, consider the following notion of continuity ([114]):

$$\lim_{t_1 \rightarrow t_2} \mathbf{E} \left[|\mathcal{V}(t_1) - \mathcal{V}(t_2)|^2 \right] \rightarrow 0 \quad (6.16)$$

in terms of sample paths. If $t_1 \rightarrow t_2$, then $\mathcal{V}(t_1, \boldsymbol{\omega}) \rightarrow \mathcal{V}(t_2, \boldsymbol{\omega})$ “for almost all $\boldsymbol{\omega}$ ” and if $\mathcal{V}(*, \boldsymbol{\omega})$ is continuous, the process is said to be continuous in sample paths. In the case of a field:

$$\lim_{x_1 \rightarrow x_2} \mathbf{E} \left[|\mathcal{V}(x_1, t) - \mathcal{V}(x_2, t)|^2 \right] \rightarrow 0, \forall t, \quad (6.17)$$

or in terms of the correlation function:

$$R_{\mathcal{V}(x_1)\mathcal{V}(x_2)}(t_1, t_2) = \iint_{L^2} \mathcal{V}(x_1, t_1) \mathcal{V}(x_2, t_2) p_{\mathcal{V}}(\mathcal{V}(x_1, t_1), \mathcal{V}(x_2, t_2)) dx_1 dx_2, \quad (6.18)$$

freezing time:

$$R_{\mathcal{V}(x_1)\mathcal{V}(x_2)}(t, t) \rightarrow 1, \exists L = (x_1 - x_2), \quad (6.19)$$

in words: if the input velocity field has a spatial correlation structure with a characteristic length L that satisfies the previous expression, two constituent stochastic processes of this field at a spatial separation $L = (x_1 - x_2)$ have an arbitrarily high correlation. In this case, the process in x_1 provides a good approximation for the process in x_2 . Since the dynamical system undergoes small vibrations, given that this is a prerequisite for the operational condition of the device, this approximation appears justified. Empirically, the order of magnitude of the displacements of the disc-shaft is at most 10^{-2}m , while spatial correlation is in the order of 10^1m . The physical interpretation of this development is that the velocity field, even though a stochastic quantity, needs to conform to continuity relationships that bind its spatial and temporal variability to provide a hydrodynamically sound model. If these continuity conditions are met, then the error in the proposed approximation is small.

3.2 modeling the velocity field

We will adapt Suptille’s [134] generalized stochastic description of the velocity field with wave-current interaction, to which an ambient turbulence component is superimposed. A similar procedure is adopted in [80], although we find the present development somewhat more general given the generalized representation of the component processes, particularly the surface elevation. The quantities involved are:

1. Intrinsic surface elevation $\eta_{int}(\mathbf{x}, t)$, characterized by its omnidirectional PSD $S_{\eta_{int}\eta_{int}}(f)$.
2. The spread function $D(f, \beta)$, from which the directional PSD is obtained.

3. The perceived particle velocity due to $\eta_{int}(\mathbf{x}, t)$, or $\mathcal{V}(z, t)$, and its intrinsic counterpart $\mathcal{V}_{int}(z, t)$.
4. The current $\mathbf{u}(t)$.
5. The ambient turbulence component $S_{VV}^{turbulence}(f)$.

Given a surface elevation process $\eta_{int}(\mathbf{x}, t)$ with PSD $S_{\eta_{int}\eta_{int}}(f)$, the directional PSD $E_{\eta\eta}(f, \beta)$ is obtained:

$$\begin{aligned} E_{\eta\eta}(f, \beta) &= S_{\eta_{int}\eta_{int}}(f) D(f, \beta) \\ \int_0^{2\pi} D(f, \beta) d\beta &= 1, \end{aligned} \quad (6.20)$$

and the particle velocity can be obtained from the potential relationship:

$$\varphi(\mathbf{x}, t) = \int_{\gamma, f} i \frac{f}{\gamma} \frac{\cosh[2\pi\gamma(h+z)]}{\sinh[2\pi\gamma h]} \exp[i2\pi(ft - \boldsymbol{\gamma}^T \mathbf{x})] dZ_{\eta\eta}, \quad (6.21)$$

with $\mathbf{x} = [x, y, z]^T$, and $\boldsymbol{\gamma} = [-\gamma \sin[\beta], \gamma \cos[\beta], 0]^T$, and with:

$$\begin{aligned} \mathcal{V}(x, t) &= \nabla \varphi(\mathbf{x}, t) \\ &= \int_{\gamma, f} \exp[i2\pi(ft - \boldsymbol{\gamma}^T \mathbf{x})] dZ_{VV} \\ dZ_{VV}(z, \boldsymbol{\gamma}, f) &= \tilde{\mathbf{A}}(z, \boldsymbol{\gamma}, f) dZ_{\eta\eta}, \end{aligned} \quad (6.22)$$

where:

$$\tilde{\mathbf{A}}(z, \beta, f_{int}(\gamma)) = \frac{2\pi f}{\sinh[2\pi\gamma h]} \begin{bmatrix} -\sin[\beta] \cosh[2\pi\gamma(h+z)] \\ \cos[\beta] \cosh[2\pi\gamma(h+z)] \\ i \sinh[2\pi\gamma(h+z)] \end{bmatrix}, \quad (6.23)$$

and $dZ_{VV} = \tilde{\mathbf{A}}(z, \boldsymbol{\gamma}, f) dZ_{\eta\eta}$. The perceived particle velocity by component, before turbulence addition, is thus expressed as:

$$\begin{aligned} S_{V_{xc}V_{xc}}(f_{int}, z_1, z_2, \beta) &= A_x^*(f_{int}, z_1, \beta) A_x(f_{int}, z_2, \beta) S_{\eta_{int}\eta_{int}}(f_{int}, \beta) \\ S_{V_{yc}V_{yc}}(f_{int}, z_1, z_2, \beta) &= A_y^*(f_{int}, z_1, \beta) A_y(f_{int}, z_2, \beta) S_{\eta_{int}\eta_{int}}(f_{int}, \beta) \\ S_{V_{zc}V_{zc}}(f_{int}, z_1, z_2, \beta) &= A_z^*(f_{int}, z_1, \beta) A_z(f_{int}, z_2, \beta) S_{\eta_{int}\eta_{int}}(f_{int}, \beta), \end{aligned} \quad (6.24)$$

where the relationship between the intrinsic frequency f_{int} and the perceived frequency f comes from the dispersion relationship:

$$f_{int}^2 = \frac{g\gamma}{2\pi} \tanh[2\pi\gamma h]. \quad (6.25)$$

Essentially, the surface elevation $\eta_{int}(\mathbf{x}, t)$ induces a particle velocity under the surface mediated by Eq. 6.21, and the interaction with current results in a frequency shift described by the dispersion relationship. The observed PSD is then:

$$\mathbf{E}_{VV}(f, z_1, z_2, \beta) = \mathbf{E}_{V_{int}V_{int}}(f_{int}, z_1, z_2, \beta) \frac{df_c}{df}, \quad (6.26)$$

to conclude the sequence, the turbulent PSD is superimposed:

$$\mathbf{E}_{VV}(f, z_1, z_2, \beta) = \mathbf{E}_{VV}(f, z_1, z_2, \beta) + S_{VV}^{turbulence}(f, z_1, z_1). \quad (6.27)$$

A von Karman PSD has been selected for the ambient turbulence as described (and empirically verified) in [88]; the hydrodynamic profile characteristics have been interpolated from the tables presented in [115].

The PSD $\mathbf{E}_{VV}(f, z_1, z_2, \beta)$ is discretized in time and space, allowing for the generation of realizations of a stochastic vector process that approaches $\mathbf{V}(\mathbf{X}, t)$. The selected parameters are shown in Tab. 6.4 for the application under development. The samples of $\mathbf{V}(\mathbf{X}, t)$ are used, as described before, to obtain the discretized force field acting over the blades using a BEMT iterative procedure. In Fig. 6.9, the two-sided PSDs of $\mathbf{V}(\mathbf{X}, t)$ at discrete depths under the sea surface are displayed, and we remark on some pertinent details:

- The amplitude of the PSD decays rapidly with depth, because the component corresponding to the surface elevation decays exponentially with depth ([33]).
- The effect of surface elevation is relevant when $z \leq \frac{\lambda}{2}$, where z is the depth. This can be expressed taking into account $\lambda = \frac{1}{\gamma}$ so $|z| \leq \frac{1}{2\gamma}$. The interval of depths used can be written as: $z(t) = H_{pile} - H_{sea} - (R_{rot} + L_b) \sin(\Omega t)$ where:
 - H_{pile} the height of the supporting pile of the turbine,
 - H_{sea} is the sea height,
 - R_{rot}, L_b are the rotor radius and blade length,
 - Ω is the intrinsic rotational speed of the turbine,
 - λ is the wavelength, γ is the spatial frequency.
- Considering the interpretation of the PSD as a frequency decomposition of the variance of a process, then the reduction in amplitude with depth suggests that $\eta_{int}(\mathbf{x}, t)$ has a predominant effect on the variance of $\mathbf{V}(\mathbf{X}, t)$.
- Reference [55] suggests that in the case of steep or irregular waves (not considered here), $\eta_{int}(\mathbf{x}, t)$ also has an important contribution to the mean of $\mathbf{V}(\mathbf{X}, t)$.

These remarks provide evidence that the stochastic model and associated simulation preserve many of the features of the physical phenomena they describe and with alternative analysis methods such as CFD simulation.

The input to the dynamical system is obtained following the developments in subsection 4.2 of Chapter 2, with the hydrodynamic loads induced by the discretized velocity field $\mathbf{V}(\mathbf{X}, t)$ following a BEMT numerical procedure, which limits the applicability of the moment propagation formulas for integral transformations established in Chapter 4.

4 Methodology

This section outlines the methods utilized to obtain and analyze the response of the system under the selected stochastic inputs. The challenges and strengths of each approach are described, and these are seen as complementary tools in the study of the problem at hand. Three methods are considered for evaluating the response \mathbf{y} , from which the design or observable variable S can be computed in terms of probabilistic descriptors or ensemble sets from which EVD and, ultimately, the reliability of the system can be estimated. The three methods start from the premise that a load sample is available, in our case, following the procedure detailed in subsection 3.2 of this chapter.

Parameter	Value
Frequency range	0.0022 – 0.43 [Hz]
Frequency step	0.0022 [Hz]
Time range	0 – 30 [s]
Time step	0.0300 [s]
Number of samples	15,000
Number of processes	10

Table 6.4: Parameters of velocity field simulation

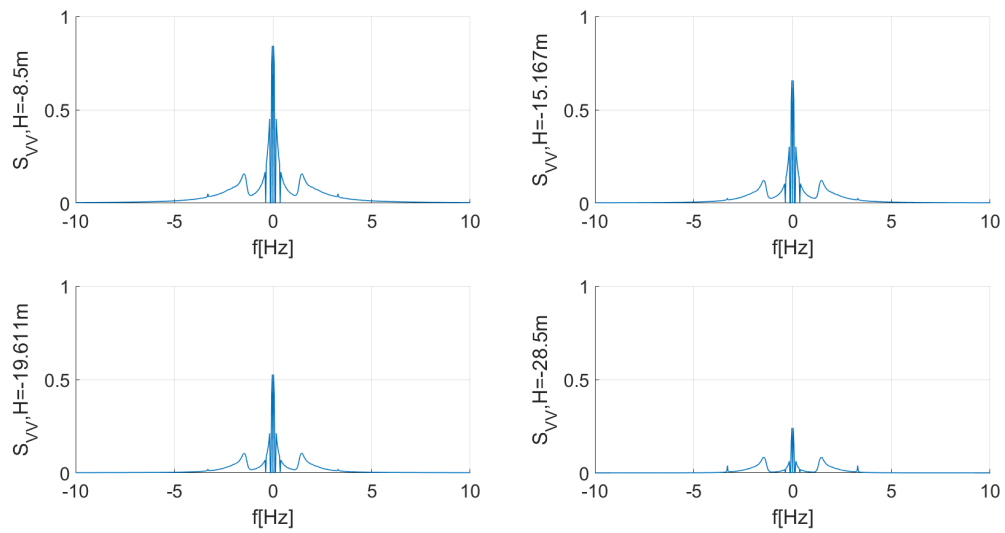


Figure 6.9: PSD of the velocity field at discrete depth point

4.1 MCS-ODE method

The Monte-Carlo simulation with ODE resolution consists of solving the forced Eq. 6.7 with each realization of the load sample, generating an ensemble of responses that can then be statistically processed to provide estimators of the probabilistic descriptors of the response. The method is easy to implement, general, and its outputs are an ensemble of responses; one may generate an ensemble of the design variable S and the limit state function G , providing what we call empirical measures of reliability. In this context, empirical refers to the fact that it is obtained from a given sample instead of an analytic or semi-analytic estimation.

Two main limitations apply to this method: on the one hand, a large number of samples is required to obtain statistically convergent results, with consequences in the required computation time and memory; on the other hand, the method is time-intensive, as each ODE has to be solved independently resulting in large computational time. Associated with the time constraints of the method comes dimensional scaling and time span scaling: the computational time required to solve one sample has a sensitive dependence on the dimension of the system and on the resolution interval. The applicability of this procedure to long integration times in systems with low dissipation and to identifying the transient-to-steady transition is impractical. However, it does provide a good estimate for the early stages of the loading process and, with some preconditioning techniques, may provide a rough estimation of the steady state.

We consider the following practical adaptation to improve the resolution of the problem, the modulating function:

$$g_{mod}(t) = \begin{cases} 1 & t > 4T_p \\ (\frac{t}{4T_p})^5 & 0 < t \leq 4T_p \end{cases}, \quad (6.28)$$

applied to the stochastic input so: $\bar{\mathbf{f}}(\mathbf{x}, t) = g_{mod}(t)\mathbf{f}(\mathbf{x}, t)$, and $\bar{\mathbf{f}}$ is taken as the effective load. This adaptation amounts to a slow and progressive application of the load to the system, and it mitigates the peak associated with the early stages of the transient regime that was discussed in the example of Chapter 5. From a numerical perspective, this modulation type improves the performance of MCS-ODE methods.

In structural reliability, a manifestation of the sample size requirements is most notable when high survival probabilities are required: by their very nature, extreme events are rare, so a precise description of the tail of the involved distributions requires a very large number of samples. Compounding these considerations is the fact that physically realistic environmental and load conditions involve correlated random processes, which demands a sample generation strategy that ensures these correlation structures in the ensemble of samples. More concretely, MCS involving statistically independent random variables benefits from the computational simplicity of independent sample generation, which can not be done for spatiotemporal correlated fields. Even when the required samples have been generated, computing the response of complex structural or mechanical systems for every generated sample constitutes the largest component of the total computational effort.

In its most basic form, the approach taken here consists of:

1. Generating the required spatio-temporal Gaussian velocity field samples from the selected sea state conditions.
2. Pre-treatment of these velocity samples to obtain the load processes over the required elements, in this case the blades of the tidal turbine.
3. Numerically solving the non-homogeneous Ordinary Differential Equations (ODE) problem.
4. Post-treatment of the response and probabilistic characterization.

The two main challenges from these steps come from 1 and 3.

To mitigate the difficulties in 1, a judicious spatial discretization scheme has been applied, selecting the relevant simulated processes to be placed in space within the diameter of action of the dynamical system. The error resulting from the spatial discretization is related to the degree of variation of the velocity field with depth. This

Algorithm 6.1 Spectral MCS method for steady-state analysis

1. Generate N_s samples of physical load vector $\mathbf{f}(t)$, denoted $\hat{\mathbf{f}}$
 2. Recover the modal parameters of the Floquet system, in Fourier domain if applicable: characteristic exponents $\boldsymbol{\rho}$, right and left periodic modes $\mathbf{R}_q, \mathbf{L}_l$, matrix of passage to state form for the load \mathbf{B}_b
 3. For each N_s :
 - (a) Compute $\hat{\mathbf{F}}(f) = \text{FT}[\hat{\mathbf{f}}(t)]$
 - (b) Apply 3.82 with $\hat{\mathbf{F}}(f)$ to obtain the frequency response of the ensemble $\hat{\mathbf{Y}}(f)$
 - (c) Compute $\hat{\mathbf{y}}(t) = \text{IFT}[\hat{\mathbf{Y}}(f)]$ to obtain the sample steady-state response of the corresponding N_s
-

variation can be measured in terms of the covariance function of the field and the smoothness of its sample paths with space but not time. From the point of view of memory handling, the generation of samples has been done in sets where each set of samples is sufficiently large to verify the basic correlation constraints prescribed for the process.

The implicit, high-order Runge-Kutta subroutine Radau IIa method of variable order (1,5,9,13) by [142] has been used in step 3, as it has been empirically verified that it provides a substantial saving in resolution time. This is conjectured to be due to the multiscale nature of the dynamical system, which results from the combination of discrete DOFs (notably the base) and modally discretized continuum elements (the blades). The relative error tolerance selected has been 10^{-6} throughout the application section.

4.2 Modal spectral MCS method

The idea of the modal spectral MCS method is capitalizing on 3.82 by applying the Fourier transform to the loads in each realization of the ensemble, producing an ensemble of loads in the frequency domain. This procedure results in an ensemble of responses in the frequency domain that corresponds to the steady-state response of the system, which can be transformed into the temporal domain using the inverse Fourier transformation to yield a time-domain steady-state ensemble of the response variables amenable to probabilistic characterization in terms of temporal moments. In the same way, the reconstructed time-domain steady-state response can serve as the basis for empirical reliability estimation. The procedure is described in 6.1.

Once the temporal samples of steady-state responses have been obtained using 6.1, it is possible to apply 6.8 to obtain the ensemble of steady-state design variable $S(t)$ and its derivative $\dot{S}(t)$.

The method has two main strengths: first, the passage to the frequency domain results in substantial savings in computational time, as highly efficient algorithms such as FFT and IFFT can be capitalized on, and the response is obtained by simple multiplication and summation of terms; second, the method provides a direct estimation of the steady-state response, circumventing the long integration times inherent to the MCS-ODE approach. In terms of limitations, the method does not provide information about time-of-arrival to the steady-state regime. Like any MCS approach, it is still constrained to large sample sizes to result in a good estimation of the desired probabilistic quantities. Additionally, the response obtained from this method is highly sensitive to errors in the determination of the Floquet characterization in the Fourier domain, in other words, the Fourier coefficients of $\mathbf{R}(t)$, $\mathbf{L}(t)$ and $\mathbf{B}(t)$.

4.3 Floquet modal convolution

The Floquet modal convolution is the same approach explored in section 4. The key relationships are reproduced here for convenience. In the Floquet modal variables \mathbf{q} , taking as input the adapted excitation \mathbf{p} , the following relationships apply:

$$\begin{aligned}
\boldsymbol{\mu}_q(t) &= \int_0^t \mathbf{h}(t-\tau) \boldsymbol{\mu}_p(\tau) d\tau \\
\boldsymbol{\mu}_{qq}(t) &= \int_0^t \int_0^t \mathbf{h}(t-\tau_1) \mathbf{R}_{pp}(\tau_1, \tau_2) \mathbf{h}(t-\tau_2)^H d\tau_1 d\tau_2 \\
\boldsymbol{\sigma}_{qq}(t) &= \int_0^t \int_0^t \mathbf{h}(t-\tau_1) \boldsymbol{\Sigma}_{pp}(\tau_1, \tau_2) \mathbf{h}(t-\tau_2)^H d\tau_1 d\tau_2 \\
\mathbf{R}_{qq}(t_1, t_2) &= \int_0^{t_2} \int_0^{t_1} \mathbf{h}(t_1-\tau_1) \mathbf{R}_{pp}(\tau_1, \tau_2) \mathbf{h}(t_2-\tau_2)^H d\tau_1 d\tau_2 \\
\boldsymbol{\Sigma}_{qq}(t_1, t_2) &= \int_0^{t_2} \int_0^{t_1} \mathbf{h}(t_1-\tau_1) \boldsymbol{\Sigma}_{pp}(\tau_1, \tau_2) \mathbf{h}^H(t_2-\tau_2) d\tau_1 d\tau_2 \\
\boldsymbol{\mu}_{qq}(t) &= \mathbf{R}_{qq}(t, t) \\
\boldsymbol{\sigma}_{qq}(t) &= \boldsymbol{\Sigma}_{qq}(t, t),
\end{aligned} \tag{6.29}$$

respectively the mean, second moment, correlation function, covariance function, and variance of \mathbf{q} . From the Floquet modal variables, the following passage to the state variable is possible:

$$\begin{aligned}
\boldsymbol{\mu}_y(t) &= \mathbf{R}(t) \boldsymbol{\mu}_q(t) \\
\boldsymbol{\mu}_{yy}(t) &= \mathbf{R}(t) \boldsymbol{\mu}_{qq}(t) \mathbf{R}^H(t) \\
\boldsymbol{\sigma}_{yy}(t) &= \mathbf{R}(t) \boldsymbol{\sigma}_{qq}(t) \mathbf{R}^H(t) \\
\mathbf{R}_{yy}(t_1, t_2) &= \mathbf{R}(t_1) \mathbf{R}_{qq}(t_1, t_2) \mathbf{R}^H(t_2) \\
\boldsymbol{\Sigma}_{yy}(t_1, t_2) &= \mathbf{R}(t_1) \boldsymbol{\Sigma}_{qq}(t_1, t_2) \mathbf{R}^H(t_2),
\end{aligned} \tag{6.30}$$

again the mean, second moment, correlation function, covariance function, and variance of \mathbf{y} . An additional development concerns the modal contribution in the forced response, which can be expressed as:

$$\mathbf{y}(t) = \sum_{i=1}^{42} \mathbf{y}_i(t), \tag{6.31}$$

where i denotes the corresponding periodic mode such that:

$$\mathbf{y}_i(t) = q_i \mathbf{R}_i(t) \tag{6.32}$$

where $\mathbf{R}_i(t) = [R_{1,i}(t) \dots R_{42,i}(t)]^T$ is the i -th column vector of $\mathbf{R}(t)$. This mode-wise decomposition can be applied to the mean response:

$$\boldsymbol{\mu}_y^{(\text{mode } i)}(t) = \mu_{q_i}(t) \mathbf{R}_i(t), i = 1, \dots, 42 \tag{6.33}$$

where $\mu_{q_i}(t)$ is the i -th element of the mean vector $\boldsymbol{\mu}_q(t)$. Finally, applying Eq. 6.8, it is possible to express the contribution of each mode to the observable of interest:

$$\boldsymbol{\mu}_S^{(\text{mode } i)}(t) = \mathbf{C} \boldsymbol{\mu}_y^{(\text{mode } i)}(t). \tag{6.34}$$

A remarkable aspect of this development is that it enables the analysis of the response in terms of mode activation. In this way, the notion that a particular sea state associated with the corresponding load process activates

a certain group of periodic modes emerges. A similar idea would apply to the variance contribution per mode. An interesting idea that will not be explored here is implementing Floquet design, or designing a system with specific periodic mode characteristics using information from load activation of the periodic modes.

The main advantage of Floquet modal convolution is that it is not constrained by ensemble stochastic convergence as the MCS-based methods do. It can be applied very efficiently if analytical expressions for the input moments are available, as shown in section 5 of Chapter 5; it can also be applied if a numerical function provides a discretized evaluation of the required moments, in the case of complex stochastic inputs this function can be constructed from MCS sampling, without much additional computation time. A key limitation concerns the required sampling to achieve an accurate evaluation of the convolution integrals: for high-frequency terms, a precise evaluation of the convolution expressions requires a very small sampling period, resulting in large arrays of data being required to obtain accurate results, with critical consequences when long integration times are required. Unlike the MCS-ODE approach, the criticality that comes with long integration does not come from the computation time, but from memory storage. Indeed, fast algorithms are available to compute the convolution of a very large size, such as Conv2_FFT ([154]), which performs 2D convolution relying on the convolution theorem and the FFT algorithm. This memory limit implies that the method, as implemented, is most applicable to the study of the transient-steady transition and may need additional adjustments to arrive at the fully developed steady state, at least for moderate-to-large dimension systems with low dissipation. By way of example, we consider the second-order moments $\mathbf{R}_{pp}(t_1, t_2)$ and $\mathbf{\Sigma}_{pp}(t_1, t_2)$, both of which scale in the following sequence:

$$\begin{aligned}
N = 42, N_t = 1 \times 10^2 &\rightarrow 0.14\text{GB} \\
N = 42, N_t = 1 \times 10^3 &\rightarrow 14.11\text{GB} \\
N = 42, N_t = 2 \times 10^3 &\rightarrow 52.60\text{GB} \\
N = 42, N_t = 5 \times 10^3 &\rightarrow 328.60\text{GB},
\end{aligned} \tag{6.35}$$

where N is the number of DOFs and N_t is the number of time-points of the selected functions.

5 Results

This section considers three regimes of the response informed by the analysis of the stochastic response of LTP systems in section 5 of Chapter 5. First, we seek to capture the approach towards the steady-state with MCS-ODE and Floquet modal convolution, using the adjustment Eq. 6.28 to mitigate the peaks associated with early transient stages and speed the approach to the steady regime. Second, we use the Floquet modal convolution to describe the transient regime for three cycles, providing the modal contribution in mean to the design variable S . Third, we use the Modal spectral MCS method to characterize the established steady-state regime for one cycle. In each case, the design variable is studied, and a reliability estimation is provided for the system under the selected failure mode on S . The reliability estimates are provided from empirical measures, that is, by reconstructing the EVD from the obtained samples of the solution; in the applicable case, the Gaussian interval estimation introduced in Chapter 5 will serve to estimate the EVD and thus the reliability. During the section, the available resistance is taken to be $R = 1.95 \times 10^5 \text{Pa}$.

5.1 Transient to steady transition

We first consider the load with the modulation in Eq. 6.28 for the MCS-ODE, adding the result obtained from Floquet modal convolution as a reference. The system is solved on the $[0, 7T_p]$ interval, but only the last three cycles, $t = [4T_p, 7T_p]$, are taken as an approximation of the vicinity of the steady-state. The responses of a selected group of DOFs are shown in Fig. 6.10 and Fig. 6.11, showing the means of G_x , θ_1 , q_{11}^s , and q_{11}^f , with

good agreement between the two approaches. As specified in Tab. 6.4, 15×10^3 realizations of the load process have been used, yielding as many response samples for the MCS-ODE method.

This first result helps establish the validity of the MCS-ODE approach from the stochastic convergence perspective, as the Floquet modal convolution is essentially a numerical evaluation of an analytical expression. Additionally, some conclusions can be reached about the computational time required for each method: the total computational time required for the MCS resolution has been $4.7 \times 10^4 s$ with parallel computation on 14 cores, whereas the Floquet modal convolution incurred in a resolution time of the order of $10^2 s$ including load conditioning. We summarize that the MCS-ODE approach is time-intensive, whereas the Floquet modal convolution is memory-intensive.

MCS-ODE characterization Taking the last three cycles $t = [4T_p, 7T_p]$ the design variable $S(t)$ has been calculated from the MCS-ODE response ensemble. The mean, variance and normalized skewness coefficient are shown in Fig. 6.12, including the moving average in the case of mean and variance. We observe that the normalized skewness $\frac{\sigma_{SSS}}{\sigma_{SS}^{3/2}}$ serves as a measure of deviation from Gaussian behavior, as this quantity is 0 for the Gaussian distribution.

The mean value of the design variable, $\mu_S(t)$ oscillates around the value of 7.6×10^4 Pa. From the moving average of the variance $\sigma_{SS}(t)$ it can be noted that it is still in growth regime, this behavior is consistent with the findings in section 5 in Chapter 5, implying that the steady-state has not yet been achieved, despite the seemingly stable value of the mean. This highlights an intrinsic limitation of the MCS-ODE: while it provides abundant information about the response, reaching the steady-state involves the consideration of long time intervals, for which the method scales poorly in terms of computational time. Concerning the normalized skewness, we observe regular peaks around 0: the design variable $S(t)$ deviates from Gaussian behavior consistently.

PGHW estimation of the EPSD The empirical samples obtained from MCS provide the basis for the PGHW estimation of the evolutionary PSD (in the sense of Priestley), as introduced in Chapters 3 and 5. The method consists of transforming the MCS solutions into the design variable using relationship Eq. 6.8, and then projecting each realization on an appropriate PGHW basis. Once this is achieved, the wavelet coefficients obtained from this projection can be used to construct an approximation to the EPSD of the design variable. The procedure requires some trial to obtain the appropriate resolution between time and frequency description.

In Fig. 6.13, the PGHW reconstructions for four arbitrary realizations of S are compared with the original solution obtained from MCS after removing the mean component of each realization. As detailed in the example of Chapter 5, this step is crucial to ensure that the selected Wavelet parameters result into a basis of Wavelets that correctly capture the features of the functions being analyzed. In this case, the selected wavelet parameters are $N_t = 25$ and $N_f = 50$. These results illustrate the fact that these parameters result in an adequate Wavelet basis that captures the features of each realization.

The EPSD in Fig. 6.14 shows oscillatory activation in the frequency bands around 9Hz and 11Hz, with the particularity that the oscillations happen out of phase from one another, although their period is that of the system: $T_p = 4.19$. The frequencies 9Hz and 11Hz correspond to the lowest frequencies of the discretized blades from the Rayleigh-Ritz discretization; the mode in each case is kinematically identical to the static deformation of a similar beam. Other oscillations in lower frequency components can be observed, too, notably around the 7Hz frequency, and around 1Hz.

These results are consistent with the expectation since the excitation introduced has been applied to the blades only, so no major amplitude involving the base DOF is dominant; additionally, from Eq. 6.8, it can be inferred that the design variable consists of a superposition of the response stochastic processes that are the blade modal variables. This representation of the EPSD also highlights the shortcomings of a two-dimensional Fourier transform in this type of scenario: the notion of time-evolution of frequency components and their associated modes is lost in such an approach, as the temporal evolution of these frequencies is decomposed and mixed into the two-dimensional frequency space. The flexibility of the PGHW provides a reasonable location in time and frequency, with an efficient numerical advantage for the study of transient events.

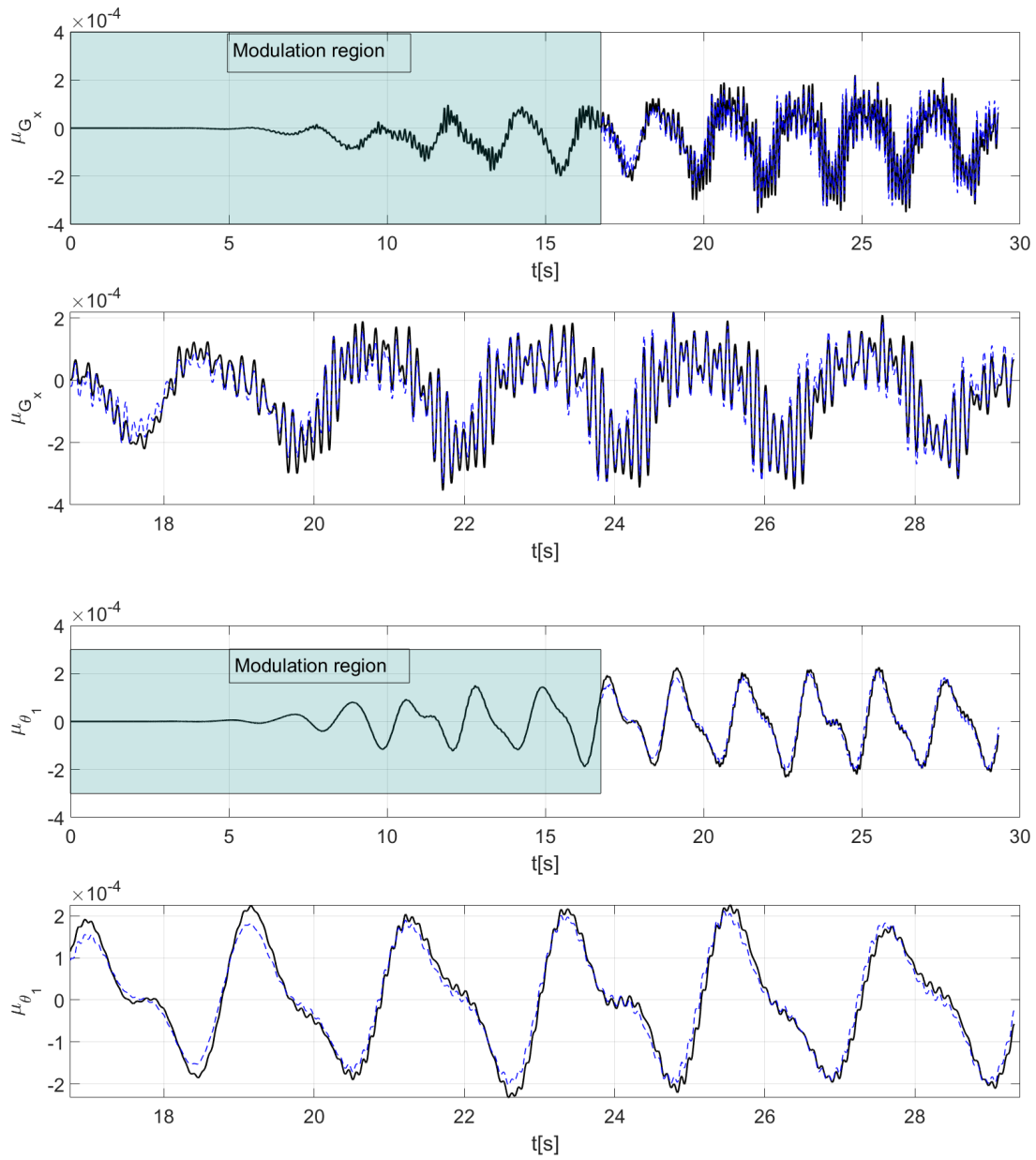


Figure 6.10: Mean response for selected DOFs, (part 1): Floquet modal convolution (black), MCS-ODE (blue), modulation interval in shade box

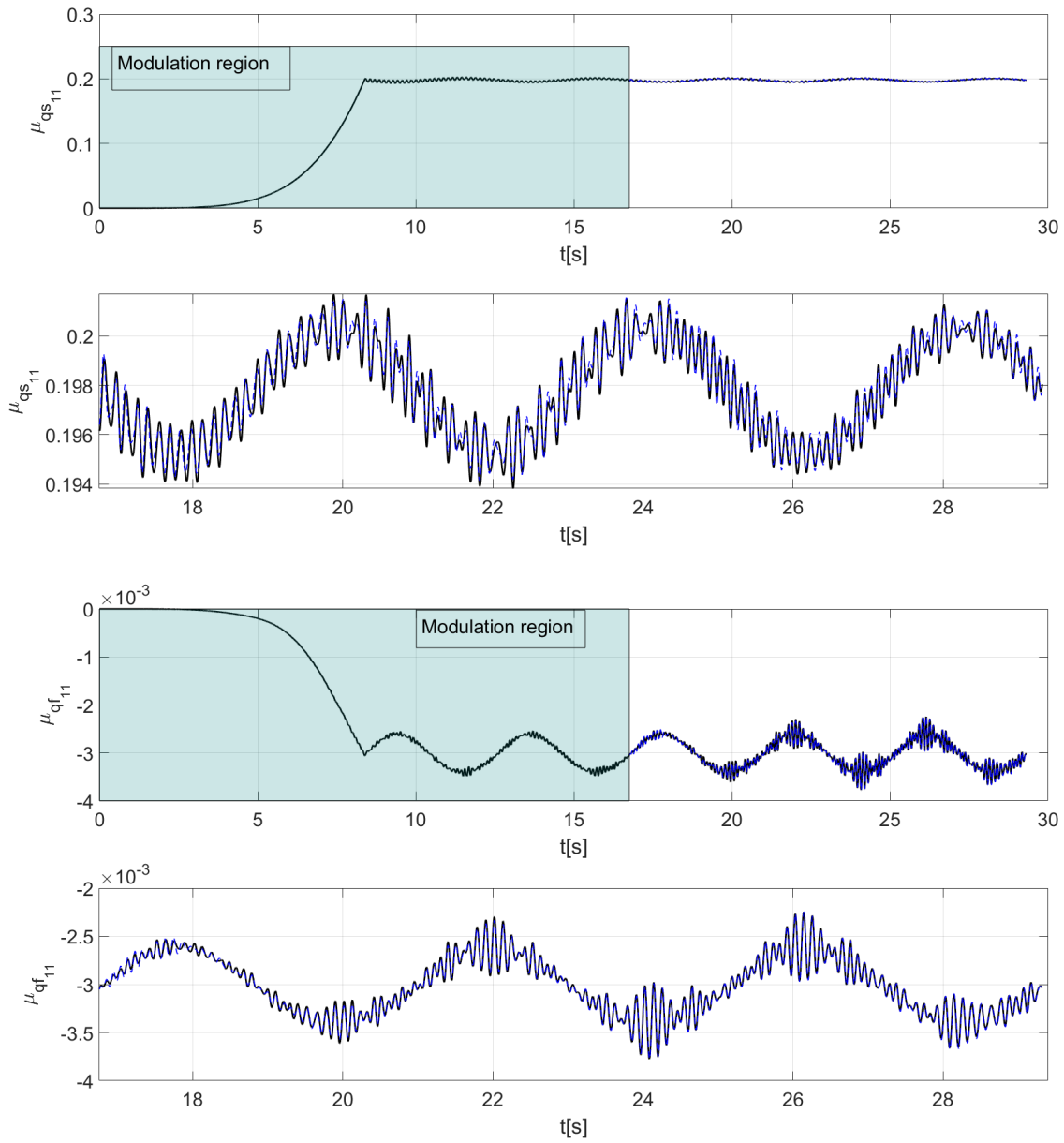


Figure 6.11: Mean response for selected DOFs, (part 2): Floquet modal convolution (black), MCS-ODE (blue), modulation interval in shade box

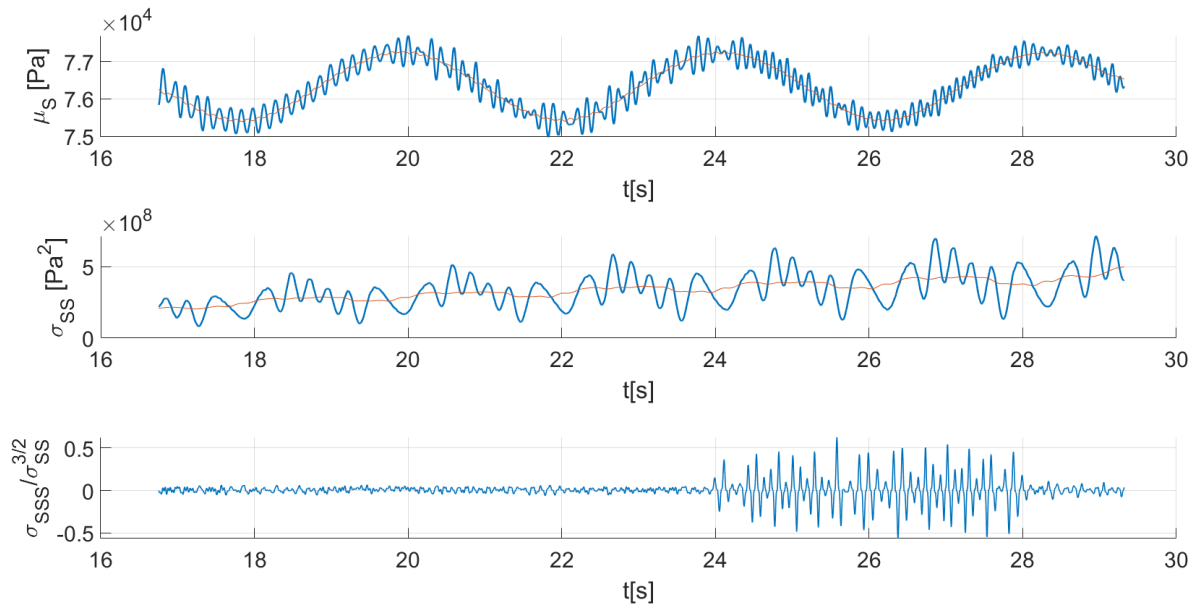


Figure 6.12: Mean, variance and skewness of $S(t)$, moving average in red, MCS-ODE method

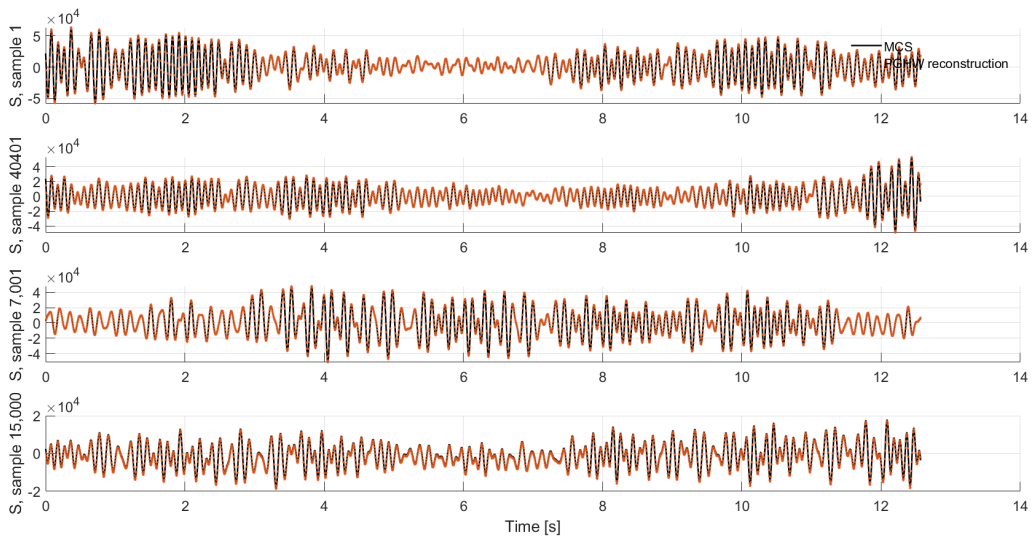


Figure 6.13: PGHW reconstruction for selected realizations of S

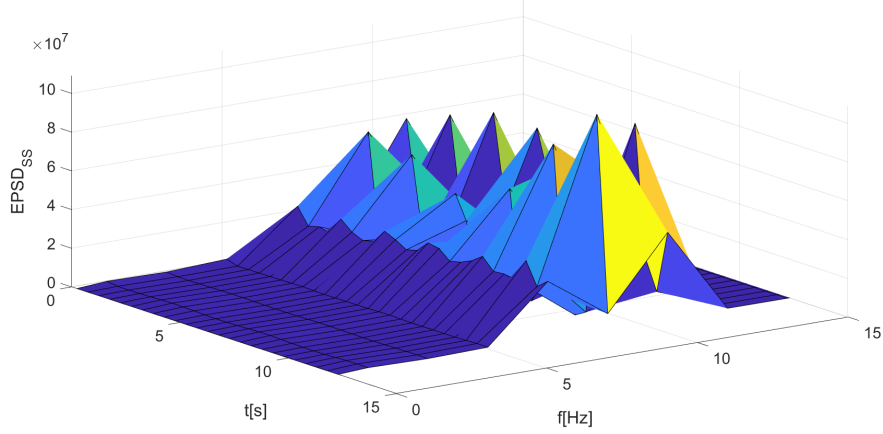


Figure 6.14: EPSS by PGHW of design variable S

MCS-ODE: EVD and reliability The EVD for the MCS-ODE method can be computed empirically from the available samples of $S(t)$, as shown in Fig. 6.15². For the selected available resistance, we can compute the probability of failure in the $[4T_p, 7T_p]$ interval:

$$P_f^1(4T_p, 7T_p) = 1 - P_{S_M}(R) \approx 4.67 \times 10^{-4}, \quad (6.36)$$

this equals a reliability level of about 99.95%. This initial result serves two main functions: first, it sketches the entire process of computing the reliability of the system from our proposed MCS-ODE method; second, it provides a concrete value to contrast with the other regimes of analysis in this section. From a practical perspective, higher levels of reliability entail lower failure probabilities, making the failure event very rare, which requires a larger number of samples to accurately estimate lower probabilities of failure and higher reliability levels. The conclusion is that if very high reliability levels are the goal, much larger MCS samples would be required, with the associated computational time requirement that has been outlined in this development. This fact serves as the motivation for the development of alternative methods.

5.2 Floquet modal convolution: early transient regime

We now turn our analysis to the early transient regime by considering the stochastic load without the modulation Eq. 6.28. From a methodological perspective, this sudden application of loads drastically increases the resolution time for the MCS-ODE method, while the Floquet modal convolution is unaffected by it. We will thus utilize the latter method and the additional developments that permit us to describe the modal contribution to the observable variable $S(t)$.

The resolution is carried out in the $[0, 3T_p]$ interval; the mean and variance of the response are shown in Fig. 6.16. The mean of the blade modal variables in the spanwise direction shows a clear dominance of the lowest mode shape of the blade; in the flapwise direction the participation of additional mode shapes can be noticed; the disc-shaft DOF which are not directly loaded begin to react to the application of load as time progresses. As expected, the variance is still in development, characteristic of the transient regime.

The mean and variance of the design variable $S(t)$ and its derivative $\dot{S}(t)$ are shown in Fig. 6.17. It is possible to see the transition of the mean $\mu_S(t)$ from an amplitude in the order of 10^5 Pa towards 10^4 Pa as in the previously analyzed regime. The consequence of $\mu_S(t)$ attaining such a high value at the very beginning of motion suggests

²The confidence bounds here are embedded in the Empirical CDF estimation algorithm, it relies on the Kaplan-Meier probabilistic estimator and applies Greenwood's formula to obtain both 95% bounds.

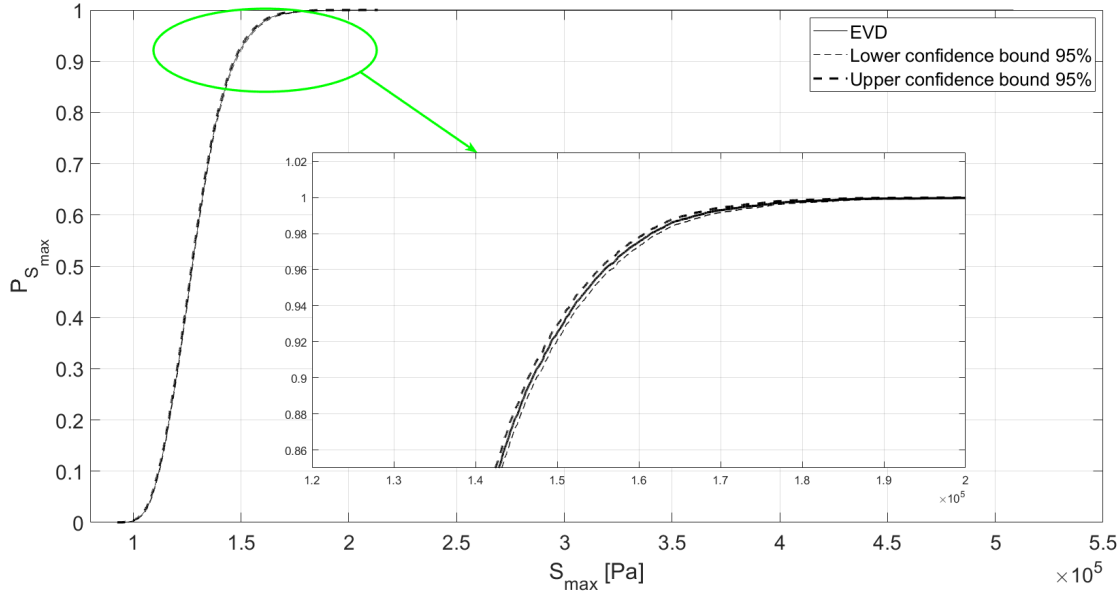


Figure 6.15: EVD estimation of $S(t)$, interval $[4T_p, 7T_p]$, MCS-ODE method

that in this regime, failure is likely to arrive in the very first cycle. This result illustrates the assertion that two distinct regimes can be distinguished: the transient one, dominated by high mean values as a result of the presence of the transient part of the response; a steady regime where the transient component has decayed, resulting in a lower magnitude of the mean and a more substantial effect of the variance in the resulting probability of failure.

The contribution to $\mu_S(t)$ by each one of the $k = 42$ periodic modes is shown in Fig. 6.18. The mode contributions have been grouped in terms of their amplitude, we remark that 4 modes have amplitudes in the order of 10^4 , 20 modes are in the order of 10^3 , the remaining 18 modes having comparatively small amplitudes.

EVD and reliability To conclude with the analysis related to the convolution moment relationships, the last period of the solution is analyzed in terms of the extreme value analysis introduced in Chapter 5. The mean and variance of $S(t)$ for this last period are represented in Fig. 6.19 to better appreciate the features, and the peak mean values are marked. The estimation of the EVD with this method is presented in Fig. 6.20.

For a sufficiently high set upcrossing level u , the likelihood of upcrossing is first best considered analyzing the mean of $S(t)$, a consequence of the discussion in Chapter 5; as the mean decays and the variance increases towards its asymptotic value, the mean is no longer the predominant factor and the direct variance interval approximation can be applied. Considering Fig. 6.20, it is clear that for the selected available resistance $R = 1.95 \times 10^5$ Pa, the system fails almost surely during the transient phase. This result is coherent, given the high value of the mean during this phase. Conversely, this result also suggests that if this early stage of loading is taken as the critical design scenario as far as extreme load is concerned, the steady-state is likely to remain in the safe region.

From a broader perspective, the loading scenario in this section is somewhat extreme. With more realistic information about the transient regime of flow and with some adjustments in the quantitative aspects of the chosen model (precise measurements of the effective damping, relaxing the hypothesis of constant spin angular

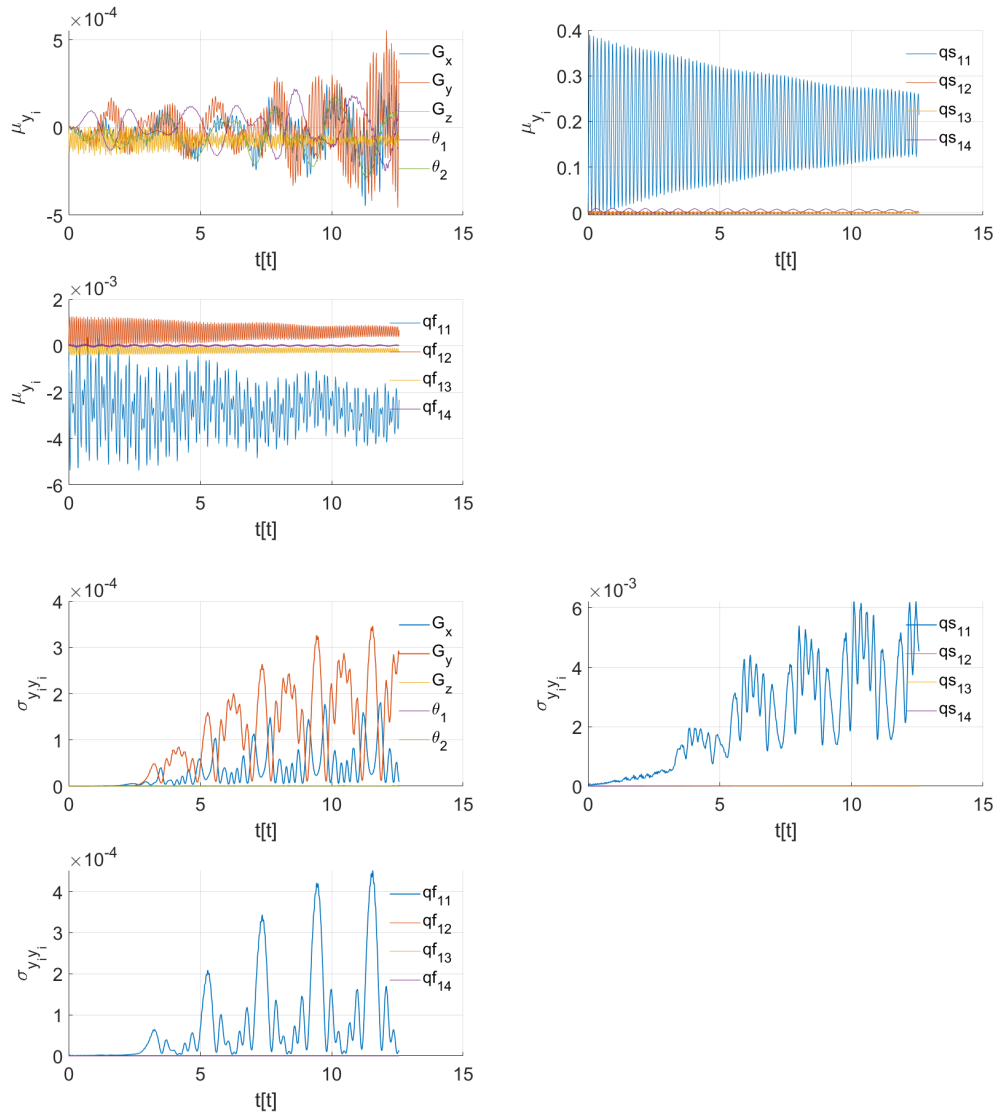


Figure 6.16: Mean (top) and variance (bottom) of state variables, disc and first blade, Floquet modal convolution

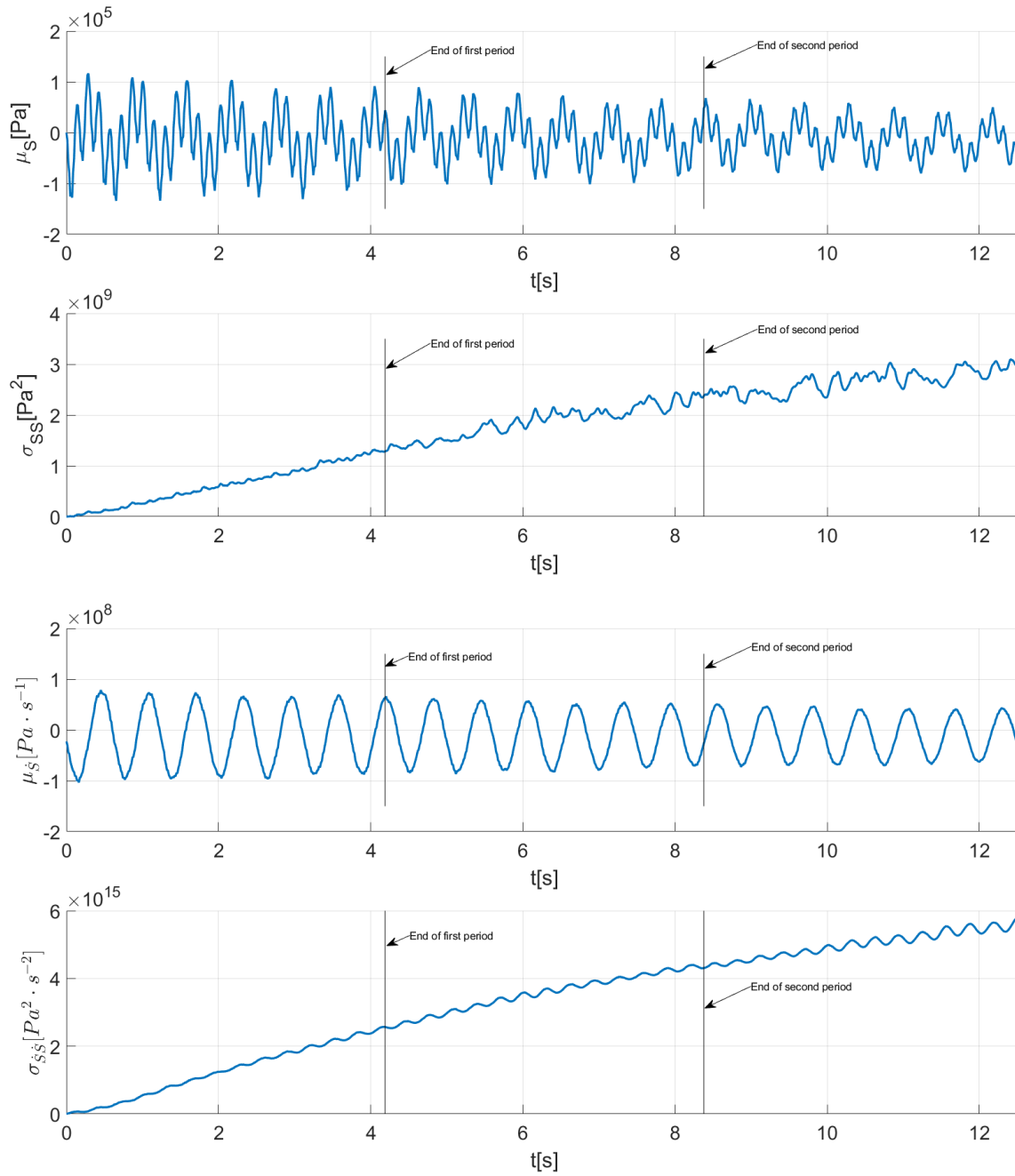


Figure 6.17: Mean and variance of $S(t)$ and $\dot{S}(t)$ on the $[0, 3T_p]$ interval, Floquet modal convolution

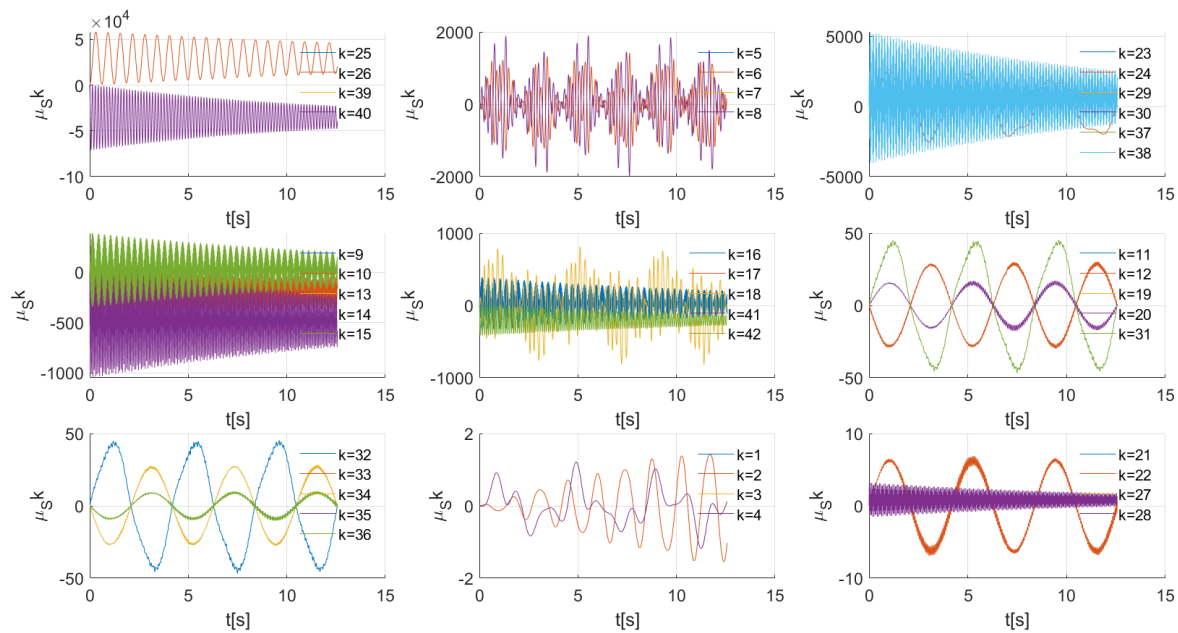


Figure 6.18: Modal decomposition of $\mu_S(t)$, Floquet modal convolution

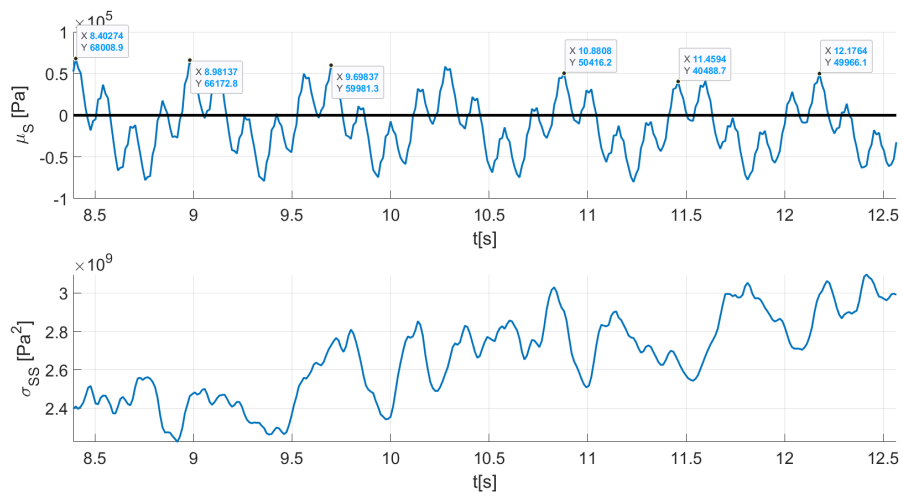


Figure 6.19: Mean and variance of $S(t)$ in the last period of analysis $[2T_p, 3T_p]$, Floquet modal convolution

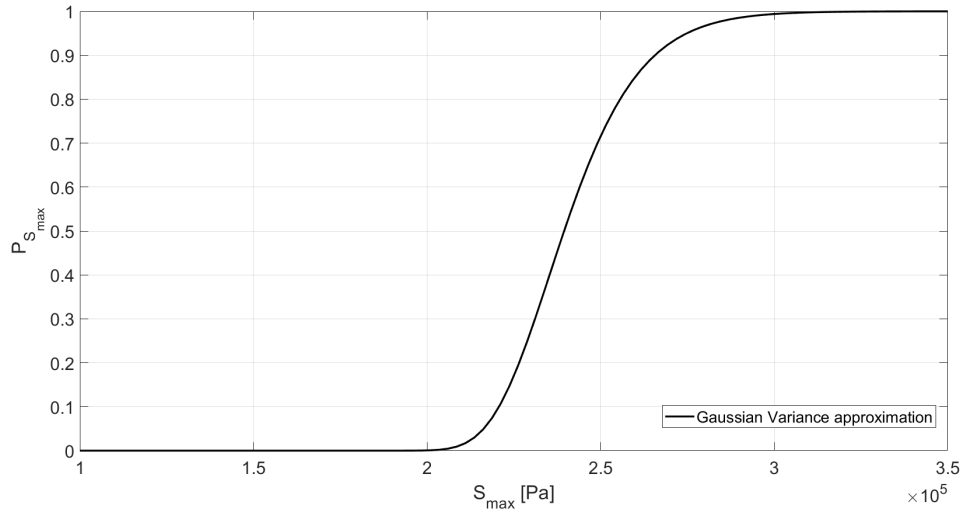


Figure 6.20: Estimation of EVD of S in last period of analysis $[2T_p, 3T_p]$, Floquet modal convolution, interval approximation method (Chapter 5)

velocity, selecting more realistic initial conditions), the convolution method presented here is fit to perform transient analysis of the response.

5.3 Steady-state

The steady-state analysis using the Modal spectral MCS method outlined in Alg. 6.1 has been performed on the system for a single period $[nT_p, (n+1)T_p]$; here n is sufficiently large for the steady-state to have been reached. The same ensemble of loads generated from the 15×10^3 velocity samples in Tab. 6.4 has been used, with the appropriate time reduction. In terms of computational aspects, the method seems substantially faster, the whole computation requiring 2.7×10^4 s, although the comparison is not ideal given the different time intervals studied. The comparison, however, helps to put into perspective the advantage of the spectral method in obtaining the steady-state response, in the sense that the approximation of the steady-state using the MCS-ODE approach would entail a substantial increase in integration time and, thus, in total simulation time.

An additional advantage of the spectral method comes from using Eq. 3.82. The expression permits the integration of the knowledge of the modal representation of the involved matrices to obtain important improvements in computational time. If any of the matrices $\mathbf{R}(t), \mathbf{L}(t)$ or $\mathbf{B}(t)$, with the corresponding matrix of Fourier coefficients for the k -th harmonic $\mathbf{R}_k, \mathbf{L}_k, \mathbf{B}_k$, have null projection over a given element of the Fourier basis $e_k = \exp\left[i\left(\frac{2\pi}{T_p}k\right)t\right]$, then the corresponding matrix of Fourier coefficients is zero and the entire term can be skipped from the sum.

As with the MCS-ODE method, the mean for selected DOFs of the response is shown in Fig. 6.21. As expected, the most active DOFs in terms of magnitude are those under direct load: the flapwise and spanwise lowest mode shapes. The mean of the two DOFs associated with the disc shows the important coupling effect, particularly among the G_x DOF and the spanwise modes of the blade. In the case of the angular DOF, the amplitude of oscillation of the mean is about 0.28 degrees (0.005 rad), a value consistent with the small angle assumption made at the modeling stage.

The mean, variance, and normalized skewness of the design variable $S(t)$ computed from the samples obtained in the Modal spectral MCS method are shown in Fig. 6.22, in a similar format to Fig. 6.12, although the moving average is omitted given the clear trend around a single value for the steady-state statistics. The orders of magnitude of mean and variance are the most remarkable feature concerning EVD analysis: 10^4 for the mean

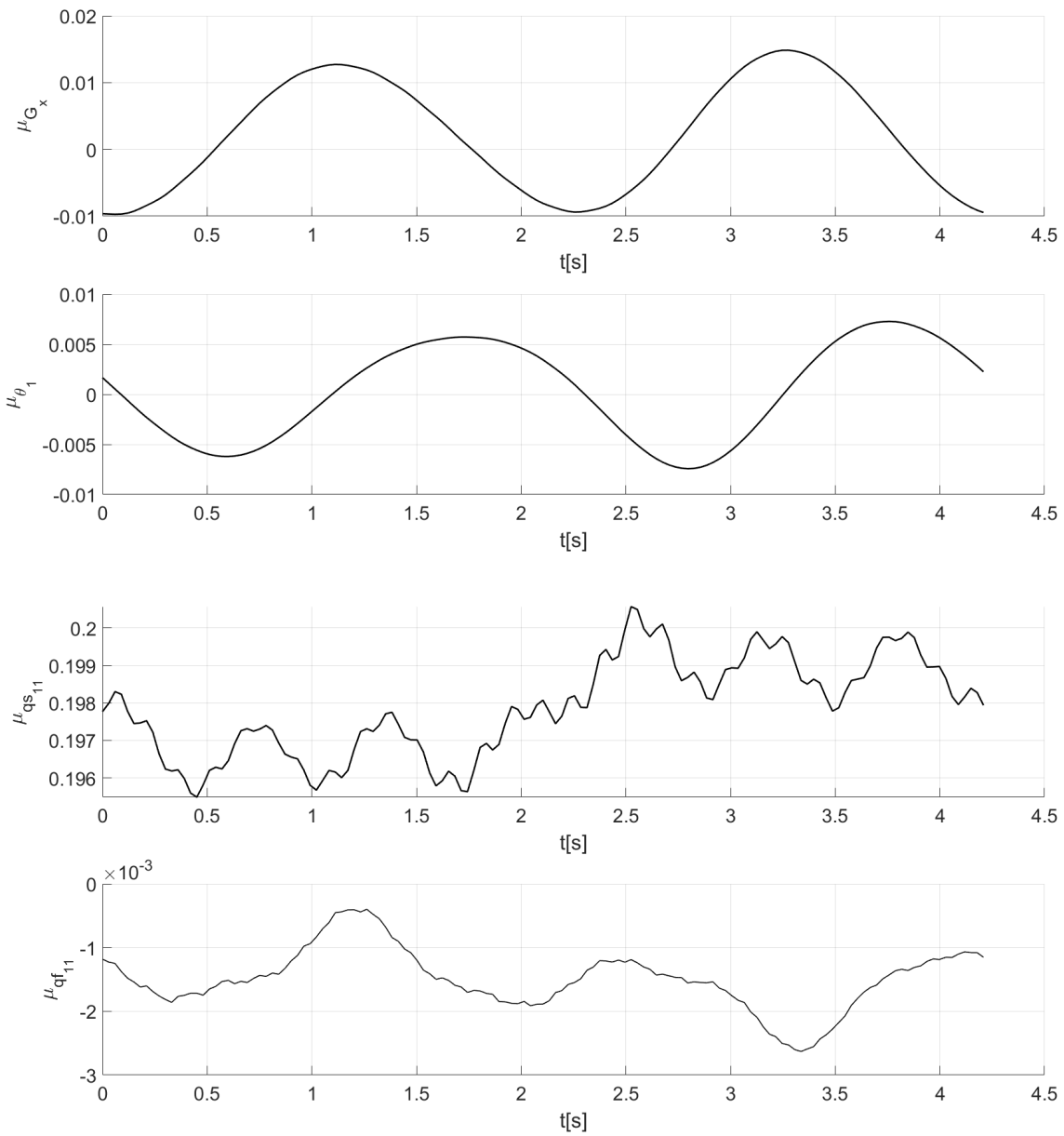


Figure 6.21: Mean response for selected DOFs, Modal spectral MCS method

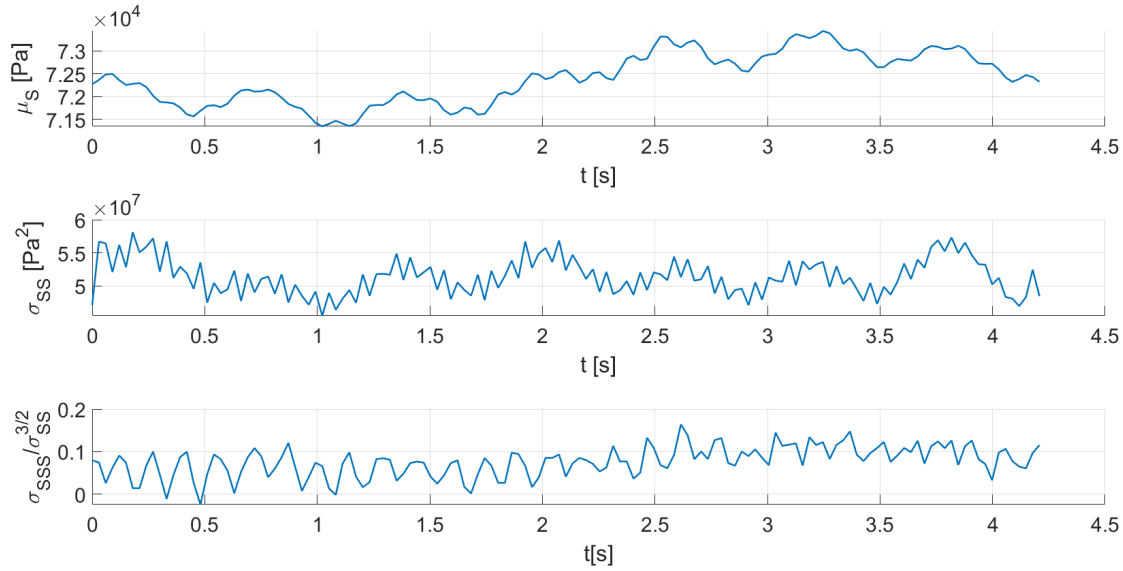


Figure 6.22: Mean, variance, and skewness of $S(t)$, Modal spectral MCS method

and 10^7 for the variance, the implication being that the consideration of mean alone, as is the case in deterministic modeling, would not provide a satisfactory assessment of the true extreme response. In a post-hoc way, this validates the choice of stochastic modeling for this type of problem. Concerning the normalized skewness coefficient, it is interesting to note the weak value of this indicator within the precision of the computations. As noted before, this coefficient is 0 of the Gaussian distribution, making it an easy test to detect non-Gaussianity, but zero skewness does not guarantee Gaussianity; it suggests a symmetric distribution. The result implies that the steady response of the design variable has an approximately symmetric distribution.

EVD and reliability The EVD of $S(t)$ is shown in Fig. 6.15; it has been calculated from the response samples obtained from the Modal spectral MCS method, along with their upper and lower 95% confidence bounds. As predicted by the values of the moment quantities of the design variable, in this scenario, the probability of the threshold established by the available resistance $R = 1.95 \times 10^5 \text{ Pa}$ is almost null. The main implication of this fact is that the limit state function is unlikely to cross into the unsafe region for the set extreme value threshold. If failure in the selected failure mode is to occur, it will do so during the early transient regime. Although it is recognized that a more exhaustive analysis could be performed, for instance, considering a much larger sample, the relationship between the transient regime and the steady-state regime holds.

5.4 Synthesis of extreme values and reliability indicators

The synthesis of the EVD analysis for the three loading scenarios considered is shown in Fig. 6.24, where the available resistance is shown in red for reference. In the steady-state, the probability of staying below the set threshold is practically 1; in the intermediate transient regime, as established earlier, the likelihood of staying below the set threshold is very high; conversely, in the early transient regime, the threshold is almost certainly crossed, resulting in failure of the system in the prescribed mode. These results suggest a very intuitive design reasoning: for extreme value analysis, the early stages of loading are the predominant consideration; the steady-state regime entails other failure modes, such as fatigue, under the assumption that the loading conditions persist in time, in which case the selected representative period of analysis could be considered as a descriptor of such loading long term history.

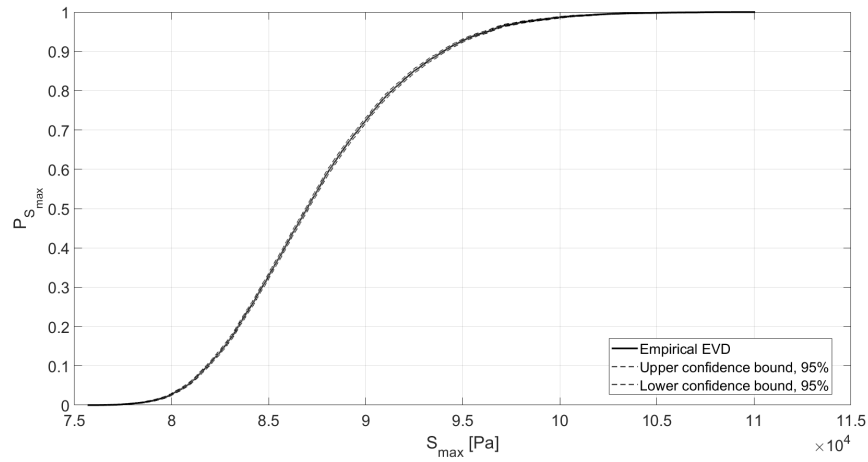


Figure 6.23: EVD estimation of $S(t)$, Modal spectral MCS method, interval $[nT_p, (n+1)T_p]$

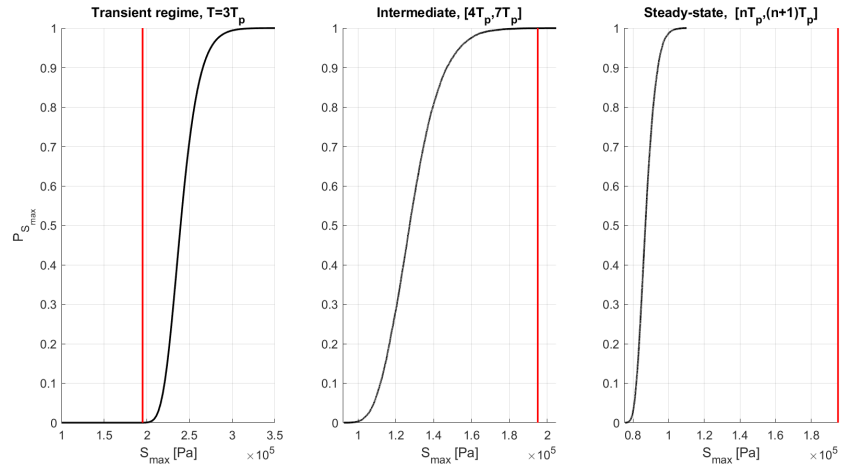


Figure 6.24: Synthesis of EVD in different regimes

From a broader perspective, we highlight the fact that this application has been developed for very particular conditions, permitting us to illustrate the proposed methods and arrive at clear conclusions for the structural analysis and design of tidal turbine blades. Once the response has been obtained from any of the proposed methodologies in any given regime, other failure modes can be easily considered by modifying the design or observable variable, and the methods established would remain viable. If lower probabilities of failure need to be assessed, conforming to established design considerations, the same methods presented here would still apply with an expanded sample in the case of MCS-based methodologies.

Conclusion and future work

« L'expérience à l'extrême du possible demande un renoncement néanmoins : cesser de vouloir être tout. »

George Bataille, L'expérience intérieure

This work aimed to study the response of a class of deterministic mechanical systems characterized by large rotations and elastic deformation elements to stochastic loads induced by environmental effects. The complexity of the problem demands a holistic approach that covers modeling decisions of the rotating mechanical system, a subset of these concerning the judicious description of the vibration of the elastic elements that are part of the system; it also covers rational modeling decisions to produce stochastic descriptions of environmental phenomena that act on the system causing its response; an effective strategy is required to obtain useful response descriptors. Much of the value of this effort rests on the applicability of the results obtained to concrete engineering practice, so a connection ought to be established with specific theories of analysis and design.

A robust analysis of previous results was established in the first chapter, offering a perspective on the evolution of the problem at hand and showing the connection with various parallel fields. The first antecedent of the rotating mechanical system is identified as the rotating beam problem, which was studied extensively in the early 20th century in helicopter and turbine design and analysis. A tendency to produce more elaborate models from this initial approach was evident in the literature. These more detailed models included aspects such as the coupled study of the rotating beam with the oscillating body supporting them: a disc on a shaft mounted on deformable supports, conventionally referred to as a rotor in much of the associated literature. However, much of the revised literature considers relatively simple descriptions of the motion of the rotor component and very particular solutions to the modeling of the rotating beam. The more elaborate models proved to yield systems of ordinary differential equations with periodic coefficients, and the connection between the study of the rotor-blade model with the theory of differential equations with periodic coefficients, Floquet theory, gained traction in the mid-20th century. It was shown that this Floquet approach extended to domains such as helicopter design and wind energy from a mechanical design and control design perspective. In parallel, a perspective of probabilistic mechanics was provided, particularly as it concerns the study of deterministic mechanical systems subjected to complex loads modeled as stochastic processes or, more broadly, as spatio-temporal stochastic fields. The problem of determining the probability of upcrossing of a certain threshold and its associate problem, the determination of the Extreme Value Distribution, were historically shown to be intimately linked to the study of the response in deterministic mechanical systems subjected to stochastic inputs.

A dynamical model for rotor-blade systems has been developed conforming to the general philosophy in this thesis: a reduced model that captures the rich behavior of the class of system under study. The theory of analytical mechanics has been integrated to produce a comprehensive description of the rotor component, modeled as a rigid body supported on elastic foundations. Three degrees of freedom in translation and two tilt angles have been included, addressing some of the limitations in much of the existing literature for this type of system, where planar motion is often assumed and decoupling in the axial direction of the shaft is enforced from a modeling perspective. The consideration of tilt has been shown to result in additional coupling and gyroscopic terms, a result that is consistent with theoretical expectations but is presented here in concrete terms. Similarly, the

deformation of elastic elements, the blades, includes the two main deformation modes: spanwise (or in-plane) and flapwise (out-of-plane). The coupling between these two flexion modes has been introduced by applying the corresponding constitutive material behavior law, addressing a simplification that appears to be pervasive in the respective literature. The description of blade vibration has been carried out in a modal form, producing an intuitive interpretation of the vibrational response in the generalized modal variables; this stands in contrast to the popular approach of spatial discretization with finite element methods. The developments strike a balance between concreteness and flexibility: although specific choices have been made, the expressions provided allow for the adaptation of the general model to different scenarios. As shown, the model can be reduced to the planar motion case with ease; it can also be implemented using different constitutive laws in the material of the blades and with the appropriate description of the modal behavior of the blade to different blade geometries.

An analysis of the rotor-blade model reveals, as theoretically expected, strong nonlinearities inherent to the general motion of the rigid body describing the rotor. While these nonlinearities have been ignored under small-angle assumptions, the result may have interesting research prospects when considered from a design perspective. While outside of the scope of this work, it is the case that certain nonlinear mechanisms have been studied for their vibration suppression characteristics (for instance, Nonlinear Energy Sinks, NES). We consider this a potential avenue for future inquiry.

The dynamical model is a system of ordinary differential equations with periodic coefficients. In this context, the existing results from Floquet theory and its implementations across many disciplines have been synthesized into a modal theory for LTP systems. The development adopted here highlights the connections among results available in the literature and presents these results as an extension of linear time-invariant (LTI) or "standard" modal analysis. The LTI frequency is replaced by the Lyapunov Characteristic Exponents; the LTI normal modes or eigenvectors are replaced with Floquet modes or periodic eigenvectors; the test solution broadly utilized in LTI analysis has been shown to have an equivalent in the modulated complex exponential form, as already proposed in works such as Xu & Garsch ([151]) and Wereley ([144]). The indeterminacy of the characteristic exponents has been elucidated from its origin in the complex logarithm function, and the formula proposed by Peters ([100, 99]), as well as his perspective on the subject, has been used to provide a cogent description of the characteristic exponents and their associated periodic eigenvectors. Instead of indeterminacy, the interpretation is more accurately characterized as a free choice of integer multiples on the imaginary part of the complex logarithm. It has also been shown by example that, because the Floquet modes diagonalize the matrix of the system, so-called "mixed" sets of characteristic exponents are viable choices. In our context, a mixed set is a set of characteristic exponents with different integer multiples added to its imaginary part. A new methodology to study and select candidate periodic eigenvectors has been proposed, based on time-frequency representations as instantiated by the PGHW class of Wavelets and making use of an intuitive yet innovative result that extends the notion of change of basis in traditional vector spaces to change of Hilbert basis in Hilbert spaces, where the corresponding Hilbert space reflects the representation basis. This approach allows the passage from the traditional Fourier basis to the polychromatic time-frequency basis formed by Periodic Generalized Harmonic Wavelets.

A new notation and moment propagation strategy has been applied in the response study, adapted from an important antecedent of this work, Suptille ([134]). The convenience of this methodology is illustrated with examples in Chapter 4, where many results from the literature are easily recovered, and the convenience for the treatment of stochastic loads is shown in the same chapter and Chapter 5 when Floquet modal theory is integrated into the description. An extensive example from offshore engineering is developed in chapter 4, the mechanical moment of a rigid pile under the effects of Morison load. The case of scalar processes and that of fields are considered, the latter requiring an integral transformation of the velocity and acceleration stochastic fields. The moment propagation scheme is contrasted with the converged Monte-Carlo simulation regarding precision and computational cost. The PDF of the response has been reconstructed employing a maximum entropy approach with 2 and 4 moments; these are equally compared to statistical analysis of the Monte-Carlo results, showing that the 4-moment PDF result is satisfactory for this type of response. The innovative aspects of the development presented are a) the modeling of inputs as spatiotemporal fields, b) the four-moment maximum entropy implementation through an optimization problem with enhanced initial point, c) intermediate results that are valid for a broad class of stochastic fields, applying the Gaussian property on the underlying velocity

field at a late stage in the development. In addition, concerning a), to our knowledge, this is a new computational approach to the handling of stochastic fields in this domain: instead of approximating the field by a discrete mesh of processes, the underlying moment functions have been implemented as numerical functions and combined with an adaptive step integration scheme. The advantage of this implementation is that the spatial discretization is automatically adjusted from tolerance constraints enforced by the integrator. The notation framework in the corresponding chapter has made this approach possible.

The proposed moment propagation strategy has been extended to the nonstationary case. First, a scalar Gaussian process is considered, where the nonstationarity comes from a periodic modulation of an underlying stationary process. Expressions for the instantaneous moments and correlation and covariance functions are provided, as before: first for the general case and later for the particular Gaussian case. The oscillating mean and variance that result from moment propagation are utilized to analyze the upcrossing of the response. The probability of the event of the response process crossing a certain level has been approximated in a simple fashion, what we refer to as the interval approximation method: the response is discretized in "nodes" of high variance, and each node is considered as an independent event, and its crossing probability is calculated using traditional expressions for stationary Gaussian processes, the total crossing probability is computed as the product of the nodal probabilities. The approach has proved very effective and coincides with the benchmarks selected to control for accuracy: two Monte-Carlo methodologies based, respectively, on statistical analysis of the response and in the direct verification of crossings of the generated ensemble. The approach appears promising to address the limitations around nongaussian processes. However, some work remains to be done on this front. Alternatively, the ubiquitous Rice formula was directly applied to the simulation results, providing the mean upcrossing number and the EVD of the response.

The Floquet modal analysis and the load modeling have revealed some important characteristics of the form of the response. First, from an applied perspective, the load acting on the class of LTP system under consideration is nonstationary, given the relative motion between flow and structure, which introduces a first form of time-dependent modulation on the loads. Second, the forced response admits a Floquet modal representation, which implies that the total forced response is a sum of terms modulated by the corresponding periodic Floquet eigenvectors.

Two methods have been proposed to study the stochastic response: a time-domain method based on the convolution of the load with the impulse response in the Floquet modal variables and a frequency-domain method based on the spectral characterization of load and Floquet periodic modes. An MCS simulation methodology has also been implemented to complement these two approaches. The strengths and limitations of each method are described. The Floquet convolution in the time domain effectively describes the transient regime; the MCS spectral method describes the steady-state regime. The tools introduced accommodate for the entire motion regime of the model.

The results obtained throughout this work have been applied to the practical problem of reliability analysis of a tidal turbine. A stochastic velocity field with wave, current, and ambient turbulence has been simulated. The dynamical model has been fitted to a horizontal axis tidal turbine with two blades. The loads have been applied over the dynamical model by implementing a BEMT numerical tool. The normal stress resulting from the maximal blade root bending moment has been defined as the failure mode, and it has been shown that this reliability problem is time-dependent on account of the nonstationary response. The probability of failure has been obtained through the estimated EVD. The approach taken in this work is slightly more general than other recent works that use stochastic modeling to describe loads. The dynamical model is more detailed than the surveyed reduced-order models found in the literature, including tilt motion, several modal degrees of freedom to describe blade vibration, and flapwise and spanwise deformation directions. Compared with full-scale, finite element models with complex CFD simulation, the advantage we identify in the present work comes from its treatment of the coupled mechanical behavior and the modal interpretation made possible by the choice of blade description and the results synthesized in the Floquet analysis of the system.

Future work

Several research avenues can be envisioned as continuations of the present work, some very direct, others tangentially related to some of our results and developments. In order of proximity, these are outlined as follows:

1. Calibrating the proposed model to an experimental setting. The theoretical results might offer useful predictions of vibratory behavior on tidal prototypes, a growing area of applied research and development.
2. Some elements of the theory of stochastic processes appear to apply to the Floquet modal representation established in this thesis, the most promising being the Priestley representation of evolutionary stochastic processes and the Wigner spectrum.
3. A possible connection between the Floquet representation of the forced response and the Karhunen–Loève decomposition of stochastic processes seems promising. The connection can be noticed from the input-output relationships established here between the covariance functions. It remains to be explored how the eigenfunctions, in the K-L sense, may be related to the eigenfunctions of the forced response of the system, which will be related to the system eigenfunctions in the Floquet sense. This treatment could provide a modal way of relating input and output and could lead to improved simulation schemes for the stochastic response.
4. The eigenvalue problem in Hill’s method is the source of an open problem in the state of the art, as the method provides a multiplicity of viable characteristic exponents and associated eigenvectors. This is often called in the literature the sorting problem or filtering problem. Hill’s method relies on Fourier series expansion of the periodic terms; its limitations have been discussed extensively in this work. A time-frequency representation has been proposed in this work, and the PGHW and a transformation theorem are the basis of the proposed methodology: Fourier expansion, resolution of the eigenvalue problem, and projection onto the selected time-frequency basis. It remains to be seen if the associated eigenvalue problem inherent to the Hill development can be directly formulated in terms of other basis functions, and whether a more efficient basis might simplify the computational effort, or ease the sorting problem. The potential of the change of basis methodology, considering other time-frequency representations, is also to be explored.
5. The nonlinearities inherent to the general rotor motion have been linearized in this work. Studying a nonlinear version of this model seems an interesting venture from the design perspective. This would imply a combination of two generalizations of the normal mode approach prevalent in LTI dynamics: one is the Floquet version presented in this thesis, and the other is that of Nonlinear Normal Modes prevalent in nonlinear systems. This would result in a modal theory of Nonlinear time-periodic systems (NLTP).
6. Vibration suppression could be studied from the framework provided here in connection with the previous point. The effects of nonlinear energy sinks (NES) or other components could be established by capitalizing on the modal and frequency representation provided here.
7. The most challenging aspect of the present work pertains to the description of general stochastic quantities. While moment propagation with PDF reconstruction has proved efficacious to the particular cases studied here, which are justified by the applications, it would be satisfactory to consider other methodologies that accommodate more general distributions. Some techniques were identified during the preparation of this thesis; these offer a direct estimation of the PDF as opposed to moment-base reconstruction or fitting. However, considerable effort is required in the complete application of these theories. Among these, we can identify: a) projection methods based on Polynomial Chaos; b) Galerkin approximate solutions of an adapted version of the Fokker-Planck-Kolmogorov equations, providing the evolution of the PDF of the response. This latter approach requires formulating the problem as a proper stochastic differential equation, an approach we have not covered in this work.

8. In relation to the previous point, extreme value theory remains challenging. While judicious approximations can be effectively exploited in some cases, and "brute force" high sampling Monte-Carlo simulation can complement this approach, as has been done in this work, a more general treatment of the subject would be desirable. Some theoretical developments were identified in the literature during the preparation of this work, but again, their application to complex models is far from trivial. In this sense, the works of Piterbarg and Konstantinides ([74]) seem to be a relevant starting point.
9. Finally, following the trends in reliability and probabilistic mechanics, the feasibility of applying machine learning strategies could be explored.

Bibliography

- [1] V. Ambekar, R. Kuppa, and S. Gupta. Multivariate Extreme Value Distributions for Vector of Non-stationary Gaussian Processes. *Procedia Engineering*, 144:504–511, 2016.
- [2] J. J. M. Baar. Extreme values of Morison-type processes. *Applied Ocean Research*, 14(1):65–68, jan 1992.
- [3] L. Bachelet, N. Driot, and J. Perret-Liaudet. A Spectral Method for Describing the Response of a Parametrically Excited System Under External Random Excitation. *Journal of Computational and Nonlinear Dynamics*, 3(1), nov 2007.
- [4] H. Bae, I. M. Boyd, E. B. Carper, and J. Brown. Accelerated Multifidelity Emulator Modeling for Probabilistic Rotor Response Study. *Journal of Engineering for Gas Turbines and Power*, 141(12), nov 2019.
- [5] A. Balestrino, A. Caiti, A. Noe', and F. Parenti. Maximum entropy based numerical algorithms for approximation of probability density functions. In *2003 European Control Conference (ECC)*. IEEE, sep 2003.
- [6] O. A. Bauchau. *Flexible Multibody Dynamics*. Springer Netherlands, 2011.
- [7] F. Bayer and R. I. Leine. Sorting-free Hill-based stability analysis of periodic solutions through Koopman analysis. *Nonlinear Dynamics*, 111(9):8439–8466, feb 2023.
- [8] B. J. Bentvelsen. *Modal analysis of structures in time-periodic elastic state*. PhD thesis, Sorbonne Université, 2018.
- [9] G. Bir. Multi-blade coordinate transformation and its application to wind turbine analysis. In *46th AIAA aerospace sciences meeting and exhibit*, page 1300, 2008.
- [10] G. S. Bir, M. J. Lawson, and Y. Li. Structural design of a horizontal-axis tidal current turbine composite blade. In *International Conference on Offshore Mechanics and Arctic Engineering*, volume 44373, pages 797–808, 2011.
- [11] B. Boashash. *Time frequency signal analysis and processing: A comprehensive reference*. Elsevier, 2003.
- [12] L. E. Borgman. Random Hydrodynamic Forces on Objects. *The Annals of Mathematical Statistics*, 38(1):37–51, 1967.
- [13] L. E. Borgman. Statistical models for ocean waves and wave forces. 8:139–181, 1972.
- [14] C. L. Bottasso and S. Cacciola. Model-independent periodic stability analysis of wind turbines. *Wind Energy*, 18(5):865–887, mar 2014.
- [15] H. Bremer. *Elastic Multibody Dynamics*. Springer Science + Business Media B.V, 2008.

- [16] L. Caracoglia. Stochastic Dynamics of Rotating Wind Turbine Blades Influenced by Turbulence and Aeroelastic Uncertainties: Recent Developments. In *Volume 7B: Dynamics, Vibration, and Control*. American Society of Mechanical Engineers, nov 2021.
- [17] W. Carnegie. Vibrations of Rotating Cantilever Blading: Theoretical Approaches to the Frequency Problem Based on Energy Methods. *Journal of Mechanical Engineering Science*, 1(3):235–240, dec 1959.
- [18] C. Cattani and A. Kudreyko. Application of Periodized Harmonic Wavelets towards Solution of Eigenvalue Problems for Integral Equations. *Mathematical Problems in Engineering*, 2010:1–8, 2010.
- [19] T. Chatterjee, A. Essien, R. Ganguli, and M. I. Friswell. The stochastic aeroelastic response analysis of helicopter rotors using deep and shallow machine learning. *Neural Computing and Applications*, 33(23):16809–16828, jul 2021.
- [20] C. Chicone. *Ordinary Differential Equations with Applications*. Springer New York, 2006.
- [21] G. Christakos. *Spatiotemporal Random Fields*. Elsevier, second edition edition, 2017.
- [22] R. H. Christensen. *Active Vibration Control of Rotor-blade Systems: Theory and Experiment*. Department of Mechanical Engineering, Technical University of Denmark, 2004.
- [23] T. Clara, J. A. C. F. D. Campos, and J. Baltazar. *Added mass effects on the natural frequencies of marine current turbine blades*. PhD thesis, MsC Thesis, KIT, Karlsruhe, 2014.
- [24] S. H. Crandall. *Random Vibration*. Published jointly by the Technology Press of the Massachusetts Institute of Technology, 1958.
- [25] P. Crimi. A method for analyzing the aeroelastic stability of a helicopter rotor in forward flight. Technical report, NASA, 1969.
- [26] F. Z. de Arcos, C. R. Vogel, and R. H. J. Willden. A parametric study on the hydrodynamics of tidal turbine blade deformation. *Journal of Fluids and Structures*, 113:103626, aug 2022.
- [27] E. Denimal and J.-J. Sinou. Advanced computational technique based on kriging and Polynomial Chaos Expansion for structural stability of mechanical systems with uncertainties. *Journal of Engineering Mathematics*, 130(1), sep 2021.
- [28] P. Diaconis. Application of the method of moments in probability and statistics. *Moments in mathematics*, 37:125–142, 1987.
- [29] S. Draycott, A. Nambiar, B. Sellar, T. Davey, and V. Venugopal. Assessing extreme loads on a tidal turbine using focused wave groups in energetic currents. *Renewable Energy*, 135:1013–1024, may 2019.
- [30] R. Durrett. *Probability: theory and examples*, volume 49. Cambridge university press, 2019.
- [31] K. Dziejciech and W. J. Staszewski. Wavelet-based transmissibility for the analysis of time-variant systems. *Mechanical Systems and Signal Processing*, 145:106918, nov 2020.
- [32] G. Failla, M. Pappatoco, and G. A. Cundari. A wavelet-based spectrum for non-stationary processes. *Mechanics Research Communications*, 38(5):361–367, jul 2011.
- [33] C. Faudot and O. G. Dahlhaug. Prediction of Wave Loads on Tidal Turbine Blades. *Energy Procedia*, 20:116–133, 2012.
- [34] F. J. Ferrante, S. R. Arwade, and L. L. Graham-Brady. A translation model for non-stationary, non-Gaussian random processes. *Probabilistic Engineering Mechanics*, 20(3):215–228, jul 2005.
- [35] G. Floquet. Sur les équations différentielles linéaires à coefficients périodiques. In *Annales scientifiques de l'École normale supérieure*, volume 12, pages 47–88, 1883.

- [36] M. Fluck and C. Crawford. A fast stochastic solution method for the Blade Element Momentum equations for long-term load assessment. *Wind Energy*, 21(2):115–128, nov 2017.
- [37] P. Friedmann, C. E. Hammond, and T.-H. Woo. Efficient numerical treatment of periodic systems with application to stability problems. *International Journal for Numerical Methods in Engineering*, 11(7):1117–1136, 1977.
- [38] P. P. Friedmann. Numerical methods for determining the stability and response of periodic systems with applications to helicopter rotor dynamics and aeroelasticity. *Computers & mathematics with applications*, 12(1):131–148, 1986.
- [39] M. I. Friswell. *Dynamics of rotating machines*. Cambridge university press, 2010.
- [40] R. Ganguli. *Finite Element Analysis of Rotating Beams*. Springer Singapore, 2017.
- [41] B. Gaurier, P. Davies, A. Deuff, and G. Germain. Flume tank characterization of marine current turbine blade behaviour under current and wave loading. *Renewable Energy*, 59:1–12, nov 2013.
- [42] G. Genta. *Dynamics of Rotating Systems*. Springer, 2005.
- [43] M. Géradin and D. J. Rixen. *Mechanical vibrations theory and application to structural dynamics*. Wiley, 2014.
- [44] T. Gmür. *Dynamique des structures: analyse modale numérique*. PPUR presses polytechniques, 1997.
- [45] C. Gong and D. M. Frangopol. An efficient time-dependent reliability method. *Structural Safety*, 81:101864, nov 2019.
- [46] M. Grigoriu. Crossings of Non-Gaussian Translation Processes. *Journal of Engineering Mechanics*, 110(4):610–620, apr 1984.
- [47] M. Grigoriu. Extremes of Wave Forces. *Journal of Engineering Mechanics*, 110(12):1731–1742, dec 1984.
- [48] S. Gupta and C. S. Manohar. Multivariate extreme value distributions for random vibration applications. *Journal of engineering mechanics*, 131(7):712–720, 2005.
- [49] S. Han and O. A. Bauchau. Simulation and stability analysis of periodic flexible multibody systems. *Multibody System Dynamics*, 50(4):381–413, may 2020.
- [50] X. Han, O. S. Jiménez, and E. Pagnacco. Response and EPSD of rotor-blade nonlinear system with non-stationary non-Gaussian stochastic excitation via PGHW method. *Computers & Mathematics with Applications*, 142:140–156, jul 2023.
- [51] M. H. Hansen. Modal dynamics of structures with bladed isotropic rotors and its complexity for two-bladed rotors. *Wind Energy Science*, 1(2):271–296, nov 2016.
- [52] A. M. Hasofer and P. Petocz. Extreme Response of the Linear Oscillator with Modulated Random Excitation. In *Statistical Extremes and Applications*, pages 503–512. Springer Netherlands, 1984.
- [53] J. He. Structural first failure times under non-Gaussian stochastic behavior. *Applied Mathematics and Mechanics*, 28(11):1487–1494, 2007.
- [54] G. W. Hill. Mean motion of the lunar perigee. *Acta Math*, 8(1):1, 1886.
- [55] M. A. Holst, O. G. Dahlhaug, and C. Faudot. CFD Analysis of Wave-Induced Loads on Tidal Turbine Blades. *IEEE Journal of Oceanic Engineering*, 40(3):506–521, jul 2015.

- [56] H. P. Hong. On the estimation of the evolutionary power spectral density. *Mechanical Systems and Signal Processing*, 190:110131, may 2023.
- [57] Z. Hu and X. Du. Time-dependent reliability analysis with joint upcrossing rates. *Structural and Multidisciplinary Optimization*, 48(5):893–907, jun 2013.
- [58] Z. Hu, H. Li, X. Du, and K. Chandrashekhara. Simulation-based time-dependent reliability analysis for composite hydrokinetic turbine blades. *Structural and Multidisciplinary Optimization*, 47(5):765–781, sep 2012.
- [59] S. Ilanko, L. Monterrubio, and Y. Mochida. *The Rayleigh-Ritz method for structural analysis*. John Wiley & Sons, 2014.
- [60] Y. Ishida and T. Yamamoto. *Linear and Nonlinear Rotordynamics: A Modern Treatment with Applications*. Wiley & Sons, 2013.
- [61] L. Isserlis. On a Formula for the Product-Moment Coefficient of any Order of a Normal Frequency Distribution in any Number of Variables. *Biometrika*, 12(1/2):134, nov 1918.
- [62] J. J. Jensen. Extreme value predictions and critical wave episodes for marine structures by FORM. *Ships and Offshore Structures*, 3(4):325–333, dec 2008.
- [63] J. J. Jensen. Extreme value predictions using Monte Carlo simulations with artificially increased load spectrum. *Probabilistic Engineering Mechanics*, 26(2):399–404, apr 2011.
- [64] O. S. Jiménez, X. Han, E. Pagnacco, and R. Sampaio. Representations of the frequency response of linear time-periodic systems: adapting to stochastic excitations. In *Proceedings of the XIX International Symposium on Dynamic Problems of Mechanics*. ABCM, 2023.
- [65] O. S. Jimenez, E. Pagnacco, E. S. de Cursi, and R. Sampaio. Estimation of the Extreme Response Probability Distribution of Offshore Structures Due to Current and Turbulence. In *Lecture Notes in Mechanical Engineering*, pages 306–322. Springer International Publishing, aug 2020.
- [66] W. Johnson. *Helicopter theory*. Courier Corporation, 2012.
- [67] J. L. Junkins. *Introduction to dynamics and control of flexible structures*. American Institute of Aeronautics and Astronautics, 1993.
- [68] B. S. Kallesøe. Equations of motion for a rotor blade, including gravity, pitch action and rotor speed variations. *Wind Energy*, 10(3):209–230, 2007.
- [69] W. G. Kelley and A. C. Peterson. *The Theory of Differential Equations*. Springer New York, 2010.
- [70] Y. A. Khulief and Y. Laejoon. Lead-lag vibrational frequencies of a rotating beam with end mass. *Computers & Structures*, 29(6):1075–1085, jan 1988.
- [71] P. K. Koliopoulos. Quasi-static and dynamic response statistics of linear SDOF systems under Morison-type wave forces. *Engineering Structures*, 10(1):24–36, 1988.
- [72] V. Konakov, V. Panov, and V. Piterbarg. Extremes of a class of non-stationary Gaussian processes and maximal deviation of projection density estimates. *Extremes*, 24(3):617–651, feb 2021.
- [73] F. Kong, S. Li, and W. Zhou. Wavelet-Galerkin approach for power spectrum determination of nonlinear oscillators. *Mechanical Systems and Signal Processing*, 48(1-2):300–324, oct 2014.
- [74] D. G. Konstant and V. I. Piterbarg. Extreme values of the cyclostationary Gaussian random process. *Journal of Applied Probability*, 30(1):82–97, mar 1993.

- [75] E. Kosko. The Free Uncoupled Vibrations of a Uniformly Rotating Beam,. *Institute of Aerophysics, University of Toronto*, March 1960.
- [76] R. Kumar, S. F. Ali, and S. Gupta. Stochastic reduced order modelling and analysis of rotating bladed discs. *Proceedings of the Royal Society A: Mathematical, Physical and Engineering Sciences*, 478(2260), apr 2022.
- [77] Y. Kumar. The Rayleigh–Ritz method for linear dynamic, static and buckling behavior of beams, shells and plates: A literature review. *Journal of Vibration and Control*, 24(7):1205–1227, feb 2017.
- [78] M. R. Leadbetter. On Crossings of Levels and Curves by a Wide Class of Stochastic Processes. *The Annals of Mathematical Statistics*, 37(1):260–267, 1966.
- [79] M. Lewis, S. P. Neill, P. Robins, M. R. Hashemi, and S. Ward. Characteristics of the velocity profile at tidal-stream energy sites. *Renewable Energy*, 114:258–272, dec 2017.
- [80] Q. Li, V. Venugopal, and N. Barltrop. Modelling dynamic loadings of a tidal stream turbine in combined wave-current-turbulence environment. *Sustainable Energy Technologies and Assessments*, 50:101795, mar 2022.
- [81] Z.-M. Li, T. Liu, H. Kang, J. Tian, J. Jing, and D. Wang. Theoretical and experimental investigations on steady-state responses of rotor-blade systems with varying rotating speeds based on a new nonlinear dynamic model. *Mechanical Systems and Signal Processing*, 184:109692, feb 2023.
- [82] G. Lindgren. A note on the extremal properties of the morison equation. *Ocean Engineering*, 11(5):543–548, jan 1984.
- [83] G. Lindgren. Gaussian Integrals and Rice Series in Crossing Distributions—to Compute the Distribution of Maxima and Other Features of Gaussian Processes. *Statistical Science*, 34(1), feb 2019.
- [84] L. D. Lutes. Counting level crossings by a stochastic process. *Probabilistic Engineering Mechanics*, 22(3):293–300, jul 2007.
- [85] L. D. Lutes and S. Sarkani. *Random vibrations: analysis of structural and mechanical systems*. Butterworth-Heinemann, 2004.
- [86] É. Mathieu. Mémoire sur le mouvement vibratoire d’une membrane de forme elliptique. *Journal de mathématiques pures et appliquées*, 13:137–203, 1868.
- [87] L. Meirovitch. *Fundamentals of vibrations*. Waveland Press, 2010.
- [88] I. A. Milne, R. N. Sharma, R. G. J. Flay, and S. Bickerton. Characteristics of the turbulence in the flow at a tidal stream power site. *Philosophical Transactions of the Royal Society A: Mathematical, Physical and Engineering Sciences*, 371(1985):20120196, feb 2013.
- [89] G. Moe. Long-term wave-force statistics for a vertical pile. *Coastal Engineering*, 2:297–311, jan 1978.
- [90] J. R. Morison, J. W. Johnson, and S. A. Schaaf. The Force Exerted by Surface Waves on Piles. *Journal of Petroleum Technology*, 2(05):149–154, may 1950.
- [91] A. Naess. Prediction of extremes of morison-type loading—An example of a general method. *Ocean Engineering*, 10(5):313–324, jan 1983.
- [92] A. Naess, O. Gaidai, and S. Haver. Efficient estimation of extreme response of drag-dominated offshore structures by Monte Carlo simulation. *Ocean Engineering*, 34(16):2188–2197, nov 2007.
- [93] A. Naess and T. Moan. *Stochastic Dynamics of Marine Structures*. 2009.

- [94] G. Najafian. Probability models for offshore structural response due to Morison wave loading. *Ocean Engineering*, 34(17-18):2289–2299, dec 2007.
- [95] D. E. Newland. *An introduction to random vibrations, spectral & wavelet analysis*. Courier Corporation, 2012.
- [96] O. M. O’Reilly. *Intermediate Dynamics for Engineers: Newton-Euler and Lagrangian Mechanics*. Cambridge University Press, 2020.
- [97] M. H. B. Osman and R. Willden. Added mass and damping forces of a floating tidal turbine undergoing pendulum motion. *Ocean Engineering*, 283:115014, sep 2023.
- [98] A. Papoulis and U. Pillai. *Probability, random variables and stochastic processes*. McGraw-Hill, fourth edition, Nov. 2001.
- [99] D. A. Peters and K. H. Hohenemser. Application of the Floquet transition matrix to problems of lifting rotor stability. *Journal of the American Helicopter Society*, 16(2):25–33, 1971.
- [100] D. A. Peters, S. M. Lieb, and L. A. Ahaus. Interpretation of Floquet Eigenvalues and Eigenvectors for Periodic Systems. *Journal of the American Helicopter Society*, 56(3):1–11, jul 2011.
- [101] T. Pflumm, L. Gaugelhofer, V. Heuschneider, F. Berghammer, and M. Hajek. Hybrid Experimental Measurement of Sectional Stiffness Properties of the MERIT Rotor Blade with Digital Image Correlation. In *Presented at 47th European Rotorcraft Forum*, volume 7, page 9th, 2021.
- [102] K.-K. Phoon, H. W. Huang, and S. T. Quek. Simulation of strongly non-Gaussian processes using Karhunen–Loeve expansion. *Probabilistic engineering mechanics*, 20(2):188–198, 2005.
- [103] D. A. Prelewicz. Response of linear periodically time varying systems to random excitation. *AIAA Journal*, 10(8):1124–1125, 1972.
- [104] A. Preumont. *Random vibration and spectral analysis*. Kluwer Academic, 1994.
- [105] A. Preumont. *Twelve lectures on structural dynamics*, volume 198. Springer, 2013.
- [106] M. B. Priestley. Evolutionary spectra and non-stationary processes. *Journal of the Royal Statistical Society: Series B (Methodological)*, 27(2):204–229, 1965.
- [107] M. B. Priestley. Power spectral analysis of non-stationary random processes. *Journal of Sound and Vibration*, 6(1):86–97, 1967.
- [108] S. Putter and H. Manor. Natural frequencies of radial rotating beams. *Journal of Sound and Vibration*, 56(2):175–185, jan 1978.
- [109] R. H. Rand. *Lecture notes on nonlinear vibrations*. 2012.
- [110] R. B. Randall, J. Antoni, and W. A. Smith. A survey of the application of the cepstrum to structural modal analysis. *Mechanical Systems and Signal Processing*, 118:716–741, mar 2019.
- [111] S. S. Rao. *Mechanical vibrations*. Prentice Hall, 2010.
- [112] S. O. Rice. Mathematical analysis of random noise. *The Bell System Technical Journal*, 23(3):282–332, 1944.
- [113] S. O. Rice. Mathematical analysis of random noise. *The Bell System Technical Journal*, 24(1):46–156, 1945.
- [114] J. E. T. Robert J. Adler. *Random Fields and Geometry*. Springer New York, 2007.

- [115] M. L. Sæterstad. Dimensioning loads for a tidal turbine. Master's thesis, Institutt for energi-og prosesssteknikk, 2011.
- [116] M. Sandsten. Time-frequency analysis of time-varying signals and non-stationary processes. *Lund University*, 2016.
- [117] G. T. Scarlett and I. M. Viola. Unsteady hydrodynamics of tidal turbine blades. *Renewable Energy*, 146:843–855, feb 2020.
- [118] P. Schinas, D. I. Manolas, V. A. Riziotis, and S. G. Voutsinas. Aeroelastic modal dynamics of floating wind turbines in anisotropic conditions based on Floquet analysis. *Journal of Physics: Conference Series*, 2265(4):042005, may 2022.
- [119] G. Schmidt. *Yakubovich, V. A./Starzhinskii, V. M., Linear Differential Equations with Periodic Coefficients, Vol. 1 und 2*, volume 56. Wiley, 1976.
- [120] S. Scholl. Fourier, Gabor, Morlet or Wigner: Comparison of Time-Frequency Transforms. *arXiv preprint arXiv:2101.06707*, 2021.
- [121] G. I. Schuëller. Developments in stochastic structural mechanics. *Archive of Applied Mechanics*, 75(10-12):755–773, aug 2006.
- [122] M. D. Shields, G. Deodatis, and P. Bocchini. A simple and efficient methodology to approximate a general non-Gaussian stationary stochastic process by a translation process. *Probabilistic Engineering Mechanics*, 26(4):511–519, oct 2011.
- [123] M. Shinozuka and C. M. Jan. Digital simulation of random processes and its applications. *Journal of sound and vibration*, 25(1):111–128, 1972.
- [124] S. C. Sinha and D. H. Wu. An efficient computational scheme for the analysis of periodic systems. *Journal of Sound and Vibration*, 151(1):91–117, 1991.
- [125] P. F. Skjoldan and M. H. Hansen. On the similarity of the Coleman and Lyapunov–Floquet transformations for modal analysis of bladed rotor structures. *Journal of Sound and Vibration*, 327(3-5):424–439, nov 2009.
- [126] M. Slama, G. Pinon, C. E. Hadi, M. Togneri, B. Gaurier, G. Germain, J.-V. Facq, J. Nuño, P. Mansilla, E. Nicolas, J. Marcille, and A. Pacheco. Turbine design dependency to turbulence: An experimental study of three scaled tidal turbines. *Ocean Engineering*, 234:109035, aug 2021.
- [127] C. G. Soares, editor. *Probabilistic Methods for Structural Design*. Springer Netherlands, 1997.
- [128] E. Souza de Cursi and R. Sampaio. *Modeling and Convexity*. Wiley Online Library, 2010.
- [129] P. D. Spanos, F. Kong, J. Li, and I. A. Kougoumtzoglou. Harmonic wavelets based excitation–response relationships for linear systems: A critical perspective. *Probabilistic Engineering Mechanics*, 44:163–173, apr 2016.
- [130] P. D. Spanos and I. A. Kougoumtzoglou. Harmonic wavelets based statistical linearization for response evolutionary power spectrum determination. *Probabilistic Engineering Mechanics*, 27(1):57–68, jan 2012.
- [131] J. M. Spires and S. C. Sinha. On the response of linear time-periodic systems subjected to deterministic and stochastic excitations. *Journal of Vibration and Control*, 2(2):219–249, 1996.
- [132] M. St Denis and W. J. Pierson. On the motions of ships in confused seas. *Trans. SnAMe*, 61:280–357, 1953.

- [133] B. Sudret. Analytical derivation of the outcrossing rate in time-variant reliability problems. *Structure and Infrastructure Engineering*, 4(5):353–362, oct 2008.
- [134] M. Suptille. *Caractérisation temporelle et spectrale de champs instationnaires non gaussiens : application aux hydroliennes en milieu marin*. PhD thesis, 2015. Thèse de doctorat de l’INSA de Rouen Normandie, INSA.
- [135] M. Suptille, E. Pagnacco, L. Khalij, J. E. Cursi, and J. Brossard. Generation of stationary Gaussian processes and extreme value distributions for high-cycle fatigue models-application to tidal stream Turbines. *Journal of the Brazilian Society of Mechanical Sciences and Engineering*, 34:640–651, 2012.
- [136] A. Tagliani. On the application of maximum entropy to the moments problem. *Journal of Mathematical Physics*, 34(1):326–337, jan 1993.
- [137] J. Thomson, B. Polagye, V. Durgesh, and M. C. Richmond. Measurements of Turbulence at Two Tidal Energy Sites in Puget Sound, WA. *IEEE Journal of Oceanic Engineering*, 37(3):363–374, jul 2012.
- [138] M. J. Tucker, P. G. Challenor, and D. J. T. Carter. Numerical simulation of a random sea: a common error and its effect upon wave group statistics. *Applied ocean research*, 6(2):118–122, 1984.
- [139] D. V. Val, L. Chernin, and D. V. Yurchenko. Reliability analysis of rotor blades of tidal stream turbines. *Reliability Engineering & System Safety*, 121:26–33, 2014.
- [140] S. Walker and P. R. Thies. A review of component and system reliability in tidal turbine deployments. *Renewable and Sustainable Energy Reviews*, 151:111495, nov 2021.
- [141] F. Y. M. Wan. Nonstationary response of linear time-varying dynamical systems to random excitation. *Journal of Applied Mechanics*, 40(2):422–428, jun 1973.
- [142] G. Wanner and E. Hairer. *Solving ordinary differential equations II*, volume 375. Springer Berlin Heidelberg New York, 1996.
- [143] S. Weber, T. Kissinger, E. Chehura, S. Staines, J. Barrington, K. Mullaney, L. Z. Fragonara, I. Petrunin, S. James, M. Lone, and R. Tatam. Application of fibre optic sensing systems to measure rotor blade structural dynamics. *Mechanical Systems and Signal Processing*, 158:107758, sep 2021.
- [144] N. M. Wereley. *Analysis and control of linear periodically time varying systems*. PhD thesis, Massachusetts Institute of Technology, 1990.
- [145] S. R. Winterstein. Nonlinear Vibration Models for Extremes and Fatigue. *Journal of Engineering Mechanics*, 114(10):1772–1790, oct 1988.
- [146] S. R. Winterstein and T. Kashef. Moment-based load and response models with wind engineering applications. *J. Sol. Energy Eng.*, 122(3):122–128, 2000.
- [147] S. R. Winterstein and C. A. MacKenzie. Extremes of nonlinear vibration: Comparing models based on moments, L-moments, and maximum entropy. *Journal of offshore mechanics and Arctic engineering*, 135(2):021602, 2013.
- [148] C. S. Withers. The moments of the multivariate normal. *Bulletin of the Australian Mathematical Society*, 32(1):103–107, aug 1985.
- [149] A. D. Wright, C. E. Smith, R. W. Thresher, and J. L. C. Wang. Vibration Modes of Centrifugally Stiffened Beams. *Journal of Applied Mechanics*, 49(1):197, 1982.
- [150] X. Xiao, Y. Zhang, and W. Shen. A stochastic analysis method of transient responses using harmonic wavelets, part 2: Time-dependent vehicle-bridge systems. *Mechanical Systems and Signal Processing*, 162:107871, jan 2022.

- [151] J. Xu and R. Gasch. Modale Behandlung linearer periodisch zeitvarianter Bewegungsgleichungen. *Archive of Applied Mechanics*, 65:178–193, 1995.
- [152] J. N. Yang. First-excursion probability in non-stationary random vibration. *Journal of Sound and Vibration*, 27(2):165–182, 1973.
- [153] E. Yazid and C. Y. Ng. Identification of time-varying linear and nonlinear impulse response functions using parametric Volterra model from model test data with application to a moored floating structure. *Ocean Engineering*, 219:108370, jan 2021.
- [154] D. Young. 2-D convolution using the FFT. <https://www.mathworks.com/matlabcentral/fileexchange/31012-2-d-convolution-using-the-fft>, 2023. Retrieved July 1, 2023.
- [155] Y. L. Young, M. R. Motley, and R. W. Yeung. Three-Dimensional Numerical Modeling of the Transient Fluid-Structural Interaction Response of Tidal Turbines. *Journal of Offshore Mechanics and Arctic Engineering*, 132(1), dec 2009.
- [156] B. Zhao, L. Xie, H. Li, S. Zhang, B. Wang, and C. Li. Reliability Analysis of Aero-Engine Compressor Rotor System Considering Cruise Characteristics. *IEEE Transactions on Reliability*, 69(1):245–259, mar 2020.
- [157] Z. Zhao, Z.-H. Lu, C.-Q. Li, and Y.-G. Zhao. Dynamic reliability analysis for non-stationary non-Gaussian response based on the bivariate vector translation process. *Probabilistic Engineering Mechanics*, 66:103143, oct 2021.
- [158] X. Y. Zheng and C. Y. Liaw. Response cumulant analysis of a linear oscillator driven by Morison force. *Applied Ocean Research*, 26(3-4):154–161, may 2004.

Appendix A

Matrix specification of various dynamical systems developed

1 The 2 DOF mass-blade

Symbols and definitions

- M mass of the disc
- r radius of the disc
- L length of the blade
- Ω angular velocity (around axis z)
- x, y, z variables in the fixed referential; X, Y, Z variables in the corotational referentials
- Φ_i mode shape i of the blade ; q_i modal variable i of the blade
- α angle of the corrotational frame with respect to the fixed frame at rest
- J_p polar moment of inertia of the disc
- A cross-section of the blade; I moment of inertia of the cross-section of the blade with respect to the Z axis
- ρ density of the blade (by volume, not by unit of length)
- K_X spring constants describing the flexibility of the base supporting the rotor, D_X damping coefficients describing energy dissipation of the base
- D_S damping coefficient on the blade .

Matrix form of the equations of motion Using the previously defined energies and Euler-Lagrange equation, the following system of equations can be established in matrix form with $\mathbf{q} = [x_h, q_1]^T$:

$$\mathbf{M}(t) \mathbf{q} + (\mathbf{D} + \mathbf{G}(t)) \dot{\mathbf{q}} + \mathbf{K} \mathbf{q} = 0. \quad (\text{A.1})$$

.The mass/inertia matrix is:

$$\mathbf{M}(t) = \begin{pmatrix} M + A\rho L & -\phi_1 \sin(\Omega t + \alpha) \\ -\phi_1 \sin(\Omega t + \alpha) & \phi_{11} \end{pmatrix}, \quad (\text{A.2})$$

with:

$$\begin{aligned} \phi_1 &= A\rho \left(\int \Phi(X) dX \right) \\ \phi_{11} &= A\rho \int \Phi(X) \Phi(X) dX. \end{aligned} \quad (\text{A.3})$$

The matrices with damping and gyroscopic effects are :

$$\mathbf{D} = \begin{pmatrix} D_x & 0 \\ 0 & D_S \phi_{11} \end{pmatrix} \quad (\text{A.4})$$

with $D_{s1} = D_S \phi_{11}$, and :

$$\mathbf{G}(t) = \Omega \begin{pmatrix} 0 & -\phi_1 \cos(\Omega t + \alpha) \\ \phi_1 \cos(\Omega t + \alpha) & 0 \end{pmatrix}. \quad (\text{A.5})$$

Quantity	Value(Units)
M	10e3[kg]
K_X	2e5[$\frac{N}{m}$]
D_X	9e3[$\frac{Ns}{m}$]
D_{s1}	10
E	25e6[Pa]
I	4.7[kg × m]
L	9[m]
ρ	211[$\frac{kg}{m^3}$]
A	1.5[m ²]
r	1[m]
Ω	1.15[$\frac{rad}{s}$]

Table A.1: Parameters

The stiffness matrix is :

$$\mathbf{K} = \begin{pmatrix} K_x & 0 \\ 0 & K_q \end{pmatrix} \quad (\text{A.6})$$

with:

$$K_q = -\phi_{11}\Omega^2 + AL(L+2r)\rho \left(\int (\Phi'_{11})^2 dX \right) \Omega^2 - 2Ar\rho \left(\int X (\Phi'_{11})^2 dX \right) \Omega^2 - A\rho \left(\int X^2 (\Phi'_{11})^2 dX \right) \Omega^2 + EI \int (\Phi''_{11})^2 dX, \quad (\text{A.7})$$

in these expressions:

- E is Young's modulus, I is the section's moment of inertia;
- A is the area of the cross-section, ρ is the density of the material;
- r is the radius of the rotor hub, L is the length of the blade;
- Integration with respect to X is done on the interval $[0, L]$, the length of the blade;
- Dot is differentiation with respect to time, prime is differentiation with respect to X .

Numerical values and parameters The previous development allows the description of different systems. The selected values of the physical parameters will be dependent on the application, and some of these require extensive experiments (particularly the damping coefficients). The parameters selected are detailed in the following table:

With these values, the numerical values of the system matrices can be written. The stiffness matrix is :

$$\mathbf{K} = \begin{pmatrix} 2e+05 & 0 \\ 0 & 7.0181e+02 \end{pmatrix} \quad (\text{A.8})$$

The damping matrix:

$$\mathbf{D} = \begin{pmatrix} 9000 & 0 \\ 0 & 10 \end{pmatrix}. \quad (\text{A.9})$$

The mode shape integrals after multiplication are:

$$\begin{aligned}\phi_1 &= 41.791 \\ \phi_{11} &= 1,\end{aligned}$$

so the mass matrix is, with $\alpha = 0$:

$$\mathbf{M}(t) = \begin{pmatrix} 12.848e+03 & -41.791 \sin(1.15t) \\ -41.791 \sin(1.15t) & 1 \end{pmatrix}. \quad (\text{A.10})$$

Finally, the gyroscopic matrix:

$$\mathbf{G}(t) = 1.15 \begin{pmatrix} 0 & -41.791 \cos(1.15t) \\ 41.791 \cos(1.15t) & 0 \end{pmatrix}. \quad (\text{A.11})$$

2 The 21 DOF model

The stiffness matrix can be decomposed in an elastic term and a term related to Ω :

$$\mathbf{K} = \mathbf{K}_E + \mathbf{K}_\Omega, \dim[21, 21] :$$

$$\mathbf{K}_E = \begin{pmatrix} \mathbf{K}_{EH} & 0 & 0 \\ 0 & \mathbf{K}_{EB1} & 0 \\ 0 & 0 & \mathbf{K}_{EB2} \end{pmatrix}. \quad (\text{A.12})$$

The elastic term can be subdivided in the following submatrices: $\mathbf{K}_{EH} \rightarrow [5, 5]$; $\mathbf{K}_{EBk} \rightarrow [8, 8]$; k designates the corresponding blade:

$$\mathbf{K}_{EH} = \begin{pmatrix} K_{XX} & 0 & 0 & 0 & K_{X\theta_2} \\ 0 & K_{YY} & 0 & K_{Y\theta_1} & 0 \\ 0 & 0 & K_{ZZ} & 0 & 0 \\ 0 & K_{Y\theta_1} & 0 & K_{\theta_1\theta_1} & 0 \\ K_{X\theta_2} & 0 & 0 & 0 & K_{\theta_2\theta_2} \end{pmatrix} \quad (\text{A.13})$$

$$K_{XX} = kx_1 + kx_2$$

$$K_{YY} = ky_1 + ky_2$$

$$K_{ZZ} = kz_1 + kz_2$$

$$K_{\theta_1\theta_1} = ky_1L_1^2 + ky_2L_2^2$$

$$K_{\theta_2\theta_2} = kx_1L_1^2 + kx_2L_2^2$$

$$K_{X\theta_2} = -kx_1L_1 - kx_2L_2$$

$$K_{Y\theta_1} = ky_1L_1 + ky_2L_2 \quad (\text{A.14})$$

$$\mathbf{K}_{EBi} = \begin{pmatrix} \mathbf{K}_{EBk}^{sj} & \mathbf{K}_{EBk}^{fj} \\ \mathbf{K}_{EBk}^{sj} & \mathbf{K}_{EBk}^{fj} \end{pmatrix} \quad (\text{A.15})$$

$$\begin{aligned}
Ks_{E_{Bk}}^{ij} &= EI_{ZZ} \int (\varphi_i^s)'' (\varphi_j^s)'' dx, i, j \in [1, 2, 3, 4] \\
Kf_{E_{Bk}}^{ij} &= EI_{YY} \int (\varphi_i^f)'' (\varphi_j^f)'' dx, i, j \in [5, 6, 7, 8] \\
Ksf_{E_{Bk}}^{ij} &= EI_{YZ} \int (\varphi_i^s)'' (\varphi_j^f)'' dx, i \in [5, 6, 7, 8], j \in [1, 2, 3, 4]
\end{aligned} \tag{A.16}$$

the matrix \mathbf{K}_Ω can be subdivided as:

$$\mathbf{K}_\Omega = \begin{pmatrix} \mathbf{K}_{HH} & \mathbf{K}_{HB1} & \mathbf{K}_{HB2} \\ \mathbf{0} & \mathbf{K}_{B1B1} & \mathbf{0} \\ \mathbf{0} & \mathbf{0} & \mathbf{K}_{B2B2} \end{pmatrix} \tag{A.17}$$

with the following form: $\mathbf{K}_{HH} \rightarrow [5, 5]$

$$\mathbf{K}_{HH} = A\rho\Omega^2 L_b \begin{pmatrix} 0 & 0 & 0 \\ 0 & 0 & 0 \\ 0 & 0 & 0 \\ 0 & -\frac{2}{3}(3rL_b + L_b^2 + 3r^2) \sin^2(t\Omega) & \frac{1}{3}((3r-1)L_b + 2L_b^2 + 3r^2) \sin(2t\Omega) \\ 0 & \frac{1}{3}((3r-1)L_b + 2L_b^2 + 3r^2) \sin(2t\Omega) & -\frac{2}{3}(3rL_b + L_b^2 + 3r^2) \cos^2(t\Omega) \end{pmatrix} \tag{A.18}$$

for $\mathbf{K}_{HB1} \rightarrow [5, 8]$:

$$\mathbf{K}_{HB1} = A_1\rho_1\Omega^2 \begin{pmatrix} \sin(t\Omega)Ks\varphi_1 & \sin(t\Omega)Ks\varphi_2 & \sin(t\Omega)Ks\varphi_3 & \sin(t\Omega)Ks\varphi_4 \\ -\cos(t\Omega)Ks\varphi_1 & -\cos(t\Omega)Ks\varphi_2 & -\cos(t\Omega)Ks\varphi_3 & -\cos(t\Omega)Ks\varphi_4 \\ 0 & 0 & 0 & 0 \\ 0 & 0 & 0 & 0 \\ 0 & 0 & 0 & 0 \\ 0 & 0 & 0 & 0 \\ 0 & 0 & 0 & 0 \\ 0 & 0 & 0 & 0 \\ \sin(t\Omega)Kfr\varphi_1 & \sin(t\Omega)Kfr\varphi_2 & \sin(t\Omega)Kfr\varphi_3 & \sin(t\Omega)Kfr\varphi_4 \\ -\cos(t\Omega)Kfr\varphi_1 & -\cos(t\Omega)Kfr\varphi_2 & -\cos(t\Omega)Kfr\varphi_3 & -\cos(t\Omega)Kfr\varphi_4 \end{pmatrix} \tag{A.19}$$

$$\mathbf{K}_{HB2} = A_2\rho_2\Omega^2 \begin{pmatrix} -\sin(t\Omega)Ks\varphi_1 & -\sin(t\Omega)Ks\varphi_2 & -\sin(t\Omega)Ks\varphi_3 & -\sin(t\Omega)Ks\varphi_4 \\ \cos(t\Omega)Ks\varphi_1 & \cos(t\Omega)Ks\varphi_2 & \cos(t\Omega)Ks\varphi_3 & \cos(t\Omega)Ks\varphi_4 \\ 0 & 0 & 0 & 0 \\ 0 & 0 & 0 & 0 \\ 0 & 0 & 0 & 0 \\ 0 & 0 & 0 & 0 \\ 0 & 0 & 0 & 0 \\ 0 & 0 & 0 & 0 \\ -\sin(t\Omega)Kfr\varphi_1 & -\sin(t\Omega)Kfr\varphi_2 & -\sin(t\Omega)Kfr\varphi_3 & -\sin(t\Omega)Kfr\varphi_4 \\ \cos(t\Omega)Kfr\varphi_1 & \cos(t\Omega)Kfr\varphi_2 & \cos(t\Omega)Kfr\varphi_3 & \cos(t\Omega)Kfr\varphi_4 \end{pmatrix} \tag{A.20}$$

$$\begin{aligned}
Ks\varphi_i &= \int \varphi_i^s dx \\
Kf\varphi_i &= \int \varphi_i^f dx \\
Kfr\varphi_i &= (rKf\varphi_i + \int x\varphi_i^f dx)
\end{aligned} \tag{A.21}$$

$$\mathbf{K}_{BkBk} = A_1 \rho_1 \Omega^2 \begin{pmatrix} K_{BkBk}^{11} & K_{BkBk}^{12} & K_{BkBk}^{13} & K_{BkBk}^{14} & 0 & 0 & 0 & 0 \\ K_{BkBk}^{21} & K_{BkBk}^{22} & K_{BkBk}^{23} & K_{BkBk}^{24} & 0 & 0 & 0 & 0 \\ K_{BkBk}^{31} & K_{BkBk}^{32} & K_{BkBk}^{33} & K_{BkBk}^{34} & 0 & 0 & 0 & 0 \\ K_{BkBk}^{41} & K_{BkBk}^{42} & K_{BkBk}^{43} & K_{BkBk}^{44} & 0 & 0 & 0 & 0 \\ 0 & 0 & 0 & 0 & 0 & 0 & 0 & 0 \\ 0 & 0 & 0 & 0 & 0 & 0 & 0 & 0 \\ 0 & 0 & 0 & 0 & 0 & 0 & 0 & 0 \\ 0 & 0 & 0 & 0 & 0 & 0 & 0 & 0 \end{pmatrix} \tag{A.22}$$

$$\begin{aligned}
K_{BkBk}^{ij} &= 2rL_b \int (\varphi_i^s)' (\varphi_j^s)' dx + L_b^2 \int (\varphi_i^s)' (\varphi_j^s)' dx \\
&\quad - 2r \int x (\varphi_i^s)' (\varphi_j^s)' dx - \int x^2 (\varphi_i^s)' (\varphi_j^s)' dx - \int (\varphi_i^s) (\varphi_j^s) dx.
\end{aligned} \tag{A.23}$$

The coefficient matrix on the time derivatives \mathbf{G} can be decomposed into two terms $\mathbf{G} = \mathbf{G}_H + \mathbf{G}_G$:

$$\mathbf{G}_H = \begin{pmatrix} \mathbf{G}_{HH} & \mathbf{0}_{[5,16]} \\ \mathbf{0}_{[16,5]} & \mathbf{0}_{[16,16]} \end{pmatrix} \tag{A.24}$$

with:

$$\mathbf{G}_{HH} = \frac{1}{3} \Omega \begin{pmatrix} 000 & 0 & 0 \\ 000 & 0 & 0 \\ 000 & 0 & 0 \\ 000 & 0 & (2A\rho L_b^3 + 6A\rho r^2 L_b + 6AprL_b^2 + 3Jp) \\ 000 - (2A\rho L_b^3 + 6A\rho r^2 L_b + 6AprL_b^2 + 3Jp) & 0 & 0 \end{pmatrix} \tag{A.25}$$

and the matrix $\mathbf{G}_G = 2A\rho\Omega G_G^{i,j}$ has the nonzero elements:

$$\begin{aligned}
G_G^{10,4} &= \cos(t\Omega)(r \int \varphi 1f(x) dx + \int x\varphi 1f(x) dx) \\
G_G^{11,4} &= \cos(t\Omega)(r \int \varphi 2f(x) dx + \int x\varphi 2f(x) dx) \\
G_G^{12,4} &= \cos(t\Omega)(r \int \varphi 3f(x) dx + \int x\varphi 3f(x) dx) \\
G_G^{13,4} &= \cos(t\Omega)(r \int \varphi 4f(x) dx + \int x\varphi 4f(x) dx) \\
G_G^{18,4} &= -\cos(t\Omega)(r \int \varphi 1f(x) dx + \int x\varphi 1f(x) dx) \\
G_G^{19,4} &= -\cos(t\Omega)(r \int \varphi 2f(x) dx + \int x\varphi 2f(x) dx) \\
G_G^{20,4} &= -\cos(t\Omega)(r \int \varphi 3f(x) dx + \int x\varphi 3f(x) dx) \\
G_G^{21,4} &= -\cos(t\Omega)(r \int \varphi 4f(x) dx + \int x\varphi 4f(x) dx)
\end{aligned} \tag{A.26}$$

$$\begin{aligned}
G_G^{10,5} &= \sin(t\Omega)(r \int \varphi 1f(x) dx + \int x\varphi 1f(x) dx) \\
G_G^{11,5} &= \sin(t\Omega)(r \int \varphi 2f(x) dx + \int x\varphi 2f(x) dx) \\
G_G^{12,5} &= \sin(t\Omega)(r \int \varphi 3f(x) dx + \int x\varphi 3f(x) dx) \\
G_G^{13,5} &= \sin(t\Omega)(r \int \varphi 4f(x) dx + \int x\varphi 4f(x) dx) \\
G_G^{18,5} &= -\sin(t\Omega)(r \int \varphi 1f(x) dx + \int x\varphi 1f(x) dx) \\
G_G^{19,5} &= -\sin(t\Omega)(r \int \varphi 2f(x) dx + \int x\varphi 2f(x) dx) \\
G_G^{20,5} &= -\sin(t\Omega)(r \int \varphi 3f(x) dx + \int x\varphi 3f(x) dx) \\
G_G^{21,5} &= -\sin(t\Omega)(r \int \varphi 4f(x) dx + \int x\varphi 4f(x) dx)
\end{aligned} \tag{A.27}$$

$$\begin{aligned}
G_G^{10,4} &= -G_G^{1,6} \\
G_G^{11,4} &= -G_G^{1,7} \\
G_G^{12,4} &= -G_G^{1,8} \\
G_G^{13,4} &= -G_G^{1,9} \\
G_G^{18,4} &= -G_G^{1,14} \\
G_G^{19,4} &= -G_G^{1,15} \\
G_G^{20,4} &= -G_G^{1,16} \\
G_G^{21,4} &= -G_G^{1,17}
\end{aligned} \tag{A.28}$$

$$\begin{aligned}
G_G^{10,5} &= -G_G^{2,6} \\
G_G^{11,5} &= -G_G^{2,7} \\
G_G^{12,5} &= -G_G^{2,8} \\
G_G^{13,5} &= -G_G^{2,9} \\
G_G^{18,5} &= -G_G^{2,14} \\
G_G^{19,5} &= -G_G^{2,15} \\
G_G^{20,5} &= -G_G^{2,16} \\
G_G^{21,5} &= -G_G^{2,17}.
\end{aligned} \tag{A.29}$$

The inertia matrix can be subdivided into a time-dependent component and a time-independent component: $\mathbf{M} = \mathbf{M}_t + \mathbf{M}_C$, with $\mathbf{M}_C = \mathbf{M}_{C1} + \mathbf{M}_{CC}$:

$$\mathbf{M}_{C1} = \begin{pmatrix} \mathbf{M}_H & 0 & 0 & 0 & 0 \\ 0 & \mathbf{M}_{B1B1}^S & 0 & 0 & 0 \\ 0 & 0 & \mathbf{M}_{B1B1}^f & 0 & 0 \\ 0 & 0 & 0 & \mathbf{M}_{B2B2}^S & 0 \\ 0 & 0 & 0 & 0 & \mathbf{M}_{B2B2}^f \end{pmatrix} \tag{A.30}$$

$$\mathbf{M}_H = \begin{pmatrix} A_1\rho_1L_b + A_2\rho_2L_b + M & 0 & 0 \\ 0 & A_1\rho_1L_b + A_2\rho_2L_b + M & 0 \\ 0 & 0 & A_1\rho_1L_b + A_2\rho_2L_b + M \\ 0 & 0 & 0 \\ 0 & 0 & 0 \\ 0 & 0 & 0 \\ 0 & 0 & 0 \\ 0 & 0 & 0 \\ J_d \frac{1}{3} A \rho L_b^3 + A \rho r^2 L_b + A \rho r L_b^2 & 0 & 0 \\ 0 & J_d \frac{1}{3} A \rho L_b^3 + A \rho r^2 L_b + A \rho r L_b^2 & 0 \end{pmatrix} \tag{A.31}$$

$$\mathbf{M}_{BkBk}^S = A_k \rho_k \begin{pmatrix} \int (\varphi_1^s)(\varphi_1^s) dx & \int (\varphi_1^s)(\varphi_2^s) dx & \int (\varphi_1^s)(\varphi_3^s) dx & \int (\varphi_1^s)(\varphi_4^s) dx \\ \int (\varphi_1^s)(\varphi_2^s) dx & \int (\varphi_2^s)(\varphi_2^s) dx & \int (\varphi_2^s)(\varphi_3^s) dx & \int (\varphi_2^s)(\varphi_4^s) dx \\ \int (\varphi_1^s)(\varphi_3^s) dx & \int (\varphi_2^s)(\varphi_3^s) dx & \int (\varphi_3^s)(\varphi_3^s) dx & \int (\varphi_3^s)(\varphi_4^s) dx \\ \int (\varphi_1^s)(\varphi_4^s) dx & \int (\varphi_2^s)(\varphi_4^s) dx & \int (\varphi_3^s)(\varphi_4^s) dx & \int (\varphi_4^s)(\varphi_4^s) dx \end{pmatrix} \tag{A.32}$$

$$\mathbf{M}_{BkBk}^f = A_k \rho_k \begin{pmatrix} \int (\varphi_1^f)(\varphi_1^f) dx & \int (\varphi_1^f)(\varphi_2^f) dx & \int (\varphi_1^f)(\varphi_3^f) dx & \int (\varphi_1^f)(\varphi_4^f) dx \\ \int (\varphi_1^f)(\varphi_2^f) dx & \int (\varphi_2^f)(\varphi_2^f) dx & \int (\varphi_2^f)(\varphi_3^f) dx & \int (\varphi_2^f)(\varphi_4^f) dx \\ \int (\varphi_1^f)(\varphi_3^f) dx & \int (\varphi_2^f)(\varphi_3^f) dx & \int (\varphi_3^f)(\varphi_3^f) dx & \int (\varphi_3^f)(\varphi_4^f) dx \\ \int (\varphi_1^f)(\varphi_4^f) dx & \int (\varphi_2^f)(\varphi_4^f) dx & \int (\varphi_3^f)(\varphi_4^f) dx & \int (\varphi_4^f)(\varphi_4^f) dx \end{pmatrix} \tag{A.33}$$

in the case of \mathbf{M}_{CC} is has the following components: $\mathbf{M}_{CC} = M_{CC}$ and:

$$M_{CC}^{i,3} = A \rho \left(\int \varphi_1^f dx \right) \tag{A.34}$$

Appendix B

Description of the stochastic load

1 Description of the stochastic load

Let $\mathcal{V}(\mathbf{X}, t)$ be a spatio-temporal stochastic field on $\{\Omega, \mathcal{F}, P\}$ describing the velocity of the fluid flow on the ocean environment. We make the following hypotheses about this field:

- The field is unidirectional: $\mathcal{V}(\mathbf{X}, t) = \begin{bmatrix} 0 \\ 0 \\ V_z \end{bmatrix}; \forall(t, \mathbf{X})$
- The field has finite moments $E[\mathcal{V}(\mathbf{X}, t)^n] = \mu_{\mathcal{V}^n(\mathbf{X})} < \infty$
- It is a gaussian, stationary field $E[\mathcal{V}(\mathbf{X}, t)] = \mu_{\mathcal{V}(\mathbf{X}, t_1)} = \mu_{\mathcal{V}(\mathbf{X})}; \text{Var}[\mathcal{V}(\mathbf{X}, t)] = \sigma_{\mathcal{V}(\mathbf{X}, t)\mathcal{V}(\mathbf{X}, t)} = \sigma_{\mathcal{V}(\mathbf{X})\mathcal{V}(\mathbf{X})}$
- The field is homogeneous in the X and Z directions, so $\mathcal{V}(\mathbf{X}, t) = \mathcal{V}(Y, t)$

our goal is to describe the effect of this load over the LTP system. From a practical perspective, this entails a problem common to tidal energy system simulation and wind turbine simulation, which we describe now:

1. The system occupies the positions $\mathbf{q}(t_i)$, with $t_i = t_{i-1} + \Delta t, t, t_i \in [T_0, T_f]$
2. The positions depend on the forces induced by the velocity $\mathbf{q}(t_i) = \mathbf{f}(\mathcal{V}(\mathbf{q}(t_i), t), t_i)$
3. Since the positions are not known before the resolution, when simulating $\mathcal{V}(\mathbf{X}, t)$ a very dense discretisation grid is required as to cover all the possible configurations of $\mathbf{q}(t_i)$; this approach is prohibitively expensive from a computational perspective and the complexity in both $[T_0, T_f]$ and $\dim[\mathbf{q}]$ is very poor

by way of example, let us consider a system where the rotor diameter is $D_{\text{sys}} = 20\text{m}$, with a simulation time of 360s; we assume that the displacements and rotations are very small, so $\mathcal{V}(Y + \Delta\mathbf{q}, t) \approx \mathcal{V}(Y, t)$; this simulation requires the generation of a grid that covers the area $A = 314.15\text{m}^2$ at each point of discretisation time. This problem is compounded by the fact that in general, the constituent random variables of $\mathcal{V}(\mathbf{X}, t)$ need to comply with a prescribed correlation structure, so the generation of $\mathcal{V}(\mathbf{X}, t)$ can not rely on independent sampling of its constituent RVs: the entire grid needs to be generated at every t_i even if just a small fraction of them are ultimately applied to the system.

We envision the following strategies to mitigate these limitations:

1. *Field interpolation*: instead of generating a fine grid for \mathcal{V} , a coarse grid is generated which is then used to interpolate the remaining required points as required from the evolution of $\mathbf{q}(t_i)$. The main drawback is related to the convergence of this approach: the interpolation has to appropriately describe the field. The criteria to ensure this relies on the smoothness of the sample paths of the processes, which ultimately depends on the covariance functions.
2. *Predictor-corrector approach*: run a first simulation assuming a non-deformable system to estimate the positions of the system, and then run a second simulation with the velocities sampled in the predictor step over the system. This approach remains computationally expensive.
3. *Semi-analytic estimation*: estimate some of the probabilistic quantities of the part of \mathcal{V} acting on the system, like the first 4 moments, the covariance function or the power spectral density. These can be estimated analytically. This provides a partial description of the processes acting on the system, so $\mathcal{V}(\mathbf{X}, t)$ incident on $\mathbf{q}(t_i)$ can be approximated as a process that fits the aforementioned statistical descriptors.

The characterisation of $\mathcal{V}(\mathbf{X}, t)$ in terms of its moments is as follows:

- Instantaneous probabilistic moments with respect to the origin:

$$\begin{aligned}
\mu_{\mathcal{V}(\mathbf{X})}(t) &= \mathbb{E}[\mathcal{V}(\mathbf{X}, t)] \\
\mu_{\mathcal{V}(\mathbf{X}_1)\mathcal{V}(\mathbf{X}_2)}(t) &= \mathbb{E}[\mathcal{V}(\mathbf{X}_1, t) \mathcal{V}(\mathbf{X}_2)] \\
\mu_{\mathcal{V}(\mathbf{X}_1)\mathcal{V}(\mathbf{X}_2)\mathcal{V}(\mathbf{X}_3)}(t) &= \mathbb{E}[\mathcal{V}(\mathbf{X}_1, t) \mathcal{V}(\mathbf{X}_2) \mathcal{V}(\mathbf{X}_3)] \\
\mu_{\mathcal{V}(\mathbf{X}_1)\mathcal{V}(\mathbf{X}_2)\mathcal{V}(\mathbf{X}_3)\mathcal{V}(\mathbf{X}_4)}(t) &= \mathbb{E}[\mathcal{V}(\mathbf{X}_1, t) \mathcal{V}(\mathbf{X}_2) \mathcal{V}(\mathbf{X}_3) \mathcal{V}(\mathbf{X}_4)] \tag{B.1}
\end{aligned}$$

- Instantaneous probabilistic moments with respect to the mean:

$$\begin{aligned}
\sigma_{\mathcal{V}(\mathbf{X}_1)\mathcal{V}(\mathbf{X}_2)}(t) &= \mathbb{E}[(\mathcal{V}(\mathbf{X}_1, t) - \mu_{\mathcal{V}(\mathbf{X}_1)}(t)) (\mathcal{V}(\mathbf{X}_2, t) - \mu_{\mathcal{V}(\mathbf{X}_2)}(t))] \\
\sigma_{\mathcal{V}(\mathbf{X}_1)\mathcal{V}(\mathbf{X}_2)\mathcal{V}(\mathbf{X}_3)}(t) &= \mathbb{E}[(\mathcal{V}(\mathbf{X}_1, t) - \mu_{\mathcal{V}(\mathbf{X}_1)}(t)) (\mathcal{V}(\mathbf{X}_2, t) - \mu_{\mathcal{V}(\mathbf{X}_2)}(t)) (\mathcal{V}(\mathbf{X}_3, t) - \mu_{\mathcal{V}(\mathbf{X}_3)}(t))] \\
\sigma_{\mathcal{V}(\mathbf{X}_1)\mathcal{V}(\mathbf{X}_2)\mathcal{V}(\mathbf{X}_3)\mathcal{V}(\mathbf{X}_4)}(t) &= \mathbb{E}[(\mathcal{V}(\mathbf{X}_1, t) - \mu_{\mathcal{V}(\mathbf{X}_1)}(t)) (\mathcal{V}(\mathbf{X}_2, t) - \mu_{\mathcal{V}(\mathbf{X}_2)}(t)) (\mathcal{V}(\mathbf{X}_3, t) - \mu_{\mathcal{V}(\mathbf{X}_3)}(t)) (\mathcal{V}(\mathbf{X}_4, t) - \mu_{\mathcal{V}(\mathbf{X}_4)}(t))] \tag{B.2}
\end{aligned}$$

- Inter-instantaneous moments:

$$\begin{aligned}
R_{\mathcal{V}(\mathbf{X}_1)\mathcal{V}(\mathbf{X}_2)}(t_1, t_2) &= \mathbb{E}[\mathcal{V}(\mathbf{X}_1, t_1) \mathcal{V}(\mathbf{X}_2, t_2)] \\
R_{\mathcal{V}(\mathbf{X}_1)\mathcal{V}(\mathbf{X}_2)\mathcal{V}(\mathbf{X}_3)}(t_1, t_2, t_3) &= \mathbb{E}[\mathcal{V}(\mathbf{X}_1, t_1) \mathcal{V}(\mathbf{X}_2, t_2) \mathcal{V}(\mathbf{X}_3, t_3)] \\
R_{\mathcal{V}(\mathbf{X}_1)\mathcal{V}(\mathbf{X}_2)\mathcal{V}(\mathbf{X}_3)\mathcal{V}(\mathbf{X}_4)}(t_1, t_2, t_3, t_4) &= \mathbb{E}[\mathcal{V}(\mathbf{X}_1, t_1) \mathcal{V}(\mathbf{X}_2, t_2) \mathcal{V}(\mathbf{X}_3, t_3) \mathcal{V}(\mathbf{X}_4, t_4)] \tag{B.3}
\end{aligned}$$

and

$$\begin{aligned}
\Sigma_{\mathcal{V}(\mathbf{X}_1)\mathcal{V}(\mathbf{X}_2)}(t_1, t_2) &= \mathbb{E}[(\mathcal{V}(\mathbf{X}_1, t_1) - \mu_{\mathcal{V}(\mathbf{X}_1)}(t_1)) (\mathcal{V}(\mathbf{X}_2, t_2) - \mu_{\mathcal{V}(\mathbf{X}_2)}(t_2))] \\
\Sigma_{\mathcal{V}(\mathbf{X}_1)\mathcal{V}(\mathbf{X}_2)\mathcal{V}(\mathbf{X}_3)}(t_1, t_2, t_3) &= \mathbb{E}[(\mathcal{V}(\mathbf{X}_1, t_1) - \mu_{\mathcal{V}(\mathbf{X}_1)}(t_1)) (\mathcal{V}(\mathbf{X}_2, t_2) - \mu_{\mathcal{V}(\mathbf{X}_2)}(t_2)) (\mathcal{V}(\mathbf{X}_3, t_3) - \mu_{\mathcal{V}(\mathbf{X}_3)}(t_3))] \tag{B.4}
\end{aligned}$$

$$\begin{aligned}
\Sigma_{\mathcal{V}(\mathbf{X}_1)\mathcal{V}(\mathbf{X}_2)\mathcal{V}(\mathbf{X}_3)\mathcal{V}(\mathbf{X}_4)}(t_1, t_2, t_3, t_4) &= \mathbb{E}[(\mathcal{V}(\mathbf{X}_1, t_1) - \mu_{\mathcal{V}(\mathbf{X}_1)}(t_1)) (\mathcal{V}(\mathbf{X}_2, t_2) - \mu_{\mathcal{V}(\mathbf{X}_2)}(t_2)) \\
&\quad (\mathcal{V}(\mathbf{X}_3, t_3) - \mu_{\mathcal{V}(\mathbf{X}_3)}(t_3)) (\mathcal{V}(\mathbf{X}_4, t_4) - \mu_{\mathcal{V}(\mathbf{X}_4)}(t_4))] \tag{B.5}
\end{aligned}$$

from these last quantities, the generalized N covariance functions, one may compute the corresponding N Power Spectral Densities (the Power Spectrum, bispectrum and trispectrum from the covariance, bicovariance and tricovariance). In the case of gaussian processes, the following quantities suffice for its complete specification:

$$\begin{aligned}
\mu_{\mathcal{V}(\mathbf{X})}(t) &= \mathbb{E}[\mathcal{V}(\mathbf{X}, t)] \\
\Sigma_{\mathcal{V}(\mathbf{X}_1)\mathcal{V}(\mathbf{X}_2)}(t_1, t_2) &= \mathbb{E}[(\mathcal{V}(\mathbf{X}_1, t_1) - \mu_{\mathcal{V}(\mathbf{X}_1)}(t_1)) (\mathcal{V}(\mathbf{X}_2, t_2) - \mu_{\mathcal{V}(\mathbf{X}_2)}(t_2))] . \tag{B.6}
\end{aligned}$$

Blade Element Theory The hydrodynamical aspects of a given section of the blade are characterized by its local chord $c(X_b)$, its lift and drag coefficients $C(X_b) = \begin{bmatrix} 0 \\ C_L \\ C_D \end{bmatrix}$, a twist angle $\theta_\beta(X_b)$. Since the rotor interaction perturbs the fluid velocity, it is convenient to supplement the previous description with the introduction of the corresponding induction factors that account for the changes in momentum on the flow: $a_x(X_b), a_z(X_b)$. The

unperturbed velocity of the fluid is $\mathcal{V}(\mathbf{X}, t) = \begin{bmatrix} 0 \\ 0 \\ -V_z \end{bmatrix}$ in the inertial referential, with norm $\|\mathcal{V}(\mathbf{X}, t)\| = \sqrt{V_z^2}$.

From Blade Element Momentum theory, this velocity becomes:

$$\begin{aligned} \mathcal{V}(\mathbf{X}, t) &= \begin{bmatrix} 0 \\ 0 \\ -(1 - a_Z(X_b))V_z \end{bmatrix} + \begin{bmatrix} -a_X(X_b)\Omega(r + X_b) \\ 0 \\ 0 \end{bmatrix} \\ &= \begin{bmatrix} -a_X(X_b)\Omega(r + X_b)\sin(\Omega t) \\ 0 \\ -(1 - a_Z(X_b))V_z \end{bmatrix} \end{aligned} \quad (\text{B.7})$$

taking into account the velocity $\dot{\mathbf{P}}_O$ of a point on the blade in the inertial referential: $\dot{\mathbf{P}}_O = \Omega \begin{bmatrix} -(r + X_b)\sin(\Omega t) \\ (r + X_b)\cos(\Omega t) \\ 0 \end{bmatrix}$,

we compute the relative velocity as follows $\mathcal{V}_{rel}(\mathbf{X}, t) = \mathcal{V}(\mathbf{X}, t) - \dot{\mathbf{P}}_O$

$$\begin{aligned} \mathcal{V}_{rel}(\mathbf{X}, t) &= \begin{bmatrix} -a_X(X_b)\Omega(r + X_b)\sin(\Omega t) \\ 0 \\ -(1 - a_Z(X_b))V_z \end{bmatrix} - \Omega \begin{bmatrix} -(r + X_b)\sin(\Omega t) \\ (r + X_b)\cos(\Omega t) \\ 0 \end{bmatrix} \\ &= \begin{bmatrix} -a_X(X_b)\Omega(r + X_b)\sin(\Omega t) - \Omega(r + X_b)\sin(\Omega t) \\ -\Omega(r + X_b)\cos(\Omega t) \\ -(1 - a_Z(X_b))V_z \end{bmatrix} \\ &= \begin{bmatrix} -(a_X(X_b) + 1)\Omega(r + X_b)\sin(\Omega t) \\ -\Omega(r + X_b)\cos(\Omega t) \\ -(1 - a_Z(X_b))V_z \end{bmatrix} \end{aligned} \quad (\text{B.8})$$

it is convenient to introduce the following substitutions: $C_{VX}(X_b) = -(a_X(X_b) + 1)\Omega(r + X_b)$; $C_{VY}(X_b) = -\Omega(r + X_b)$; $C_{VZ}(X_b) = -(1 - a_Z(X_b))V_z$, which allows to recognize:

$$\mathcal{V}_{rel}(\mathbf{X}, t) = \begin{bmatrix} C_{VX}(X_b)\sin(\Omega t) \\ C_{VY}(X_b)\cos(\Omega t) \\ C_{VZ}(X_b)V_z \end{bmatrix} \quad (\text{B.9})$$

in an unidirectional flow, the only stochastic component corresponds to the Z direction.

The forces on a given point on a blade is:

$$\mathbf{F}(X_b, t) = \frac{1}{2}\rho_w c(X_b)\mathcal{V}_{rel}^2(\mathbf{X}, t)C(X_b) \quad (\text{B.10})$$

it requires the evaluation of the square of the relative velocity:

$$\begin{aligned} \mathcal{V}_{rel}^2(\mathbf{X}, t) &= \frac{1}{8} (8\Omega^2 a_x^2 (X_b + r)^2 \sin^2(t\Omega) + 16\Omega^2 a_x (X_b + r)^2 \sin^2(t\Omega) + 8V^2 a_z^2 - 16V^2 a_z \\ &\quad - 8r\Omega^2 X_b \cos(2t\Omega) - 2r\Omega^2 X_b \cos(4t\Omega) + 10r\Omega^2 X_b - 4\Omega^2 X_b^2 \cos(2t\Omega) - \Omega^2 X_b^2 \cos(4t\Omega) \\ &\quad + 5\Omega^2 X_b^2 - 4r^2 \Omega^2 \cos(2t\Omega) - r^2 \Omega^2 \cos(4t\Omega) + 5r^2 \Omega^2 + 8V^2) \end{aligned} \quad (\text{B.11})$$

which we separate into a deterministic and a random component $\mathcal{V}_{rel}^2(\mathbf{X}, t) = \mathcal{V}_{rand}^2(\mathbf{X}, t) + \mathcal{V}_{det}^2(\mathbf{X}, t)$:

$$\mathcal{V}_{rand}^2(\mathbf{X}, t) = V_z^2(a_z - 1)^2 \quad (\text{B.12})$$

$$\mathcal{V}_{det}^2(\mathbf{X}, t) = \frac{1}{2} \Omega^2 (X_b + r)^2 \sin^2(t\Omega) (2a_x^2 + 4a_x + \cos(2t\Omega) + 3). \quad (\text{B.13})$$

If V_z is gaussian stationary process, we can immediately conclude that:

$$\begin{aligned} \mu_{V_z^2(\mathbf{x})} &= \sigma_{V_z(\mathbf{x})V_z(\mathbf{x})} + \mu_{V_z(\mathbf{x})}^2 \\ \mu_{V_z^4(\mathbf{x})} &= \mu_{V_z(\mathbf{x})}^4 + 6\mu_{V_z(\mathbf{x})}^2 \sigma_{V_z(\mathbf{x})V_z(\mathbf{x})} + 3\sigma_{V_z(\mathbf{x})V_z(\mathbf{x})}^2 \\ \mu_{V_z^6(\mathbf{x})} &= \mu_{V_z(\mathbf{x})}^6 + 15\mu_{V_z(\mathbf{x})}^4 \sigma_{V_z(\mathbf{x})V_z(\mathbf{x})} + 45\mu_{V_z(\mathbf{x})}^2 \sigma_{V_z(\mathbf{x})V_z(\mathbf{x})}^2 + 15\sigma_{V_z(\mathbf{x})V_z(\mathbf{x})}^3 \\ \mu_{V_z^8(\mathbf{x})} &= \mu_{V_z(\mathbf{x})}^8 + 28\mu_{V_z(\mathbf{x})}^6 \sigma_{V_z(\mathbf{x})V_z(\mathbf{x})} + 210\mu_{V_z(\mathbf{x})}^4 \sigma_{V_z(\mathbf{x})V_z(\mathbf{x})}^2 + 420\mu_{V_z(\mathbf{x})}^2 \sigma_{V_z(\mathbf{x})V_z(\mathbf{x})}^3 + 105\sigma_{V_z(\mathbf{x})V_z(\mathbf{x})}^4 \end{aligned} \quad (\text{B.14})$$

$$\Sigma_{V_z^2(\mathbf{x}_1)V_z^2(\mathbf{x}_2)}(\tau) = 2\Sigma_{V_z^2(\mathbf{x}_1)V_z^2(\mathbf{x}_2)}(\tau) + 4\mu_{V_z(\mathbf{x}_1)}\mu_{V_z(\mathbf{x}_2)}\Sigma_{V_z(\mathbf{x}_1)V_z(\mathbf{x}_2)}(\tau) \quad (\text{B.15})$$

$$\begin{aligned} \Sigma_{V_z^2(\mathbf{x}_1)V_z^2(\mathbf{x}_2)V_z^2(\mathbf{x}_3)}(\tau_1, \tau_2) &= 8 \left[\mu_{V_z(\mathbf{x}_1)}\mu_{V_z(\mathbf{x}_2)}\Sigma_{V_z(\mathbf{x}_1)V_z(\mathbf{x}_3)}(\tau_2 - \tau_1)\Sigma_{V_z(\mathbf{x}_2)V_z(\mathbf{x}_3)}(\tau_2) \right. \\ &\quad + \mu_{V_z(\mathbf{x}_2)}\mu_{V_z(\mathbf{x}_3)}\Sigma_{V_z(\mathbf{x}_1)V_z(\mathbf{x}_2)}(\tau_1)\Sigma_{V_z(\mathbf{x}_1)V_z(\mathbf{x}_3)}(\tau_2 - \tau_1) \\ &\quad + \mu_{V_z(\mathbf{x}_1)}\mu_{V_z(\mathbf{x}_3)}\Sigma_{V_z(\mathbf{x}_1)V_z(\mathbf{x}_2)}(\tau_1)\Sigma_{V_z(\mathbf{x}_2)V_z(\mathbf{x}_3)}(\tau_2) \\ &\quad \left. + \Sigma_{V_z(\mathbf{x}_1)V_z(\mathbf{x}_2)}(\tau_1)\Sigma_{V_z(\mathbf{x}_1)V_z(\mathbf{x}_3)}(\tau_2 - \tau_1)\Sigma_{V_z(\mathbf{x}_2)V_z(\mathbf{x}_3)}(\tau_2) \right] \end{aligned} \quad (\text{B.16})$$

Force projection Assuming a force $\mathbf{F}(X_b, t)$ defined on $R_{rot} \leq X_b \leq L_b; t_0 \leq t \leq t_f$:

$$\begin{aligned} C_F(t) &= \int_{R_{rot}}^{L_b} \mathbf{F}(X_b, t) dx \\ C_F^2(t) &= \int_{R_{rot}}^{L_b} \|\mathbf{F}(X_b, t)\|^2 dx \end{aligned} \quad (\text{B.17})$$

we seek to express $\mathbf{F}(X_b, t)$ in the following projection basis $\varphi_i(x)$, where each of these functions are such that $\int_{R_{rot}}^{L_b} \varphi_i(x) \varphi_j(x) dx = \delta_{ij}$. We have:

$$\begin{aligned} C_{\varphi_i}(t) &= \int_{R_{rot}}^{L_b} \mathbf{F}(X_b, t) \varphi_i(x) dx \\ C_{\varphi}(t) &= \sum_{i=1}^N C_{\varphi_i}(t) \end{aligned} \quad (\text{B.18})$$

from Rayghley's theorem:

$$\int_{R_{rot}}^{L_b} \|\mathbf{F}(X_b, t)\|^2 dx = \sum_{i=1}^{\infty} \|C_{\varphi_i}(t)\|^2 \quad (\text{B.19})$$

since a truncated basis is used, we adjust the projections to ensure $\int_{R_{rot}}^{L_b} \|\mathbf{F}(X_b, t)\|^2 dx = \sum_{i=1}^N \lambda_i \|C_{\varphi_i}(t)\|^2$.

Appendix C

Energy expression of beam from continuum mechanics and material constitutive laws

The general displacement for a continuum is:

$$\begin{aligned} U_x &= U_x(X, Y, Z, t) \\ U_y &= U_y(X, Y, Z, t) \\ U_z &= U_z(X, Y, Z, t) \end{aligned} \quad (\text{C.1})$$

the Green strain tensor:

$$\mathbf{E} = \begin{pmatrix} E_{xx} & E_{xy} & E_{yz} \\ E_{xy} & E_{yy} & E_{zy} \\ E_{yz} & E_{zy} & E_{zz} \end{pmatrix} \quad (\text{C.2})$$

with:

$$\begin{aligned} E_{xx} &= \frac{\partial U_x}{\partial X} + \frac{1}{2} \left(\left(\frac{\partial U_x}{\partial X} \right)^2 + \left(\frac{\partial U_y}{\partial X} \right)^2 + \left(\frac{\partial U_z}{\partial X} \right)^2 \right) \\ E_{yy} &= \frac{\partial U_y}{\partial Y} + \frac{1}{2} \left(\left(\frac{\partial U_x}{\partial Y} \right)^2 + \left(\frac{\partial U_y}{\partial Y} \right)^2 + \left(\frac{\partial U_z}{\partial Y} \right)^2 \right) \\ E_{zz} &= \frac{\partial U_z}{\partial Z} + \frac{1}{2} \left(\left(\frac{\partial U_x}{\partial Z} \right)^2 + \left(\frac{\partial U_y}{\partial Z} \right)^2 + \left(\frac{\partial U_z}{\partial Z} \right)^2 \right) \end{aligned} \quad (\text{C.3})$$

and:

$$\begin{aligned} E_{xy} &= \frac{1}{2} \left(\frac{\partial U_x}{\partial Y} + \frac{\partial U_y}{\partial X} \right) + \frac{1}{2} \left(\frac{\partial U_x}{\partial X} \frac{\partial U_x}{\partial Y} + \frac{\partial U_y}{\partial X} \frac{\partial U_y}{\partial Y} + \frac{\partial U_z}{\partial X} \frac{\partial U_z}{\partial Y} \right) \\ E_{xz} &= \frac{1}{2} \left(\frac{\partial U_x}{\partial Z} + \frac{\partial U_z}{\partial X} \right) + \frac{1}{2} \left(\frac{\partial U_x}{\partial X} \frac{\partial U_x}{\partial Z} + \frac{\partial U_y}{\partial X} \frac{\partial U_y}{\partial Z} + \frac{\partial U_z}{\partial X} \frac{\partial U_z}{\partial Z} \right) \\ E_{yz} &= \frac{1}{2} \left(\frac{\partial U_y}{\partial Z} + \frac{\partial U_z}{\partial Y} \right) + \frac{1}{2} \left(\frac{\partial U_x}{\partial Y} \frac{\partial U_x}{\partial Z} + \frac{\partial U_y}{\partial Y} \frac{\partial U_y}{\partial Z} + \frac{\partial U_z}{\partial Y} \frac{\partial U_z}{\partial Z} \right). \end{aligned} \quad (\text{C.4})$$

From these expressions and with a constitutive law, the stresses are obtained as $\sigma_{ij} = C_{ijkl} \epsilon_{kl}$, where C_{ijkl} is a tensor describing the material behavior. The stress allows for the definition of strain energy densities:

$$W(\epsilon_{ij}) = \int_0^{\epsilon_{ij}} \sigma_{ij} d\epsilon_{ij}. \quad (\text{C.5})$$

The Euler-Bernoulli beam is a uni-dimensional model, so:

$$\begin{aligned} U_x &= U_x(X, Y, Z, t) \\ U_y &= U_y(X, t) \\ U_z &= U_z(X, t), \end{aligned} \quad (\text{C.6})$$

furthermore, it entails:

$$U_x(X, Y, Z) = -Y \frac{\partial U_y}{\partial X} - Z \frac{\partial U_z}{\partial X}. \quad (\text{C.7})$$

From these assumptions we can simplify:

$$\begin{aligned}\frac{\partial U_x}{\partial X} &= -Y \frac{\partial^2 U_y}{\partial X^2} - Z \frac{\partial^2 U_z}{\partial X^2} \\ \frac{\partial U_x}{\partial Y} &= -\frac{\partial U_y}{\partial X} \\ \frac{\partial U_x}{\partial Z} &= -\frac{\partial U_z}{\partial X}\end{aligned}\tag{C.8}$$

and:

$$\begin{aligned}E_{xx} &= \left(-Y \frac{\partial^2 U_y}{\partial X^2} - Z \frac{\partial^2 U_z}{\partial X^2}\right) + \frac{1}{2} \left(\left(-Y \frac{\partial^2 U_y}{\partial X^2} - Z \frac{\partial^2 U_z}{\partial X^2}\right)^2 + \left(\frac{\partial U_y}{\partial X}\right)^2 + \left(\frac{\partial U_z}{\partial X}\right)^2 \right) \\ E_{yy} &= \frac{\partial U_y}{\partial Y} + \frac{1}{2} \left(\left(-\frac{\partial U_y}{\partial X}\right)^2 + \left(\frac{\partial U_y}{\partial Y}\right)^2 + \left(\frac{\partial U_z}{\partial Y}\right)^2 \right) \\ E_{zz} &= \frac{\partial U_z}{\partial Z} + \frac{1}{2} \left(\left(-\frac{\partial U_z}{\partial X}\right)^2 + \left(\frac{\partial U_y}{\partial Z}\right)^2 + \left(\frac{\partial U_z}{\partial Z}\right)^2 \right) \\ E_{xy} &= \frac{1}{2} \left(-\frac{\partial U_y}{\partial X} + \frac{\partial U_y}{\partial X} \right) + \frac{1}{2} \left(\left(-Y \frac{\partial^2 U_y}{\partial X^2} - Z \frac{\partial^2 U_z}{\partial X^2}\right) \left(-\frac{\partial U_y}{\partial X}\right) + \frac{\partial U_y}{\partial X} \frac{\partial U_y}{\partial Y} + \frac{\partial U_z}{\partial X} \frac{\partial U_z}{\partial Y} \right) \\ E_{xz} &= \frac{1}{2} \left(-\frac{\partial U_z}{\partial X} + \frac{\partial U_z}{\partial X} \right) + \frac{1}{2} \left(\left(-Y \frac{\partial^2 U_y}{\partial X^2} - Z \frac{\partial^2 U_z}{\partial X^2}\right) \left(-\frac{\partial U_z}{\partial X}\right) + \frac{\partial U_y}{\partial X} \frac{\partial U_y}{\partial Z} + \frac{\partial U_z}{\partial X} \frac{\partial U_z}{\partial Z} \right) \\ E_{yz} &= \frac{1}{2} \left(\frac{\partial U_y}{\partial Z} + \frac{\partial U_z}{\partial Y} \right) + \frac{1}{2} \left(\left(-\frac{\partial U_y}{\partial X}\right) \frac{\partial U_x}{\partial Z} + \frac{\partial U_y}{\partial Y} \frac{\partial U_y}{\partial Z} + \frac{\partial U_z}{\partial Y} \frac{\partial U_z}{\partial Z} \right).\end{aligned}$$

Now:

$$\begin{aligned}E_{xx} &= \left(-Y \frac{\partial^2 U_y}{\partial X^2} - Z \frac{\partial^2 U_z}{\partial X^2}\right) + \frac{1}{2} \left(\left(Y \frac{\partial^2 U_y}{\partial X^2}\right)^2 + \left(Z \frac{\partial^2 U_z}{\partial X^2}\right)^2 + 2YZ \frac{\partial^2 U_y}{\partial X^2} \frac{\partial^2 U_z}{\partial X^2} + \left(\frac{\partial U_y}{\partial X}\right)^2 + \left(\frac{\partial U_z}{\partial X}\right)^2 \right) \\ E_{yy} &= \frac{1}{2} \left(\frac{\partial U_y}{\partial X} \right)^2 \\ E_{zz} &= \frac{1}{2} \left(\frac{\partial U_z}{\partial X} \right)^2\end{aligned}\tag{C.9}$$

$$\begin{aligned}
E_{xy} &= \frac{1}{2} \left(Y \frac{\partial^2 U_y}{\partial X^2} \frac{\partial U_y}{\partial X} + Z \frac{\partial^2 U_z}{\partial X^2} \frac{\partial U_y}{\partial X} \right) \\
E_{xz} &= \frac{1}{2} \left(Y \frac{\partial^2 U_y}{\partial X^2} \frac{\partial U_z}{\partial X} + Z \frac{\partial^2 U_z}{\partial X^2} \frac{\partial U_z}{\partial X} \right) \\
E_{yz} &= \frac{1}{2} \left(-\frac{\partial U_y}{\partial X} \frac{\partial U_x}{\partial Z} \right).
\end{aligned} \tag{C.10}$$

The constitutive law for an isotropic material are expressed as follows:

$$\begin{bmatrix} \sigma_{xx} \\ \sigma_{yy} \\ \sigma_{zz} \\ \sigma_{yz} \\ \sigma_{xz} \\ \sigma_{xy} \end{bmatrix} = \begin{bmatrix} \lambda + 2\mu & \lambda & \lambda & 0 & 0 & 0 \\ \lambda & \lambda + 2\mu & \lambda & 0 & 0 & 0 \\ \lambda & \lambda & \lambda + 2\mu & 0 & 0 & 0 \\ 0 & 0 & 0 & \mu & 0 & 0 \\ 0 & 0 & 0 & 0 & \mu & 0 \\ 0 & 0 & 0 & 0 & 0 & \mu \end{bmatrix} \begin{bmatrix} E_{xx} \\ E_{yy} \\ E_{zz} \\ 2E_{yz} \\ 2E_{xz} \\ 2E_{xy} \end{bmatrix}, \tag{C.11}$$

the linear part of strain energy V can be obtained considering the linear terms: $E_{xx} = -Y \frac{\partial^2 U_y}{\partial X^2} - Z \frac{\partial^2 U_z}{\partial X^2}$; $E_{yy} = 0$; $E_{zz} = 0$; $E_{xy} = 0$; $E_{xz} = 0$; $E_{yz} = 0$:

$$\begin{aligned}
E_{xx}^2 &= \left(-Y \frac{\partial^2 U_y}{\partial X^2} - Z \frac{\partial^2 U_z}{\partial X^2} \right)^2 \\
&= Y^2 \left(\frac{\partial^2 U_y}{\partial X^2} \right)^2 + Z^2 \left(\frac{\partial^2 U_z}{\partial X^2} \right)^2 + YZ \frac{\partial^2 U_y}{\partial X^2} \frac{\partial^2 U_z}{\partial X^2}
\end{aligned} \tag{C.12}$$

$$\begin{aligned}
V &= (\lambda + 2\mu) \int_A \int_{L_b} Y^2 \left(\frac{\partial^2 U_y}{\partial X^2} \right)^2 + Z^2 \left(\frac{\partial^2 U_z}{\partial X^2} \right)^2 + YZ \frac{\partial^2 U_y}{\partial X^2} \frac{\partial^2 U_z}{\partial X^2} dx dA \\
&= (\lambda + 2\mu) I_{ZZ} \int_{L_b} \left(\frac{\partial^2 U_y}{\partial X^2} \right)^2 dx \\
&\quad + (\lambda + 2\mu) I_{YY} \int_{L_b} \left(\frac{\partial^2 U_z}{\partial X^2} \right)^2 dx \\
&\quad + (\lambda + 2\mu) I_{YZ} \int_{L_b} \left(\frac{\partial^2 U_y}{\partial X^2} \frac{\partial^2 U_z}{\partial X^2} \right) dx
\end{aligned} \tag{C.13}$$

with $I_{ZZ} = \int_A Y^2 dA$; $I_{YY} = \int_A Z^2 dA$; $I_{YZ} = \int_A YZ dA$.

Appendix D

Generation of stochastic processes

This annex describes some of the methods that permit the numerical simulation of a prescribed stochastic process, simulation being understood as the generation of samples or realizations of said process. The importance of generation methods comes from the fact that the entire branch of Monte-Carlo methodologies for probabilistic mechanics requires the availability of an ensemble of the processes considered as inputs; since MCMs tend to be very general in their scope of application, they tend to serve as benchmark for new approaches in problems involving uncertainties. Most of the results here pertain to a very particular, if widely utilized, class of process: stationary centered Gaussian processes. From the stationary centered Gaussian case, more complex processes can be constructed by relatively simple means: addition and multiplication by the appropriate quantities permit the scaling of mean and variance, preserving Gaussianity; polynomial transformations produce generally non-Gaussian processes that are useful in the modeling of loads; multiplication by a time-modulating function results in Gaussian non-stationary processes.

The following notation will be employed to denote the distribution of a given random variable:

- $\mathcal{U}(a, b)$ Uniform distribution with parameters a, b .
- $\mathcal{R}(\sigma)$ Rayleigh distribution with parameter σ .
- $\mathcal{N}(\mu, \sigma)$ Gaussian distribution with mean μ and variance σ .

1 Preliminaries

Let Ω be a sampling space with associated sigma-algebra \mathcal{F} and probability measure \mathbb{P} , forming the probability space $\{\Omega, \mathcal{F}, \mathbb{P}\}$. A random variable x with distribution \mathbb{P} is characterized by its CDF:

$$P_x(a) = \mathbb{P}[x \leq a], a \in \Omega \quad (\text{D.1})$$

from where we define a stochastic process as a group of random variables indexed by a time variable:

$$X(t) = x_t, \quad (\text{D.2})$$

if a spatial domain $\mathbf{r} = (x, y, z)$ is considered, then it is possible to establish a scalar spatiotemporal stochastic field:

$$\mathcal{X}(\mathbf{r}, t) = \mathcal{X}_r(t), \quad (\text{D.3})$$

or also a vector spatiotemporal stochastic field:

$$\mathcal{X}(\mathbf{r}, t) = \begin{pmatrix} \mathcal{X}_r^x(t) \\ \mathcal{X}_r^y(t) \\ \mathcal{X}_r^z(t) \end{pmatrix}. \quad (\text{D.4})$$

Unlike random variables, the CDF of a stochastic process does not provide a complete description of processes and fields; more concretely, the marginal CDF of a stochastic process reads:

$$P_X(x, t) = \mathbb{P}[X(t) \leq x], \quad (\text{D.5})$$

the finite-dimensional distributions (FDDs) of the process are the joint CDFs of a finite number of the constituent random variables, for instance the second-order distributions read:

$$P_{XX}(x_1, x_2, t_1, t_2) = \mathbb{P}[X(t_1) \leq x_1, X(t_2) \leq x_2], \quad (\text{D.6})$$

and similarly, the $n - th$ order distributions read:

$$P_{X\dots X}(x_1, \dots, x_n, t_1, \dots, t_n) = \mathbb{P}[X(t_1) \leq x_1, \dots, X(t_n) \leq x_n]. \quad (\text{D.7})$$

An analogous partial characterization applies to spatiotemporal stochastic fields in terms of finite-dimensional distributions, the key distinction being the spatial dimension on which these are indexed.

1.1 Karhunen-Loève representation

The Karhunen-Loève representation is introduced here because it will facilitate the interpretation of the formulas of key methods presented here. The process $X(t)$ of mean $\mu_X(t) = \mathbb{E}[X(t)]$ and covariance function $\Sigma_{XX}(t_1, t_2) = \mathbb{E}[(X(t_1) - \mu_X)(X(t_2) - \mu_X)]$, variance $\sigma_{XX}(t_i) = \Sigma_{XX}(t_i, t_i)$, allows the following Karhunen-Loève (K-L) representation:

$$X(t) = \mu_X(t) + \sum_{i=1}^M \sqrt{\lambda_i} \zeta_i f_i(t) \quad (\text{D.8})$$

where the M is the order of the K-L series, and $f_i(t), \lambda_i$ are eigenfunctions and eigenvalues of the following eigenvalue problem:

$$\int_D \Sigma_{XX}(t_1, t_2) f_i(t_2) dt_2 = \lambda_i f_i(t_1), \quad (\text{D.9})$$

with ζ_i a set of uncorrelated random variables verifying:

$$\begin{aligned} \mathbb{E}[\zeta_i] &= 0 \\ \mathbb{E}[\zeta_i \zeta_j] &= \delta_{ij}. \end{aligned} \quad (\text{D.10})$$

In the case of a stationary Gaussian process, then $\zeta_i \rightarrow \mathcal{N}(0, 1)$.

2 Simulation of Gaussian processes

The following quantities fully determine a Gaussian process $X(t)$:

1. Its mean function $\mu_X(t)$
2. Its covariance function $\Sigma_{XX}(t_1, t_2)$, or its correlation function $R_{XX}(t_1, t_2)$, or its Power Spectral Density (PSD) $S_{XX}(f)$; these three quantities provide equivalent information about the process.

We consider a Gaussian process $X(t)$ which is stationary up to the second order, $\mu_X(t) = \mu_X$ and $\Sigma_{XX}(t_1, t_2) = \Sigma_{XX}(\tau)$, where $\tau = t_2 - t_1$; and centered, $\mu_X = 0$. We recall, from the Wiener-Khinchin theorem, the following relationships:

$$\begin{aligned} S_{XX}(f) &= \text{FT}[\Sigma_{XX}(\tau)] \\ \sigma_{XX} &= \int_{-\infty}^{\infty} S_{XX}(f) df, \end{aligned} \quad (\text{D.11})$$

the covariance function and the PSD are FT pairs; the practical interpretation of the PSD is that of a decomposition of the variance in the frequency domain. Additionally, the shape of the PSD allows for the classification of processes in two groups: narrowband processes, where the magnitude of the PSD is clustered in the vicinity of a given frequency, and broadband processes, where the magnitude of the PSD is spread across a wide interval of frequency values.

Method 1: Harmonic function with random amplitude The process is approximated with the following formula:

$$X(t) = \sum_{i=1}^N A_i \cos[2\pi f_i t] + B_i \sin[2\pi f_i t] \quad (\text{D.12})$$

with $A_i, B_i \rightarrow \mathcal{N}(0, \sqrt{S_i \Delta f_i})$ a set of independent Gaussian random variables of mean 0 and variance $\sigma_i = \sqrt{S_i \Delta f_i}$; the pair (f_i, S_i) corresponds to the i -th discretized frequency and associated value of the PSD. To note, in the discretization:

$$\begin{aligned} \Delta f_i &= \frac{f_{i+1} - f_{i-1}}{2} \\ \Delta f_1 &= f_2 - f_1 \\ \Delta f_N &= f_N - f_{N-1}. \end{aligned} \quad (\text{D.13})$$

Notice that this approximation of the process is Gaussian in distribution for any given N , as it is a sum of Gaussian variables.

The algorithmic implementation of this method has the form:

1. Define time interval of the observation $t \in [T_{in}, T_f]$, frequency discretization N , and number of samples N_S .
2. Compute the N discretized pairs (f_i, S_i) .
3. Compute the discretized variance terms $\sigma_i = \sqrt{S_i \Delta f_i}$.
4. Generate $N \times N_S$ pairs of $(A_i, B_i) \rightarrow \mathcal{N}(0, \sqrt{S_i \Delta f_i})$, these pairs being statistically independent.
5. Perform the sum in formula Eq. D.12.

Method 2: Random phase and random amplitude Formula Eq. D.12 can be rewritten as:

$$X(t) = \sum_{i=1}^N C_i \cos[2\pi f_i t + \phi_i], \quad (\text{D.14})$$

where $C_i = \sqrt{A_i^2 + B_i^2}$ and $\phi_i = \arctan\left(-\frac{B_i}{A_i}\right)$; it can be shown ([138]) that if $(A_i, B_i) \rightarrow \mathcal{N}(0, \sqrt{S_i \Delta f_i})$, then $C_i \rightarrow \mathcal{R}(\sqrt{S_i \Delta f_i})$ and $\phi_i \rightarrow \mathcal{U}(0, 2\pi)$. The algorithmic implementation of this method has the form:

1. Define the time interval of the observation $t \in [T_{in}, T_f]$, frequency discretization N , and number of samples N_S .
2. Compute the N discretized pairs (f_i, S_i) .
3. Generate $N \times N_S$ independent random variables $\phi_i \rightarrow \mathcal{U}(0, 2\pi)$ and $C_i \rightarrow \mathcal{R}(\sqrt{S_i \Delta f_i})$.
4. Perform the sum in formula Eq. D.14.

It should be stressed that formula Eq. D.14, when used with $C_i = \sqrt{2S_i \Delta f_i}$ (non-random amplitude), produces samples that converge to the Gaussian distribution only asymptotically: $N \rightarrow \infty$, as a result of the central limit theorem. While this approach may be useful in theoretical developments where the limit can be imposed, simulation imposes a high requirement on N to approach Gaussianity in distribution. Consequently, the method with non-random C_i is not recommended in practical settings.

Method 3: Random amplitude with IFFT algorithm The random amplitude method can be implemented with the aid of the Inverse Fast Fourier Transform (IFFT) algorithm, resulting in a substantial reduction of the computational time cost. First, we note the following identities:

$$\begin{aligned}\exp[i2\pi f_i t] &= \cos[2\pi f_i t] + i \sin[2\pi f_i t] \\ \operatorname{Re}[\exp[i2\pi f_i t]] &= \cos[2\pi f_i t] \\ \sin[2\pi f_i t] &= \cos\left[2\pi f_i t - \frac{\pi}{2}\right],\end{aligned}\tag{D.15}$$

so we may write Eq. D.12 in the following form:

$$\begin{aligned}X(t) &= \sum_{i=1}^N A_i \cos[2\pi f_i t] + B_i \sin[2\pi f_i t] \\ &= \sum_{i=1}^N A_i \cos[2\pi f_i t] + B_i \cos\left[2\pi f_i t - \frac{\pi}{2}\right] \\ &= \sum_{i=1}^N A_i \operatorname{Re}[\exp[i2\pi f_i t]] + B_i \operatorname{Re}\left[\exp[i2\pi f_i t] \exp\left[-i\frac{\pi}{2}\right]\right] \\ &= \operatorname{Re}\left[\sum_{i=1}^N D_i \exp[i2\pi f_i t]\right],\end{aligned}\tag{D.16}$$

with $D_i = (A_i - B_i)$, and the sum is equivalent to an Discrete Inverse Fourier Transform. Concerning D_i , since A_i, B_i are independent, we may write:

$$\begin{aligned}\mu_{D_i} &= \mu_{A_i} + \mu_{B_i} = 0 \\ \sigma_{D_i D_i} &= \mu_{D_i D_i} \\ &= \operatorname{E}[A_i^2 + B_i^2 - 2A_i B_i] \\ &= \sigma_{A_i A_i} + \sigma_{B_i B_i} \\ &= 2\sqrt{S_i \Delta f_i},\end{aligned}\tag{D.17}$$

which means that $D_i \rightarrow \mathcal{N}(0, 2\sqrt{S_i \Delta f_i})$.

The algorithmic implementation of this method has the form:

1. Define time interval of the observation $t \in [T_m, T_f]$, frequency discretization N , and number of samples N_S .
2. Compute the N discretized pairs (f_i, S_i) .
3. Compute the discretized variance terms $\sigma_i = 2\sqrt{S_i \Delta f_i}$.
4. Generate $N \times N_S$ values of $D_i \rightarrow \mathcal{N}(0, 2\sqrt{S_i \Delta f_i})$.
5. Use the IFFT algorithm to evaluate Eq. D.16.

2.1 Multivariate case

In the case of i processes, the prescribed spectral matrix reads:

$$\mathbf{S}(f) = \begin{pmatrix} S_{11}(f) & S_{12}(f) & \dots & S_{1i}(f) \\ S_{12}^*(f) & S_{22}(f) & & \dots \\ \dots & & & \dots \\ S_{1i}^*(f) & & & S_{ii}(f) \end{pmatrix} \quad (\text{D.18})$$

where $S_{ij}^*(f)$ denotes the complex conjugate of $S_{ij}(f)$. The correlation of any two processes is ρ_{ij} , with which one can express the coherence function:

$$\gamma_{ij}(f) = \rho_{ij} \exp[i\phi_{ij}]. \quad (\text{D.19})$$

The methods for univariate processes can be extended, for instance:

$$X_p(t) = \sum_{i=1}^N \sum_{q=1}^n M_{ipq} \cos[2\pi f_{iq}t + \arg[H_{pq}(f_i)] + \phi_{ij}], \quad (\text{D.20})$$

where i and j are frequency indexes, and p denotes the corresponding process, and additionally:

$$\begin{aligned} H(f_i) &= S^{\frac{1}{2}}(f_i) \\ M_{ipq} &= |H_{pq}(f_i)| \sqrt{\Delta f_i} \\ \phi_{ij} &\rightarrow U(0, 2\pi) \\ f_{iq} &= f_i + \frac{q}{n} \Delta f_i. \end{aligned} \quad (\text{D.21})$$

The Inverse Fourier Transform method reads:

$$X_p(t) = \sum_{q=1}^n \sum_{i=1}^N C_{ipq} \exp[i2\pi f_{iq}t] \quad (\text{D.22})$$

$$\begin{aligned} |C_{ipq}| &= M_{ipq} \\ \arg(C_{ipq}) &= \arg[H_{pq}(f_i)] + \phi_{iq} \\ \phi_{iq} &\rightarrow U(0, 2\pi). \end{aligned} \quad (\text{D.23})$$

Karhunen-Loève connection We write, from Eq. D.8 and Eq. D.16:

$$\begin{aligned} X(t) &= \sum_{i=1}^M \sqrt{\lambda_i} \zeta_i f_i(t) \\ X(t) &= \sum_{i=1}^N D_i \exp[i2\pi f_i t], \end{aligned} \quad (\text{D.24})$$

by identification:

$$\begin{aligned} f_i(t) &= \exp[i2\pi f_i t] \\ D_i &= \sqrt{\lambda_i} \zeta_i, \end{aligned}$$

and considering $\zeta_i \rightarrow \mathcal{N}(0, 1)$ then:

$$\begin{aligned}\mu_{D_i} &= 0 \\ \sigma_{D_i D_i} &= \lambda_i \sigma_{\zeta_i} \zeta_i \\ &= \lambda_i.\end{aligned}$$

This suggests that the methods presented in this section can be interpreted as instances of the K-L series representation of the corresponding Gaussian processes: with eigenfunctions $f_i(t) = \exp[i2\pi f_i t]$, eigenvalues λ_i associated to the PSD discretization (f_i, S_i) and Δf_i , and basis $\zeta_i \rightarrow \mathcal{N}(0, 1)$.

3 Simulation of non-Gaussian processes

The topic of non-Gaussian simulation remains an active field of research, a consequence of the challenges involved in such a task. The difficulties involved in the simulation of non-Gaussian processes are caused, in no small part, by the fact that the class “non-Gaussian” encompasses a very broad type of process with very different characteristics. Phoon’s algorithm is included in this section, the aim being to provide a concise illustration of the type of adjustments that are required to extend K-L-based stochastic simulation into the realm of the non-Gaussian.

K-L Phoon’s algorithm ([102])

1. Generation of m samples using $X_M^{(k)}(t) = \sum_{i=1}^M \sqrt{\lambda_i} \zeta_i^{(k)} f_i(t)$, with k the iteration number and m the number of samples,
2. Estimate the marginal CDF: $\hat{F}_M^{(k)}(y|t) = \frac{1}{n} \sum_{m=1}^n I(X_M^{(k)}(t) \leq y)$, where I is the indicating function, 1 if $X_M^{(k)}(t) \leq y$, 0 otherwise,
3. Transform the samples to match the prescribed CDF: $\eta_M^{(k)} = F^{-1}[\hat{F}_M^{(k)}(X_M^{(k)})]$
4. Estimate the new $\zeta_i^{(k)}$ with $\zeta_i^{(k+1)} = \frac{1}{\sqrt{\lambda_i}} \int_D [\eta_M^{(k)} - E[\eta_M^{(k)}]] f_i(t) dt$
5. Transform $\zeta_i^{(k+1)}$ to unit variance (LHS is suggested to minimize cross-correlations among these variables)
6. Iterate through steps 1 to 5 until the target CDF is achieved

Résumé

Un grand nombre de technologies reposent sur des machines ou des structures qui peuvent être suffisamment bien décrites par un modèle rotor-pâle avec des pâles constituées d'éléments de poutre attachés radialement et subissant des vibrations transversales. Or les chargements agissants sur ces systèmes peuvent être de nature aléatoire et très complexes, en particulier pour des applications telles que les hydroliennes ou les machines hydrocinétiques. Pour l'analyse et la conception de ces systèmes en tenant compte des considérations de fiabilité, un modèle mécano-probabiliste intégrant les aspects mécaniques du système de rotor-pâle et les différents aspects du processus de chargement stochastique est d'intérêt. L'approche fiabiliste permet d'améliorer les systèmes et les structures du point de vue du coût, de la sécurité et de la performance.

D'un point de vue théorique, certaines limitations peuvent être identifiées par rapport aux travaux précédents dans le domaine des modèles rotor-pâle, de la dynamique stochastique, de la fiabilité et de l'analyse des valeurs extrêmes. Elles comprennent les problèmes de dimensionnalité du modèle dynamique, qui limitent la capacité d'analyse stochastique fine ; la non prise en compte de certaines coordonnées du mouvement ; ainsi que des hypothèses de simplification strictes sur les chargements stochastiques considérés, la gaussiannité et la stationnarité étant les plus courantes.

Pour répondre aux questions précédemment identifiées, une première étape est la construction d'un nouveau modèle dynamique pour le système rotor-pâle. Il s'agit d'un modèle d'ordre réduit, établi sur la base d'informations préliminaires provenant des domaines de la dynamique des rotors, des vibrations et de la mécanique des milieux continus, tenant compte des variables de conception les plus importantes. La philosophie préalable à sa création se base sur la capture des principales caractéristiques vibratoires et mécaniques de ce type de système physique, tout en conservant une dimension réduite afin de faciliter l'analyse stochastique de la réponse. Une description détaillée de la construction du modèle est présentée, y compris l'analyse cinématique et énergétique du système, le schéma de discrétisation modale qui permet une représentation efficace des vibrations des pales et la reconstruction de la réponse physique.

Le modèle rotor-pâle ainsi établi entre dans la catégorie des systèmes de Floquet : un système d'équations différentielles ordinaires avec des coefficients temporels, aussi dit problème mécanique non-standard. Pour traiter ce type de système, la théorie modale de Floquet est exploitée. Une revue synthétique de cette théorie est d'abord présentée, capitalisant à la fois les avancées numériques et les perspectives d'interprétation dans des domaines très différents : de la dynamique des hélicoptères à la théorie moderne des équations différentielles ordinaires, en passant par la mécanique appliquée et la dynamique des rotors. À partir de cette base théorique, nous présentons une discussion approfondie sur l'application et l'interprétation des modes périodiques de Floquet et des exposants caractéristiques de Lyapunov ; les méthodes de détermination de ces quantités sont présentées et évaluées de manière critique. Les exposants caractéristiques du système de Floquet sont interprétés comme une généralisation des caractéristiques vibratoires clés pour les systèmes invariants dans le temps : fréquence vibratoire naturelle et amortissement modal ; Une généralisation du diagramme de Campbell, nommé diagramme de Campbell-Lyapunov, est proposée par l'étude paramétrique de l'évolution de la fréquence du système en fonction de la vitesse angulaire propre, ou, de manière équivalente, la fréquence de l'excitation paramétrique.

La réponse déterministe du système de Floquet dans le domaine des fréquences est obtenue en utilisant la méthode de Hill. Une démonstration nouvelle est proposée pour l'équation reliant la réponse en fréquence du système aux sollicitations. Elle apporte une certaine clarté dans l'application de la formule, ce qui facilite l'amélioration de certains aspects de sa mise en œuvre numérique. Cette équation sert de base à la méthode de

Monte-Carlo spectrale, qui fournit la réponse en régime établi du système rotor-pâle en cas d'entrées stochastiques. Une stratégie innovante est également proposée pour l'analyse modale des systèmes de Floquet, basée sur un outil temps-fréquence particulier : l'ondelette harmonique généralisée périodique. Elle établit une connexion entre la méthode traditionnelle de Hill dans le domaine des fréquences et le domaine temps-fréquence des ondelettes, sélectionnées par un schéma de projection parmi les bases de Hilbert. Plus généralement, l'ondelette harmonique généralisée est utilisée tout au long de cette thèse comme outil pour estimer des quantités instationnaires telles que le spectre évolutif de la réponse qui caractérise un système de Floquet.

La propagation des moments statistiques est choisie comme principale stratégie pour la description des réponses mécaniques, en raison des complexités inhérentes à la caractérisation stochastique de ces processus. À cette fin, une méthodologie systématique pour la propagation des moments est élaborée et illustrée. La méthodologie et la notation associée sont discutées en détail, et des exemples du génie offshore sont utilisés pour montrer l'efficacité de l'approche proposée en comparaison des publications de référence dans ce domaine. La théorie modale de Floquet et la propagation des moments ont ainsi été combinées pour établir des expressions analytiques de convolution multidimensionnelles reliant les quantités probabilistes de la sollicitation d'entrée stochastique à la réponse du système rotor-pâle. Ces expressions constituent la base de la méthode semi-analytique proposée pour caractériser les réponses par les moments. Les particularités de la méthode, ses avantages et ses limites, ainsi que plusieurs aspects d'implémentation numérique sont discutés. La propagation des moments obtenue, la densité de probabilité de la réponse peut alors être reconstruite par une méthode d'estimation basée sur le principe d'Entropie maximale, pour finalement obtenir la distribution des valeurs extrêmes.

Après avoir étudié les processus instationnaires obtenus par une modulation uniforme de processus stationnaires, des relations de propagation des moments sont déduites pour cette classe de processus et sa dérivée temporelle. Nous présentons une analyse détaillée de la relation entre les moments de ce type de processus et les franchissements d'un certain seuil atteint par le processus et, finalement, la distribution des valeurs extrêmes. Cette analyse est à l'origine d'une méthodologie proposée pour estimer la distribution des valeurs extrêmes des processus instationnaires et non gaussiens : la méthode d'approximation par intervalles, dont la simplicité et les performances surprenantes sont un point fort de cette thèse.

L'ensemble des développements théoriques et méthodologiques ainsi produits nous ont permis de traiter une étude de fiabilité de pales d'hydroliennes. Certains défis de la conception mécanique dans ce domaine sont résumés, ainsi que les tendances actuelles en termes de modélisation stochastique des états de mer et de sollicitations sur la turbine. L'analyse de Floquet du système simplifié est réalisée, ce qui permet d'obtenir la caractérisation modale périodique correspondante. Un modèle stochastique de vague-courant-turbulence est utilisé pour décrire le processus de vitesse d'écoulement agissant sur l'hydrolienne, et trois méthodologies sont mises en œuvre pour obtenir les réponses du système dans différents régimes de mouvement. Pour chaque cas, des estimateurs de fiabilité sont obtenus et comparés. Les résultats illustrent la faisabilité des solutions proposées pour résoudre ce type de problème. En particulier, la combinaison des modèles de sollicitations par des processus stochastiques élaborés et de modèles dynamiques d'ordre réduit capables de tenir compte des variables de conception essentielles.

Abstract

Many technologies rely on machines or structures that can be effectively described by a rotor-blade model: a rotor component with continuum elements attached radially undergoing transverse vibrations. The loads acting over these systems can be quite complex, particularly for such applications as tidal or hydrokinetic turbines; the complexity of these loads makes them good candidates to be described through stochastic modeling tools. The usefulness of a mechano-probabilistic model integrating the mechanical aspects of the rotor-blade model and the different elements of the stochastic load process includes the analysis and design of such systems under reliability considerations. The reliability approach results in improved systems and structures from the cost, safety, and performance perspective.

From a theoretical perspective, certain limitations can be identified concerning the previous works in the joint domain of rotor-blade models, stochastic dynamics, reliability, and extreme value analysis. The limitations include dimensionality issues in the dynamical model, which hampers the capability of insightful or refined stochastic analysis; neglect of specific coordinates of motion; stringent simplification hypotheses on the stochastic loads considered- Gaussianity and stationarity being the most common.

Our first step is to construct a new dynamical model for rotor-blade systems to address the previously identified issues. The model is of reduced order, established by the careful consideration of preliminary information from the fields of rotordynamics, vibration theory, and continuum mechanics; the philosophy of its inception has been to capture key vibrational and mechanical features of this type of physical system while maintaining a reduced dimension to facilitate stochastic analysis of the response. A detailed description of the construction of the model is presented, including the kinematic and energetic analysis of the system, the modal discretization scheme that allows the efficient representation of blade vibration, and the recovery of design variables from the response.

The mathematical rotor-blade model falls under the category of a Floquet system, a system of Ordinary Differential Equations with time-periodic coefficients. To treat this type of system, the modal theory of Floquet has been harnessed. A synthetic review of Floquet theory is presented, capitalizing on technical advances and interpretation insights in different domains: helicopter dynamics to the modern theory of ordinary differential equations, passing through applied mechanics and rotordynamics. From this theoretical foundation, we present an in-depth discussion on applying and interpreting Floquet Periodic Modes and Lyapunov Characteristic Exponents; the methods for determining such quantities are presented and critically evaluated. The Characteristic exponents of the Floquet system are interpreted as a generalization of the vital vibrational characteristics for time-invariant systems: natural vibrational frequency and damping ratio; the generalization of the Campbell diagram, the Campbell-Lyapunov diagram, is proposed as a parametric study of the evolution of the system's frequency with the spin angular velocity or equivalently the frequency of parametric excitation. An innovative strategy is put forward for the modal analysis of Floquet systems; it is based on a particular time-frequency tool: the Periodic Generalized Harmonic Wavelet; it establishes a connection between the traditional method of Hill in the Frequency domain and the time-frequency domain of the selected Wavelets using a projection scheme among Hilbert bases. More broadly, the PGHW is used throughout the thesis to estimate nonstationary quantities, such as the response evolutionary spectra that characterize Floquet systems.

The response of the Floquet system on the frequency domain is obtained using Hill's method. A new demonstration is presented for the equation relating the system's frequency response and the load's Fourier transform. This new demonstration clarifies the application of the formula, which facilitates improving some numerical as-

pects of the implementation. This spectral equation serves as the basis for the proposed Floquet-based spectral Monte-Carlo, a method that provides the steady-state response of the rotor-blade system under stochastic input.

Owing to the inherent complexities of stochastic characterization, moment propagation is selected as the primary strategy for response description. To this end, a systematic methodology for moment propagation is constructed and exemplified. The method and associated notation are discussed in detail, and examples from offshore analysis problems are used to contrast the efficacy of our approach with benchmark publications in this domain. Moment propagation is combined with a Maximum Entropy PDF estimation method to reconstruct the PDF of the response and, ultimately, the distribution of extreme values of the response quantity.

Floquet's modal theory and moment propagation have been combined to establish analytical expressions relating the probabilistic quantities of the stochastic input load with the response of the rotor-blade system. These multidimensional convolution expressions are the basis of a proposed semi-analytical method to characterize the system's response through its moments. The particularities of the method, its advantages and limitations, and several computational aspects are discussed.

After studying nonstationary processes obtained by uniform modulation of stationary processes, moment propagation relationships are deduced for this class of process and its temporal derivative. We present a detailed analysis of the relationship between the moments of this type of process and the crossings over a certain threshold attained by the process and, ultimately, the extreme value distribution. This analysis is the origin of a proposed methodology to estimate the extreme value distribution of nonstationary processes: the interval approximation method, its simplicity, and surprising performance are a highlight of the present work.

The theoretical and methodological developments obtained throughout this work are put together in a case study corresponding to the blade reliability of tidal turbines. Some challenges to the mechanical design in this field are summarized, as well as current trends in stochastic modeling of sea states and loadings over the turbine. The Floquet analysis of a simplified generic system is performed, obtaining its corresponding modal characterization. A stochastic wave-current-turbulence model describes the flow velocity process acting over the tidal turbine, and three methodologies are used to obtain the system's response under different regimes of motion. The reliability estimators are obtained for each case and compared. The results illustrate the feasibility of the proposed techniques to solve this type of problem, particularly the combination of elaborate stochastic load processes and reduced-order dynamical models that capture important design variables.